Pathogenesis of Mitochondrial Dysfunction in Skeletal Muscle

Hannah Sophia Rosa

MSci

This thesis is submitted for the degree of Doctor of Philosophy at Newcastle University

Wellcome Trust Centre for Mitochondrial Research

Institute of Neuroscience.

January 2017

Author's declaration

This thesis is submitted for the degree of Doctor of Philosophy at Newcastle University. The research was conducted in the Wellcome Trust Centre for Mitochondrial Research, Institute of Neuroscience, and is my own work if not stated otherwise. The research was completed under the supervision of Professor Sir D.M. Turnbull, Professor R.W. Taylor and Dr H.A.L. Tuppen from August 2013 to December 2016.

I certify that none of the material offered in this thesis has been previously submitted by me for a degree or any other qualification at any other university.

Abstract

Mitochondrial diseases are amongst the most prevalent genetic disorders, however little is known about genetic and cellular mechanisms behind disease pathogenesis and progression. Elucidating such mechanisms can help identify targets for novel therapeutic measures and improve patient care by informing the implementation of clinical regimens and providing clearer information on prognoses. This project aims to improve the understanding of the molecular mechanisms behind the pathogenesis of mitochondrial dysfunction in muscle and the genetic and biochemical changes occurring over time in patients with mitochondrial disease.

Firstly, a longitudinal study combines immunofluorescent and molecular genetic techniques to assess biochemical and genetic changes over time in serial skeletal muscle biopsies from patients with m.3243A>G or single, large-scale mtDNA deletions, the two largest groups in the MRC Centre Mitochondrial Disease Patient Cohort. Further investigation into the relationship between the genetic and biochemical defects in patients with single, large-scale mtDNA deletions is carried out by applying a single-fibre approach. Here, muscle fibres are classified by their biochemical defect and laser microdissected for genetic analysis to determine deletion level and mtDNA copy number.

These studies find that: (i) changes to mutation level, mtDNA copy number and biochemical defect occur over time in skeletal muscle of mitochondrial disease patients; (ii) these changes are inconsistent in magnitude and direction across groups of patients and (iii) the biochemical threshold for deficiency is affected by the size and location of single, large-scale mtDNA deletions.

In addition, a real time PCR assay for the quantification of mitochondrial DNA copy number from homogenate tissue has been optimised to improve accuracy through the use of additional gene markers.

Acknowledgements

I would firstly like to thank my supervisory team, Professor Sir Doug Turnbull, Professor Rob Taylor and Dr. Helen Tuppen for their continued support and guidance over the last few years. I am sincerely grateful for all the advice you have given me on so many occasions. A special thanks to Helen for answering all of my questions about, well everything really, and for sharing in my frustration during the many real-time related nightmares.

I would like to thank the 'The Barbour Foundation', who funded my PhD studies and showed a keen interest throughout. I would further like to thank the many people who I have collaborated with, or who have contributed to the research presented in this thesis. Thank you to all the patients who took part in the various studies, and the research nurses, particularly Alex Bright, who collected many samples for me. Thanks to Mariana Rocha for putting up with my craziness during all that single fibre analysis. I will never be the same again. I would also like to thank John Grady for his help with the modelling of disease progression and general statistical wizardry. I should further thank John for suggesting we develop a new copy number assay and then leaving for Australia before we finished analysing all the data. I am also grateful for the training and support provided by Dr. Trevor Booth and Dr. Alex Laude at the Bioimaging Facility where I spent many long hours. I would like to extend my thanks to Dr Yi Ng for providing me with the clinical details I needed for the various studies, and Tom Holden and Gavin Falkous for dealing with all the tissue requests I sent in. And to Julie Murphy for letting me get involved with the public engagements activities.

There are really too many people to thank individually, so a massive shout out to the whole MRG. Many of you are like family, in that I didn't chose to be stuck sat next to you for three years but what could I do about it (you know who you are). A few special mentions though. Thanks to Jono for being an awesome flatmate for the last however many months. Career advice – remember to feed the sandwich. Drs Reeve and Russell – thanks for the puppy therapy. Amy 'Pablo' Vincent and Ewen 'Mystio' Sommerville…what to say…ta for putting up with me, I don't know how you do it. I know I can be a little shady at times but reading is fun-da-mental! And to the Reeve lab posse (+1), Chenny FromDaBlock, DonnaBeth, NishNash and Bobosaurus Rex for providing constant entertainment, most of the time without even realising it. I should also congratulate Pav, Tianhong, Ash and Catherine for surviving the last few months with me slowly declining into madness.

Finally I would like to thank my family for their ongoing support since I moved up North seven years ago. Especially to my sister Anelise who never fails to put a smile on my face.

Table of contents

List of figures

List of Tables

List of equations

Publications

- Amy E. Vincent, Hannah S. Rosa, Charlotte L. Alston, John P. Grady, Karolina A. Rygiel, Mariana C. Rocha, Rita Barresi, Robert W. Taylor, Doug M. Turnbull (2016) 'Dysferlin mutations and mitochondrial dysfunction', *Neuromuscular Disorders*, 26(11), 782-788

- Amy E Vincent, Hannah S Rosa, Karolina A Rygiel, Anne Grünewald, Mariana C Rocha, Gavin Falkous, John P Grady, Kathryn White, Tracey Davey, Basil Petrof, Avan A Sayer, Cyrus Cooper, Robert W Taylor, Doug M Turnbull, Martin Picard (2016) 'Clonally Expanded mtDNA Deletions in Human Skeletal Muscle Originate as a Proliferative Perinuclear Niche' *Cell metabolism* (submitted -under review)

- Elizabeth A Stoll, Nevena Karapavlovic, Hannah Rosa, Michael Woodmass, Karolina Rygiel, Kathryn White, Douglass M Turnbull, Chris G Faulkes (2016) 'Naked mole-rats maintain healthy skeletal muscle and Complex IV mitochondrial enzyme function into old age' *Aging* (Epub ahead of publication)

Abbreviations

ADP	Adenosine diphosphate
AH	Alper's Huttenlocher syndrome
ATP	Adenosine Triphosphate
β2M	Beta-2-microglobulin
Ca^{2+}	Calcium ion
COX	Cytochrome c Oxidase
CPEO	Chronic Progressive External Opthalmoplegia
Cq	Threshold cycle of quantification
dH_2O	Distilled water
D-Loop	Displacement loop
DNA	Deoxyribonucleic Acid
dNTP	Deoxynucleotide
DRP	Dynamin-related proteins
EDTA	Ethylenediaminetetraacetic acid
ETC	Electron transport chain
FADH	Flavin adenine dinucleotide
Fe-S	Iron-sulphur
GAPDH	Glyceraldehyde 3-phosphate dehydrogenase
GTP	Guanosine triphosphate
H^+	Proton
H_2O	Water
HCl	Hydrochloric acid
H strand	Heavy strand
HSP	Heavy strand promotor
IMF	Intermyofibrillar
IMM	Inner mitochondrial membrane
IMS	Intermembrane space
Kb	Kilobase

KSS	Kearn-Sayre Syndrome
LB	Lysogeny broth
L strand	Light strand
Leu	Leucine
LHON	Leber's hereditary optic neuropathy
LS	Leigh Syndrome
LSP	Light strand promotor
Lys	Lysine
M	Molar
MELAS	Mitochondrial Enchephalomyopathy, Lactic Acidosis and Stroke-like episodes
MERRF	Myoclonic Epilepsy with Ragged Ref Fibres
MIDD	Maternally inherited diabetes and deafness
$MgCl_2$	Magnesium Chloride
ml	millilitre
mM	millimolar
mRNA	messenger Ribonucleic Acid
mtDNA	Mitochondrial DNA
mtSSB	Mitochondrial Single Strand Binding protein
mt-tRNA	mitochondrial transfer Ribonucleic Acid
Na^+	Sodium ion
NADH	Nicotinamide adenine dinucleotide
NARP	Neuropathy, ataxia, and retinitis pigmentosa
nDNA	nuclear DNA
NGS	Normal goat serum
nm	nanometer
nM	nanomolar
NMDAS	Newcastle Mitochondrial Disease Adult Scale
O_D	Optical density
O_H	Origin of heavy strand replication
O_L	Origin of light strand replication

OMM	Outer mitochondrial membrane
OPA1	Optic Atrophy 1
OXPHOS	Oxidative phosphorylation
PBS	Phosphate buffered saline
PCR	Polymerase Chain Reaction
PEO	Progressive External Opthalmoplegia
Pi	Inorganic Phosphate
POLG	Polymerase Gamma
POLMRT	Mitochondrial RNA polymerase
PS	Pearson Syndrome
Rcf	Relative Centrifugal Force
rCRS	Revised Cambridge reference sequence
RITOLS	Ribonucleotide incorporation throughout the lagging strand
ROS	Reactive Oxygen Species
RNA	Ribonucleic Acid
RRF	Ragged Red Fibre
SDH	Succinate Dehydrogenase
SKM	Skeletal Muscle
SS	Subsarcolemmal
TAE	Tris-Acetate EDTA
TCA	Tricarboxylic Acid
TFAM	Transcription Factor A, Mitochondrial
tRNA	transfer ribonucleic acid
T_m	Melting temperature
TWINKLE	Twinkle helicase
UNG	Uracil-N glycoslyase
VDAC	Voltage Dependant Anion Channel
µm	micromolar
µl	microliter

Chapter 1: Introduction

1.1 Mitochondrial origins

The original theory on mitochondrial origins, known as the endosymbiotic theory, was proposed by Margulis in 1971. The theory describes a symbiotic relationship formed between a free eubacterium that had been integrated into a primitive eukaryotic host by endosymbiosis. This relationship provided the eubacterium with access to metabolic substrates and physical protection, in exchange for a constant supply of respiration-derived ATP (adenosine triphosphate). This theory proposes the fusion event occurred subsequent to the formation of the cell nucleus in the host. An alternative theory, termed the 'hydrogen hypothesis', instead postulated that a hydrogen-producing eubacterium was engulfed by a hydrogen-dependent archaebacterium leading to the concurrent formation of the mitochondrion and nucleus (Martin and Müller, 1998). Both theories agree that, over a large period of reductive evolution, the organelle became essential to the survival of the bacterial endosymbiont and most genes were transferred to the nucleus of the host.

Whole genome sequencing of the α-proteobacterium *Rickettsia prowazekii* (Andersson *et al.,* 1998) revealed genes encoding components of the tricarboxylic acid (TCA) cycle and respiratory chain complexes phylogenetically similar to those found in mitochondria (Andersson and Kurland, 1999; Dyall and Johnson, 2000). Further analysis of the cytochrome *b* and cytochrome *c* oxidase I genes confirmed α-proteobacteria, specifically within the Rickettsiaceae family, were the evolutionary ancestors of the mitochondrion (Sicheritz-Ponten *et al.*, 1998).

1.2 Mitochondrial structure

Mitochondria are commonly depicted as single rod-shaped organelles encapsulated by a double membrane (Figure 1.1) and measuring approximately 2µm in length and 0.5µm in diameter (Palade, 1953). Early visualisation of mitochondrial structure by light microscopy

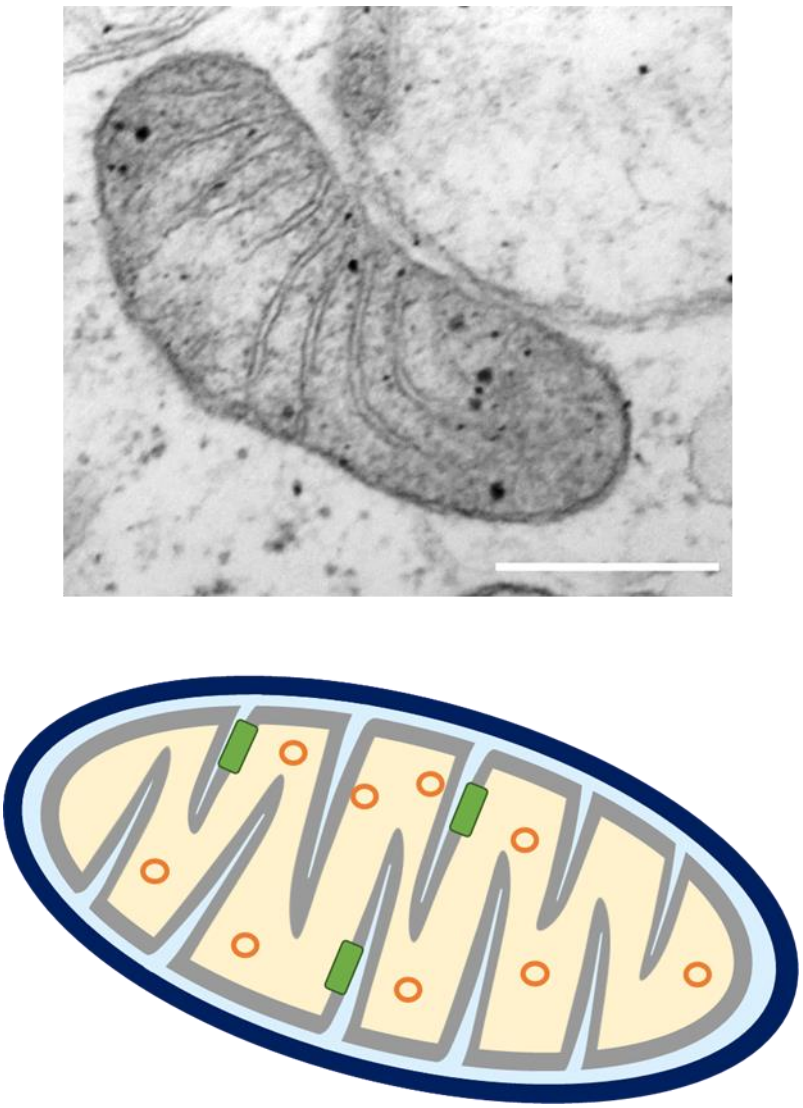

Figure 1.1: Mitochondrial structure: Electron micrograph of a mitochondrion (top, image provided by Dr Amy Reeve) with a schematic (bottom) showing the outer mitochondrial membrane (dark blue), intermembrane space (light blue), inner mitochondrial membrane (grey), mitochondrial matrix (light orange), mitochondrial DNA molecules (orange circles) and oxidative phosphorylation system (green boxes).

determined an outer and inner membrane, with the latter forming several invaginations termed ‘cristae mitochondriales’ (Palade, 1952). The use of electron microscopy resolved these details further to reveal a smooth outer membrane and folded inner membrane (Palade, 1953).

The outer mitochondrial membrane (OMM) acts as a physical barrier between the cytoplasm and contents of the mitochondria, regulating the movement of molecules between the compartments. Small ions of <10kDa can diffuse freely from the cytosol across the OMM via a voltage-dependent anion channel (VDAC), known as porin, into the intermembrane space. Import of larger proteins requires the translocase of the outer membrane (TOM) and translocase of the inner membrane (TIM) (Truscott *et al.,* 2003; Ahmed and Fisher, 2009).

The inner mitochondrial membrane (IMM) acts as a scaffold upon which respiratory chain complexes can be assembled and subsequently used for the generation of the electrochemical gradient required for oxidative phosphorylation (Munn, 1974). The IMM is essentially impermeable to polar molecules and ions so transport into the mitochondrial matrix is regulated by several transporter proteins (Wagner *et al.,* 2009). Using electron tomography, Mannella *et al*. (1997) observed that the IMM is composed of two distinct regions connected via cristae junctions; the inner boundary membrane (IBM) and the cristae membrane (CM) (Frey and Mannella, 2000). Immunoelectron microscopy performed on wild-type yeast cells revealed an uneven protein distribution between the IBM and the CM. The IBM, contains numerous proteins involved in mitochondrial fusion and the transport of nuclear-encoded proteins. The CM is rich in proteins involved in oxidative phosphorylation, protein synthesis, iron/sulphur cluster biogenesis and the transport of mtDNA-encoded proteins (Vogel *et al.,* 2006). More recently, respiratory chain complexes have been shown to distribute differently between the IBM, which contains a large proportion of complex II, and the CM, where complexes I, III and IV and ATP synthase are located (Cogliati *et al.,* 2016; Wilkins *et al.,* 2013).

The invagination of the IBM at regular intervals forms cristae junctions. These tubular structures are regulated by mitochondrial cristae organising system (MICOS) proteins. As the cristae reach further into the mitochondrial matrix, respiratory chain complexes are seen on the IBM and CM, with ATP synthase dimerising at the apex of the cristae (Paumard *et al.,* 2002; Strauss *et al*., 2008). It has also been suggested that the presence of ATP synthase localises respiratory chain complexes to the CM (Vogel *et al.,* 2006). Furthermore, the sub-

compartments of the IMM are proposed to be dynamic with the protein distribution dependent on the physiological state of the cell (Vogel *et al.,* 2006; Zick *et al.,* 2009).

The innermost compartment of the mitochondrion holds the mitochondrial matrix. This houses multiple copies of mtDNA, which have been shown to associate with the IMM (He *et al.,* 2007), as well as the machinery required for protein translation and transcription and various enzymes of the TCA cycle.

1.3 Mitochondrial dynamics

While mitochondria are often portrayed as singular, isolated organelles, they usually exist in a dynamic network allowing for exchange of nutrients and mtDNA (Bereiter-Hahn and Voth, 1994; Chen and Chan, 2004). This arrangement is key to normal mitochondrial function, as evidenced by pathogenic mutations in the nuclear-encoded proteins regulating the fission and fusion processes.

1.3.1 Fusion

Fusion of the OMM and IMM are co-ordinated, however in instances where IMM fusion is impaired, OMM fusion can still occur normally (Westermann, 2010). Vital to the process of mitochondrial fusion are mitofusin proteins (Mfn1 and Mfn2), a subgroup of dynamin-related proteins (DRPs), with GTPase activity, which are highly conserved across yeast, worms, flies and mammals (Escobar-Henriques and Anton, 2012). Mfn1 and Mfn2 each contain two hydrophobic coiled-coil heptad repeats (HR1 and HR2) located on the OMM. The HR2 repeat is required for docking, acting as a tether between adjacent mitochondria before fusion (Koshiba *et al.,* 2004). The GTPase activity of the protein provides sufficient energy for the fusion of the OMM (Westermann, 2010).

Fusion of the IMM in mammals is mediated by another DRP called OPA1 (optic atrophy 1) (Cipolat *et al.,* 2004) which is present at the IMM in long and short isoforms (Delettre *et al.,* 2001). The long, membrane anchored isoforms protrude into the inter-membrane space and promote the tethering of the two IMM of the fusing mitochondria following OMM fusion.

Short isoforms, produced by processing of the larger isoforms, are soluble and facilitate the fusion of the two IMM (Escobar-Henriques and Anton 2013). Both long and short isoforms are required for fusion (DeVay *et al*., 2009; Herlan *et al*., 2003; Song *et al*., 2007). In the event of low membrane potential, fusion has been shown to be prevented by cleavage of Opa1 (Head *et al.,* 2009).

1.3.2 Fission

Early genetic screens of yeast first determined the involvement of Drp1 and Fis1 in mitochondrial fission (Bleazard *et al.,* 1999; Mozdy *et al.,* 2000). Drp1, the mammalian homologue of Dnm1, is a dynamin-related protein located in the cytoplasm, although a proportion of it is recruited to the OMM by Fis1 in order to carry out fission. Mutations in Drp1 have been shown to induce highly connected networks of mitochondria (Smirnova *et al.,* 2001). Fis1 is a small protein, localised to the OMM by a single transmembrane domain (James *et al.,* 2003). While Fis1 is required for the recruitment of Dnm1 in yeast (Mozdy *et al.,* 2000), knockdown of Fis1 does not affect Drp1 recruitment in mammals (Lee *et al.,* 2004). Depletion of Fis1 has been shown to result in tubular networks of mitochondria (Westermann 2010).

The process of fusion firstly requires recruitment of Drp1 to the OMM by Fis1. Here, multiple units of Drp1 form a self-assembled helical oligomer (Legesse-Miller *et al.,* 2003; Mears *et al.,* 2011). This structure wraps around the mitochondrial membrane and constricts at specific fission sites in a process driven by GTP hydrolysis (Westermann 2010). Fission is completed by the severance of the inner and outer mitochondrial membrane (Youle and van der Bliek 2012).

1.4 Oxidative phosphorylation and ATP synthesis

Mitochondria are commonly described as the ‘powerhouses of the cell’ due to their major role in the production of ATP. Approximately 80% of the cellular energetic demand is met by ATP synthesis via oxidative phosphorylation. This process begins outside of the

mitochondria, in the cytosol where glucose is broken down into pyruvate via glycolysis (Berg, 2002a) (Equation 1.1).

$$Glucose + 2NAD^+ + 2ADP + 2P_i \rightarrow 2Pyruvate + 2NADH + 2H^+ + 2ATP + 2H_2O$$

Equation 1.1: Glycolysis

Pyruvate is then transported across the double mitochondrial membrane into the matrix, where it is converted into acetyl CoA by the enzyme pyruvate dehydrogenase (Equation 1.2).

$$Pyruvate + CoA + NAD^+ \rightarrow Acetyl\ CoA + NADH + H^+ + CO_2$$

Equation 1.2: Pyruvate decarboxylation

Acetyl CoA is a key substrate in the tricarboxylic acid (TCA) cycle (Krebs and Johnson 1937), the overall equation for which is shown below (Equation 1.3), and can also be sourced by the oxidation of fatty acids in the mitochondria. Along with the other major substrates NAD^+ and FADH, acetyl CoA is fed into the TCA cycle by transferring its acetyl group to oxaloacetate, producing citrate. This reaction is catalysed by citrate synthase and releases CoA as a by-product, which feeds back to react with another pyruvate molecule to begin the cycle again. Through a further seven enzymatic reactions, oxaloacetate is regenerated to continue the cycle (Berg, 2002b).

$$Acetyl\ CoA + 3NAD^+ + FAD + ADP + P_i + 2H_2O \rightarrow CoA + 3NADH + 2H^+ + FADH_2 + ATP + CO_2$$

Equation 1.3: Outcome of the TCA cycle

Four transmembrane multimeric complexes (I-IV) and two mobile electron carriers (coenzyme Q and cytochrome *b*) located at the IMM make up the electron transport chain

(ETC) which, together with ATP synthase (complex V), comprise the OXPHOS system (Figure 1.2). Reducing agents NADH and $FADH_2$, produced by the TCA cycle, are essential components of the oxidative phosphorylation (OXPHOS) process (Hatefi, 1985; Saraste, 1999). These act as electron carriers, donating electrons to complex I (in the case of NADH) and complex II (in the case of $FADH_2$) of the ETC. Energy released from this transfer of electrons at complexes I, III and IV drives the movement of hydrogen ions (H^+) from the matrix to the inter-membrane space (Smeitink *et al.*, 2001). This generates an electrochemical gradient which is used by ATP synthase to generate ATP from ADP and inorganic phosphate (P_i), as described by the chemiosmotic theory proposed by Mitchell (1961).

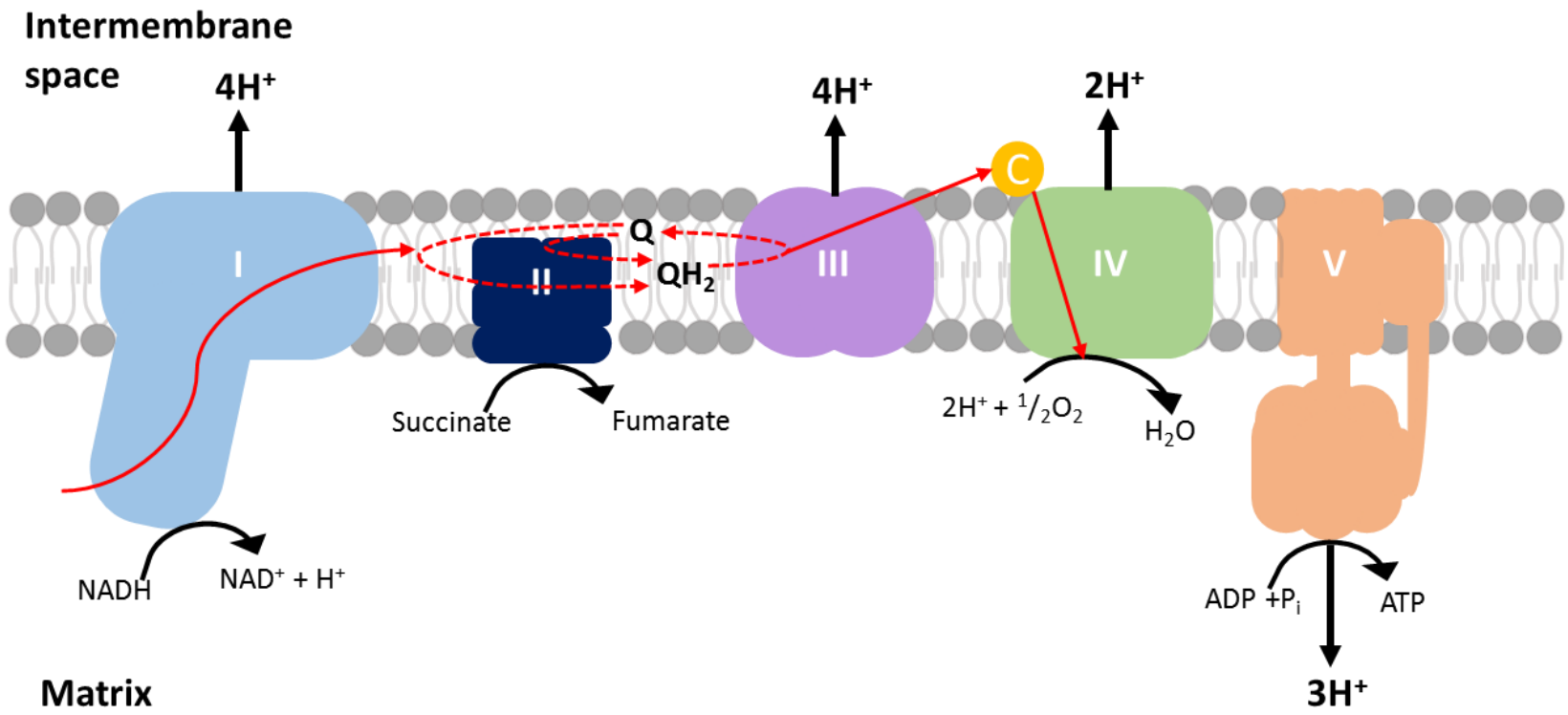

Figure 1.2: Oxidative phosphorylation. Complexes I-V are shown in the inner mitochondrial membrane. The transfer of electrons from complex I to IV, shown by the solid red lines, is coupled with the pumping of protons from the matrix to the intermembrane space to create an electrochemical gradient for ATPase (complex V) to convert ADP and P*i* (inorganic phosphate) to ATP. The roles of the individual complexes are described later in the chapter.

1.4.1 Complex I - NADH: Ubiquinone oxidoreductase

Complex I, also known as NADH dehydrogenase, is the largest of the OXPHOS complexes with a molecular mass of 980kDa (Hirst *et al.,* 2003) and 45 subunits identified (Carroll *et al.,* 2006; Zhu *et al.,* 2016). Seven of these subunits are encoded by mtDNA: *MT-ND1-6* and *MT-ND4L* (Walker *et al.,* 1992) and make up a group of 14 conserved 'core' subunits with seven nuclear-encoded subunits. An additional 31 nuclear-encoded 'supernumerary' subunits complete the complex (Zhu *et al.,* 2016). The complex has a characteristic L-shape (Hofhaus *et al.,* 1991), where one arm is embedded in the lipid bilayer of the IMM, and the other protrudes into the matrix (Grigorieff 1999; Hofhaus, 1991). The mtDNA-encoded subunits are highly hydrophobic and are therefore located within the membrane arm (Zickermann *et al.,* 2009)

There are three functional modules within complex I (Brandt 2006). The N-module is situated in the peripheral arm of the complex, protruding into the matrix. In this module, NADH is oxidised by the primary electron acceptor, a flavin mononucleotide (FMN) (Walker *et al.,* 1992). The electron is subsequently transferred through a series of seven iron-sulphur clusters in the Q-module, also located within the peripheral arm of complex I (Sazanov 2007). This module contains the ubiquinone reduction site. The transfer of two electrons from NADH to ubiquinone is coupled with the translocation of four protons across the IMM to the inter-membrane space. This is facilitated by the proton-pumping action of the P-module, located in the membrane-bound portion of the complex (Efremov *et al.,* 2010; Sazanov, 2015) (Figure 1.3). The overall reaction is shown in ***Equation 1.4: Complex I reaction*** *(Berg* et al., *2012c)*Equation 1.4.

$$NADH + Q + 5H^{+}_{matrix} \rightarrow NAD^{+} + QH_2 + 4H^{+}_{ims}$$

Equation 1.4: Complex I reaction (Berg *et al.,* 2012c)

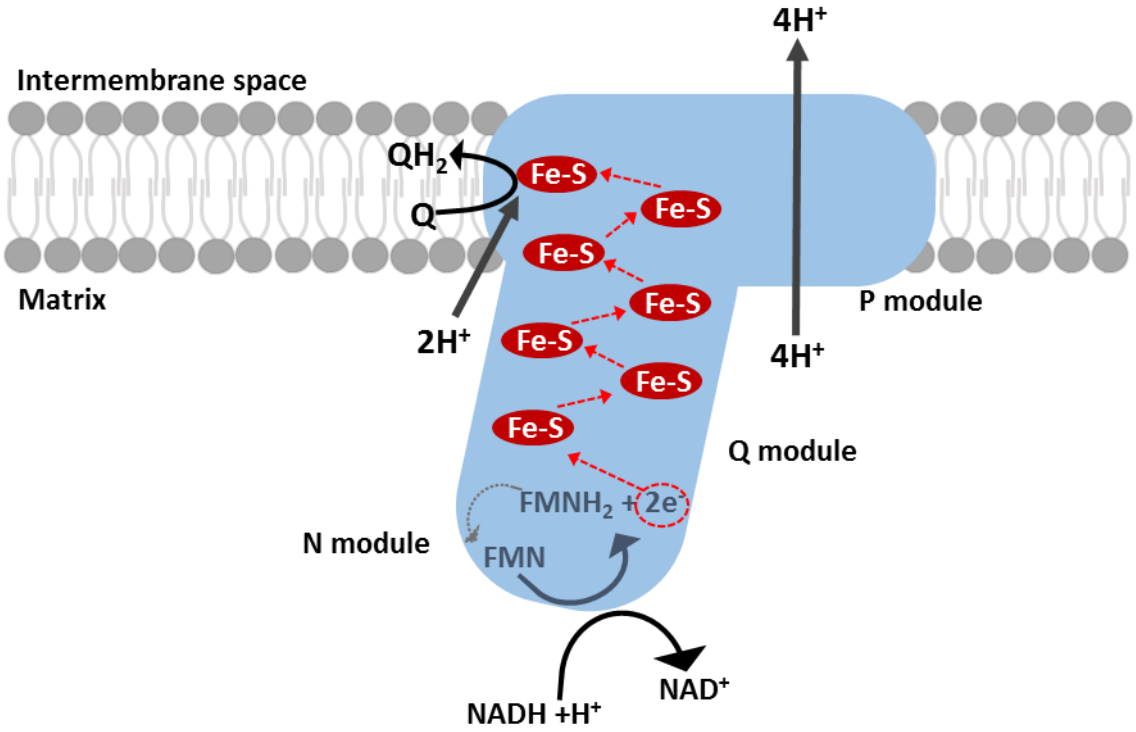

Figure 1.3: Schematic of complex I. The path of electrons is shown by the red dotted lines. Electrons are donated by NADH and are transferred through several iron-sulphur clusters (Fe-S) to ubiquinone (Q), reducing it to ubiquinol (QH_2). This is coupled with the pumping of four protons (H^+) to the intermembrane space.

Defects in complex I are the most frequently observed OXPHOS defects in humans. These can be caused by a number of mutations in the mitochondrial or nuclear genes encoding structural subunits or assembly factors of complex I (Mimaki *et al.,* 2012).

1.4.2 Complex II - Succinate dehydrogenase

Complex II, also referred to as succinate-ubiquinone oxidoreductase, is the only complex of the OXPHOS system whose subunits are entirely nuclear-encoded. It is also the smallest complex, comprised of only four subunits SDHA-D. SDHA and SDHB form a catalytic dimer protruding into the matrix, with a series of iron-sulphur clusters between FAD, in SDHA, and the ubiquitin binding site at the IMM. SDHC and SDHD are hydrophobic subunits, therefore

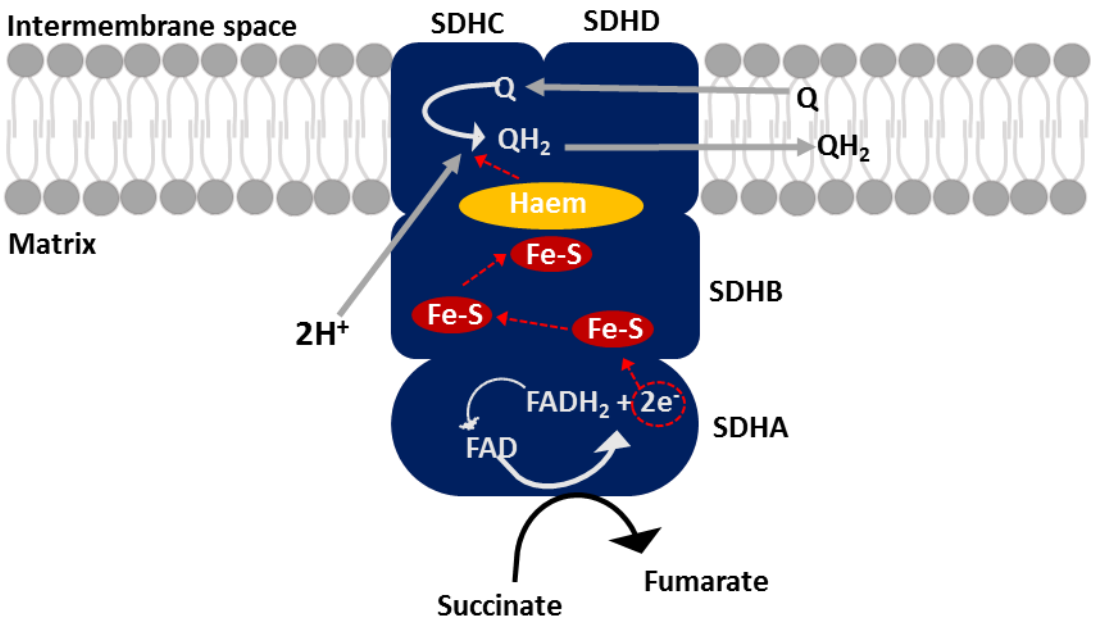

Figure 1.4: Schematic of complex II. The path of electrons is shown by the red dotted line through iron-sulphur clusters (Fe-S) and haem to reduce ubiquinone (Q) to ubiquinol (QH_2).

anchoring complex II to the IMM. Unlike the other complexes of the OXPHOS system, complex II is not involved in the translocation of protons across the IMM. Instead, it catalyses the conversion of succinate to fumarate, thereby producing $FADH_2$, which donates electrons for the reduction of ubiquinone to ubiquinol (Hagerhall 1997) (Figure 1.4). The equation for this reaction is shown below (Equation 1.5).

$$succinate + Q \rightarrow fumarate + QH_2$$

Equation 1.5: Complex II reaction (Berg *et al.,* 2012c)

Mutations in complex II genes are usually associated with a tumorigenic phenotype, thought to be caused by an increase in ROS production or stabilisation of hypoxia inducible factor I (HIF1) (Hoekstra and Bayley, 2013). Isolated complex II deficiency accounts for only approximately 2% of mitochondrial disease (Alston *et al.,* 2012).

1.4.3 Ubiquinone (coenzyme Q)

Ubiquinone is a small, hydrophobic electron carrier that moves freely in the IMM. It is reduced by a single electron to form ubisemiquinone, while complete reduction by a second electron produces ubiquinol (Lodish *et al.,* 2000a).

1.4.4 Complex III - Cytochrome bc1

Complex III consists of 11 subunits, of which only one – cytochrome *b* – is encoded by mtDNA (*MT-CYB*) (Sen and Beattie, 1986). This complex houses a number of essential redox components including two b-type haems (b_L and b_H), one c-type haem (c_1) an iron-sulphur cluster (the Rieske centre) and ubiquinone. These are involved in the transfer of two electrons from ubiquinol to cytochrome *c*, coupled with the translocation of two protons into the inter-membrane space, via the protonmotive Q cycle (Mitchell, 1975). Briefly, one electron is transferred to the Rieske centre, subsequently passing to cytochrome c_1 and cytochrome *c*. A second electron is transferred to haem b_L then to haem b_H before reducing ubiquinone to an ubisemiquinone anion. This process repeats itself so that haem b_H this time reduces the ubisemiquinone intermediate created in the previous cycle, forming ubiquinol (Trumpower, 1990) (Figure 1.5). This reaction is shown in Equation 1.6.

$$2QH_2 + Q + 2Cytc_{oxidised} + 2H^+_{matrix} \rightarrow 2Q + QH_2 + 2Cytc_{reduced} + 4H^+_{ims}$$

Equation 1.6: Complex III reaction (Berg *et al.,* 2012c)

Disease caused by mutations in complex III genes are rare in humans (Fernández-Vizarra and Zeviani, 2015). Phenotypes associated with complex III abnormalities are similar to other OXPHOS defects. One such condition, Leber's hereditary optic neuropathy (LHON) has been associated with mutations affecting complex III (Brown *et al.,* 1992).

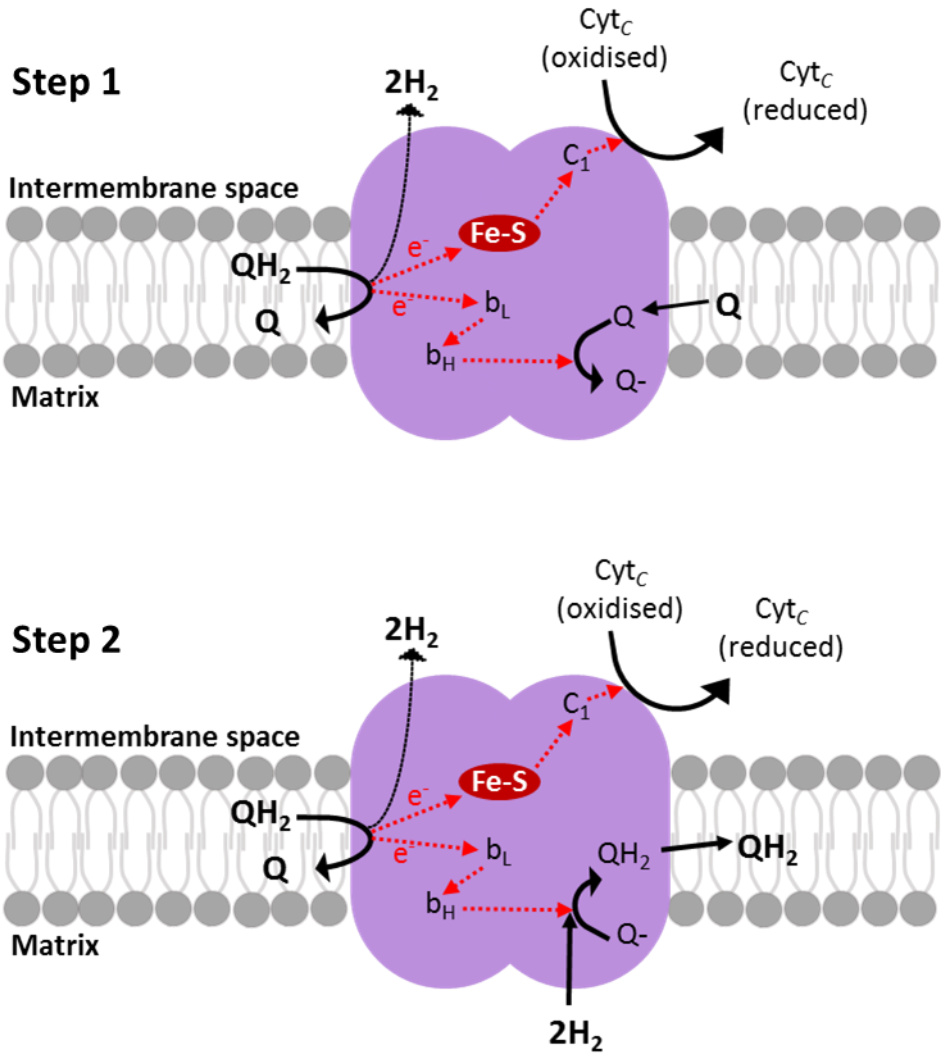

Figure 1.5: Schematic of complex III. The path of electrons is shown by the dotted red line. In step one, one electron from ubiquinol (QH_2) is transferred to cytochrome *c* (Cyt_c), while another partially reduces ubiquinone (Q) to ubisemiquinone (Q-). Step two also transfers one electron to Cyt_c, with another electron reducing the ubisemiquinone to ubiquinol (QH_2).

1.4.5 Cytochrome c

Cytochrome *c* is a nuclear encoded haem-containing protein with a molecular weight of 13kDa. It is localised to the IMM and acts as a mobile electron carrier between complex III and complex IV. Cytochrome *c* has an additional role in apoptosis, described in section 1.5.4 (Huttemann *et al.*, 2011).

1.4.6 Complex IV – Cytochrome c oxidase (COX)

Complex IV (200kDa) is the terminal electron acceptor, reducing molecular oxygen to produce water. This complex comprises of 13 subunits, of which three (S1-S3) are encoded by mtDNA (*MT-COI, MT-COII* and *MT-COIII,* respectively) (Tsukihara *et al.,* 1996). The active site, consisting of $haem_{a3}$ and Cu_B, is located in S1 in the transmembrane region. S2 and S3 are associated with S1 at the transmembrane region, however no direct contact is made. In total, four electrons are required for the reduction of one molecule of oxygen, thought to be a rate-limiting step in the mammalian ETC (Huttemann *et al.,* 2011). Therefore, complex IV cycles through four phases, each of which transfers an electron to the catalytic site via Cu_A and $haem_a$ (Faxen *et al*., 2005). The first two electrons lead to the reduction of $haem_{a3}$ and Cu_B, which allow O_2 to bind, leading to the formation of a peroxide bridge. The next two electrons follow the same path, except the binding of two protons this time cleaves the peroxide bridge. A further two protons are required to complete the reduction of O_2 to $2H_2O$ (Faxen *et al*., 2005) (Figure 1.6). This process is coupled with translocation of four protons to the inter-membrane space (Equation 1.7) (Diaz 2010).

$$4Cytc_{reduced} + 8H^{+}_{matrix} + O_2 \rightarrow 4Cytc_{oxidised} + 2H_2O + 4H^{+}_{ims}$$

Equation 1.7: Complex IV reaction (Berg *et al.,* 2012c)

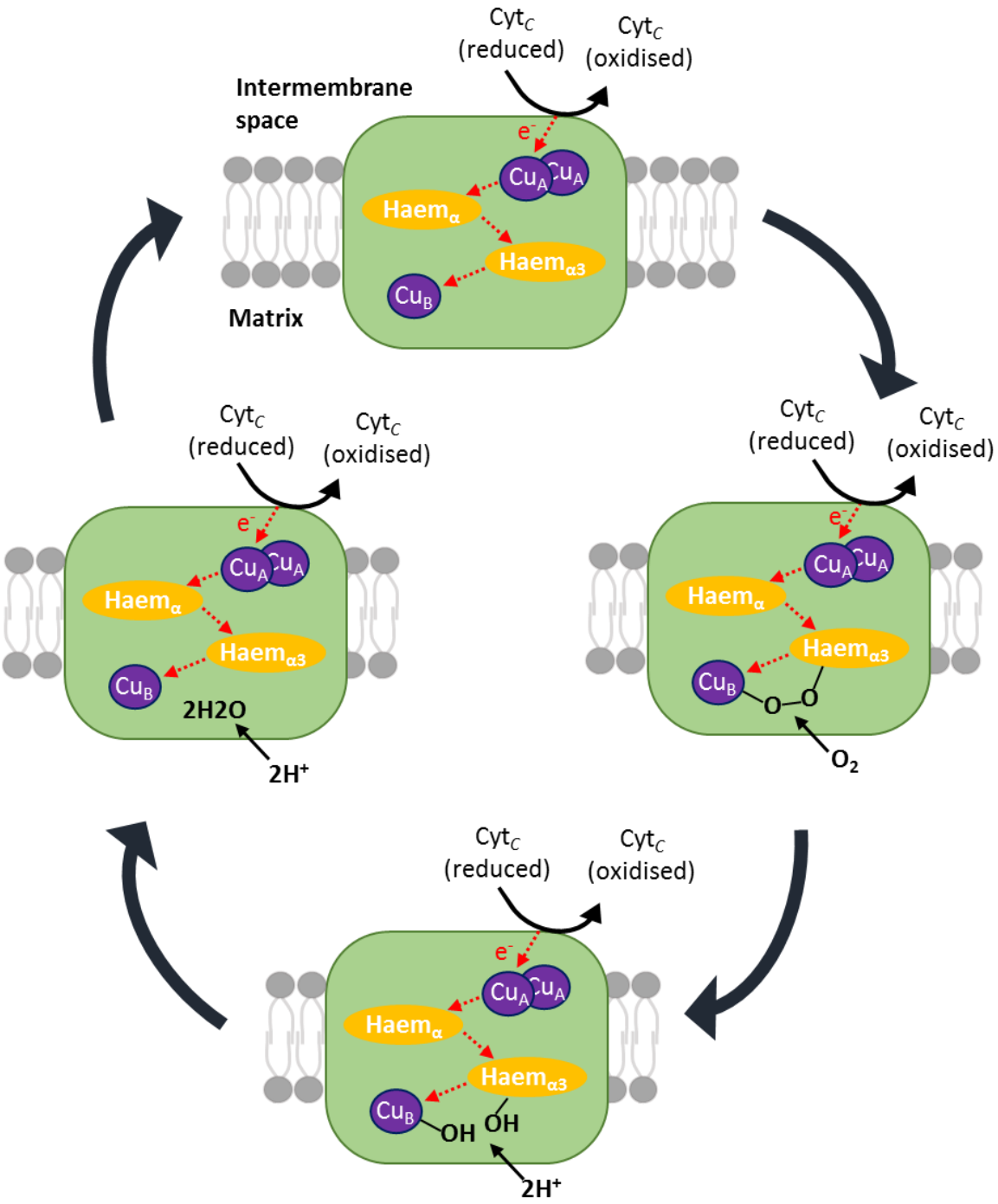

Figure 1.6: Schematic of complex IV. The path of electrons (e^-) donated by cytochrome *c* (Cyt_c) is shown by the dotted red line. Complex IV cycles through four states each transferring an electron to the active site of $heam_{a3}$ and Cu_B.

1.4.7 Complex V – ATP synthase

In the final step of the OXPHOS process, ATP synthase catalyses the conversion of ADP and inorganic phosphate (P_i) to ATP. Complex IV is a relatively large subunit, approximately 500kDa. There are 16 subunits, of which two are encoded by mtDNA (*MT-ATP6* and *MT-ATP8*). Structurally, this complex is split into two domains; the F_0 and F_1. These domains act as rotating motors, which work bi-directionally to hydrolyse ATP as well as producing it (Elston *et al.,* 1998). The F_0 domain, located in the IMM, is formed from an ab complex and ring of c-subunits forming a proton channel. The F_1 domain is found on the matrix side of the IMM and contains the binding site for ADP and P_i. This domain comprises five subunits; α, β, γ, δ and ε. A cylinder of alternating α and β subunits (three of each) is formed around a central coiled γ subunit and a stalk of γ and ε interacts with the F_0 domain (Elston *et al.,* 1998) (Figure 1.7).

In the presence of a sufficient electrochemical gradient, protons flow through the channel in the F_0 domain causing rotation of the rotary ring through the pronation and depronation of glutamate residues of the ring of c-subunits (Zhou *et al.,* 1997; Elston *et al.,* 1998). This leads to the rotation of the γ and ε stalk of F_1, causing the rotation of the F_1 αβ cylinder. Upon rotation, the β subunits of the cylinder change conformation to one of three states (open, loose or tight) (Abrahams *et al.,* 1994; Noji *et al.,* 1997). In the open conformation, ADP and Pi bind to the catalytic site. With further rotation, the conformation changes to become tight, and sufficient energy is produced to phosphorylate ADP and produce ATP. A final rotation results in the loose conformation where the catalytic site is empty (Figure 1.7). Each 360° rotation produces 3ATP molecules coupled with the translocation of eight protons (Watt *et al.,* 2010). Therefore, the production of each ATP molecule by this complex has a biogenic cost of 2.7 protons (Ferguson 2010).

Mutations in complex V genes lead to severe phenotypes, characterised by brain lesions, particularly affecting the striatum. Mitochondrial disorders caused by complex V mutations include neuropathy, ataxia and retinitis pigmentosa (NARP) and Leigh Syndrome (Schon *et al.,* 2001).

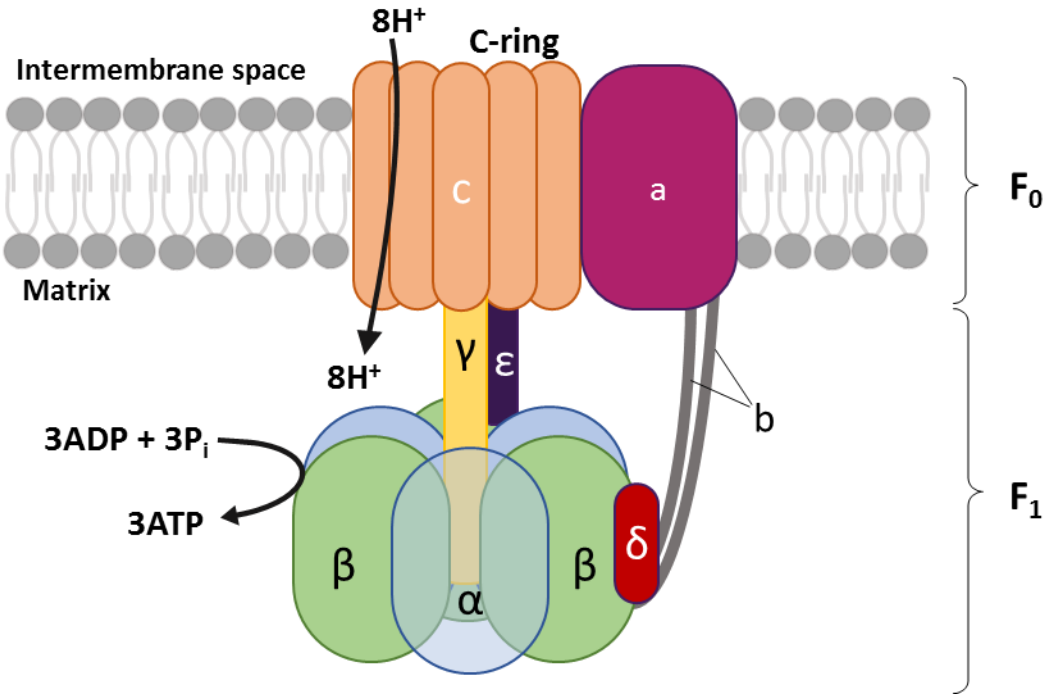

Figure 1.7: Schematic of complex V. Protons flow through the c-ring along the electrochemical gradient causing rotation of the αβ cylinder and the conversion of ADP and P_i to ATP.

1.4.8 Supercomplexes

Initially, supercomplexes composed of complexes III and IV were isolated from bacteria (Berry and Trumpower, 1985; Sone *et al.,* 1987; Iwasaki *et al.,* 1995). Evidence for supercomplexes in mammalian mitochondria was first presented in bovine heart mitochondria (Schägger and Pfeiffer, 2000). Almost all complex I was found to be associated with complex III, and a supercomplex consisting of complexes I+III+IV (termed the 'respirasome') was identified. Further evidence for supercomplexes was presented in electron microscopy images showing interactions between complexes in isolated supercomplexes (Schäfer *et al.,* 2006). Additional studies using bovine heart mitochondria suggest most supercomplexes exist as either I_1III_2 or $I_1III_2IV_1$, with the first acting as a building block for the respirasome (Schäfer *et al.,* 2006). The formation of supercomplexes is suggested to occur by firstly assembling an intermediate of complex I, without the catalytic core, to act as a scaffold onto which complexes III and IV are added. Only when the NADH

dehydrogenase catalytic core of complex I is incorporated is the respirasome functional (Moreno-Lastres *et al.,* 2012).

A number of structural and functional advantages of the formation of supercomplexes have been suggested. Binding sites for electron carriers are aligned on successive complexes allowing for improved efficiency in electron transfer (Schãfer *et al.,* 2007). Additionally, supercomplexes prevent the destabilisation and degradation of the component complexes, and reduce the leakage of protons and electrons, which also improves the efficiency of the ETC (Lenaz and Genova, 2010). The interconnected nature of these ETC complexes could have implications regarding combined respiratory chain deficiency often seen in disease. For example, in mitochondrial disease, mutations affecting the structure or function of a particular complex often result in deficiency of additional complexes (Moreno-Lastres *et al.,* 2012; Enriquez, 2016).

1.5 Other mitochondrial functions

1.5.1 Iron-sulphur clusters

Mitochondria play a key role in cellular iron metabolism and are a major site for haem synthesis and the formation and maturation of iron-sulphur (Fe-S) clusters in eukaryotic cells (Lill *et al.,* 1999; Wang and Pantopoulos, 2011). This function is highly conserved across eukaryotes, with primitive mitochondria (mitosomes) shown to contain some of the proteins required for this process (Tovar *et al.,* 2003). Fe-S clusters are primarily involved in the transport of electrons, and are therefore essential to the OXPHOS process in mitochondria. A number of Fe-S clusters are located within complexes I, II and III of the ETC where they facilitate the transfer of electrons by redox reactions cycling Fe^{2+} and Fe^{3+} (Schultz and Chan, 2001).

The iron sulphur cluster (ISC) pathway, occurring inside mitochondria, feeds into the cytosolic and nuclear Fe-S cluster formation pathways, in addition to providing for mitochondrial proteins (Kispal *et al.,* 1999; Gerber *et al.,* 2004). The import of cellular iron into the mitochondria is facilitated by mitoferrin (Mfrn1 and Mfrn2), a member of the

mitochondrial solute carrier family located in the IMM (Shaw *et al.,* 2005; Paradkar *et al.,* 2009). Subsequent Fe-S cluster biogenesis is a multi-stage process requiring the highly conserved scaffold protein ISCU (Agar *et al.,* 2000). Alternative scaffold proteins, such as ISCA and NFU1 are required for maturation of particular subsets of Fe-S proteins (Krebs *et al.,* 2001; Tong *et al.,* 2003). ISCS, a cysteine desulphurase, forms a complex with ISCU and provides sulphur to the Fe-S cluster formation process (Tong and Rouault, 2000; Urbina *et al.,* 2001). The activity of ISCS in this complex is mediated by frataxin, a nuclear-encoded Fe-binding protein localised to the mitochondria (Yoon and Cowan, 2003). It has been suggested that frataxin could be the source of iron for this pathway (Bencze *et al.,* 2006), although the exact source is yet to be identified. The delivery of Fe-S clusters from ISCU to target proteins requires GLRX5 (glutaredoxin) and a number of chaperones (Mühlenhoff *et al.,* 2003; Mapolelo *et al.,* 2013; Barupala *et al.,* 2016).

1.5.2 ROS production

The mitochondrial OXPHOS system is a significant source of reactive oxygen species (ROS) (Jensen, 1966; Boveris *et al.,* 1972), although the endoplasmic reticulum and peroxisomes also contribute to cellular ROS levels (Brown and Borutaite, 2012). Complexes I and III are major producers of mitochondrial ROS (Turrens and Boveris, 1980; Sena and Chandel, 2012), although complex I is considered the predominant producer when ATP is not being produced and a high NADH:NAD^+ ratio is present in the matrix (Murphy 2009). The leaking of electrons from complexes I and III of the ETC causes partial reduction of oxygen to create superoxide anions, O_2^-. Complex III produces O_2^- radicals on both sides of the IMM, whereas complex I ROS are produced in the matrix only. These O_2^- radicals are precursors to the formation of hydrogen peroxide, H_2O_2 (Loschen *et al*., 1974), catalysed by copper/zinc superoxide dismutase in the inter-membrane space or manganese superoxide dismutase in the matrix. H_2O_2 then diffuses into the cytoplasm where it is converted to water by glutathione peroxidases (Turrens, 2003).

Historically, ROS were considered harmful to the cell, however they are now recognised as playing a key role in cell signalling pathways (Finkel, 1998; Rhee *et al.,* 2000). Regulation of basal levels of ROS can facilitate cell differentiation, metabolic adaptation, immune cell

activation and autophagy (Sena and Chandel, 2012). However, fluctuations in ROS levels impact cell signalling and excessive levels, unable to be buffered by the cells antioxidant systems, can result in damage to lipids, proteins and nucleotides. Ultimately, the damage caused by excessive levels of ROS leads to cell death by necrosis or apoptosis (Sena and Chandel, 2012).

1.5.3 Calcium signalling and homeostasis

Calcium ions (Ca^{2+}) are important signalling molecules with fundamental roles including the regulation of ATP production (Griffiths and Rutter, 2009), induction of apoptosis (Orrenius *et al.,* 2003) and regulation of intercellular communication (Hofer *et al.,* 2000). In muscle, Ca^{2+} signalling is involved in the mediation of contraction mechanisms, and so intercellular Ca^{2+} concentration must be tightly regulated for effective muscle function (Gehlert *et al.,* 2015).

Mitochondria play a crucial role in the homeostasis of cytosolic Ca^{2+} levels (Kirichok *et al.,* 2004). Ca^{2+} moves across the OMM by VDAC (Simamura *et al.,* 2008) and is imported across the IMM into the matrix by the mitochondrial calcium uniporter (MCU) (Kirichok *et al.,* 2004). Once in the matrix, Ca^{2+} acts as a signalling molecule causing an increase in respiratory chain function and ATP production (Denton *et al.,* 1980; McCormack *et al.,* 1990). An excessive accumulation of Ca^{2+} to toxic levels can trigger apoptosis by opening the mitochondrial permeability transition pore (PTP) leading to permeabilisation of the IMM, mitochondrial swelling and cytochrome *c* release (Mattson and Chan, 2003; Giorgi *et al.,* 2008). Therefore, mitochondrial Ca^{2+} efflux is mediated by the Na^{+}/Ca^{2+} exchanger (Palty *et al.,* 2010) in a 3:1 ratio, respectively (Boyman *et al.,* 2013).

1.5.4 Apoptosis

Apoptosis, or programmed cell death, is required for the removal of damaged or unwanted cells (Kerr *et al.,* 1972). Induction of apoptosis by the extrinsic pathway is mediated by the extracellular ligand activation of death receptors. Mitochondria play a pivotal role in apoptosis (Hockenberry *et al.,* 1990) via the intrinsic pathway, which is triggered by DNA damage, oxidative stress and calcium overload. As previously mentioned, build-up of

organellar Ca^{2+} causes permeabilisation of the IMM and release of cytochrome *c* into the cytosol. Here, cytochrome *c* binds to apoptotic protease activating factor 1 (Apaf1), facilitating the formation of the apoptosome. Subsequent activation of caspase-9 results in a downstream signalling cascade activating execution procaspases and eventually leading to cell death (Kroemer *et al.,* 1998; Wang and Youle, 2009). Regulation of the intrinsic pathway is via the Bcl-2 family of proteins which comprises pro-apoptotic Bax and Bak, and anti-apoptotic Bcl-2. Activation of pro-apoptotic Bax and Bak leads to aggregation of these proteins at the OMM and induces the release of cytochrome *c* into the cytosol (Wei *et al*., 2001).

1.6 Mitochondrial Turnover

1.6.1 Biogenesis

Mitochondrial biogenesis is tightly regulated to cater for cell-specific energy requirements. The chief regulator of this process, which occurs in the nucleus, is peroxisome proliferator-activated receptor gamma (PPARγ) co-activator 1a (PGC1α) (Puigserver *et al.,* 1998; Jornayvaz and Shulman, 2010). PGC1α is activated in response to low ATP levels or growth signals, via phosphorylation by AMP protein kinase (AMPK) or deacetylation by Sirtuins (SIRT1) (Zong *et al.,* 2002; Hardie *et al.,* 2012). Downstream targets of activated PGC1α include nuclear transcription factors, such as NRF1 and NRF2 (Wu *et al.,* 1999), leading to increased expression of TFAM (Virbasius and Scarpulla, 1994), which is subsequently imported into the mitochondria, increasing synthesis of mtDNA-encoded proteins (Kelly and Scarpulla, 2004).

1.6.2 Mitophagy

Damaged mitochondria can be selectively degraded by a process known as mitophagy (Kanki and Klionsky 2008). Fission has been shown to occur prior to mitophagy (Duvezin-Caubet *et al.,* 2006; Twig *et al.,* 2008), isolating the damaged mitochondria from the network. There are two key proteins involved in mitophagy, Pink1 and Parkin. Under normal conditions, the serine threonine kinase Pink1 is imported into the intermembrane space where it is cleaved by presenilin-associated rhomboid-like (PARL) protein (Meissner *et al.,* 2011). Following a

loss of membrane potential, however, Pink1 is no longer imported and cleaved, accumulating at the OMM and recruiting the E3 ubiquitin ligase Parkin (Narendra *et al.,* 2008). This leads to the ubiquitination of several OMM proteins, including VDAC and Mfn, signalling autotrophic factors (Okatsu *et al.,* 2012) and ultimately resulting in the formation of the autophagosome which facilitates mitochondrial degradation (Nguyen *et al.,* 2016).

1.7 Mitochondrial genome

Mitochondria have their own genome (Nass and Nass, 1963) in the form of a 16,569bp, double stranded molecule, located in the mitochondrial matrix. In total, the mitochondrial DNA (mtDNA) comprises 37 genes, encoding 22 transfer RNAs (mt-tRNAs), 13 hydrophobic proteins involved in the OXPHOS system and two ribosomal RNAs (mt-rRNAs) (Anderson *et al.,* 1981; Andrews *et al.,* 1999). Most of these genes are located on the outer, guanine-rich heavy strand, whereas the inner, cysteine-rich light strand holds only 8 tRNA genes and one protein-encoding gene (*MT-ND6*) (Figure 1.8).

The mtDNA is compact, with no introns present. One or two non-coding base-pairs separate genes, except in the case of *MT-ATP6* and *MT-ATP8*, where there is a region of overlap between these two genes. There is only one non-coding region, known as the D-loop. This region, extending approximately 1kb in human mtDNA, contains the major control elements for mtDNA transcription and is the site of origin for heavy strand replication (Arnberg *et al.,* 1971; Kasamatsu *et al.,* 1971; Shadel and Clayton, 1997).

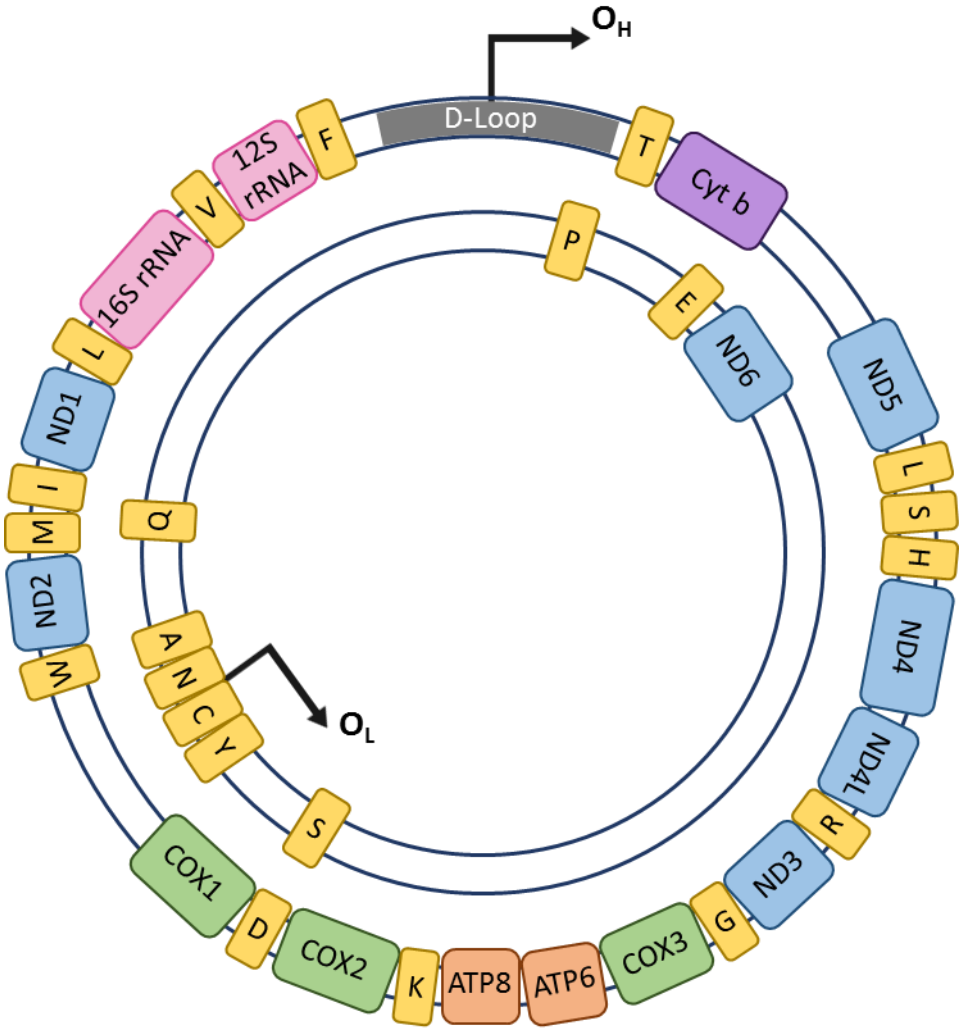

Figure 1.8: The human mitochondrial genome. The double-stranded genome encodes 37 genes in total encoding 13 polypeptides (complex I = blue, complex III = purple, complex IV = green, complex V = orange), 22 mt-tRNAs (yellow) and 2 mt-rRNAs (pink). Origins of heavy (O_H) and light (O_L) strand replication are shown. Image adapted courtesy of Dr John Grady.

With the exception of erythrocytes, mammalian cells contain multiple mitochondria, each of which carries approximately 2-10 copies of mtDNA (Bogenhagen and Clayton 1974). Therefore, the number of mtDNA copies per cell ranges up to an estimated 10,000 copies dependent upon the cellular energy requirements (Lightowlers *et al.,* 1997). Within the mitochondrial matrix, mtDNA molecules are packaged as small protein-DNA complexes, approximately 100nm, known as nucleoids (Satoh and Kuroiwa, 1991; Kukat *et al.,* 2011). Located in close association with the IMM (Albring *et al.,* 1997), each nucleoid contains a number of mtDNA molecules estimated between 1.4 (Kukat *et al.,* 2011) and 3 copies

(Brown *et al.,* 2011). Mitochondrial transcription factor A (TFAM) is abundant in nucleoids along with other proteins involved in the replication and transcription machinery such as the mitochondrial DNA helicase (TWINKLE), single-stranded DNA binding protein (mtSSB) and mitochondrial DNA polymerase (Polγ) (Spellbrink *et al.,* 2001; Garrido *et al.,* 2003; Chen and Butow, 2005).

1.7.1 Transcription

There are three sites of transcription initiation, one light-strand promotor (LSP) and two heavy-strand promotors (HSP1, HSP2), all generating polycistronic molecules. The LSP, located in the D-loop, produces a single transcript for all genes present on the light strand. Similarly, all heavy strand genes are transcribed from HSP2, located in the mitochondrial tRNA phenylalanine gene (*MT-TF*). However HSP1, found in the D-loop, transcribes only genes for the two rRNAS, 12S and 16S, and the intervening mt-tRNAs phenylalanine and valine (Montoya *et al.,* 1982; Chang and Clayton, 1984; Zollo *et al.,* 2012) (Figure 1.9).

Prior to the initiation of transcription, TFAM binds upstream of the promotor causing mtDNA to undergo a conformational change. This allows access for mitochondrial RNA polymerase (POLMRT) and mitochondrial transcription factors B1 and B2 (TFB1 and TFB2) to initiate transcription (Fisher *et al.,* 1987; Dairaghi *et al.,* 1995). Elongation is mediated by mitochondrial transcription elongation factor (TEFM), which associates with POLMRT, before mitochondrial transcription termination factor (mTERF) is incorporated to terminate the transcription process (Rebelo *et al.,* 2011). Polycistronic transcripts are then processed according to the proposed tRNA punctuation model, whereby the cloverleaf structure of tRNAs on nascent transcripts recruits processing enzymes mitochondrial ribonuclease P (RNaseP) and Z (RNaseZ), which cleave the tRNA at the 5’ and 3’ ends, respectively. Further modifications are made with the addition of a CCA triplet to the 3’ end of tRNAs and polyadenylation of mRNA 3’ end before translation can begin (Ojala *et al.,* 1981; Rorbach and Minczuk, 2012).

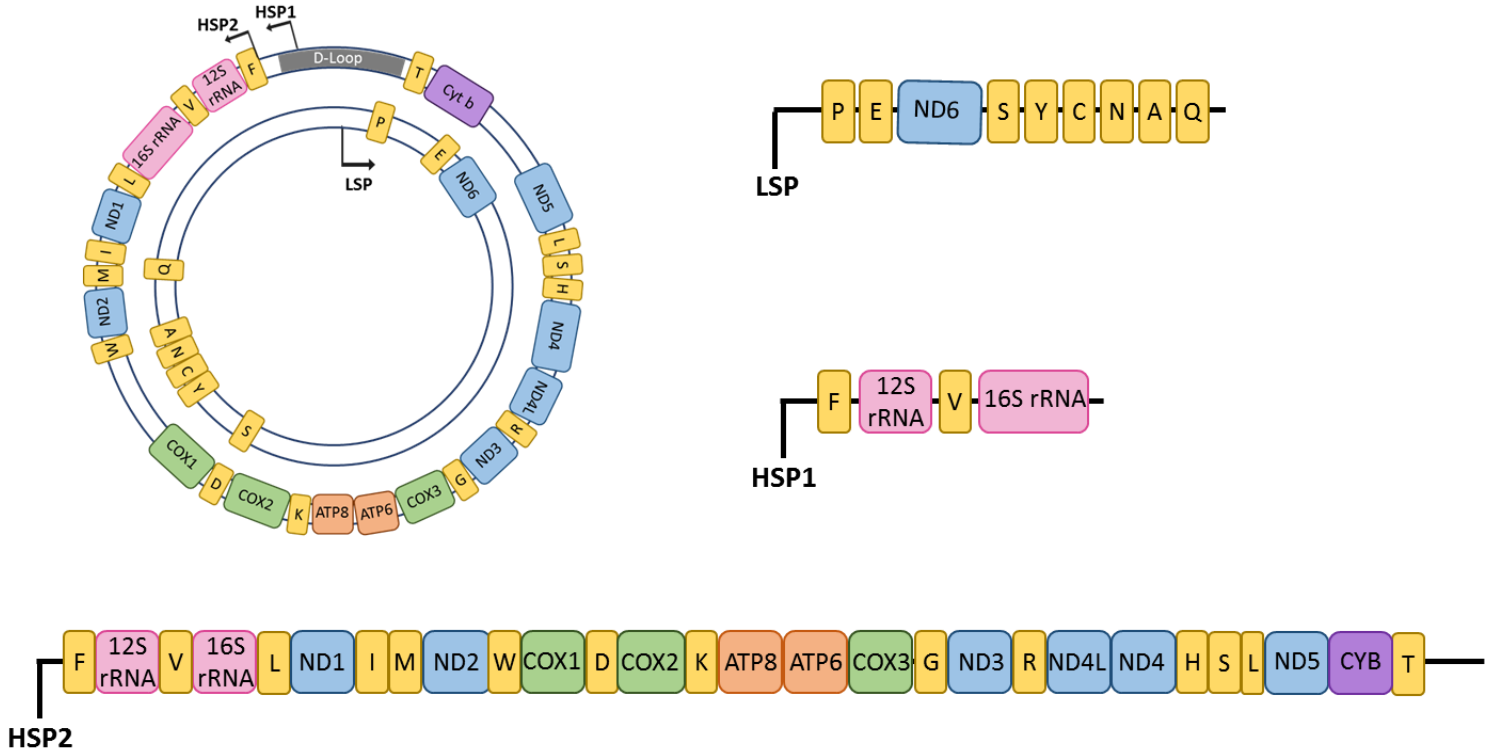

Figure 1.9: Mitochondrial DNA transcription. Polycistrons produced from LSP, HSP1 (both in the D-loop) and HSP2 (in *MT-TF*). LSP and HSP2 produce transcripts of the entire light and heavy strands respectively, whereas HSP1 transcribes only four genes on the heavy strand.

1.7.2 Translation

There are three phases of mitochondrial translation: initiation, elongation and termination (Smits *et al.,* 2010). This process occurs in the mitochondrial matrix within the mitoribosomes, more protein-rich than their cytosolic and bacterial counterparts. Mitoribosomes consist of approximately 80 nuclear-encoded proteins (O'Brien *et al.,* 2003) and two mitochondrial rRNAs split between a small 28S subunit and a large 39S subunit (Smits *et al.,* 2007). Nuclear-encoded initiations factors (IF2 (Ma and Spremulli, 1995) and IF3 (Koc and Spremulli, 2002)), elongation factors (mtEFTu (Ling *et al.,* 1997), mtEFTs (Xin *et al.,* 1995) and mtEFG (Hammarsund *et al.,* 2001)) and release factor (RF1) are also required for the translation process (Smits *et al.,* 2010). Protein synthesis is carried out by the 22 mt-tRNAs, rather than the 31 required for translation of nuclear genes (Barell *et al.,* 1980).

1.7.3 Replication

The mitochondrial genome replicates throughout the cell cycle, independently of the nuclear genome (Bogenhagen and Clayton 1977). Although turnover in post-mitotic cells, such as skeletal muscle and neurons, is slower than in mitotic cells (Wang *et al.,* 1997), the process reportedly takes 60-75 minutes (Clayton, 1982; Korr *et al.,* 1998). The mechanism of mtDNA replication is yet to be determined, with several competing theories proposed to date. The earliest proposed mechanism is the 'asynchronous' or 'strand-displacement' model of replication (Clayton, 1982). Here, replication is initiated at the origin of heavy strand replication (O_H) and continues until the origin of light strand replication (O_L) is exposed and light-strand replication is initiated. Evidence of replication intermediates resistant to single-strand nucleases lead to the development of an alternative 'synchronous' theory (Holt *et al.,* 2000), whereby replication occurs bi-directionally following initiation from more than one region (incorporating *MT-ND5*, *MT-ND6* and *MT-CYB*) and terminating at O_H (Bowmaker *et al.,* 2003). More recently, a third mechanism known as RITOLS (ribonucleotide incorporation throughout the lagging strand) has been proposed based on activity of RNaseH, an enzyme which acts on RNA/DNA hybrids, on replication intermediates. This model is similar to the asynchronous model but involves the binding of RNA to the lagging strand during synthesis of the leading H-strand, which is subsequently converted to DNA (Yasukawa *et al.,* 2006) (Figure 1.10).

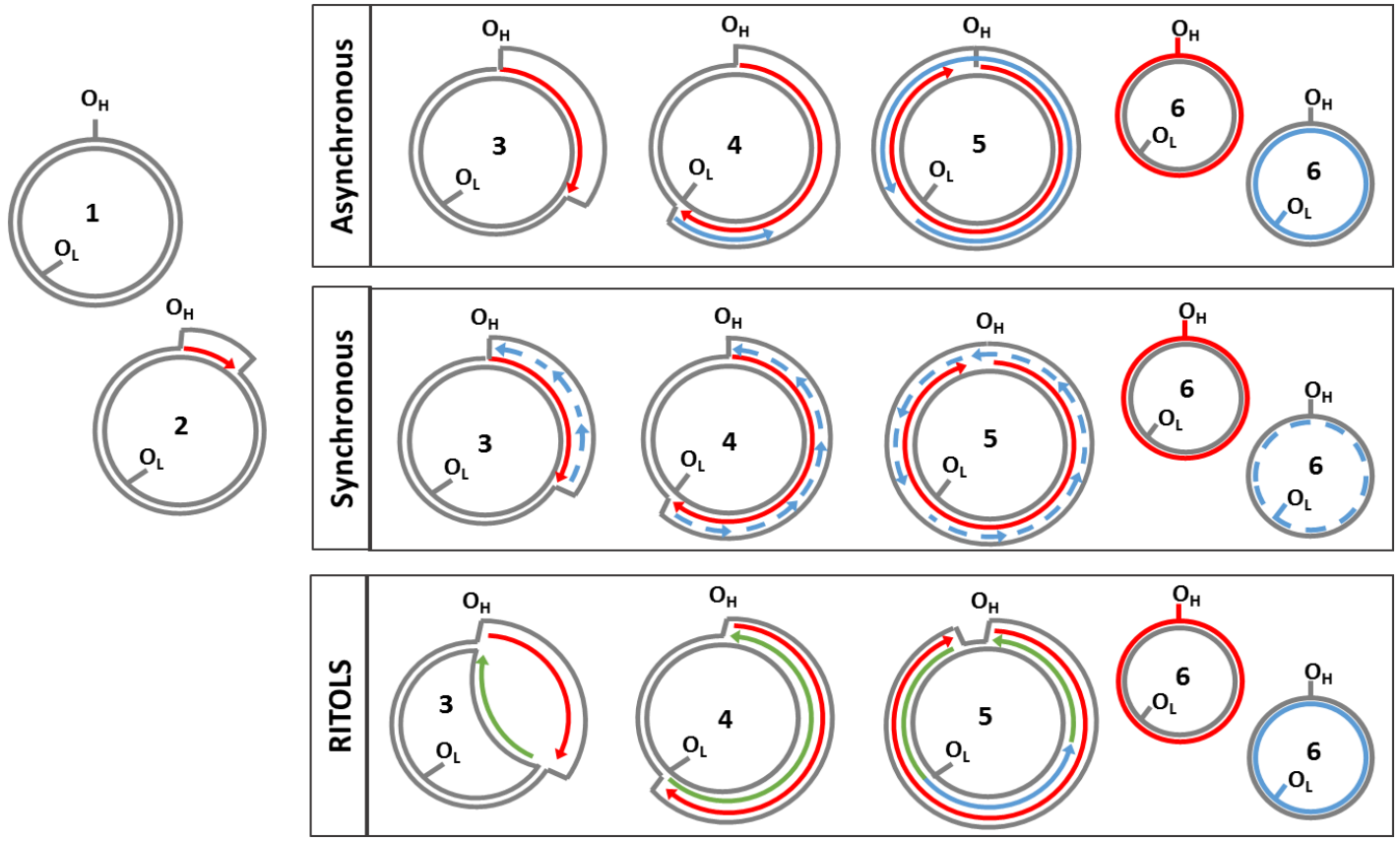

Figure 1.10: Mitochondrial DNA replication. The models of replication, described in section 1.7.3 are shown. Steps 1 and 2 are common to all models, with later steps 3-6 shown for each one. Existing, template DNA is shown in grey and synthesis of the H-strand and L-strand are shown in red and blue respectively. RNA incorporated as part of the RITOLS model is shown in green. Original figure provided courtesy of Dr. Amy Reeve and adapted using Holt et al 2000.

The mtDNA replication machinery is comprised of nuclear-encoded proteins with currently known components including the mitochondrial polymerase γ (polγ), TWINKLE DNA helicase, mitochondrial single-stranded binding protein (mt-SSB) and mitochondrial RNA polymerase (POLMRT) (Korhonen *et al.,* 2004; McKinney and Oliveira, 2013) (Figure 1.11). Polγ comprises a heterotrimer of a catalytic PolγA subunit and two accessory PolγB subunits (Lestienne, 1987) and carries out synthesis by extension of an RNA primer synthesised by POLMRT (Wanrooij *et al.,* 2008; Young and Copeland, 2016). Unwinding of the mtDNA is facilitated by TWINKLE helicase (Spelbrink *et al.,* 2001) ahead of the replication fork, while single-stranded mtDNA is stabilised and protected from nucleolysis by mt-SSB which also enhances TWINKLE and polγ activity (Curth *et al.*, 1994, Korhonen *et al.,* 2003).

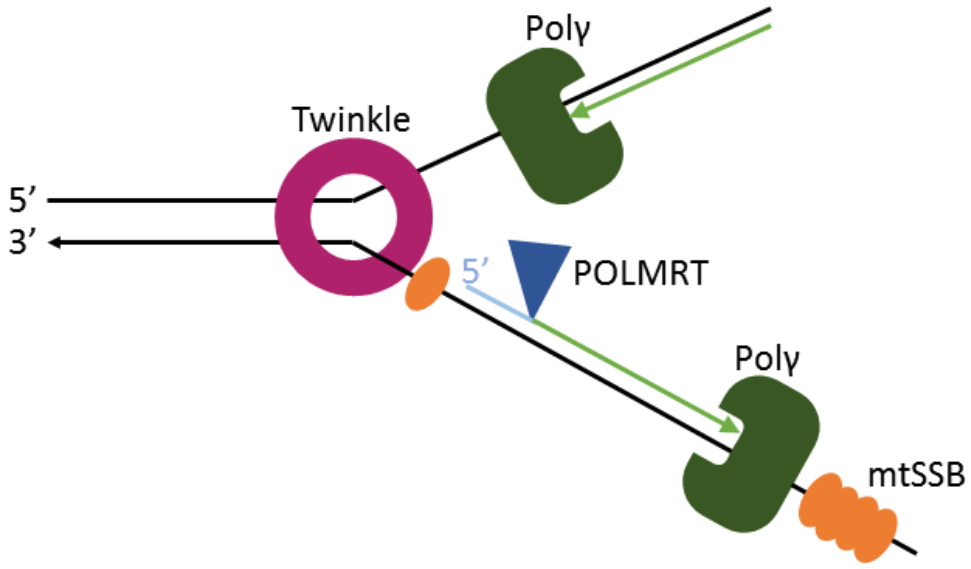

Figure 1.11: Mitochondrial DNA replication machinery. mtDNA is unwound by Twinkle helicase and stabilised by mtSSB while polγ carries out synthesis of nascent DNA (green line) from an RNA primer (blue line) produced by POLMRT. Figure adapted from Young and Copeland 2016

1.8 Mitochondrial genetics

1.8.1 Mutagenesis and repair mechanisms

The mutation rate of mtDNA has been estimated at 10-fold greater than that of the nuclear genome (Brown *et al.,* 1979). This is in part owing to the proximity of the mtDNA, packaged in nucleoids at the IMM, to the ROS producing sites of the OXPHOS system. In addition, mutations can arise due to erroneous replication and incorporation of modified nucleotides (Kamiya, 2003; Boesch *et al.*, 2011). mtDNA undergoes replication much more frequently than nuclear DNA and is therefore subject to a higher rate of replication errors. For example, polγ has been shown to have a high error rate, generating single-stranded regions of mtDNA at the site of double-strand breaks (Kunkel and Loeb 1981). Furthermore, the compact nature of mtDNA means mutations occur in coding regions, thus are likely to have more of a pathogenic effect.

The repair mechanisms for mtDNA mutations are less robust than those used by the nuclear genome (Clayton 1982), although there are some similar pathways involved (Larsen *et al.,* 2005). Such repair mechanisms include base-excision repair (BER) (Stierum *et al.,* 1999) and single-strand break repair (SSB) (Hegde *et al.,* 2012).

1.8.2 Copy number regulation

The number of copies of mtDNA per cell varies, for example 100,000 copies are present in mature oocytes (Shoubridge and Wei 2007), compared with 3600 in skeletal muscle fibres (Miller *et al.,* 2003). While this is thought to be associated with the cell-specific energy requirement and associated mitochondrial mass, the exact mechanisms tightly regulating mtDNA copy number have not been elucidated. A recent method suggesting epigenetic regulation of mtDNA replication was proposed based on correlations between mtDNA copy number and the methylation of CpG islands around the polγ gene (Kelly *et al.,* 2012). This would provide long-term, rather than homeostatic, regulation of mtDNA copy number. Alternative hypotheses include regulation by TFAM (Pohjoismäki *et al.,* 2006), the size of dNTP pools (Tang *et al.,* 2000) or the cellular ATP requirements (Clay Montier *et al.,* 2009).

1.8.3 Heteroplasmy and homoplasmy

Due to the multicopy nature of the mitochondrial genome, subpopulations of wild-type and mutant mtDNA species, harbouring polymorphic or pathogenic variants, can co-exist within the same cell (Holt *et al.,* 1988). This mixture of genomes is termed heteroplasmy, which commonly refers to the proportion of the mutant mtDNA present in a cell or tissue, generally expressed as a percentage of the total mtDNA population. This is an important feature of mitochondrial genetics and plays a fundamental role in the phenotypic expression of mtDNA mutations. Homoplasmy, on the other hand, refers to a state where all mtDNA molecules are identical, whether wild-type or mutant (Taylor and Turnbull 2005).

In muscle, heteroplasmy has been shown to vary between and along muscle fibres (Sciacco *et al.,* 1994). Furthermore, there is variation in heteroplasmy between tissues and organs of the same individual (Shanske *et al.,* 2004). Longitudinal studies of heteroplasmy have shown that levels decrease over time in mitotic tissues like blood (Rahman *et al.,* 2001), yet accumulate in post-mitotic tissues such as brain and skeletal muscle (Larsson, 1990; Weber *et al.,* 1997). These changes over time are discussed further in chapters 3 and 4 relating to the m.3243A>G point mutation and single, large-scale mtDNA deletions respectively.

1.8.4 Threshold effect

Mutations of mtDNA are functionally recessive (Saconni *et al.,* 2008). Low levels of heteroplasmy do not typically result in a biochemical or clinical phenotype as any defects can be compensated for by the high proportion of wild-type mtDNA molecules. However, accumulation of the mutated mtDNA species above a pathological threshold level results in respiratory chain deficiency and mitochondrial dysfunction, as there are insufficient wild-type mtDNA molecules remaining to support normal mitochondrial function (Sciacco *et al.,* 1994) (Figure 1.12).

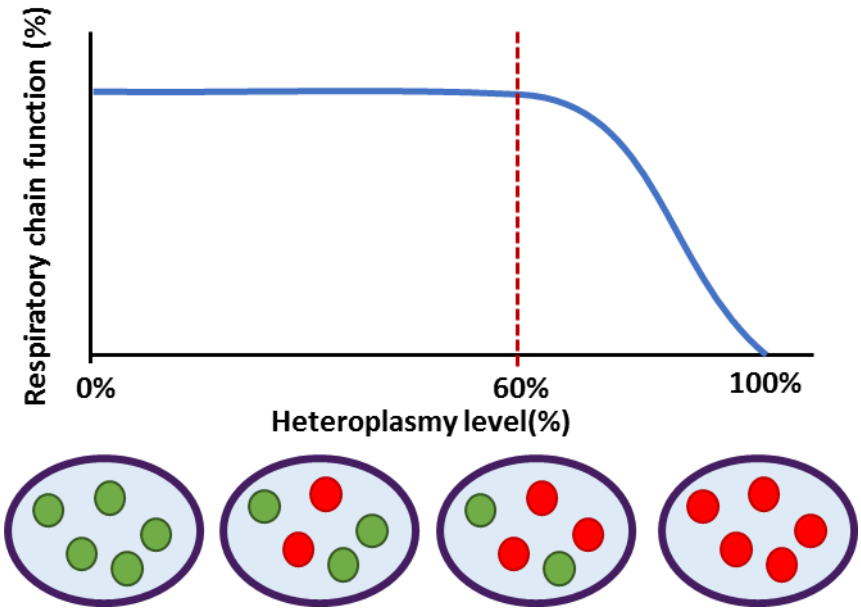

Figure 1.12: Mitochondrial threshold effect. Respiratory chain function (blue line) is maintained at 100% until the heteroplasmy level, (the proportion of mutant (red) mtDNA to wild-type (green) mtDNA)) reaches a threshold level, indicated here at 60% by the dotted red line. After the threshold level is reached, respiratory chain function begins to decline.

The critical threshold level has been shown to vary between different tissues. For example mitochondria isolated from rat tissues showed a lower threshold for complex I deficiency in brain relative to muscle, liver, heart and kidney, whereas muscle showed greater vulnerability to complex IV defects (Rossignol *et al.,* 1999). More recently, extra-ocular muscles were reported as having a lower threshold for OXPHOS defects than was seen in skeletal muscle from patients with single, large-scale mtDNA deletions (Greaves *et al.,* 2010).

The threshold level also varies between different types of mutation. Point mutations involving mt-tRNA genes have an estimated threshold level of 90% based on studies in *trans*mitochondrial cybrids (Chomyn *et al.,* 1992; Yoneda *et al.,* 1995). Analysis of muscle fibres from patients with MERRF or MELAS has revealed threshold levels of approximately 80% for m.8344A>G (Taylor and Turnbull, 2005) and 90% for m.3243A>G (Schoffner *et al.,*

1990). However, a lower estimate of 50% heteroplasmy has been suggested as the biochemical threshold level for m.3243A>G in skeletal muscle (Jeppesen *et al.,* 2006).

The biochemical threshold level for single, large-scale mtDNA deletions is generally lower than that for point mutations, estimated at approximately 50-60% by studies using *trans*mitochondrial cybrids (Hayashi *et al.,* 1991; Porteous *et al.,* 1998). However, a much higher threshold level of 70-90% has been reported in patient skeletal muscle (Sciacco *et al.,* 1994). This variation in threshold levels could be due to the genetic and phenotypic heterogeneity of these mutations, which is explored in further detail in chapter five.

1.8.5 Clonal expansion of mtDNA mutations

A single mutated mtDNA molecule can clonally expand to become the predominant mtDNA species within a cell. This impacts the extent of mitochondrial dysfunction and the biochemical phenotype of the cell, particularly if the heteroplasmy level is raised over the threshold level, towards homoplasmy. The precise mechanism by which clonal expansion occurs remains unsolved, however a number of theories have been put forward.

The earliest model to be proposed was clonal expansion by replicative advantage (Wallace, 1992). This model, also known as the 'survival of the smallest', suggests that mtDNA molecules with larger deletions have a replicative advantage owing to their smaller size. While some studies have provided evidence to support this model (Fukui and Moraes, 2009; Diaz *et al.,* 1997), others have found no evidence of a replicative advantage for smaller mtDNA molecules under normal physiological conditions (Diaz *et al.,* 2007; Campbell *et al.,* 2014). Furthermore, this model is not applicable to the accumulation of point mutations over time.

An alternative theory, clonal expansion by selective advantage, was offered by de Grey (1997). Here it was suggested that mutant mtDNA species hinder the respiratory capability of the mitochondrion, leading to a reduction in free radical production. Subsequently,

turnover of dysfunctional mitochondria is slower and mutant mtDNA species are able to accumulate. This model only applies where mtDNA mutations have already undergone sufficient clonal expansion to impact on the respiratory capacity of the mitochondria. It also implies that accumulation of mutant mtDNA species would primarily occur in mitotic tissues with high rates of mitochondrial turnover, and therefore offers no consideration for the accumulation of mtDNA mutations in post-mitotic tissues.

The most recent model put forward by Elson *et al.* (2001) suggests that relaxed replication of mtDNA alone is sufficient to cause an accumulation of a single mtDNA mutant species over a time via random genetic drift. Although this theory is supported by mathematical models, there is some dispute between predictions of COX-deficiency and physiological observations (Campbell *et al.,* 2014).

1.8.6 Maternal inheritance and the bottleneck

Inheritance of mtDNA follows a non-Mendelian pattern and is instead strictly maternally inherited (Giles *et al.,* 1980), although there is one documented case of paternal inheritance of mtDNA with a deletion in *MT-ND2* (Schwartz and Vissing, 2002), yet this has not been reported by others. Paternal mtDNA is thought to be eliminated by selective proteasomal degradation (Kaneda *et al.,* 1995; Sutovsky *et al.,* 2000) or autophagy post-fertilization (Al Rawi *et al.,* 2011), although degradation prior to fertilisation has also been reported (Luo *et al.,* 2013). Mutations in mtDNA are passed from mother to child, however there is great variability in the heteroplasmy levels and phenotypic expression across generations (Taylor and Turnbull 2005).

This variation in heteroplasmy levels in offspring is attributed to the genetic bottleneck. The most widely accepted mechanism describes an initial reduction in mtDNA copy number from the oocyte post-fertilisation to the primordial germ cell, prior to re-amplification of mtDNA resulting in random shifts in heteroplasmy between generations (Jenuth *et al.,* 1996; Cree *et al.,* 2008). Heteroplasmy levels in offspring are thought to be determined by random genetic drift during replication in the oocyte (Brown *et al.,* 2001).

1.9 Mitochondrial disease: Pathogenic mutations

The prevalence of mitochondrial disease due to nuclear and mitochondrial DNA mutations is estimated at 1 in 4300, according to a recent study of adults in the North East of England (Gorman *et al.,* 2015). In clinically affected adults, the minimum prevalence of mtDNA mutations was 1 in 10,400, with an additional 1 in 9300 adults and children deemed at risk. These figures are similar to previous estimates from a study of patients from the same region (Schaefer *et al.,* 2008) and conclude the minimum prevalence rate for mtDNA mutations is 1 in 5000. Adult mitochondrial disease attributed to mutations in the nuclear genome were reported in 2.9 per 100,000 (1 in 34,400). Obtaining an accurate estimate for mitochondrial disease prevalence is made challenging by the genetic and clinical heterogeneity of this group of diseases.

1.9.1 Point mutations in mtDNA

Point mutations in mtDNA were first identified as a cause of mitochondrial disease in patients with Leber's hereditary optic neuropathy (Wallace *et al.,* 1988). These single base pair substitutions are typically maternally inherited, as opposed to occurring sporadically, and more than half are located in tRNA genes (Schon *et al.,* 2012) (Figure 1.13). These commonly cause a decrease in activity of OXPHOS subunits, particularly complexes I and IV (Mariotti *et al.,* 1994). The most common point mutation is the m.3243A>G transition in *MT-TL1*, the mitochondrial $tRNA^{Leu(UUR)}$, first described in patients with mitochondrial encephalopathy, lactic acidosis and stroke-like episodes (MELAS) in 1990 (Goto *et al.,* 1990). This mutation, and its associated biochemical and clinical phenotypes, will be discussed in further detail in Chapter Three.

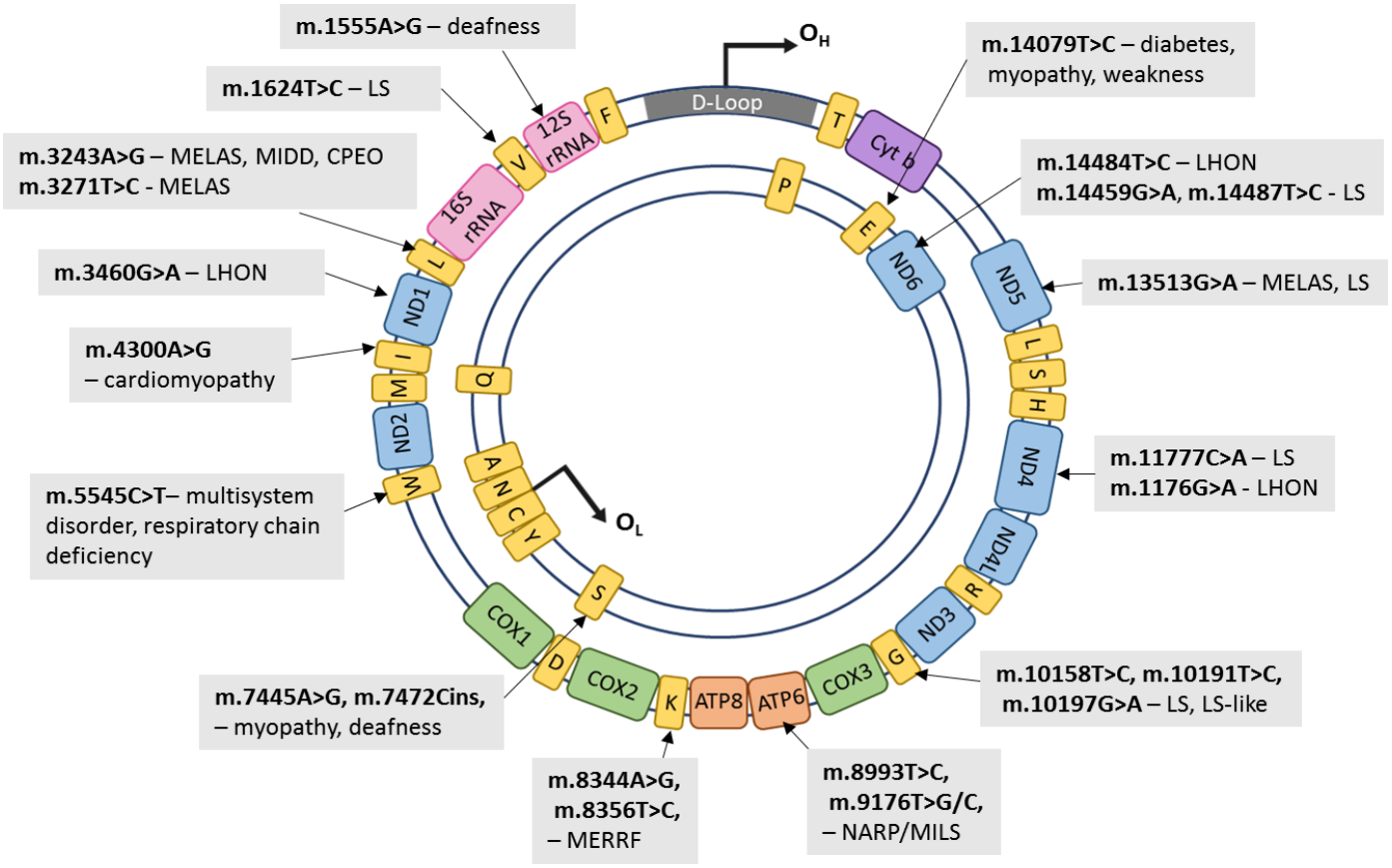

Figure 1.13: Point mutations associated with disease. Point mutations occur across the genome (genes indicated by arrows), causing a range of clinical phenotypes. Abbreviations: LHON=Leber's hereditary optic neuropathy; LS=Leigh's syndrome; MELAS=mitochondrial encephalopathy, lactic acidosis and stroke-like episodes; NARP= neuropathy, ataxia and retinitis pigmentosa; MILS=maternally inherited LS; MERRF=myoclonic epilepsy and ragged red fibres; MIDD=maternally inherited diabetes and deafness; CPEO=chronic progressive external ophthalmoplegia. Adapted from original provided by Dr. John Grady.

The m.8344A>G mutation in *MT-TK* (mitochondrial tRNA lysine) was identified in patients with myoclonic epilepsy and ragged red fibres (MERRF) (Schoffner *et al.,* 1990; Yoneda *et al.,* 1990), a multisystem disorder characterised by myoclonus and a range of neurological symptoms such as epilepsy, ataxia and dementia. The overall prevalence of this mutation is much lower than that of m.3243A>G, at just 0.7 per 100,000 (Gorman *et al.,* 2015), however it is found in 80% of patients with MERRF phenotype (Wu *et al.,* 2010). m.8344A>G results in a loss of taurine modification of the $tRNA^{Lys}$ at the wobble position which impedes translation and leads to ribosomal stalling (Yasukawa *et al.,* 2001), resulting in reduced protein synthesis (Chomyn *et al.,* 1991; Yoneda *et al.*, 1994).

Pathogenic point mutations in genes encoding subunits of complexes involved in OXPHOS have also been identified (Ylikallio and Suomalainen, 2012). 90% of point mutations associated with LHON, the most prevalent condition under the umbrella of mitochondrial disease (Gorman *et al.,* 2015), are located in complex I genes, e.g m.3460G>A in *MT-ND1* (Howell *et al.,* 1991), m.11778G>A in *MT-ND4* (Wallace *et al.,* 1988) and m.14484T>C in *MT-ND6* (Johns *et al.,* 1992). These near homoplasmic mutations selectively affect retinal ganglion cells in the optic nerve (Schon 2012).

MT-ATP6 is the site of the m.8993T>G point mutation associated with NARP (Holt *et al.,* 1990; Schon *et al.,* 2001). This mutation has also been found in patients with Leigh's syndrome, a progressive neurological disorder with infantile onset often resulting in childhood mortality. This condition is characterised post-mortem by the observation of necrotic lesions in the thalamus, basal ganglia and brain stem (Leigh and Thompson 1951). Other mutations in this gene, e.g. m.9176T>G and m.9176T>C, have also been associated with Leigh's syndrome (Carrozzo *et al.*, 2001; Thyagarajan *et al.*, 1995).

1.9.2 Single, large-scale mtDNA deletions

Single, large-scale deletions of mtDNA are the most common form of mtDNA rearrangement. These deletions can vary in size and location across the mitochondrial genome and have a collective prevalence of approximately 1.5 in 100,000 (Gorman *et al.,*

2015). Clinically, single, large-scale mtDNA deletions are associated with a broad range of phenotypes from relatively mild chronic progressive external ophthalmoplegia (CPEO) (Moraes *et al.,* 1989) to more severe conditions such as Pearson's syndrome (PS) (Pearson *et al.*, 1979) and Kearns-Sayre syndrome (KSS) (Kearns & Sayre, 1958). The genetic, biochemical and clinical features of single, large-scale mtDNA deletions are discussed in more detail in chapters four and five.

Typically single, large-scale mtDNA deletions are thought to occur sporadically during oogenesis (Krishnan *et al.,* 2008) or embryonic development (Zeviani *et al.,* 1990; Marzuki *et al.,* 1997), by a mechanism which is still being debated. An early model, suggested by Schoffner *et al.* (1989), proposed deletion formation by slipped-strand mispairing during replication (Figure 1.14). Here, single-strand repeats on the parent heavy strand mis-anneal with homologous repeats on the parent light strand, creating a single-stranded loop of parent heavy strand DNA. The loop is subsequently degraded and the heavy strand ends are ligated. Replication of the daughter heavy strand continues, producing a deleted mtDNA molecule. While this model may explain why so many deletions are located in the major arc, it is based on the asynchronous model of replication and requires large regions of unprotected single-stranded mtDNA, which are not thought to occur. Furthermore, if deletion formation were linked to replication, mitotic tissues would be expected to accumulate deletions at a much higher rate than post-mitotic tissues due to replication occurring more frequently in these tissues (Krishnan *et al.,* 2008). However, single, large-scale mtDNA deletions have been shown to be rare in mitotic tissues, such as the colon (Taylor *et al.,* 2003), whereas they are commonly seen in post-mitotic tissues, accumulating with age (Cortopassi *et al.,* 1992; Melov *et al.,* 1995; Kraytsberg *et al.,* 2006).

A more recent mechanism proposed by Krishnan *et al.* (2008) claims that deletions are formed during the repair of double-stranded breaks. These breaks occur frequently as intermediates in the restoration of the replication fork following stalling. Exonuclease activity in the repair of double-stranded breaks generates single-stranded regions, which anneal with microhomologous sequences (Haber *et al.,* 2000) leading to deletions via the repair or degradation of the exposed single-stranded DNA. This mechanism is consistent

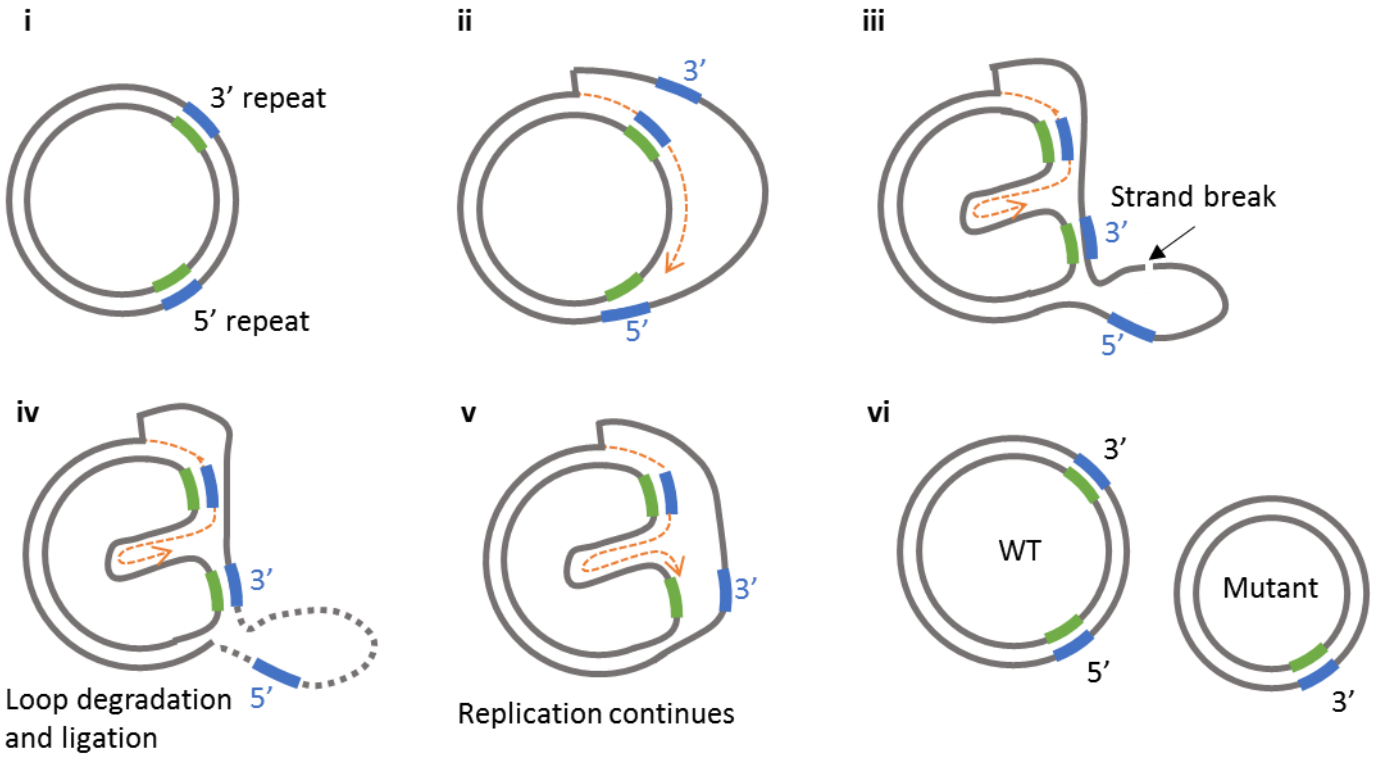

Figure 1.14: Formation of single, large-scale mtDNA deletions by replication. Direct repeats, labelled 3' and 5', are present in mtDNA (i). Replication begins, with nascent DNA (orange dotted line) displacing the heavy strand (ii). Repeats misanneal causing the formation of a single-stranded loop (iii), which is degraded (iv) before replication continues (v) generating a wild-type molecule of mtDNA and a second mutant species with a deletion. Adapted from Krishnan et al (2008).

with the flanking repeat sequences seen with deletions (Samuels *et al.,* 2004) and is more in keeping with the distribution of these mutations in mitotic and post-mitotic tissues.

1.9.3 Nuclear DNA mutations

The nuclear genome is vital to so many aspects of mitochondrial function, encoding structural subunits of complexes in the OXPHOS system as well as proteins required for complex assembly, transcription and translation, regulation of mitochondrial dynamics and mtDNA maintenance (Schon *et al.,* 2012). Nuclear DNA mutations often have secondary effects on mtDNA resulting in multiple deletions and mtDNA depletion and have been associated with a wide spectrum of conditions. Mutations in *POLG*, encoding polγ, compromise enzyme function leading to a depletion in mtDNA to pathogenically low levels in patients with Alpers-Huttenlocher (AH) syndrome (Naviaux *et al.,* 1999; Davidzon *et al.,* 2005). AH is a multisystem condition with infantile onset, characterised by developmental delay, liver failure and intractable seizures (Naviaux and Nguyen, 2004; Davidzon *et al.*, 2005; Isohanni *et al*., 2011). Mutations in the same gene have also been associated with progressive external ophthalmoplegia (PEO), a milder condition with adult onset and symptoms including ptosis and generalised myopathy (Van Goethem *et al.,* 2001). Mutations in *PEO1*, the gene-encoding the DNA helicase Twinkle, have also been associated with mtDNA depletion and multiple deletions (Spelbrink *et al.,* 2001). Here, an impaired helicase activity leads to a PEO phenotype with adult onset (Spinazzola and Zeviani, 2005).

1.10 Diagnosis of mitochondrial disease

The diagnosis of mitochondrial disease is complicated by the genetic and clinical heterogeneity of the conditions. Following clinical evaluation by a multidisciplinary team, further laboratory investigations are carried out to determine a genetic diagnosis, which could provide key information regarding inheritance and prognosis to clinicians and patients. An algorithm for these investigations, adapted from McFarland *et al.* (2010), is presented in Figure 1.15.

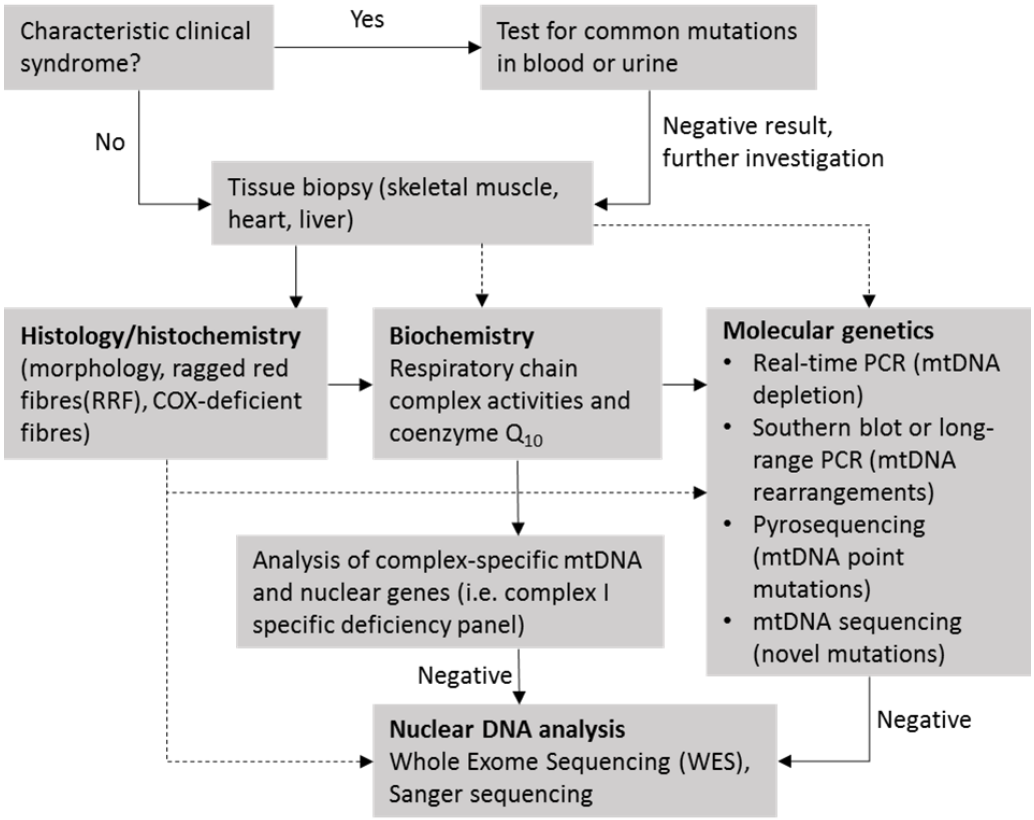

Figure 1.15: Algorithm for investigations in the diagnosis of mitochondrial disease. (Adapted from McFarland *et al.* 2010)

Skeletal muscle biopsies are considered the 'gold standard' in the diagnosis of mitochondrial disease, allowing for histological, biochemical and molecular genetic analyses to be performed (Taylor *et al.,* 2004; Hardy *et al.,* 2016). While other affected organs, such as brain or liver, may harbour tissue-specific pathologies there are concerns over the safety of performing biopsies of these tissues (Bourgeois and Tarnopolsky, 2004).

Histochemical analysis of skeletal muscle sections in the transverse orientation can reveal hallmarks of mitochondrial dysfunction. For example, the Gomori trichrome stain (Engel and Cunningham 1963) enables visualisation of mitochondria in the subsarcolemmal regions, which selectively uptake the red component of the stain. A pathological accumulation of subsarcolemmal mitochondria is identified as a 'ragged red fibre' and is characteristic of the condition MERRF, although present in other mitochondrial myopathies (Figure 1.16A). The use of COX/SDH dual histochemistry (Johnson *et al.,* 1983) highlights the characteristic mosaic pattern of COX-deficiency across fibres in a muscle section. The first reaction for COX (complex IV) produces a brown precipitate when cytochrome *c* is active, thereby indicating the presence of functional mitochondria. A sequential reaction for SDH (complex II) highlights COX-negative fibres by producing a blue precipitate. This allows for the categorisation of fibres as COX-positive, -intermediate or -negative across the section (Figure 1.16B). This same protocol also identifies segmental COX-deficiency in fibres when viewed in the longitudinal plane (Murphy *et al.,* 2008) (Figure 1.16C). These histological hallmarks are also seen in aging muscle and so the age of the patient must be considered when reviewing these findings. It is also important to note that only complex IV deficiency is evaluated here, and so the absence of any negative fibres does not mean an absence of respiratory chain dysfunction, as a different complex may be affected. A recently developed immunofluorescence protocol somewhat addresses this issue by quantitatively analysing levels of complex I and complex IV together (Rocha *et al.,* 2015) (Figure 1.16D). This method is used throughout this thesis and is described in section 2.5.2.

In addition to the histochemical evaluations of patient skeletal muscle, biochemical assessments can be carried out to determine enzyme activity levels and ATP production. These require fresh skeletal muscle for the isolation of mitochondria (Janssen *et al.,* 2003) and can prove useful in narrowing down the diagnosis of mitochondrial syndromes (Taylor *et al.,* 2004). Determination of the specific genetic defect in patient skeletal muscle requires molecular genetic analyses performed on DNA extracted from homogenate tissue: long-range PCR and Southern blotting can identify mtDNA rearrangements, while point mutations of the mtDNA or nuclear gene defects can be identified via sequencing (Chinnery and Turnbull, 1997)

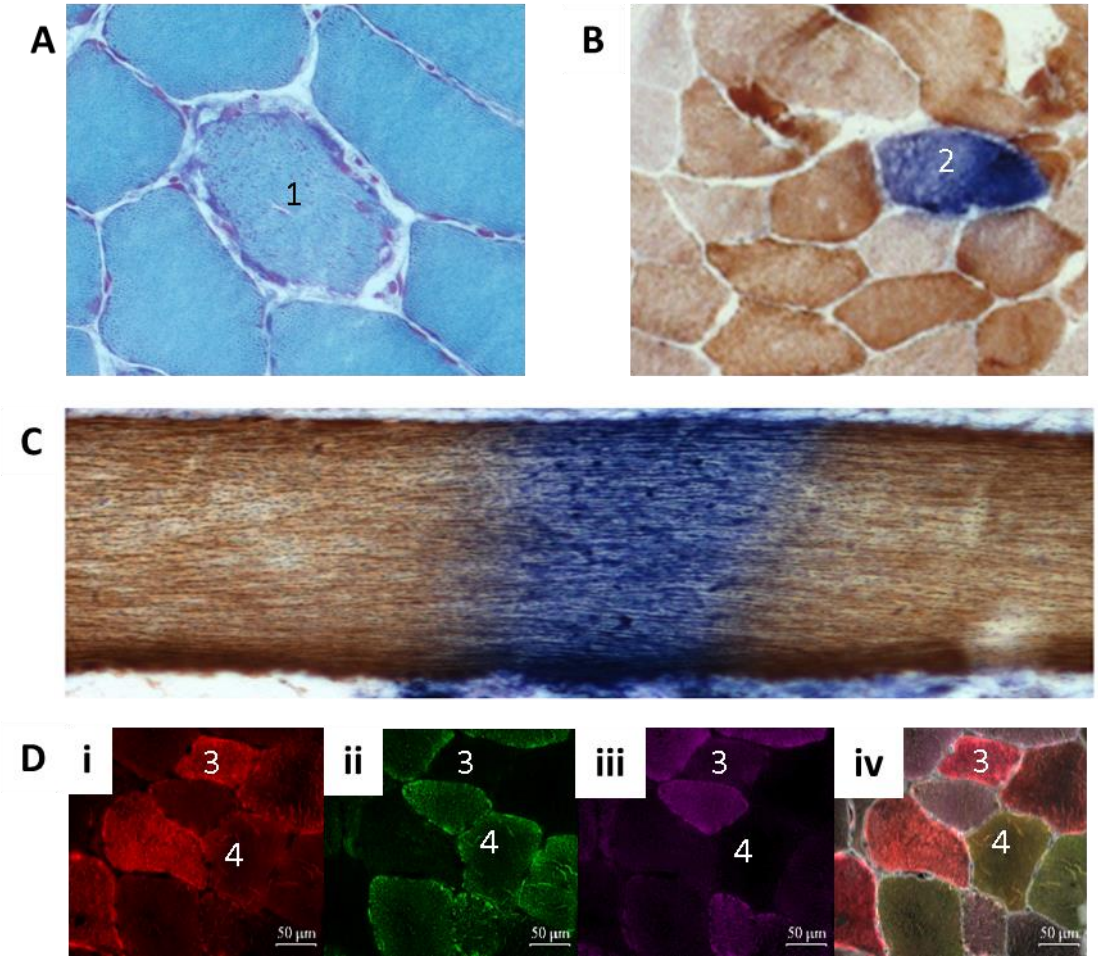

Figure 1.16: Hallmarks of mitochondrial dysfunction in skeletal muscle. (A) Gomori trichrome stain to detect ragged red fibres (fibre 1). (B) Sequential COX/SDH histochemistry highlights COX-negative fibres in blue (fibre 2), while brown fibres indicate normal COX activity. (C) COX/SDH histochemistry on skeletal muscle fibre viewed longitudinally shows segmental COX deficiency (blue). (D) A quantitative immunofluorescence protocol using antibodies against porin (i), COXI (complex IV subunit) (ii), NDUFB8 (complex I subunit) (iii) to determine levels of complex I and complex IV normalised to mitochondrial mass. Fibres deficient for complex IV (fibre 3) and complex I (fibre 4) are shown in each channel and the merged image (iv).

1.11 Skeletal muscle

The formation of skeletal muscle fibres occurs during embryogenesis (Yusuf and Brand-Saberi, 2012). Mononuclear myoblasts cluster together and fuse to form multinucleated myotubes, which continue to fuse forming muscle fibres, which are arranged in parallel in the longitudinal plane. Unfused myoblasts become satellite cells which act as stem cells in the regeneration of muscle fibres. (Leiber, 2010).

1.11.1 Structure of skeletal muscle

Muscle fibres are grouped together to form fascicles, supported by a thick perimysium which allows for the entry of the capillary network and motor neurons to innervate fibres (Gillies and Lieber, 2011). A muscle is formed from a collection of fascicles surrounded by the epimysium, the outer layer of the muscle which is continuous with that of the tendon (MacIntosh *et al.,* 2006).

Each muscle fibre consists of bundles of myofibrils, arranged in parallel and surrounded by the sarcolemma and endomysium (Lieber, 2010). Myofibrils occupy 85-90% of the muscle fibre volume, and are composed of repeating contractile units, approximately 2.5-3µm, called sarcomeres (Dubowitz, 2007). Sarcomeres are separated at the Z-bands and contain thin actin and thick myosin myofilaments as well as associated proteins involved in muscle contraction (Hanson and Huxley, 1953). (Figure 1.17).

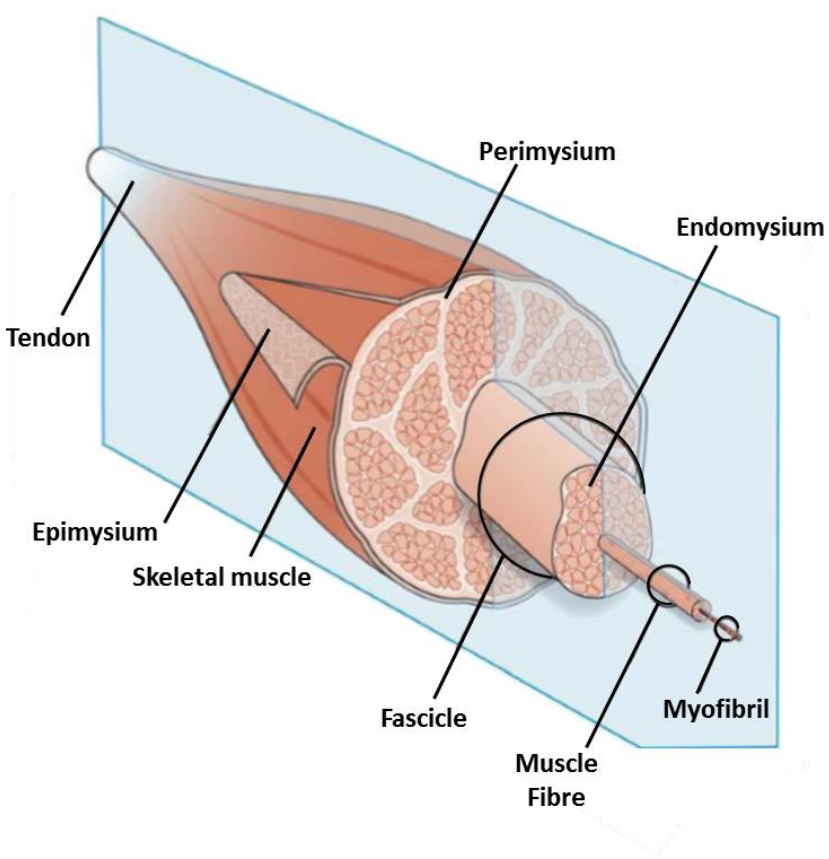

Figure 1.17: Schematic of the structure of skeletal muscle. Muscle fibres (consisting of bundles of myofibrils) are grouped to form fascicles, supported by the perimysium. Groups of fascicles make up a skeletal muscle which is surrounded by the epimysium. Adapted from figure provided by Dr Mariana Rocha (original provided courtesy of Professor Richard Lieber).

1.11.2 Skeletal muscle fibre types

In humans, muscle fibres can be grouped according to their morphology, metabolic capabilities and their contractile strength (Table 1.1). Type I fibres have high oxidative and low glycolytic activity, whereas type II fibres rely predominantly on glycolytic metabolism. Type II fibres can be further divided into two groups, where type IIa fibres are an intermediate between type I and IIx relying on both oxidative and glycolytic metabolism (Brooke and Kaiser 1970). Fibre types can also be differentiated by their contractile strength and susceptibility to fatigue (Schiaffino *et al.,* 1970). Type I fibres are thereby known as slow twitch fatigue resistant. Type IIa fibres are fast twitch fatigue resistant and type IIx fibres are fast twitch, fatigue sensitive. The difference in metabolic characteristics is mirrored by the mitochondrial content of the muscle fibre types, with oxidative type I fibres possessing more mitochondria than glycolytic type II fibres (MacIntosh *et al.,* 2006).

Characteristics	Type I (Slow)	Type IIa (Fast-resistant)	Type IIx (Fast-fatigable)
Fibre diameter	Small	Medium	Large
Mitochondria	Rich	Rich	Poor
Oxidative activity	High	High	Low
Glycolytic activity	Low	High/ intermediate	High
Contraction speed	Slow	Fast	Fast
Fatigues resistance	High	Low/ Intermediate	Low

Table 1.1: Characteristics of muscle fibres types. Adapted from (MacIntosh *et al.,* 2006) and (Hopkins, 2006).

Most skeletal muscles display variable proportions of each fibre type, which can also vary within different regions of the same muscle (Johnson *et al.,* 1973). For example, the tibialis anterior contains a higher proportion of type I fibres than the quadriceps. An age-related preferential decline in the proportion of type II fibres has been observed (Lexell *et al.,* 1995). Conley *et al.,* (2007) report more mitochondrial dysfunction (as measured by ATP depletion

and mitochondrial uncoupling) in muscles with a higher proportion of type II fibres, possibly contributing to the loss of these fibres with age.

The muscle fibre makes up only a portion of the motor unit, which also comprises the motor neuron. A single motor neuron influences muscle fibre phenotype through the frequency of electrical discharges (Buller *et al.,* 1960). Discharges at 10 and 100Hz trigger changes in gene expression resulting in slow and fast-twitch phenotypes (Schiaffino *et al.,* 1999). Each motor neuron innervates hundreds of muscle fibres. Within each motor unit, fibres are of the same type and are randomly scattered throughout the muscle.

Despite the different mitochondrial loads of muscle fibre types, they are rarely accounted for in studies on mitochondrial disease utilising patient skeletal muscle biopsies. This is a major limitation of such studies and may be a contributing factor to the inconsistent biochemical and histopathological reports, particularly those featuring analysis of single muscle fibres.

1.11.3 Mitochondrial organisation in muscle

There are two subcellular populations of mitochondria in skeletal muscle. 20% of mitochondria are localised to the subsarcolemmal (SS) region in peri-nuclear clusters. The remaining 80% of mitochondria, classed as intermyofibrillar (IMF), are distributed in pairs at the z-bands of the sarcomeres (Milner *et al.,* 2000). As such, these mitochondria form a relatively rigid network compared to other cells such as neurons (Huang *et al.,* 2013).

In addition to contrasting subcellular localisation, SS and IMF mitochondria also differ in their activity, function and susceptibility to apoptosis. SS mitochondria are thought to produce energy for the function of the membrane and nuclei, whereas IMF mitochondria produce energy for use in the muscle contraction process, consistent with their location within contractile units (Hood *et al.,* 2001). Furthermore, IMF mitochondria have shown higher levels of respiratory chain activity in rats (Ferreira *et al.,* 2010), and a higher susceptibility to apoptosis (Adhihetty *et al.,* 2005).

1.12 Overall aims and objectives

Mitochondrial disease encompasses a highly heterogeneous group of conditions with a wide spectrum of clinical phenotypes associated with a broad range of mutations occurring in the mitochondrial and nuclear genomes. Such heterogeneity presents challenges in the diagnosis and treatment of patients, and as such there is no cure for mitochondrial disease. Furthermore, evaluating patient prognosis is complicated as little is known about the pathogenic mechanisms behind the onset and progression of these conditions. Elucidating these genetic and cellular mechanisms could greatly improve the current understanding of disease pathogenesis, providing potential candidates for future therapeutic measures and improving patient care by providing clearer information on prognoses. Therefore, this work aims to improve understanding of the molecular mechanisms behind the pathogenesis of mitochondrial dysfunction in muscle, and the genetic and biochemical changes occurring over time with disease progression.

First, longitudinal studies were conducted using two skeletal muscle biopsies from patients with either m.3243A>G point mutation or single, large-scale mtDNA deletions, the two most common mutations in the MRC Mitochondrial Disease Cohort. These studies aimed to determine whether any changes to heteroplasmy level, mtDNA copy number or respiratory chain deficiency occurred over time by performing immunofluorescent and molecular genetic analyses.

Next, a single fibre approach was applied to skeletal muscle biopsies from patients with single, large-scale deletions with the overall aim of better understanding the relationship between the genetic status (i.e. the deletion size, location and level, as well as mtDNA copy number) and the respiratory chain defect (i.e. the level of complex I and IV deficiency) on a cellular level. A more specific aim was to identify the threshold levels for complex I and IV deficiency in patients harbouring different deletion species to determine the role of the size and location of the deletion on the extent of the respiratory chain defect.

Finally, a novel real-time PCR assay for the determination of mtDNA copy number was optimised. The current protocol can be subject to variability, particularly when DNA concentration is low. Therefore, the aim of this project was to evaluate whether the addition of a multicopy gene target (*RNA18S*) to the current protocol would improve quantitative accuracy and precision.

Chapter 2: Materials and Methods

2.1 Materials

2.1.1 Consumables

Aerosol resistant pipettes	Starlab UK Ltd, Milton Keynes
Coverslips (22x22mm, 22x40mm, 22x50mm)	MSD, Hoddesdon, UK
Microfuge tubes (0.6ml, 1.5ml, 2.0ml)	Starlab UK Ltd, Milton Keynes
0.2ml Thin-walled PCR tubes	Starlab UK Ltd, Milton Keynes
Falcon tubes (15ml, 50ml)	BD Biosciences UK, Oxford
Gilson pipetteman (P10, P20, P200, P1000)	Gilson Scientific UK, Dunstable
Pipette tips (10µl, 20µl, 200µl, 1ml)	Starlab UK Ltd, Milton Keynes
Pasteur pipettes	VWR International Ltd, Lutterworth, UK
Superfrost slides	MSD UK, Hoddesdon
Whatman filter paper	Fisher Scientific UK Ltd., Loughborough
24-well plates	Starlab UK Ltd, Milton Keynes
MicroAmp® Optical 96-Well Reaction Plate	Fisher Scientific UK Ltd., Loughborough
StarSeal advanced polyolefin film	Starlab UK Ltd, Milton Keynes
Hydrophobic pen	Daido Sangyo, Japan
Scalpels	Swann Morton, Sheffield, UK
Cap strips, domed	Starlab UK Ltd, Milton Keynes
QIAmp DNA Mini Kit (50)	Qiagen UK, Manchester

2.2 Solutions

2.2.1 DNA loading dye

0.25% (w/v) Bromophenol Blue

0.25% (w/v) Xylene Cyanol

30% (v/v) Glycerol

2.2.2 Gel pouring buffer/running buffer (1L)

100ml 10x TAE

900ml NANOpure water

2.2.3 Electrophoresis buffer (1L)

100ml 10x TAE

900ml NANOpure water

2.2.4 Single cell lysis buffer (500µl)

250µl 1% Tween 20

50µl 0.5M TrisHCl pH8.5

5µl proteinase K

195µl dH_2O

2.2.5 TBST (2L)

121g Trizma base

90g NaCl

5ml Tween 20

2L dH_2O

HCl to pH 7.6

2.2.6 LB Broth (250ml)

3.75g Bacto™ Agar

2.50g Bacto™ Tryptone

1.25g Bacto™ Yeast Extract

2.50g NaCl

250ml dH_2O

2.3 Reagents

2.3.1 Immunofluorescent staining

Trizma base	Sigma-Aldrich Company Ltd., Dorset, UK
Sodium chloride (NaCl)	Sigma-Aldrich Company Ltd., Dorset, UK
Hydrochloric acid (HCl)	VWR International Ltd, Lutterworth, UK
Tween-20	Sigma-Aldrich Company Ltd., Dorset, UK
4% Paraformaldehyde (PFA)	Santa Cruz Biotechnology, Dallas, TX, USA
Normal goat serum (NGS)	Sigma-Aldrich Company Ltd., Dorset, UK
Ethanol (AnalR)	MSD, Hoddesdon, UK
Methanol (AnalR)	MSD, Hoddesdon, UK
Phosphate buffered saline (PBS) tablets	Sigma-Aldrich Company Ltd., Dorset, UK
Prolong Gold mounting media	Fisher Scientific UK Ltd., Loughborough

2.3.2 Gel Electrophoresis

Agarose	Bioline Reagents Limited, London, UK
Tris acetate EDTA 10x	Sigma-Aldrich Company Ltd., Dorset, UK
SYBR® Safe DNA Gel Stain	Fisher Scientific UK Ltd., Loughborough
Bromophenol blue	Sigma-Aldrich Company Ltd., Dorset, UK
Xylene cyanol	Sigma-Aldrich Company Ltd., Dorset, UK
Glycerol	Sigma-Aldrich Company Ltd., Dorset, UK
100bp ladder	Norgen Biotek Corps, Ontario, Canada
1Kb ladder	Promega UK, Southampton

2.3.3 DNA extraction, amplification and sequencing

Ethanol	Fisher Scientific UK Ltd, Loughborough
Proteinase K Solution	Fisher Scientific UK Ltd., Loughborough
Tris-HCl	Sigma-Aldrich Company Ltd., Dorset, UK
Tween-20	Sigma-Aldrich Company Ltd., Dorset, UK
GoTaq® Hot Start Polymerase Kit	Promega UK, Southampton
GoTaq® G2 Flexi DNA Polymerase Kit	Promega UK, Southampton
10mM dNTPs	Roche Diagnostics Ltd, Sussex, UK
10mM dNTPs	Takara Bio Europe, France
Standard PCR primers	Eurofins Genomics, Ebersburg, Germany
Realtime PCR primers	Eurofins Genomics, Ebersburg, Germany
Realtime PCR probes	Eurofins Genomics, Ebersburg, Germany
Taqman universal PCR mastermix (with UNG)	Fisher Scientific UK Ltd., Loughborough
Nuclease-free water	Fisher Scientific UK Ltd., Loughborough
PyroMark Binding Buffer	Qiagen UK, Manchester
PyroMark Annealing Buffer	Qiagen UK, Manchester
PyroMark Gold Q24 Reagents	Qiagen UK, Manchester
Pyrosequencing primers	Eurofins Genomics, Ebersburg, Germany
Sepharose beads	GE Healthcare, UK
PyroMark Wash Buffer concentrate	Qiagen UK, Manchester
NaOH	Sigma-Aldrich Company Ltd., Dorset, UK

TSAP Thermosensitive Alkaline Phosphatase	Promega UK, Southampton
Exonuclease I	Fisher Scientific UK Ltd., Loughborough
BigDye® Terminator v3.1 Cycle Sequencing	Fisher Scientific UK Ltd., Loughborough
Performa® DTR V3 96-Well Short Plate	EdgeBio, San Jose, CA, USA

2.3.4 Cloning and transformation

Agencourt®AMPure®XP	Beckman Coulter UK Ltd., High Wycombe
PCR polishing kit	Agilent Technologies UK, Stockport
T4 DNA ligase	Promega UK, Southampton
Restriction enzymes	New England Biolabs UK Ltd., Hitchin
2x ligation buffer	Promega UK, Southampton
JM109 competent cells	Promega UK, Southampton
SOC medium	Sigma-Aldrich Company Ltd., Dorset, UK
Bacto™ Agar	BD Biosciences UK, Oxford
Bacto™ Tryptone	BD Biosciences UK, Oxford
Bacto™ Yeast Extract	BD Biosciences UK, Oxford
NaCl	Sigma-Aldrich Company Ltd., Dorset, UK
Ampicillin (100mg/ml)	Sigma-Aldrich Company Ltd., Dorset, UK
Glycerol	Sigma-Aldrich Company Ltd., Dorset, UK

2.4 Clinical Data

2.4.1 Mitochondrial Disease Patient Cohort (UK)

The MRC-funded Mitochondrial Disease Patient Cohort Study is run by The National Commissioning Group (NCG) for Rare Mitochondrial Diseases of Adults and Children. The study aims to recruit a cohort of 1500 patients with clinically diagnosed mitochondrial disease. This cohort is managed by the MRC centre for translational research in Neuromuscular Disease. To date (31/08/2016), there are a total of 1383 patients in the cohort, with 373 (26.9%) diagnosed with the m.3243A>G point mutation and 172 (12.4%) with single, large-scale mtDNA deletions. Clinical details, including Newcastle Mitochondrial Disease Adult Scale (NMDAS) scores, of patients who have given fully informed consent are stored on a secure database and can be accessed by authorised individuals only. This resource was accessed for this study for the purpose of monitoring the progression of clinical symptoms for a selection of patients with m.3243A>G or single, large-scale mtDNA

deletion mutations, which required collating all available NMDAS evaluation scores on record.

2.4.2 Newcastle Mitochondrial Disease Adult Scale (NMDAS)

Evaluating the course and progression of mitochondrial disease is complicated by the diverse spectrum of clinical symptoms presented by patients, which can range greatly in terms of severity. The NMDAS is a validated clinical tool (Schaefer *et al.,* 2006) used in practice since 2005 to quantitatively evaluate the clinical status of patients with mitochondrial disease. The assessment is split into three sections focussing on 1) a subjective report on current function as completed by the patient, 2) system specific involvement to be determined by both the patient and clinician and 3) a subjective clinical assessment. In all there are 29 fields, each assigned a score of 0-5 with 0 indicating normal function and 5 reflecting the poorest level of function in this field, generating a maximum total score of 145 (Appendix I). Data collected from NMDAS assessments are stored in the MRC Mitochondrial Disease Cohort Database (http://mitocohort.ncl.ac.uk). All recorded NMDAS data for patients involved in this project were accessed in order to quantitatively assess clinical progression. In all cases, the measure for respiratory function was removed from the NMDAS evaluation due to concerns regarding the reliability of spirometry in the measurement of forced vital capacity (FVC) for this score. Further information on the use of NMDAS scores will be given in later chapters.

2.4.3 Ethical approval for use of Human Tissue

Access to tissue excess to diagnostic requirements and consented for use in research, stored in the NHS Highly Specialised Mitochondrial Diagnostic Service, was granted by Newcastle and North Tyneside 1 Research Ethics Committee (reference 2002/205). The assessment of patients and collection of skeletal muscle biopsies for use in the investigation of mitochondrial disease progression was approved by the Newcastle and North Tyneside 2 Research Ethics Committee (reference 11/NE/0337). Ethical approval for storage of this tissue was granted by the Newcastle and North Tyneside 1 Research Ethics Committee (reference 08/H0906/28+5). The collection of control tissue samples for DNA extraction was approved by Newcastle and North Tyneside 1 Research Ethics Committee (reference 12/NE/0395). Ethical approval for the use of patient and control tissue for the single-fibre study was granted by the Newcastle and North Tyneside Local Research Ethics Committees (reference 09/H0906/75). All experiments were carried out in accordance with the approved

guidelines and written informed consent was received from all participants prior to beginning the study.

2.5 Immunohistochemical Methods

2.5.1 Cryosectioning

Skeletal muscle blocks obtained by needle biopsy were snap-frozen by immersion in iso-pentane (Merck) cooled to -160°C using liquid nitrogen (BOC). Samples were then stored at -80°C in the NHS Highly Specialised Rare Mitochondrial Disease Laboratory with restricted access. Frozen skeletal muscle biopsy blocks were mounted in a transverse orientation onto Whatman filter paper using OCT cryo-embedding matrix (Raymond Lamb). Sections of varying thickness (10-20µm), depending on the subsequent protocol, were cut onto glass slides using the Cryo-star HM 560M cryostat which was maintained at -20°C. Skeletal muscle sections were left to air dry at room temperature for one hour before storing at -80°C until required for further use.

2.5.2 Immunofluorescent histochemistry of frozen tissue for detection of OXPHOS subunits

This protocol is reported and described in detail by Rocha *et al*., (2015). Skeletal muscle sections were removed from storage at –80°C and left to air dry for one hour at room temperature. A hydrophobic pen was used to draw a liquid-blocking border around each section to prevent the antibody cocktail from running off the section during later incubations. Sections were fixed in cold 4% paraformaldehyde (PFA) for three minutes. After washing in 1xTBST (section 2.2.5) for five minutes, sections were permeabilised via a methanol gradient. This consisted of placing the sections in 70% methanol for 10 minutes, 95% methanol for 10 minutes and then 100% methanol for 10 minutes before repeating this sequence in reverse (100% methanol for 10 minutes, 95% methanol for 10 minutes and then 70% methanol for 10 minutes). Following the methanol gradient, sections were washed three times in 1xTBST, each for five minutes. 100µl of 10% normal goat serum (NGS) were applied to each section and left for one hour at room temperature in a humidified chamber for blocking. Sections were then incubated with the primary antibody cocktail for laminin, COX-I, VDAC1, NDUFB8 (Table 2.1) overnight at 4°C in a humidified chamber. No OXPHOS control (NOC) sections were incubated with laminin antibody only, under the same conditions.

After washing with 1xTBST (3x five minutes), all sections were incubated with a cocktail of secondary antibodies (Alexa Fluor® 405nm or 750nm, with 488nm, 546nm and biotinylated IgG1) (Table2.1) for two hours at 4°C and subsequently with streptavadin conjugated with Alexa-Fluor 647 for two hours at 4°C. Finally, sections were washed with 1xTBST and mounted in Prolong Gold mounting media. Mounted sections were left to dry for one hour at room temperature before storing at -20°C until imaging.

Antibody	Host	Dilution	Company (cat.no.)
Primary antibodies			
Laminin (IgG)	Rabbit	1:50	Sigma-Aldrich (L9393)
COX-I (IgG2a)	Mouse	1:100	Abcam (Ab14705)
VDAC1 (IgG2b)	Mouse	1:100	Abcam (Ab14734)
NDUFB8 (IgG1)	Mouse	1:100	Abcam (Ab110242)
Secondary antibodies			
Anti-rabbit IgG (H+L) Alexa Fluor® 405nm	Goat	1:200	ThermoFisher Scientific (A-31556)
Anti-Rabbit IgG (H+L) Alexa Fluor® 750nm	Goat	1:200	ThermoFisher Scientific (A- 21039)
Anti-mouse IgG2a Alexa Fluor® 488nm	Goat	1:200	ThermoFisher Scientific (A-2113)
Anti-mouse IgG2b Alexa Fluor® 546nm	Goat	1:200	ThermoFisher Scientific (A-21143)
Anti-mouse IgG1– Biotin-XX	Goat	1:200	ThermoFisher Scientific (A10519)
Streptavadin, Alexa Fluor® 647nm	Goat	1:100	ThermoFisher Scientific (S32357)

Table 2.1: Antibodies for immunofluorescent detection of OXPHOS complexes.

2.5.3 Immunofluorescent histochemistry for determining muscle fibre type

20µm sections of skeletal muscle were removed from storage at -80°C and left to dry at room temperature for up to one hour. A hydrophobic pen was used to draw a border around each section. After washing briefly in 1xTBST, 100µl of 5% NGS were applied to each section as a blocking agent for one hour at room temperature. A cocktail of primary antibodies diluted in 5% NGS(Table 2.2) was then applied to each section, which were left to incubate overnight at 4°C in a humidified chamber.

Sections were washed in 1xTBST three times, each for five minutes, before incubation with a cocktail of secondary antibodies (Table 2.2) for 150 minutes at 4°C in a dark, humidified chamber. Whilst kept in the dark, sections were washed three times in 1xTBST, each for five minutes, and coverslips mounted using Prolong Gold mounting media. Sections were left to dry in the dark at room temperature for one hour before storing at 4°C until imaging.

Antibody	Host	Dilution	Company (cat.no.)
Primary antibodies			
Laminin (IgG)	Rabbit	1:50	Sigma-Aldrich (L9393)
BA-F8-s (IgG2b) = MHC slow type I	Mouse	1:200	DSHB (11/5/15-43µg/ml)
SC-71-s (IgG1) = MHC type IIa	Mouse	1:200	DSHB (3/3/16-26µg/ml)
6H1-s (IgM) = MHC type IIx	Mouse	1:15	DSHB (4/7/16-64µg/ml)
Secondary antibodies			
Anti-rabbit IgG (H+L) Alexa Fluor® - 405nm	Goat	1:200	ThermoFisher Scientific (A-31556)
Anti-mouse IgG2b Alexa Fluor® – 488nm	Goat	1:200	ThermoFisher Scientific (A-21141)
Anti-mouse IgG1 Alexa Fluor® – 546nm	Goat	1:200	ThermoFisher Scientific (A-21123)
Anti-mouse IgM Alexa fluor – 647nm	Goat	1:200	ThermoFisher Scientific (A21238)

Table 2.2: Antibodies for immunofluorescent detection of skeletal muscle fibre types. Primary antibodies against myosin heavy chains (MHC), shown with their associated fibre types, were provided by the Developmental Studies Hybridoma Bank (DSHB).

2.5.4 Immunofluorescent microscopy

Fluorescent images of skeletal muscle biopsies were captured at 20x magnification using an Axio Imager M1 microscope (Carl Zeiss), fitted with an AxioCam MRm monochrome digital camera and filter cubes suitable for detection of light at 405nm, 488nm, 546nm, 647nm and 750nm. This microscope was also equipped with a motorised stage allowing for tiled mosaic images of complete muscle biopsy sections to be captured. Images were acquired using Zen 2 (Blue edition) software, with the Tiles and Positions module enabled for mosaic images. Exposure times were set for each channel to avoid pixel saturation and were kept consistent across all sections within a staining batch. Images were stored as .czi files and exported to

uncompressed Tagged Image File Format (tiff). Mosaic images were first stitched in Zen 2 processing suite before saving and exporting as previously described.

2.5.5 Densitometric analysis using Imaris software

For earlier experiments (detailed in chapters three and four) stitched .czi files were opened in Imaris software (version 7.7.2, Bitplane). A surface was created over the 405nm channel to form a mask over laminin-positive muscle fibre boundaries. A second surface was then added, based around the first, which created a layer over the remaining image. Unwanted areas of the second surface, i.e. those covering blood vessels or nerves, were manually removed leaving only those covering individual muscle fibres. The mean optical density (OD) of each channel was measured in the OXPHOS stained sections using this software (ODCOX-I, ODNDUFB8, ODporin). Measurement of ODCOX-I, ODNDUFB8 and ODporin in the NOC sections was also made as an indication of background signal intensity. Data were saved as a .csv file for upload to R studio inc. (version 0.97.551***)***.

2.5.6 Densitometric analysis using ImmunoAnalyser Software

In more recent experiments (described in chapter five), stitched .czi files were uploaded to an in-house designed software coded in MatLab R2015a (Mathworks), herein referred to as ImmunoAnalyser, designed by Dr John Grady. Low resolution .jpg images were created for each channel, as well as merged channels 1, 2 and 3 and channels 2, 3 and 4. Muscle fibre boundaries were automatically mapped using the .jpg file for the laminin channel by contrast analysis and size selection. Any fibres missed by the automated process were manually drawn and added to the map. A surface was then created over each muscle fibre using the boundary map as a guide. This was applied to the .jpg files of individual channels so that OD measurements for each channel could be made for each muscle fibre. OD data were saved as a .csv file format for upload to the Mitochondrial Immunofluorescence Analysis online tool (http://research.ncl.ac.uk/mitoresearch/).

2.5.7 Data analysis

Analysis of OD data from Imaris software was performed by R studio using a script written and developed by Dr John Grady. More recent experimental data collected using the ImmunoAnalyser was analysed by the Mitochondrial Immunofluorescence Analysis online

tool. Both these methods perform the same analysis of the raw OD data. OD were corrected for background signal (as described in Rocha *et al.,* 2015) and log transformed to normalise the data (OD_TCOX-I, OD_TNDUFB8, OD_Tporin). An equal number of fibres was randomly sampled from each control biopsy and plots of OD_TCOX-I vs OD_Tporin and OD_TNDUFB8 vs OD_Tporin were generated. Linear regression analyses of these data provided a predicted level of COX-I and NDUFB8 for each fibre based on its porin level. An estimation of the deviation of the level of COX-I and NDUFB8 from this predicted level is presented as a z_score, used to classify fibres as shown in Table 2.3.

Classification	z_score boundaries (sd)
Porin	
Very low	z<-3.0
Low	-3.0<z<-2.0
Normal	-2.0<z<+2.0
High	+2.0<z<+3.0
Very high	z>+3.0
COX-I and NDUFB8	
Positive	z>-3.0
Intermediate positive	-4.5<z<-3.0
Intermediate negative	-6.0<z<-4.5
Negative	z<-6.0

Table 2.3: Fibre classifications based on z_scores. Individual fibres are classified based on z-score boundaries (sd=standard deviations) for porin, COX-I and NDUFB8.

2.6 Single cell laser capture microdissection

2.6.1 Preparation of muscle sections for single cell laser microdissection

20µm thick sections of skeletal muscle were cut onto glass slides and stored at -80°C until subjected to immunofluorescence staining protocols. After imaging, these sections were placed in 1x PBS (one PBS tablet per 100ml dH_2O) and left on a rocking platform at 4°C overnight to remove the coverslips. Sections were then dehydrated by immersion in an ethanol gradient (70% ethanol for 10 minutes; 95% ethanol for 10 minutes; 100% ethanol for 10 minutes, 100% ethanol for 10 minutes) before storing at -20°C until ready for single cell laser microdissection.

2.6.2 Laser capture microdissection of single muscle fibres

Sections were left to dry at room temperature for one hour. Laser microdissection was carried out using the PALM Microbeam system (Zeiss). Laser settings were calibrated using control tissue of the same thickness. Selected fibres were drawn around at 20x magnification using PALM RoboSoftware 4.6 (Zeiss) and laser microdissected into 15µl lysis buffer (section 2.2.4), with one fibre placed into each 0.2ml PCR tube (Figure 2.1). PCR tubes containing single fibres were kept on ice before centrifugation at 16800rcf to remove contents from the caps.

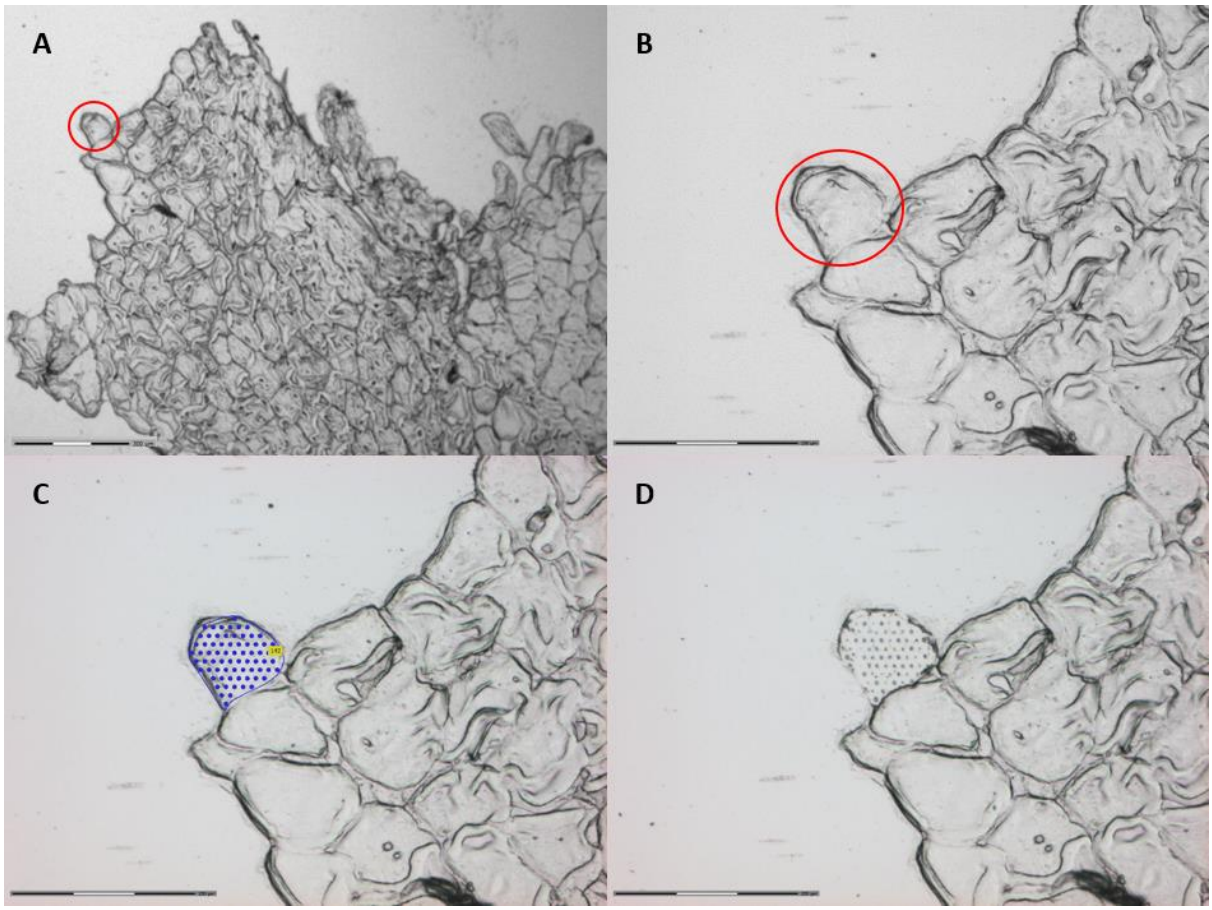

Figure 2.1: Isolation of single muscle fibres by laser capture microdissection. Muscle sections (20µm thick) were viewed using the PALM Microbeam system at 5x magnification to locate fibres of interest (encircled) (A). The fibre of interest was viewed at 20x magnification (B) and traced around, the solid blue line indicating the cut path of the laser (C). The fibre is removed into the cap of 0.2ml PCR tube containing lysis buffer (D). Scale bars: 5x magnification = 300µm; 20X magnification = 150µm.

2.6.3 Single cell lysis

0.2ml PCR tubes containing 15µl lysis buffer and single laser-microdissected muscle fibres were placed on an ABI Veriti 96-well thermal cycler (Applied Biosystems). The lysis reaction was carried out under the conditions described in Table 2.4. Following lysis, samples were stored at -80°C until use in further molecular genetic protocols.

	Temperature	Duration
Activation of proteinase K enzyme	55°C	3 hours
Deactivation of proteinase K enzyme	95°C	10 minutes

Table 2.4: Single cell lysis reaction conditions.

2.7 DNA extraction from human tissues

2.7.1 Homogenisation of frozen skeletal muscle

Before beginning the tissue homogenisation, an empty 1.5ml microcentrifuge tube was weighed. Muscle was placed in a porcelain mortar, chilled with liquid nitrogen, and manually ground with a porcelain pestle. Liquid nitrogen was used to keep the samples and instruments cool throughout the process. Powdered tissue was transferred to a 1.5ml microcentrifuge tube using a chilled scalpel. The microcentrifuge tube was then re-weighed and the sample mass calculated. A maximum of 25mg of muscle tissue was accepted for each 1.5ml microcentrifuge tube, with any excess removed to another tube. In between stages of this process, muscle tissue samples were kept in liquid nitrogen.

2.7.2 DNA purification from frozen skeletal muscle

Isolation of DNA from homogenised skeletal muscle samples was performed using a QIAamp DNA Mini Kit (Qiagen) according to the manufacturer's guidelines as outlined in the 'DNA Purification from Tissues' protocol in the QIAamp DNA Mini and Blood Mini Handbook (06/2012). For the final elution stage, 100µl Buffer AE were added to the centre of the membrane and allowed to incubate at room temperature for five minutes before centrifugation at full speed for one minute.

2.7.3 DNA purification from urine

Urine samples were collected in 50ml Falcon tubes and centrifuged at 160rcf for 10 minutes to generate a pellet of urinary sediment. The supernatant was removed and the pellet was re-suspended in 1ml sterile PBS. DNA was extracted from the urinary sediment using a QIAamp DNA Micro Kit (Qiagen) according to the manufacturer's guidelines, outlined in the protocol 'Isolation of Genomic DNA from Urine' (QIAamp DNA Micro Handbook 12/2014). For elution of DNA from the spin column, 50µl of Buffer AE were added to the centre of the membrane and left to incubate at room temperature for five minutes before centrifugation at full speed for one minute.

2.7.4 DNA purification from buccal swabs

Dacron buccal swabs were separated from the stick using scissors into a 2ml microcentrifuge tube. DNA was extracted from buccal swabs using a QIAamp DNA Mini Kit (Qiagen) as outlined in the manufacturer's guidelines 'DNA purification from Buccal Swabs (Spin Protocol)' (QIAamp DNA Mini and Blood Mini Handbook 05/2016). Following the spin column purification, outlined in steps 1-9 of the protocol, 100µl buffer AE were added for elution of DNA instead of 150µl. This was to increase the final DNA concentration.

2.7.5 DNA purification from hair

Hair samples were cut to approximately 2cm lengths into 2ml microcentrifuge tubes with 150µl sterile PBS. DNA was isolated from these samples using the QIAamp DNA Micro Kit (Qiagen) by adapting the manufacturer's protocol for 'Isolation of Genomic DNA from Laser-Microdissected Tissues' (QIAamp DNA Micro Handbook 12/2014). 300µl buffer ATL were added along with 20µl proteinase K and the sample was mixed by pulse-vortexing for 15 seconds before being placed in a thermomixer to incubate at 56°C for three hours. Following centrifugation to remove drops from the lid, a further 250µl buffer ATL were added to the sample with 50µl buffer AL. The solution was thoroughly mixed by pulse vortexing for 15 seconds to ensure sufficient lysis. 50µl 10% ethanol were added to the sample, which was then mixed by pulse-vortexing and incubated for five minutes at room temperature. Again, the sample was centrifuged to remove any liquid from the cap. The lysate was transferred to the QIAamp MinElute column without wetting the rim and centrifuged at 5510rcf for one minute. Flow-through was discarded and the spin column placed in a clean 2ml collection tube. 500µl Buffer AW1 were added to the spin column and then centrifuged at 5510rcf for

one minute. After discarding flow through and placing the column in a clean collection tube, the step was repeated with 500µl Buffer AW2. To dry the membrane, the spin column was centrifuged at full speed (16873rcf) for three minutes while empty. The column was then transferred to a clean 1.5ml microcentrifuge tube and 50µl Buffer AE added to the centre of the membrane. This was left to incubate at room temperature for five minutes to maximise the DNA yield before a final centrifugation step at 16873rcf for one minute.

2.7.6 DNA purification from whole blood

Isolation of DNA from human blood samples was performed using a QIAamp DNA Mini Kit (Qiagen). 40µl proteinase K were added to 600µl whole blood sample along with 600µl Buffer AL. After pulse vortexing for 15 seconds to mix, the sample was incubated at 56°C for 10 minutes while shaking using a Thermomixer (Eppendorf). Droplets were removed from the lid by centrifugation and 600µl 100% ethanol added to the sample before pulse-vortexing and centrifugation once more. 600µl sample was transferred to the spin column, without wetting the rim, and centrifuged at 5510rcf for one minute. This step was repeated until the entire sample had been passed through the spin column. The remaining steps follow the manufacturer's protocol as outlined in the QIAamp DNA Mini and Blood Mini Handbook (05/2016), eluting into a final volume of 100µl Buffer AE.

2.7.7 DNA concentration and storage

The concentration of DNA extracted from homogenate tissues was measured using the Nanodrop ND-1000 spectrophotometer (Labtech International). Extracted DNA was stored as 10µl aliquots at -20°C, or -80°C for long-term storage.

2.8 Real time PCR

2.8.1 Preparation of reagents

All primers used in real time PCRs (polymerase chain reactions) were reconstituted using nuclease-free water under the Microflow OMNI PCR workstation (ASTEC). Primer and probe stocks were then diluted in nuclease free water to 10µM and 5µM working stocks, respectively, and stored at -20°C in 100µl aliquots. Prior to use, the 96-well plate, adhesive film, microcentrifuge tubes and nuclease-free water were placed in a PCR UV cabinet (Bio Air Instruments) for at least 30 minutes to reduce contamination.

2.8.2 Standard curves

A standard curve consisting of a 10-fold serial dilution of plasmid DNA was loaded in triplicate on each plate. A number of plasmids were engineered for the creation of standard curves for the various real time PCR assays used in this project (Table 2.5). Plasmids p.7D1 and p.7D1.β2M were engineered by Dr Helen Tuppen prior to the start of this work. A detailed protocol for the creation of plasmids p.MTCN1 and p.MTCN2 is provided in chapter six.

Plasmid	Genes
p.7D1	*MT-ND1*, *MT-ND4*, *MT-Dloop*
p.7D1.β2M	*MT-ND1*, *MT-ND4*, *MT-Dloop*, *β2M*
p.MTCN1	*MT-ND1*, *MT-ND4*, *MT-Dloop*, *β2M*, *RNA18S*
p.MTCN2	*MT-ND1*, *MT-ND4*, *MT-Dloop*, *β2M*, *RNA18S*, *MT-RNR2*, *GAPDH*

Table 2.5: Plasmids engineered for use as standard curve DNA.

Average Cq values for each standard were plotted against the dilution factor on a base-10 semi-logarithmic plot and a line of best fit applied. This graph was used to calculate the reaction efficiency using Equation 2.8:

$$E = 10^{-\frac{1}{slope}}$$

$$\%\, Efficiency = (E - 1) * 100$$

Equation 2.8: Calculating efficiency of real-time PCR reactions. E=efficiency; slope = gradient of standard curve.

The standard curve was accepted if $R^2 > 0.990$ and the reaction efficiency was between 90-110% (represented by a gradient of -3.1 to -3.5). This was then used for absolute quantification of sample genes.

2.8.3 mtDNA deletion level assay

Deletion level was determined using multiplex *MT-ND1*/*MT-ND4* Taqman® real-time PCR assay, as previously described by Krishnan et al. (2007). Primers and probes used in this protocol are detailed in Table 2.6. 5µl sample DNA were added to 15µl of mastermix,

consisting of 10µl TaqMan® Universal Master Mix II (with UNG), 300nM forward and reverse primers for *MT-ND1* and *MT-ND4*, 100nM molecular probes for *MT-ND1* and *MT-ND4* and nuclease-free water. Patient DNA samples were used at approximately 0.01ng/µl, in order to produce a Cq value between 20-30 and within the range of the standard curve. Plates were sealed with adhesive film and mixed thoroughly by vortexing for 10 seconds. The plate underwent centrifugation at 300rcf for two minutes before loading into the ABI StepOnePlus™ Real-Time PCR System (Applied Biosystems). The reaction was carried out under the cycling conditions in Table 2.7. Data were analysed using ABI StepOne software v2.0 (Applied Biosystems).

Target	Position	Sequence	Tm(°C)	Length (nt)	%GC
Primers					
*MT-ND1*_F	nt.3485-3504	5’-CCCTAAAACCCGCCACATCT-3’	58.5	20	55
*MT-ND1*_R	nt.3553-3532	5’-GAGCGATGGTGAGAGCTAAGGT-3’	60.0	22	55
*MT-ND4*_F	nt.12087–12109	5’-CCATTCTCCTCCTATCCCTCAAC-3	57.9	23	52
*MT-ND4*_R	nt.12170–12140	5’–CACAATCTGATGTTTTGGTTAAACTATATTT-3’	52.5	31	26
β2M _F	nt.8969-8990	5’-CCAGCAGAGAATGGAAAGTCAA -3’	55.8	22	45
β2M _R	nt.9064-9037	5’-TCTCTCTCCATTCTTCAGTAAGTCAACT-3’	57.4	28	40
Probes					
MT-ND1	nt.2966-2987	VIC-5’-CCATCACCCTCTACATCACCGCCC-3’-MGB	64.2	24	63
MT-ND4	nt.12111–12138	6FAM-5’-CCGACATCATTACCGGGTTTTCCTCTTG-3’-MGB	61.6	28	50
β2M	nt.9006-9032	6FAM-5’-ATGTGTCTGGGTTTCATCCATCCGACA-3’-MGB	61.7	27	48

Table 2.6: Primers and probes used in standard real-time PCR protocols. F=forward, R=reverse primers; GenBank accession numbers: *MT-ND1* and *MT-ND4* = NC_012920.1 (Revised Cambridge Reference Sequence (rCRS)); *β2M* = NG_012920.1. Tm=melting temperature.

Process	Temperature (°C)	Time	Cycles
UNG amperase activity	50°C	2 minutes	1 cycle
Initial denaturation	95°C	10 minutes	1 cycle
Denaturation	95°C	15 seconds	40 cycles
Primer annealing and Extension	60°C	1 minute	

Table 2.7: Cycling conditions for real-time PCR reactions.

2.8.4 Determining mtDNA copy number in homogenate tissue

In homogenate skeletal muscle DNA samples, total mtDNA copy number was calculated as the ratio of the number of copies of the mitochondrial *MT-ND1* gene to the single-copy nuclear gene *β2M*. A singleplex Taqman® real-time PCR assay was used to measure the level of *β2M*. 5µl sample DNA at concentration 1ng/µl were added to 15µl of mastermix containing 10µl TaqMan® Universal Master Mix II (with UNG), 300nM forward and reverse primers for *β2M* (Table 2.6), 100nM molecular probes for *β2M*, 3mM $MgCl_2$ and nuclease-free water.

MT-ND1 copy number was measured in a separate reaction using sample DNA at a concentration 1:100 that used for the *β2M* assay. This was necessary due to the vast difference in the abundance of these two genes in the sample. By using different sample concentrations, Cq values for both genes were comparable and within the optimum range of 20-30. This dilution factor was addressed and accounted for during the final calculations. 5µl diluted sample DNA were added to 15µl of mastermix, consisting of 10µl TaqMan® Universal Master Mix II (with UNG), 300nM forward and reverse primers for *MT-ND1* (Table 2.6), 100nM molecular probes for *MT-ND1* and nuclease-free water. Plates were sealed and underwent vortexing and centrifugation before the reaction was carried out as described in section 2.8.3.

Levels of *MT-ND1* and *β2M* were measured using the standard curve method. *MT-ND1* copy number was multiplied by 100 to account for the relative dilution factor against *β2M*. The ratio of *MT-ND1*:*β2M* was calculated to indicate the number of copies of mtDNA present per copy of the *β2M* gene. The *β2M* gene is a single copy gene and so to account for its presence on both chromosomes the ratio of *MT-ND1*:*β2M* was doubled, giving the total copies of

mtDNA present per nucleus. It is important to note that this figure does not reflect the total mtDNA copy number per cell as skeletal muscle fibres are multinucleated.

2.9 Pyrosequencing

2.9.1 Pre-pyrosequencing PCR

To determine heteroplasmy levels of *m.3243A>G* mutation, a fragment of 210bp length spanning the mutation site was generated and amplified using primers described in Table 2.8. The PCR mastermix (1x) consisted of 5µl 5x GoTaq Flexibuffer, 2mM $MgCl_2$, 0.2µl GoTaq Hot Start Polymerase (GoTaq® Hot Start Polymerase Kit, Promega), 1nM dNTPs (Roche), 500nM 5'-biotin forward and reverse primer (IDT) made up to volume with 13.8µl DEPC-treated water (Life Technologies). 1µl sample DNA was added to 24µl mastermix per well, in triplicate. A positive control, with known heteroplasmy level of 85%, and negative control with 0% heteroplasmy were also run in triplicate alongside a no template control. The reaction was carried out on an ABI Veriti 96-well thermal cycler (Applied Biosystems) with run conditions as listed in Table 2.9.

5µl PCR product were electrophoresed through a 2.0% agarose gel containing SYBR® Safe DNA Gel Stain (4µl per 100ml) (Invitrogen). Samples were mixed with 1µl loading dye (section2.2.1) and loaded alongside 100bp DNA ladder. Gels were placed in electrophoresis buffer (section 2.2.3) at 120V for approximately 30 minutes. Amplicons were visualised using the ChemiDoc MP imaging system (Biorad). PCR products were stored at 4°C for use in the pyrosequencing protocol.

Primer	Position	Sequence	Tm (°C)	Length	%GC
F	nt.3143-3163	5'-TAAGGCCTACTTCACAAAGCG-3’	55.8	21	48
R	nt.3353-3331	5'-GCGATTAGAATGGGTACAATGAG-3’	54.8	23	43
S	nt.3258-3244	5'-ATGCGATTACCGGGC-3’	53.9	15	60

Table 2.8: Primers used for pyrosequencing protocol. F=forward; R=reverse; S=sequencing. GenBank accession number NC_012920.1 (rCRS).

Process	Temperature	Duration	Cycles
Initial Denaturation	95ºC	10 minutes	1
Denaturation	95ºC	30 seconds	
Primer annealing	62ºC	30 seconds	30
Extension	72ºC	1 minute/kb	
Final Extension	72ºC	10 minutes	1
Hold	4ºC	∞	

Table 2.9: Cycling conditions for PCR step of-pyrosequencing protocol.

2.9.2 Post-PCR Pyrosequencing

Quantitative pyrosequencing was performed using the Pyromark Q24 platform (Qiagen). 10µl PCR product generated in section 2.9.1 were added to 70µl binding buffer mixture (2µl Sepharose beads, 40µl Binding Buffer, 28µl deionised water) per well of a 24-well plate. Binding of the amplicons to the Sepharose beads was facilitated by mechanical agitation on a shaking platform for 10 minutes. A handheld vacuum pump and compressor (Welch) were used to capture the beads and move them through sequential washes in 70% ethanol (five seconds), 0.2M NaOH (five seconds) and wash buffer (Qiagen). The beads were released into a shallow-well containing 25µl annealing buffer mixture (24.25µl annealing buffer, 300nM sequencing primer (Table 2.8)) and heated to 80°C for two minutes. Samples were left to cool at room temperature for at least five minutes to allow for annealing of the pyrosequencing primer.

Appropriate volumes of dNTPs, enzyme and substrate, as determined by Pyromark Q24 software, were aliquoted into the pyrosequencing cassette which was then loaded into the Q24 Pyrosequencer (Qiagen) along with the 24-shallow-well plate containing DNA. Pyromark Q24 software was used to calculate the heteroplasmy of the m.3243A>G mutation as described previously (White *et al*., 2005).

2.10 Cloning and transformation

2.10.1 Standard PCR for amplification of insert DNA

A fragment of DNA containing the locus of interest was generated by standard PCR amplification. 24µl mastermix (Table 2.10) were added to 0.2ml PCR tubes, followed by 1µl sample DNA. Tubes were pulse-vortexed 10 times and spun down at 8609rcf for 10 seconds

before placing into an ABI Veriti 96-well thermal cycler (Applied Biosystems) under the conditions described in Table 2.11.

Reagent	1x mastermix (24µl)
5x colourless GoTaq Flexi Buffer	5.00µl
$MgCl_2$ (25mM)	2.50µl
dNTPs (10mM, 2.5mM each)	2.50µl
Forward Primer (10µM)	1.00µl
Reverse Primer (10µM)	1.00µl
GoTaq G2 Flexi DNA polymerase (5U/µl)	0.13µl
DNA (1-100ng)	1.00µl

Table 2.10: Mastermix for standard PCR. GoTaq polymerase concentration is provided in units (U)/µl.

Process	Temperature	Duration	Cycles
Initial Denaturation	95ºC	2 minutes	1
Denaturation	95ºC	30 seconds	
Primer annealing	60ºC	30 seconds	33
Extension	72ºC	1minute/kb	
Final Extension	72ºC	7 minutes	1
Hold	4ºC	∞	

Table 2.11: Cycling conditions for standard PCR

2.10.2 Agarose gel electrophoresis

To visualise and confirm the results of PCR amplification, products were resolved by gel electrophoresis. 1µl loading dye (section 2.2.1) was added to 5µl amplicons before loading samples onto agarose gel (% agarose composition determined by amplicon size). The gel was submersed in electrophoresis buffer (section 2.2.3) and subjected to 120V for approximately 30 minutes to one hour, depending on amplicon size. Amplicons were visualised using the ChemiDoc MP imaging system and Image Lab software (BioRad).

2.10.3 DNA clean-up

PCR products generated in section 2.10.1 were made up to 50µl volume with nuclease free water. Agencourt®AMPure®XP beads were added to each sample, at 1.8x volume (90µl for 50µl sample DNA), mixed gently by pipetting and left at room temperature for five minutes. Samples underwent a pulse spin before being placed on a magnetic rack for three minutes to attract and localise the DNA-bound beads. The supernatant was removed and 500µl freshly-

made 70% ethanol was used to wash the beads for 30 seconds, rotating the tube to mix the sample while on the magnetic rack. The supernatant was removed and the wash step repeated. Once again, the ethanol supernatant was removed and the remaining sample spun down to remove any excess ethanol. The beads were then air-dried with an open cap for four minutes at room temperature before resuspension in 25µl nuclease-free water, mixed by vortex for 10 seconds and pulsed in the microcentrifuge. The sample was placed on the magnetic rack for one minute to separate the beads from the DNA in solution. The supernatant, containing the sample DNA, was removed to a microcentrifuge tube for assessment of concentration by Nanodrop and DNA polishing.

2.10.4 Polishing to create blunt-ended fragments

10µl of clean PCR amplicon, from 2.4.11.1, were added to 1µl 10mM dNTP mix (Takara), 1.3µl 10x polishing buffer and 1µl cloned Pfu DNA polymerase (PCR polishing kit, Agilent Technologies). The reaction mixture was incubated at 72° for 30 minutes using an ABI Veriti 96-well thermal cycler (Applied Biosystems).

2.10.5 Digestion/ligation reaction

Plasmid pcDNA^{TM}3.1 (ThermoFisher Scientific) was the original vector used for the construction of plasmid p.7D1 and p.7D1.β2M by Dr Helen Tuppen. Plasmids p.MTCN1 and p.MTCN2, engineered by myself for the work carried out in chapter six, used p.7D1.β2M and p.MTCN1 as vectors, respectively. For each vector the required quantity of insert fragment DNA was calculated using Equation 2.9.

$$\frac{ng\ of\ vector \times kb\ of\ insert}{kb\ of\ vector} \times insert{:}\ vector\ molar\ ratio\ = ng\ of\ insert$$

Equation 2.9: Calculating the insert fragment DNA concentration

For a 10µl reaction volume, the mastermix consisted of 5µl 2x ligation buffer, 1µl T4 DNA ligase (1-3units/µl), 0.5µl restriction enzyme (20units/µl) added to appropriate quantities of vector and insert, and made up to volume with nuclease free water. The reaction mixture was placed in a thermal cycler (Veriti 96 well thermal cycler, Applied Biosystems) for incubation at 37°C for one hour, followed by 10 minutes at 80°C for enzyme deactivation.

2.10.6 LB agar plates

Agar plates were produced using 1.5% w/v Bacto™ Agar, 1.0% w/v Bacto™ Tryptone, 0.5% w/v Bacto™ Yeast extract (BD), 1.0% w/v NaCl (Sigma) mixed in deionised water and autoclaved to approximately 120°C. After allowing the molten agar to cool to around 55°C, and in the proximity to a Bunsen burner flame, 0.1% v/v ampicillin (Sigma) was added and mixed by gentle shaking. Plates were poured and allowed to set before storing at 4°C for up to four weeks.

2.10.7 Transformation of competent cells

Competent JM109 cells (Promega) were thawed on ice in 50µl aliquots. 5µl ligation product were added to one aliquot of JM109 competent cells, referred to as the positive sample, with another aliquot kept as a negative plasmid control. Cells were left on ice for a further 20 minutes then given a heat shock at 42°C for 50 seconds before being returned to ice for two minutes. In proximity to a Bunsen burner flame, 950µl SOC medium were added to the positive and negative plasmid control aliquots, as well as a clean microcentrifuge tube to act as a negative cell control. Samples were placed in an orbital shaker (Sanyo) at 37°C for 90 minutes to allow for cell growth. Following incubation, samples were spun down at 583rcf for 10 minutes, the supernatant was removed and 100µl SOC medium were added to each sample in proximity to a flame. The positive sample was diluted to create 100µl of 10%, 20% and 70% solutions (using 10µl, 20µl and 70µl aliquots respectively, and making up to volume with SOC medium). 100µl of each of the positive dilutions and the negative plasmid and cell controls were plated on agar plates. An empty plate was set aside as a negative plating control. Plates were incubated at 37°C overnight.

2.10.8 Confirmation of insert

Approximately 50 individual colonies were picked from the 10% positive sample growth plate and streaked onto a grid plate. Plates were incubated at 37°C for eight hours to allow for sufficient growth of the colony clones. A portion of each clone was picked and lysed in 10µl nuclease free water by heating at 95°C for 10 minutes. Standard PCR was performed as described in 2.4.8.2 to confirm the presence of the fragment. Final confirmation of the insertion of the fragment was obtained by Sanger sequencing.

2.10.9 Sanger Sequencing

5µl PCR product were added in duplicate to wells of a 96-well plate. 1.5µl ExoSap (1µl 1U/µl TSAP with 0.5µl 20U/µl Exo1) were added to each well. The plate was covered, mixed by vortex machine and centrifuged before incubation for 15 minutes at 37°C followed by a further 15 minutes at 80°C in a thermal cycler. BigDye mastermix (3µl 5x sequencing buffer, 3µl BigDye, 1µl forward or reverse primer (10µM) and 7µl dH_2O) was made for each primer used in the PCR. 13µl BigDye mastermix were added to each well and the plate covered, mixed and spun down before loading onto an ABI Veriti 96-well thermal cycler (Applied Biosystems) with the run conditions described in Table 2.12.

To clean up the sequencing products, a Performa® DTR V3 96-Well Short Plate underwent centrifugation for five minutes to drain buffer from the wells into a clean 96-well plate. The PCR product was added to the appropriate wells of the Performa® DTR V3 96-Well Short Plate and collected into a clean 96-well plate via centrifugation for five minutes. The 96-well plate containing PCR products was loaded onto the ABI 3130xl Genetic Analyzer (Applied Biosystems) for sequencing according to the manufacturer's protocol. Sequences were visualised using Finch TV software (Geospizer).

Process	Temperature	Duration	Cycles
Initial Denaturation	96ºC	2 minutes	1
Denaturation	95ºC	30 seconds	
Primer annealing	60ºC	30 seconds	33
Extension	72ºC	1minute	
Final Extension	72ºC	7 minutes	1
Hold	4ºC	∞	

Table 2.12: Cycling conditions for PCR step of Sanger Sequencing protocol

2.10.10Glycerol stocks for long-term storage

After confirming the presence of the insert fragment in the plasmid, further material was picked from the corresponding colony clone on the grid plate into five 15ml Falcon tubes containing 5ml of LB broth (1.0% w/v Bacto™ Tryptone, 0.5% w/v Bacto™ Yeast extract (BD), 1.0% w/v NaCl (Sigma) with 0.1% v/v ampicillin). Tubes were incubated at 37°C overnight in a shaking incubator (Sanyo) along with a negative control of LB broth and ampicillin only. The following morning, 0.5ml LB culture was added to 30% glycerol LB broth and snap-frozen in liquid nitrogen. This glycerol stock was then transferred to -80°C freezers for long-term storage.

2.10.11DNA extraction from bacterial cultures

A QIAprep Spin Miniprep Kit (Qiagen) was used to extract DNA from the remaining LB culture. The tubes of overnight bacterial culture underwent centrifugation at 14549$_{rcf}$ for three minutes at room temperature to produce a single pellet. DNA extraction was then completed as per the manufacturer's guidelines detailed in 'Protocol: Plasmid DNA Purification using the QIAprep Spin Miniprep Kit and a Microcentrifuge' (QIAprep Miniprep Handbook 05/2012). The concentration of the extracted DNA product was measured using the Nanodrop. Aliquots of the final DNA extraction product were stored at -20°C for use in real-time PCR assays.

2.11 Statistical analysis

Statistical analysis was carried out in GraphPad Prism v5.02 (GraphPad Software Inc.) and Minitab 17.0 (Minitab Inc.) software. Normality of datasets was assessed prior to selection of parametric or non-parametric tests. Graphs featuring linear and non-linear regression analysis display 95% confidence intervals, unless otherwise stated. A statistically significant result is considered when $p<0.05$. Further information on the specific statistical tests applied will be provided in the relevant chapters.

Chapter 3: Disease progression in patients with the m.3243A>G *MT-TL1* transition mutation

3.1 Introduction

3.1.1 The m.3243A>G mutation: pathogenic mechanisms

The m.3243A>G transition mutation in *MT-TL1* was first described by Goto *et al.* (1990) using PCR techniques to sequence mitochondrial tRNA genes in 26 patients with mitochondrial encephalopathy lactic acidosis and stroke-like episodes (MELAS) and one with CPEO. This mutation affects nucleotides A14 and U8 in a highly conserved region of the dihydrouridine loop (D-loop) of mt-tRNA$^{Leu(UUR)}$ (Figure 3.1). Early studies using *trans*mitochondrial cybrid cells confirmed the presence of the m.3243A>G mutation resulted in compromised protein synthesis and respiratory chain activity (Chomyn *et al.,* 1992; King *et al.,* 1992). A number of pathogenic mechanisms underlying the cellular and clinical phenotypes associated with the m.3243A>G mutation have been suggested and are described below.

The earliest proposed mechanism was based upon altered transcription termination observed *in vitro* by Hess *et al.* (1991). The mTERF binding site spans a 28bp region of *MT-TL1* within which the m.3243A>G mutation lies (Kruse *et al.,* 1989). In the presence of the m.3243A>G mutation, Hess *et al.* (1991) report that binding of human mitochondrial transcription termination factor (mTERF) is compromised, possibly leading to altered synthesis of 16S and 12S rRNA. However, studies *in vivo* have not observed a defect in transcription termination, possibly due to a compensatory over-expression of mTERF or increase in transcription rate buffering the effect of reduced mTERF binding (Chomyn *et al.,* 1992; Koga *et al*., 1993).

It has also been suggested that a reduction in the availability of mt-tRNA$^{Leu(UUR)}$ could contribute to the pathogenicity of the m.3243A>G mutation. Börner *et al.* (2000) evaluated total and mutant populations of mtDNA, free mt-tRNA$^{Leu(UUR)}$ and aminoacylated mt-tRNA$^{Leu(UUR)}$ in 8 patients with the m.3243A>G mutation and MELAS/related symptoms (seven muscle biopsies and one lymphoblastoid cell line). In four patients, the proportion of

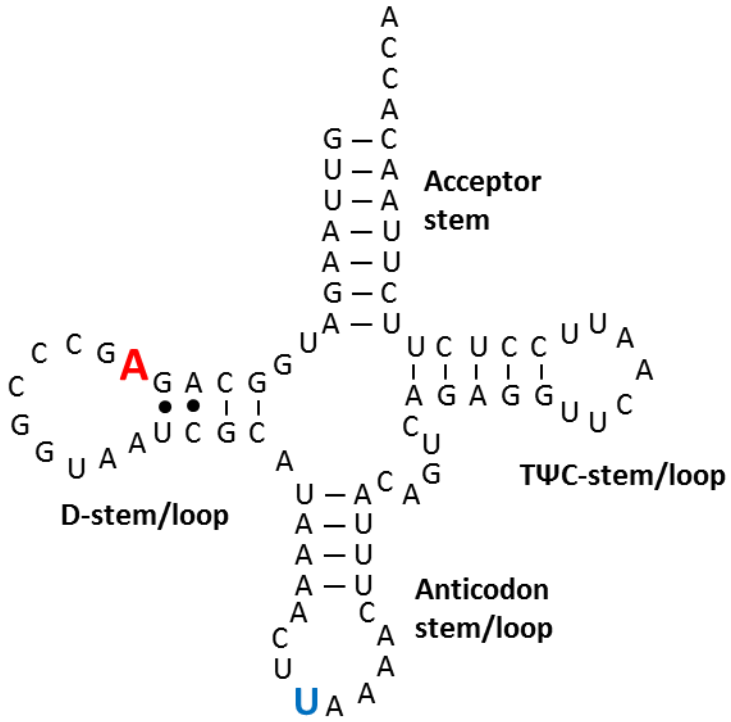

Figure 3.1: Cloverleaf structure of mt-tRNA$^{Leu(UUR)}$. The A14 residue of the D-loop (shown in red) is affected by the m.3243A>G mutation, in the presence of which it is substituted for a G- residue. The uridine residue situated at the wobble position (shown in blue) is subject to post-transcriptional modification to become 5-taurinomethyluridine (τm^{5}U). Adapted from Wittenhagen and Kelley (2002).

mutant tRNA$^{Leu(UUR)}$ in the total tRNA$^{Leu(UUR)}$ pool was decreased, compared to the proportion of mutant mtDNA present in the tissue. This suggested a reduction in expression of the mutant tRNA$^{Leu(UUR)}$ in half of the patients studied, and was not related to mtDNA heteroplasmy level. Furthermore, six patients showed a decrease in the proportion of aminoacylated mutant tRNA$^{Leu(UUR)}$ when compared to the mutant mtDNA level. Only one patient sample maintained equal proportions of mutant in mtDNA, tRNA$^{Leu(UUR)}$ and aminoacylated tRNA$^{Leu(UUR)}$. As such, the authors concluded that the mutation had a variable impact on the expression of mt-tRNA$^{Leu(UUR)}$ and the availability of the aminoacylated tRNA molecule across patients, alluding to the involvement of additional factors contributing to pathogenicity.

The effect of the m.3243A>G mutation on post-transcriptional modification of the mt-tRNA$^{Leu(UUR)}$ is central to another proposed mechanism of pathogenicity. It has been shown

in *trans*mitochondrial cybrid cells that the presence of this mutation prevents the taurine modification of uridine (5-taurinomethyluridine (τm^5U)) at the wobble position (Yasukawa *et al.,* 2000; Suzuki *et al.,* 2002). This modification reinforces the tertiary, L-shaped structure of mt- $tRNA^{Leu(UUR)}$ (Helm *et al.,* 1998), and is required to facilitate effective recognition of codons by the tRNA. Indeed, Kirino *et al.* (2004) have shown that $tRNA^{Leu(UUR)}$ molecules lacking the τm^5U modification resulted in a severe and specific reduction in UUG translation in *trans*mitochondrial cybrid cells. This indicated that the m.3243A>G mutation amplifies the translation defect, possibly due to the de-stabilisation of the tertiary structure of the tRNA. Of further interest, Kirino *et al.* (2004) note the high abundance of UUG codons in the *MT-ND6* gene, pertinent to the observation that complex I activity is often reduced in patients with m.3243A>G mutation (Goto *et al.,* 1992). However, others have reported no relationship between the translation of UUR codons and the synthesis of these mitochondrial proteins (Chomyn *et al.,* 1992).

Several mutations in the *MT-TL1* gene (m.3243A>G, m.3244G>A, m.3258T>C, m.3271T>C and m.3291T>C) associated with the MELAS phenotype have been shown to prevent the τm^5U modification (Kirino *et al.,* 2005). This study also reported normal τm^5U modification in patient tissue or *trans*mitochondrial cybrid lines harbouring alternative *MT-TL1* mutations associated with non-MELAS phenotypes (m.3242G>A, m.3250T>C, m.3254C>T and m.3280A>G). This would suggest a strong correlation between the clinical phenotype and the presence of the τm^5U modification. While this can be said for the MELAS phenotype studied by Kirino *et al.* (2005), it may not be the case for other phenotypes associated with the m.3243A>G mutation.

The final, and most recently proposed mechanism of pathogenicity is based on reports of tRNA dimerisation induced by the presence of the m.3243A>G mutation (Wittenhagen and Kelley, 2002). The mutation introduces a self-complementary hexanucleotide (5'GGGCCC; G= mutation site) into the conserved D-loop, disrupting the native tertiary structure and facilitating dimerisation of the tRNA. To characterise the molecular effects of the dimerisation, *in vitro* tests using tRNA constructs found a reduction in the aminoacylation activity in the presence of the mutation. This was partially rescued by the addition of a second mutation, designed to disrupt the dimerisation process. As aminoacylation was not

fully restored in the absence of the tRNA dimer, it was concluded that this mechanism was not exclusively the cause of m.3243A>G pathogenicity (Wittenhagen and Kelley, 2002).

3.1.2 Epidemiology and clinical features associated with the m.3242A>G mutation

The m.3243A>G *MT-TL1* transition mutation is the most prevalent point mutation of mtDNA, affecting an estimated 1 in 12,800 adults (Gorman *et al.,* 2015). The mutation was first described by Goto *et al.* (1990) in patients with MELAS, a term created by Pavlakis *et al.* (1984) to describe a phenotype distinct from KSS and MERRF. Unlike KSS, MELAS patients do not present with ophthalmoplegia or retinal degeneration. The phenotype also differs from MERRF by the absence of myoclonus (Pavlakis *et al*., 1984). Clinical criteria for the diagnosis of MELAS were outlined by Hirano *et al.* (1992); (i) stroke-like episodes occurring before 40 years of age, (ii) encephalopathy characterised by seizures, dementia or both and (iii) lactic acidosis, RRFs or both. In addition to the typical MELAS phenotype, additional common symptoms were identified as recurrent headaches, sensorineural hearing loss, short stature, ataxia, vomiting and blindness. The m.3243A>G mutation is now recognised as the most common cause of MELAS, accounting for up to 80% of cases (Goto *et al.,* 1991). In a recent study of 129 patients with m.3243A>G mutation recruited to the MRC Centre Mitochondrial Disease Cohort, Nesbitt *et al.* (2013) record only 10% of patients with this genotype presenting classical MELAS phenotype.

This mutation is also a cause of CPEO in patients who do not harbour single, large-scale mtDNA deletions (Moraes *et al.,* 1993), and was noted in the original account of the m.3243A>G mutation (Goto *et al.,* 1990). Nesbitt *et al.* (2013) report that CPEO in patients with m.3243A>G is most often seen in combination with a number of non-classical symptoms (6% of their cohort) such as proximal myopathy, ataxia and migraine. In 2% of patients, PEO is presented alongside MELAS.

The most common phenotype associated with this mutation is maternally inherited diabetes and deafness (MIDD). This syndrome was first recorded by van den Ouweland *et al.* (1992) during the study of an m.3243A>G pedigree with non-insulin dependent diabetes mellitus (NIDDM). The authors reported sensorineural hearing loss as a common additional symptom, which was later also observed in pedigrees from a Dutch/French NIDDM population. This phenotype was introduced as MIDD by van den Ouweland *et al.* (1994) and

has been described in association with a spectrum of clinical symptoms ranging including macular pattern dystrophy, cardiomyopathy and mitochondrial renal disease (Guillausseau *et al.,* 2001). MIDD was reported by Nesbitt *et al.* (2013) in 30% of cases with m.3243A>G mutation, the most commonly observed phenotype in this cohort. 5% of patients showed an overlap between MIDD and CPEO, while 6% presented a combination of MIDD and MELAS.

As well as the defined phenotypes described above, m.3243A>G mutation has been associated with non-classical syndromes, as noted for 28% of patients in Nesbitt *et al.* 2013. The clinical spectrum of these symptoms includes proximal myopathy (27%), ataxia (24%), migraine (23%) and seizures (18%). In addition to the wide range of clinical phenotypes associated with the m.3243A>G mutation, 9% of patients were recorded as asymptomatic. Given the diversity of clinical phenotypes accompanying this mutation, the molecular and cellular mechanisms driving disease progression are difficult to decipher and, as such, are poorly understood.

3.1.3 Genetic and biochemical features associated with m.3243A>G

Biochemical studies identify reduced activity of both complex I and complex IV in muscle biopsies from patients with m.3243A>G, although complex I seems to be more commonly affected. Out of 19 patients, Mariotti *et al.* (1995) report nine with reduced complex I activity, compared to just three with reduced complex IV. Similarly Goto *et al.* (1992) present compromised complex I activity in 13 out of 40 MELAS patients. Only seven patients in this group had low complex IV activity, four of which also saw complex I affected. Similar observations are made by Jeppesen *et al.* (2006) and Morgan-Hughes *et al.* (1995).

Unlike the histochemical findings, the relationship between biochemical activity and mutation load is not so consistently reported. While Mariotti *et al.,* (1995) describe a correlation between complex I activity and mutation level, no such relationship is seen for complex IV. Furthermore, a number of studies conclude no association between heteroplasmy level and complex I or –IV activity in m.3243A>G patients (Jeppesen *et al.,* 2006; Ciafaloni *et al.,* 1992; Morgan-Hughes *et al.,* 1995).

Post-mortem studies investigating the tissue-specific distribution of the m.3243A>G mutation have reported some conflicting findings. Ciafaloni *et al.* (1991) reported a uniform

segregation of the mutation across five tissues, yet Shiraiwa *et al.* (1993) noted a range of heteroplasmy levels from 22-95% across 32 tissues. Although a tissue-specific threshold of vulnerability is proposed by Ciafaloni *et al.* (1991), both studies conclude that a straightforward correlation between heteroplasmy level, organ dysfunction and clinical phenotype is non-existent.

The distribution of m.3243A>G among patient tissues has been shown to be non-random and tissue-specific by Chinnery *et al.* (1997), who also note a correlation between heteroplasmy level and the rate of cell turnover in a tissue. Analysis of samples from a 24-week old foetus showed little variation in mutant load across six tissues (Matthews *et al.,* 1994). The authors conclude that the tissue-specific distributions of the m.3243A>G mutation are likely due to selection pressures on the wild-type and mutant mtDNA species acting throughout life. The analysis of four adult tissues from three embryonic germ layers (buccal mucosa = ectoderm; leucocytes and skeletal muscle = mesoderm; urinary epithelium = endoderm) did show a range in heteroplasmy level across the tissue types and uniform distribution within germ layers (Frederikson *et al*., 2006).

The proportion of m.3243A>G mutation in patient tissue has been investigated by several studies using skeletal muscle biopsies. Typically, these studies compare patients displaying MELAS symptoms with those presenting milder phenotypes such as PEO (Moraes *et al.,* 1993; Petruzzella *et al.,* 1994; Mariotti *et al.,* 1995) and mitochondrial myopathy (Sylvestri *et al.,* 2000), with a higher mutation load unanimously observed in the more severely affected MELAS patients. This correlation between heteroplasmy level and disease severity was further supported by Koga *et al.* (2000), who observed decreasing mutation loads (measured in SKM) across five unrelated m.3243A>G probands with Leigh syndrome (92%), MELAS (74% & 87%), PEO (33%) and MIDD (5%).

Many studies have also quantified the proportion of COX-deficient and ragged-red fibres (RRFs) in patients by COX-histochemistry protocols. In general, the observed proportion of COX-deficient or –negative fibres in patients with m.3243A>G mutation is lower than that seen in patients harbouring single, large-scale or multiple mtDNA deletions (Zierz *et al.,* 2015). In patients with MELAS, the majority of RRFs are COX-positive, whereas COX-negative RRFs are predominant in PEO (Moraes *et al.,* 1993; Petruzzella *et al.,* 1994; Mariotti *et al.,*

1995) and myopathic phenotypes (Sylvestri *et al.,* 2000). Single fibre analyses performed by Petruzzella *et al.* (1994) and Sylvestri *et al.* (2000) show a higher level of heteroplasmy in COX-negative RRFs, declining in COX-positive RRFs and then further in COX-normal fibres. These findings indicate a potential relationship between the genetic status and respiratory chain deficiency of muscle fibres.

3.1.4 Disease progression and prognosis

Studying clinical progression in patients with m.3243A>G mutation is challenging due to the variety of phenotypes expressed and the fact that patients can present throughout life. It is important to consider that in addition to the worsening of existing symptoms over time, the emergence of new symptoms with age may contribute to overall disease progression. A few studies have evaluated clinical data from large cohorts in attempts to understand the relationships between different symptoms and how they manifest and progress over time in order to determine useful prognostic factors. One such study by Mancuso *et al*. (2014) showed common symptoms at disease onset to be hearing loss, generalised seizure and diabetes, with features including stroke-like episodes, muscle weakness, ataxia and cardiac involvement more common on follow-up assessment.

There have been very few genetic studies looking at changes in tissues harbouring the m.3243A>G mutation over time, and those that have predominantly focussed on blood samples (T'Hart *et al*., 1996; Rahman *et al*., 2001; Pyle *et al*., 2007; Mehrazin *et al*., 2009). These studies show a decrease in heteroplasmy in all patients (n= 69) at a rate of 0.6-1.4% per year. However, this is likely due to loss of the mutation in the highly replicative blood stem cells and may be very different in other tissues (McDonnell *et al.,* 2004). There have been only two longitudinal studies investigating changes in patient skeletal muscle biopsies, identifying a decrease in heteroplasmy in one patient (Kawakami *et al*., 1994) and increase in percentage COX-deficient fibres in another (Chinnery *et al*., 2003).

It is evident that disease progression in patients with m.3243A>G mutation is not a uniform experience with some patients showing a rapid decline in clinical condition while others can remain relatively stable for a number of years. Understanding the mechanisms behind disease progression can help identify prognostic factors which could improve the quality of

information available to patients regarding their expected clinical progression as well as informing clinicians on appropriate treatment strategies.

3.2 Aims

This longitudinal study used serial skeletal muscle biopsies, the "gold standard" tissue for diagnosis of mitochondrial disease, from patients with m.3243A>G mutation (n=6) over intervals of 4.0-14.3 years. The study aimed to determine whether any changes to (i) the nature or magnitude of the biochemical defect, (ii) heteroplasmy level or (iii) total mtDNA copy number are occurring over time and whether the behaviour of these genetic and cellular characteristics are associated with clinical disease progression, as measured using the Newcastle Mitochondrial Disease Adult Scale (NMDAS) (Schaefer *et al*., 2006).

3.3 Methods

3.3.1 Patients and controls

Patients with m.3243A>G mutation were selected from the MRC Centre Mitochondrial Disease Patient Cohort. Only six patients with this mutation had serial skeletal muscle biopsies available for use in this study (Table 3.1). Skeletal muscle biopsies collected from these patients for diagnostic purposes were approved for access by the Newcastle and North Tyneside 1 committee (REC 2005/202). Additional skeletal muscle biopsies required for this project were collected under REC reference 11/NE/0337 (Newcastle and North Tyneside 2), with informed signed consent from all participants, and stored at the NHS Highly Specialised Rare Mitochondrial Disease Laboratory in Newcastle (REC 08/H0906/28+5).

Three skeletal muscle biopsies were obtained from controls for use in this project (Table 3.2). Tissue from controls 1 and 2 was obtained following orthopaedic surgery with patient consent for the donation of tissue for use by Newcastle University for research purposes (REC 09/H1010/20 (NorthWest – Haydock. R&D number 5004)). Access to control 3 (disease control) was granted under REC reference 2005/202 as excess to diagnostic requirements.

Patient	Interval (years)	Biopsy one				Biopsy two			
		Age	Muscle	Symptoms	NMDAS	Age	Muscle	Symptoms	NMDAS
P1 (F)	4.0	54.6	LG	Mild hearing loss, GI dysmotility	4.0	58.6	LQ	Mild hearing loss, GI dysmotility, ataxia	4.2
P2 (F)	11.2	23.9	LQ	Ataxia	*R	35.1	LQ	Ataxia, deafness, SLE, myopathy, fatigue	8.5
P3 (M)	13.6	32.8	LQ	Asymptomatic	*R	46.4	RQ	Asymptomatic	0.0
P4 (M)	13.9	40.9	LG	Deafness, diabetes, fatigue	*R	54.8	RQ	Deafness, diabetes, fatigue, ataxia, myopathy, dysphonia/dysarthria	12.0
P5 (F)	14.2	29.3	LQ	N/A	*R	43.5	RQ	Diabetes, deafness, GI dysmotility, LVH	13.8
P6 (F)	14.3	59.1	RQ	Deafness, LVH, ptosis, myopathy, fatigue, migraine,	*R	73.4	LQ	Deafness, ataxia, LVH, ptosis, myopathy, fatigue	14.0

Table 3.1: Patients with m.3243A>G selected from the MRC Centre Mitochondrial Disease Patient Cohort. GI=Gastrointestinal; RQ=right quadriceps; LQ=left quadriceps; LG=left gastrocnemius; NMDAS=Newcastle Mitochondrial Disease Adult Scale; *R = retrospective clinical data only. Scaled NMDAS scores are recorded within one year of the muscle biopsy date. Where patient biopsies were collected before 2005, no NMDAS data is available and so retrospective scoring is required (*R).

Control (sex)	Age at biopsy	Classification
C1(M)	18	Orthopaedic surgery
C2(M)	46	Orthopaedic surgery
C3(F)	63	Disease control

Table 3.2: Control cases used for quantitative immunofluorescent analysis of complex I and complex IV in skeletal muscle biopsies. Skeletal muscle biopsies were obtained from three controls, either during orthopaedic surgery or as excess to diagnostic requirements.

3.3.2 Post mortem tissue

Tissue was collected post mortem from five patients with m.3243A>G mutation (Table 3.3). Samples from multiple muscles from each case were collected and stored at the NHS Highly Specialised Rare Mitochondrial Disease Laboratory in Newcastle (REC 2005/202). DNA was extracted from muscle blocks as described in section 2.7.2 and stored at -80°C until use for molecular genetic analysis.

3.3.3 NMDAS

All recorded NMDAS data for these six patients was collated for analysis of clinical disease progression. Multiple NMDAS assessments were available for all but one patient (P6). Due to the subjective nature of part one of the NMDAS assessment, scores from this section were removed from the final analysis, leaving total NMDAS scores calculated from sections two and three only. Total scores were scaled to account for unassessed fields by dividing the total score by the number of assessed fields, and then multiplying by the total number of fields.

Patient (sex)	Age at death	Muscles biopsied	Clinical details
PM1 (F)	59	Biceps, diaphragm, gastrocnemius, psoas, quadriceps, tibialis, triceps	MELAS, MIDD, pseudo-obstruction
PM2 (M)	45	Biceps, diaphragm, gastrocnemius, paraspinal, psoas, quadriceps, tibialis, triceps	MELAS *[1]
PM3 (M)	35	Biceps, psoas, quadriceps	Myopathy, cardiomyopathy, renal tubule acidosis
PM4 (M)	30	Biceps, quadriceps	Diabetes, ptosis, PEO, cardiomyopathy, deafness
PM5 (M)	20	Diaphragm, psoas	Mild deafness *[2]

Table 3.3 Post-mortem cases with m.3243A>G mutation. Multiple muscles were biopsied from six post-mortem cases with m.3243A>G. Cases included had at least two different muscle types biopsied. MELAS = mitochondrial encephalopathy, lactic acidosis and stroke-like episodes; MIDD = maternally inherited diabetes and deafness; PEO = progressive external ophthalmoplegia. *[1] previously published case = patient 3 in Lax *et al.* (2016). *[2] previously published case = case 1 in Ng *et al.* (2016).

.

3.3.4 Statistical modelling of clinical progression

All statistical modelling was performed by Dr. John Grady. Box-Cox (Box and Cox, 1964) indicated the square root was the optimal transform for total NMDAS scores in order to satisfy normality assumptions. The transformed data were then used in a random effects mixed model where total NMDAS scores were the dependent variables and age at assessment was the sole independent variable. The model included a random effect of the gradient with respect to age, which generated a gradient for each individual patient. This model was constrained to have no intercept, such that the NMDAS score at birth is fixed at zero. The rate of clinical progression for each patient is represented by the gradient calculated by the model.

3.3.5 Immunofluorescent staining of cryosectioned skeletal muscle biopsies

10µm sections were cut from patient and control skeletal muscle biopsies and left to dry before storing at -80°C. Sections were allowed to dry at room temperature for up to one hour prior to beginning the protocol outlined in section 2.5.2. Fluorescent images were acquired at 20x magnification using an Axio Imager M1 microscope (Carl Zeiss) and processed with AxioVison software (Carl Zeiss). Images were analysed using Imaris (version 7.6.5, Bitplane) and R script as described in sections 2.5.5 and 2.5.7.

3.3.6 Cloning (to make plasmid p.7D1. β2M)

A plasmid construct was engineered for use as a standard curve. A 275bp portion of the *β2M* gene (GenBank accession number NG_012920.1) was amplified by forward primer 5'-TCCAAAGATTCAGGTTTACTCACG-3' (nt.8941-nt.8964) and reverse primer 5'-CCCACTTAACTATCTTGGGCTGT-3' (nt.9215 -nt.9193). Plasmid p7D1 (Rygiel *et al.,* 2015), containing a portion of the *MT-ND1* gene, was cut with *Sma1* restriction enzyme and *β2M* template inserted by blunt-ended ligation to produce plasmid p7D1.β2M (7469bp). Incorporation of the *β2M* sequence was confirmed by Sanger sequencing as outlined in section 2.10.9.

3.3.7 Pyrosequencing for determination of m.3243A>G heteroplasmy level

The PCR and pyrosequencing protocols are outlined in section 2.9. Patient DNA samples were split into two batches for pyrosequencing. P1, P2 and P3 were run on the same plate

and P4, P5, and P6 were batched together on a separate plate. Each patient sample was diluted to approximately 10ng/µl and loaded in triplicate alongside a positive control (85% heteroplasmy), negative control (0% heteroplasmy) and a no-template control (no DNA). m.3243A>G heteroplasmy level was calculated using Pyromark Q24 software as described by White *et al.* (2012).

3.3.8 Real-time PCR assay for determination of mtDNA copy number

A six-point standard curve comprising a 1:10 serial dilution of p.7D1.β2M was prepared and loaded in triplicate onto each sample plate. Patient DNA samples were first diluted to 10ng/µl concentration for the *β2M* assay, and then diluted 1:100 in nuclease-free water for the *MT-ND1* assay. Each patient sample was loaded in sextuplicate onto six replicate plates, as required for a 10% mean detectable difference in mtDNA copy number (Grady *et al.,* 2014). As for the pyrosequencing protocol, patients were batched and serial biopsies were loaded onto the same plate. Further details of the *MT-ND1* and *β2M* assays are provided in sections 2.8.3 and 2.8.4, respectively.

3.4 Results

3.4.1 Clinical changes as indicated by NMDAS scores

Total NMDAS scores were recorded at multiple assessments for all patients in this study, with the exception of P6. These scores are shown alongside those from patients with m.3243A>G mutation in the MRC Centre Mitochondrial Disease Patient Cohort (n=104) in Figure 3.2 . Longitudinal modelling using these scores highlights the course of disease progression in our patients from birth to current disease burden, as recorded by the most recent total NMDAS score. All six patients in this study were within the boundaries of the cohort in terms of clinical presentation. Based on the trajectories of their predicted disease progression, one patient appeared asymptomatic (P3), two were quite mildly affected (P1 & P6) and three presented moderate levels of disease severity (P2, P4, & P5).

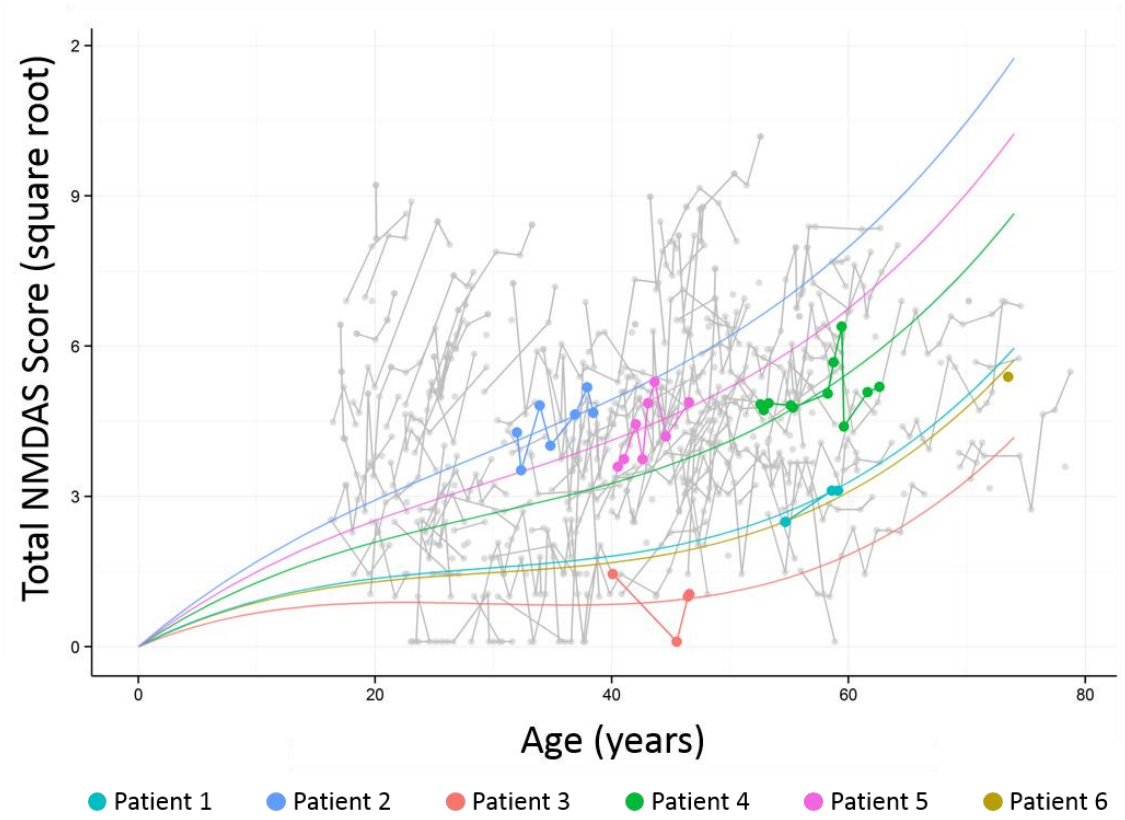

Figure 3.2: Scaled total NMDAS scores Total NMDAS scores were recorded and scaled (square-root transformed) for each patient in this study (n=6) and the MRC Centre Mitochondrial Disease Patient Cohort (n=104). Lines show the estimated disease progression from birth calculated from longitudinal mixed modelling for patients in this study (coloured) and those with m.3243A>G mutation in the cohort.

Muscular phenotypes were recorded for a number of patients in this study. P2, P4, P5 and P6 have presented with myopathy during NMDAS assessments, however this is usually mild and scores no higher than 3 (P2). Furthermore, these patients have more prominent clinical features associated with other tissues and organs: P2 and P6 display multisystem involvement commonly with ataxia and hearing loss; P4 and P5 present with diabetes (Table 3.1). P1 and P3 have no recorded myopathy score. Exercise intolerance is also common to all patients, with the exception of asymptomatic P3, yet other muscle-related phenotypes such as ptosis and CPEO are rare features in this group.

3.4.2 Mitochondrial Respiratory Chain (mtRC) profiles

Quantitative immunofluorescence was performed on a 10µm section of skeletal muscle from biopsy one and two of each patient. Fluorescent images (Figure 3.3) were analysed to determine the levels of COX-I and NDUFB8 in each muscle fibre of the biopsy section (3.3.5). Figure 3.4 shows the z_scores for COX-I plotted against NDUFB8 for each fibre in skeletal

muscle biopsies from patients with m.3243A>G mutation. These graphs display the profile of deficiency in these biopsies, referred to as the mtRC profile. Rocha *et al.,* (2015) have shown these profiles to be characteristic to specific mtDNA mutations, with m.3243A>G presenting an r-shaped profile. This is indicative of complex I deficiency preceding a deficiency of complex IV. This mtRC profile is apparent in P1 (biopsy one), P2 (both biopsies), P4 (biopsy two), P5 (biopsy two) and P6 (biopsy two). Biopsy two from P1 displays a unique mtRC profile in this group, however it is still compatible with m.3243A>G associated disease. The mtRC profiles from P3 reflect the asymptomatic nature of the clinical condition, as all fibres are classified as positive for COX-I and NDUFB8. The remaining biopsies (biopsy one from P4, P5 and P6) show profiles similar to those of P3, with a small minority of fibres showing any deficiency in COX-I or NDUFB8. This is perhaps due to the biopsy being taken earlier in the disease course, when the biochemical defect was not as well established as in biopsy two.

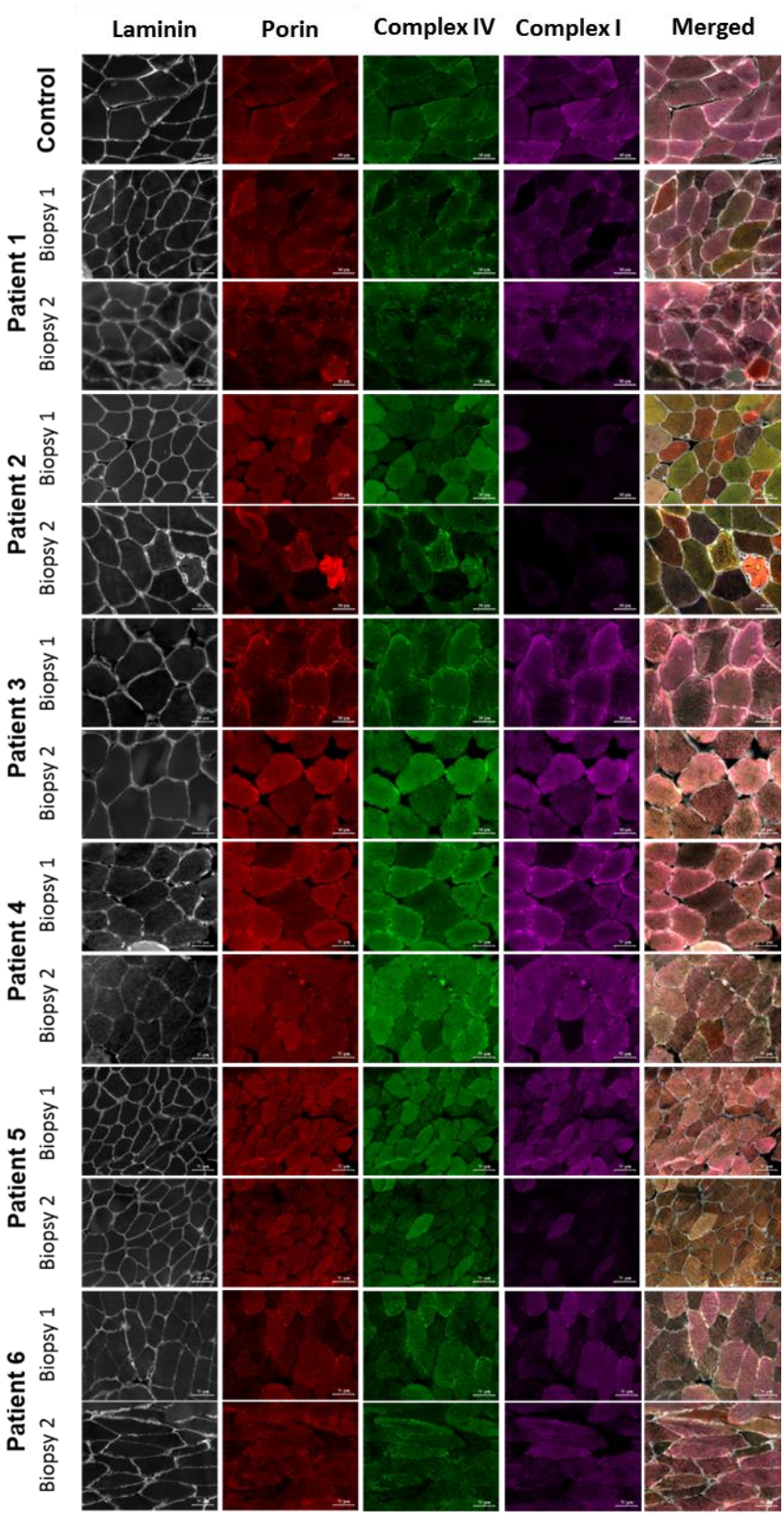

Figure 3.3: Quadruple immunofluorescence staining of skeletal muscle. Levels of porin (VDAC1), complex IV (COX-I) and complex I (NDUFB8) were quantified using laminin as a marker for muscle fibre boundaries. Fluorescent images were acquired from control and patient tissue at 20x magnification, scale bar 50µm.

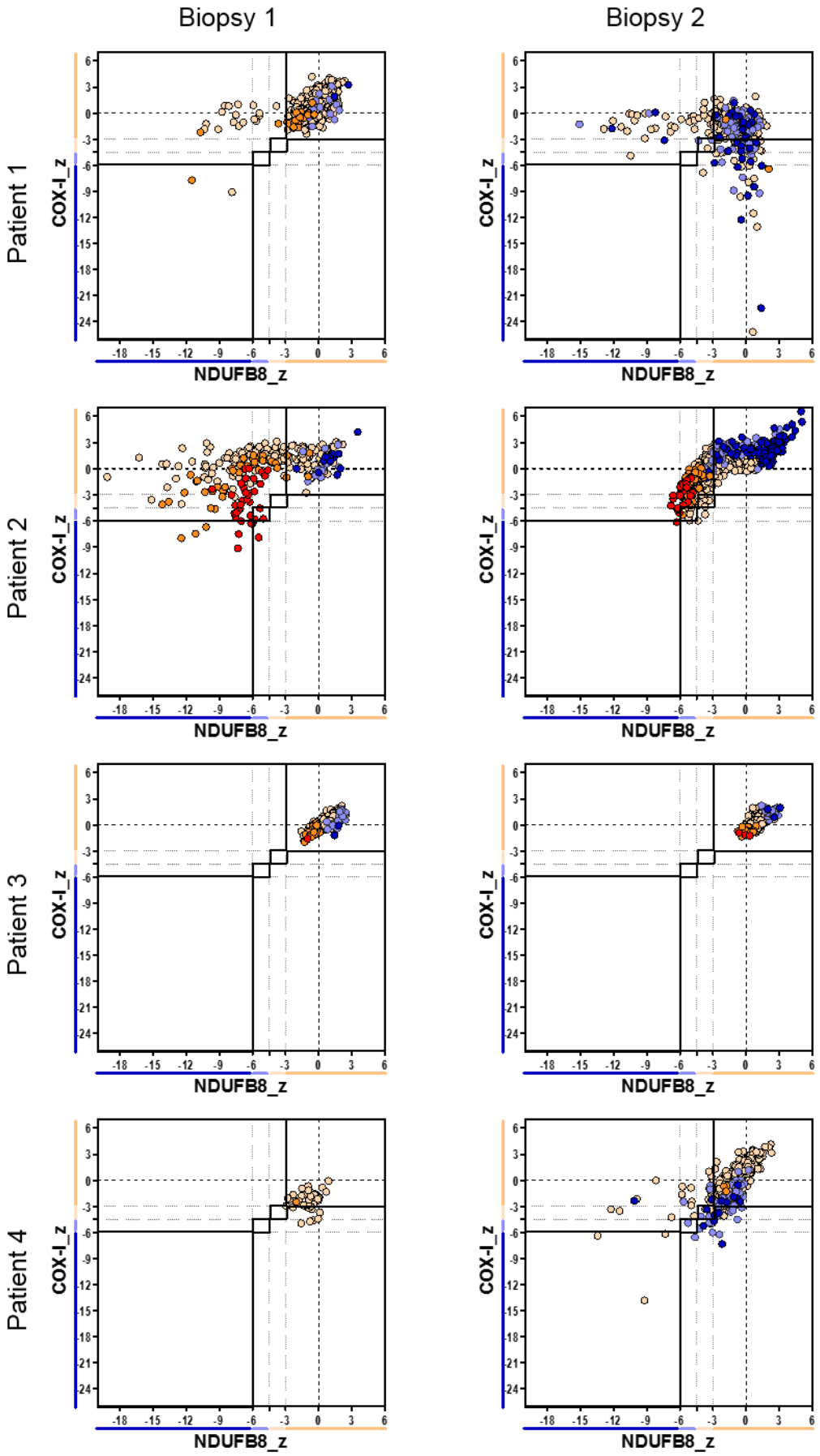
Biopsy 1
Biopsy 2
Patient 1
Patient 2
Patient 3
Patient 4
COX-I_z
NDUFB8_z

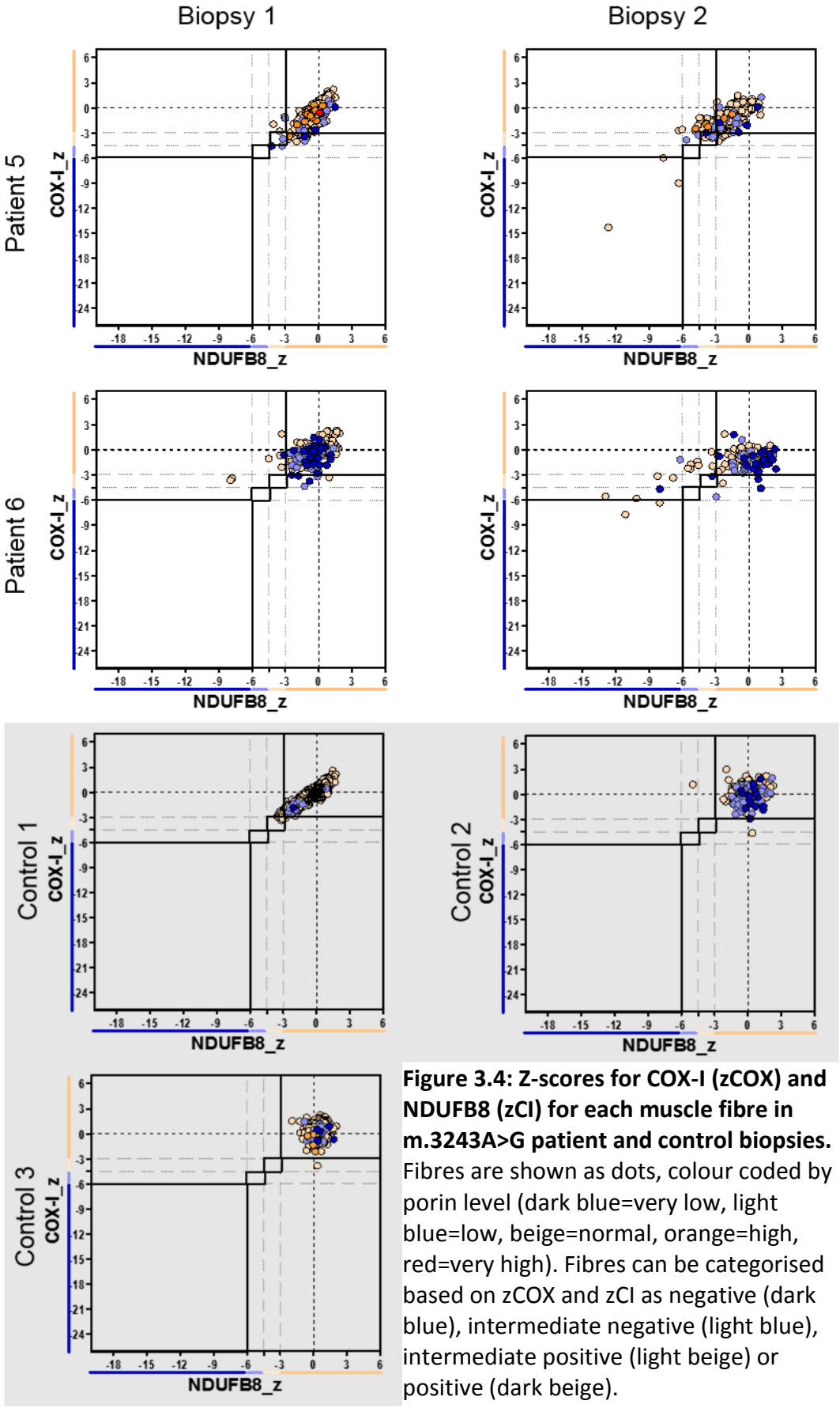

Figure 3.4: Z-scores for COX-I (zCOX) and NDUFB8 (zCI) for each muscle fibre in m.3243A>G patient and control biopsies. Fibres are shown as dots, colour coded by porin level (dark blue=very low, light blue=low, beige=normal, orange=high, red=very high). Fibres can be categorised based on zCOX and zCI as negative (dark blue), intermediate negative (light blue), intermediate positive (light beige) or positive (dark beige).

3.4.3 Respiratory chain defect: Complex I

The level of complex I in each fibre was determined by quantitative immunofluorescence, as described in section 3.3.5. The distribution of complex I levels across all fibres in each biopsy is shown in Figure 3.5, alongside heteroplasmy and total mtDNA copy number (grey boxes). A Mann-Whitney U-test was performed using complex I z-scores to determine the median complex I level for each biopsy, and calculate the change in median from biopsy one to biopsy two. P1, P2, P3 and P5 all show changes to the median level of complex I from biopsy one to biopsy two. However, these changes are not significant and are inconsistent in terms of direction, with P1 and P5 showing decreases in complex I levels over time, P2 and P3 showing increases, and P4 and P6 showing negligible changes (Figure 3.6A). The rate of change of complex I level, as determined by the change divided by the interval length, is variable in terms of magnitude across the group (Figure 3.6B). The importance of accounting for the interval length in the evaluation of these data is highlighted by P1 and P5. These patients have similar levels of complex I at biopsy one, yet P5 shows a much greater decline then P1 by the time biopsy two is taken. When considering the interval length for P1 (4y) and P5 (14y), complex I levels are shown to decline at a similar rate each year in both patients, therefore the greater decrease in complex I levels observed in P5 can be attributed to the much longer time between biopsies.

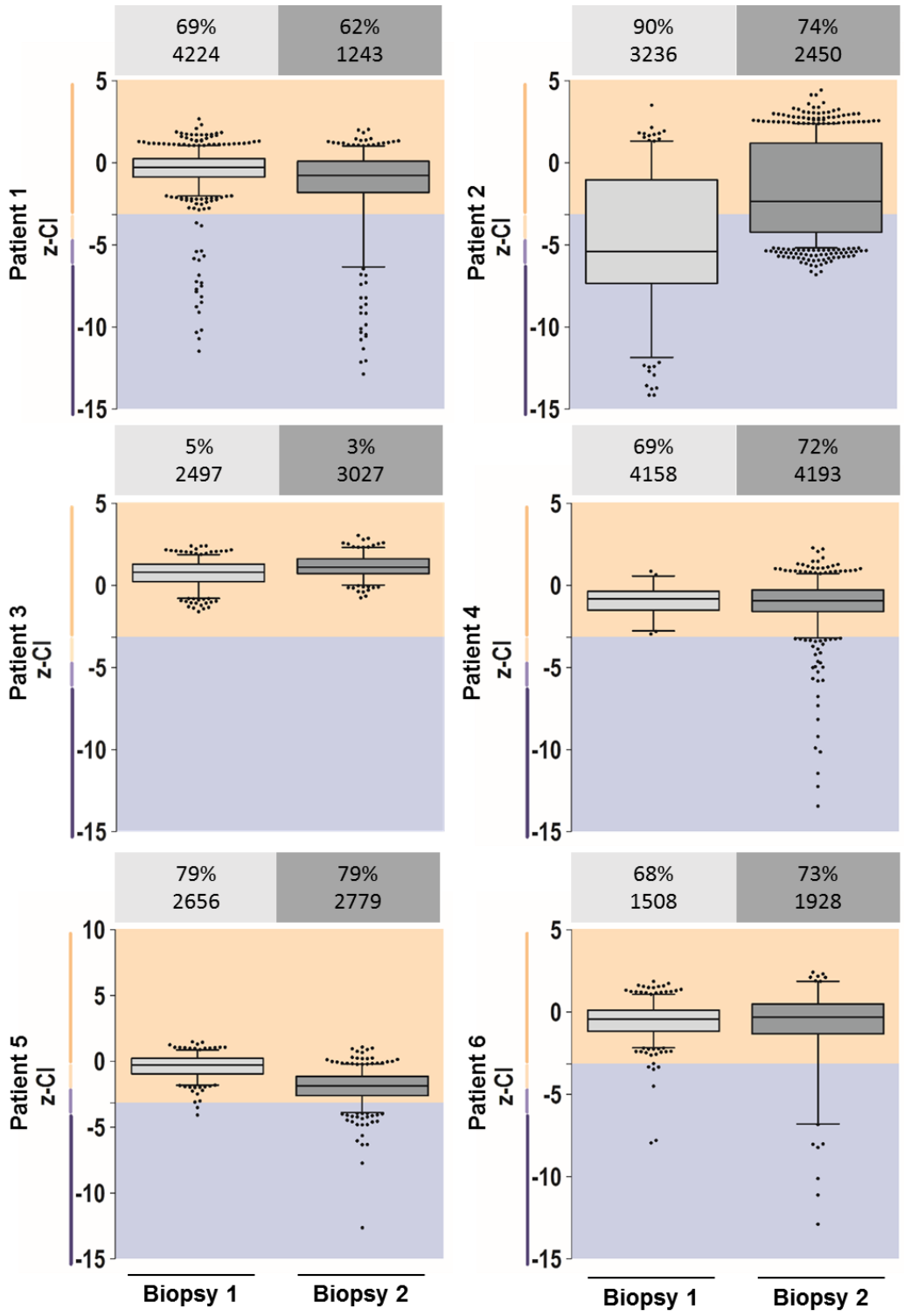

Figure 3.5 Distribution of complex I levels in serial biopsies from patients with m.3243A>G mutation. z-scores for complex I (z_CI) are shown for biopsy one (light grey) and biopsy two (dark grey) for each patient. Boxplots show median and inter-quartile range of z_CI with whiskers extending to the 5th-95th percentile. Outliers are indicated by black dots. Fibres are categorised as positive (shown against a beige background) or deficient (against a blue background). Deficient fibres are comprised of those classified as intermediate positive (-3>z>-4.5, light beige), intermediate negative (-4.5>z>-6.0, light blue) or negative (z<-6) for complex-1 as indicated on the Y axis. Deletion level (%) and total mtDNA copy number are shown in the boxes above each graph (biopsy one=light grey; biopsy two=dark grey).

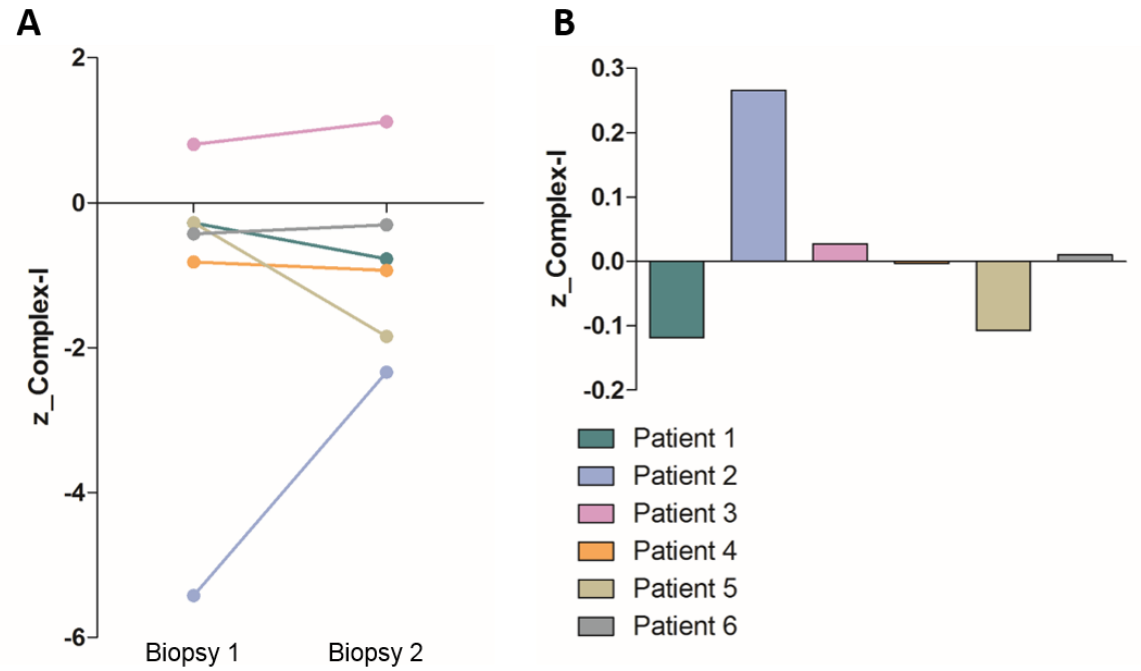

Figure 3.6: Median complex I levels in patients with m.3243A>G mutation. (**A**) median z_score for complex I in biopsy one and biopsy two (**B**) change per year to median z_score for complex I.

Figure 3.7 shows the proportion of fibres from each biopsy with various biochemical profiles for complex I. With the exception of P2, the proportion of fibres defined as negative for complex I is small, ranging from 0% (P3, biopsy one) to 5.7% (P6, biopsy two). The high proportion of intermediate and negative fibres seen in biopsy one from P2 could be related to the moderate disease severity recorded for this patient, as indicated by the rate of disease progression (section 3.4.1). Although P4 and P5 display similar levels of clinical severity, the younger age at biopsy for P2 may account for the different biochemical profiles.

P3, who is clinically asymptomatic, shows no change from the 100% complex I positive fibres measured in biopsy one. The high proportion of complex I negative fibres in P2 biopsy one is reduced to <1% by biopsy two, with fibres moving into the intermediate positive and positive categories, alongside the increase in median complex I z_score. The remaining four patients can be assigned to two groups: P1 and P5 show movement of fibres from the positive to intermediate positive category, with minor changes to the proportion of intermediate negative and negative populations; P4 and P6 show a much larger increase to the complex I negative proportion of fibres (Figure 3.7).

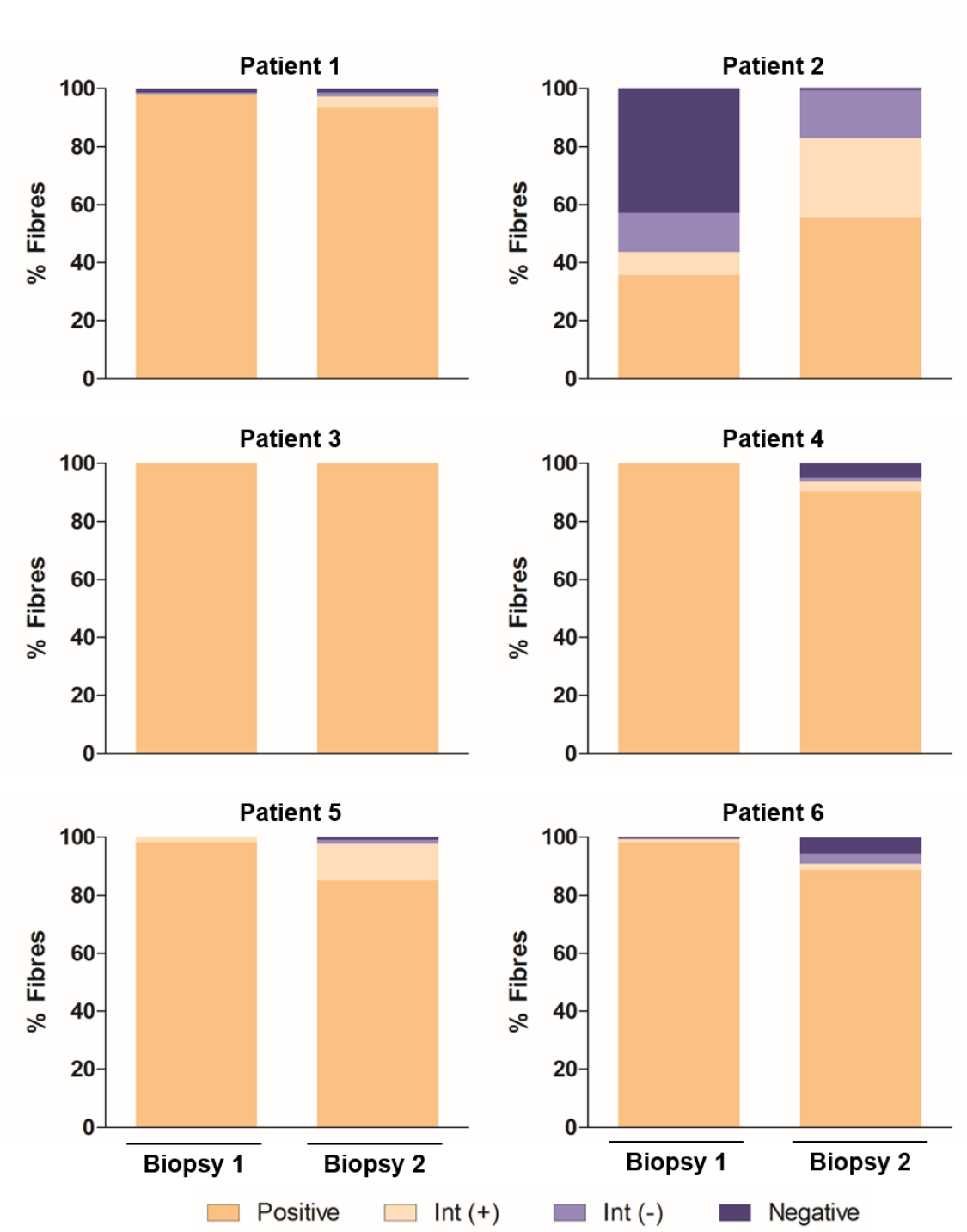

Figure 3.7: Distribution of fibres by biochemical profile for complex I in serial biopsies from patients with m.3243A>G mutation. Fibres are classified as positive (z>-3, beige), intermediate positive (-3>z>-4.5, light beige), intermediate negative (-4.5>z>-6.0, light blue) or negative (z<-6, dark blue). The percentage of fibres of each class from biopsies one and two are displayed.

In order to more clearly observe the changes to the biochemical profiles of these biopsies, fibres were grouped as either positive or deficient, with the latter comprising fibres classified as intermediate positive, intermediate negative and negative for complex I. As previously

mentioned, P3 showed no change to the distribution of fibres. A decrease in the proportion of deficient fibres over time in P2 was also expected, due to the large reduction in the percentage of complex I negative fibres between biopsies. The remaining patients, however, showed an increase in the proportion of complex I deficient fibres from biopsy one to biopsy two (Figure 3.8A). The rate of increase in these patients is similar at approximately 1% per year (Figure 3.8B).

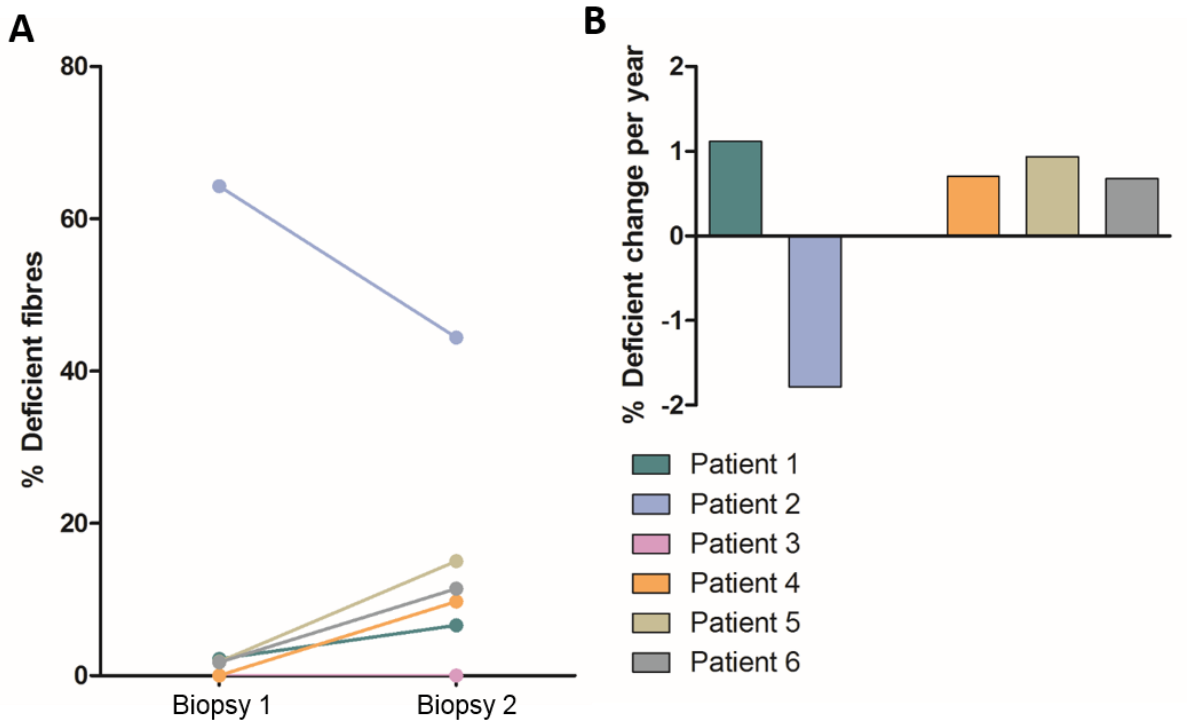

Figure 3.8: The proportion of complex I deficient fibres in patients with m.3243A>G mutation. (**A**) The proportion of complex I deficient fibres in biopsies one and two. (**B**) The change per year to proportion of complex I deficient fibres in each patient.

3.4.4 Respiratory chain defect: Complex IV

The level of COX-I in each fibre was determined by quantitative immunofluorescence (section 3.3.5). Figure 3.9 shows the distribution of complex IV levels, as represented by z_COX, in each biopsy. A Mann-Whitney U-test was performed to determine the median levels of complex IV and the changes to median levels occurring from biopsy one to biopsy two. All patients, with the exception of P3, show a change to the median level of complex IV over time. However, as for complex I, there is no consistent trend regarding the direction of this change, with P1, P5 and P6 showing a reduction over time, P4 showing an increase and P2 and P3 showing negligible changes (Figure 3.10A). The rate of change of median complex IV levels is also inconsistent in terms of magnitude (Figure 3.10B).

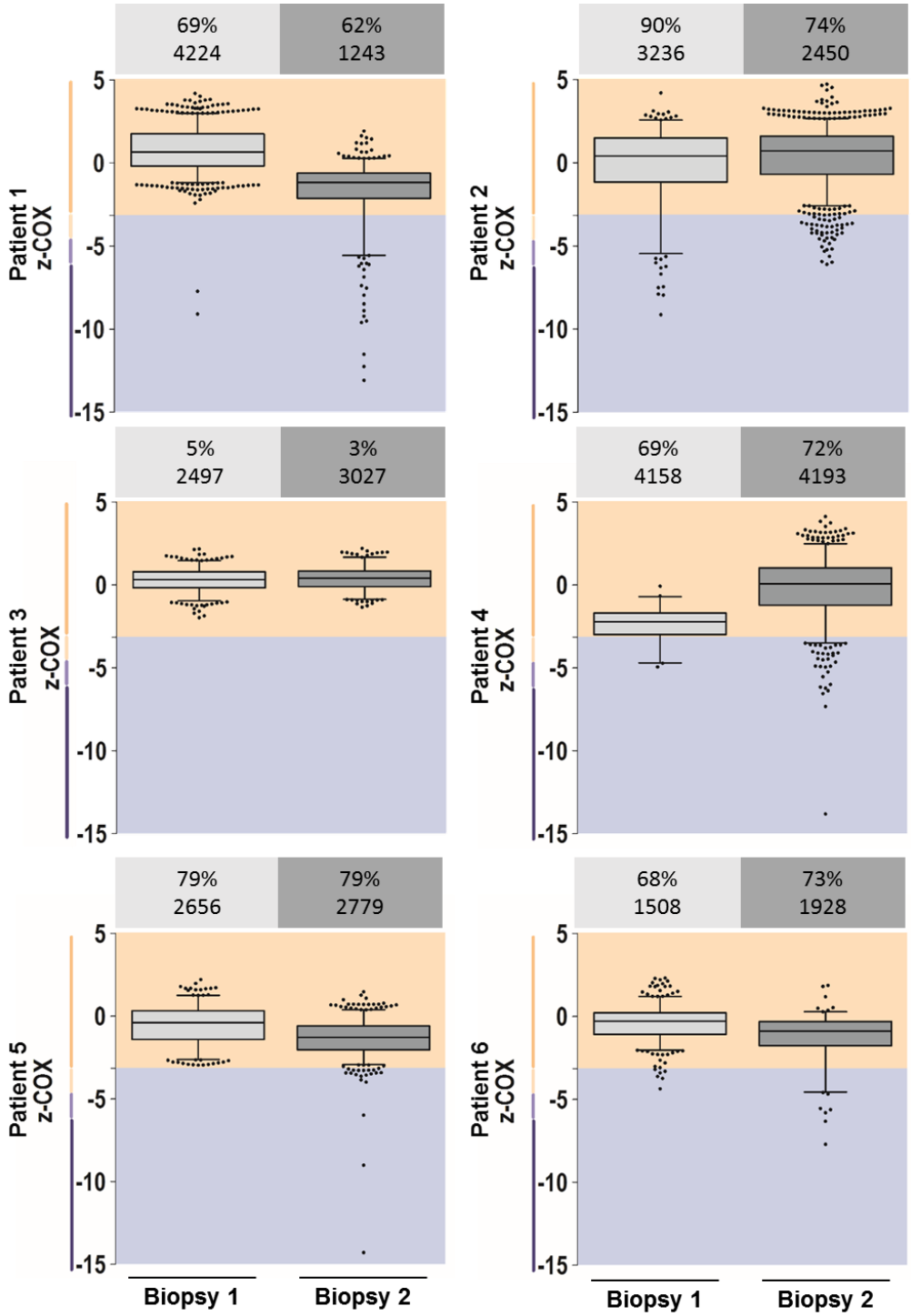

Figure 3.9: Distribution of complex IV levels in serial biopsies from patients with m.3243A>G mutation. z-scores for complex IV (z_COX) are shown for biopsy one (light grey) and biopsy two (dark grey) for each patient. Boxplots show median and inter-quartile range of z_COX with whiskers extending to the 5th-95th percentile. Outliers are indicated by black dots. Fibres are categorised as positive (shown against a beige background) or deficient (against a blue background). Deficient fibres are comprised of those classified as intermediate positive (-3>z>-4.5, light beige), intermediate negative (-4.5>z>-6.0, light blue) or negative (z<-6) for complex I as indicated on the Y axis. Deletion level (%) and total mtDNA copy number are shown in the boxes above each graph (biopsy one=light grey; biopsy two=dark grey).

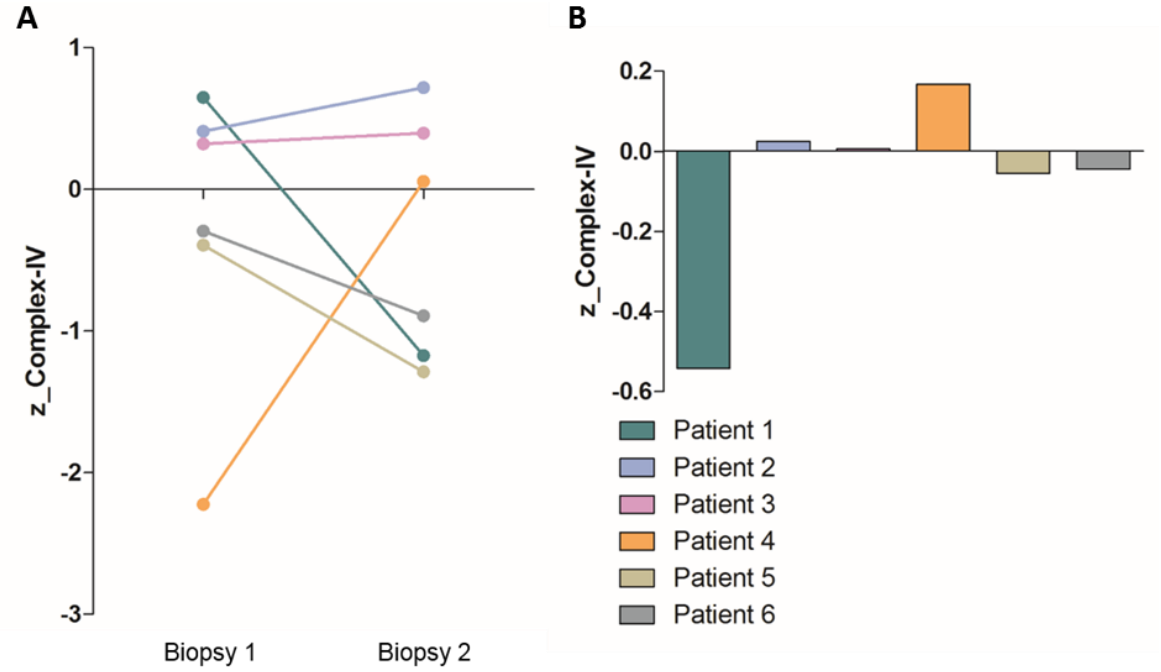

Figure 3.10: Median complex IV levels in patients with m.3243A>G mutation. (A) median z_score for complex IV in biopsy one and biopsy two **(B)** change per year to median z_score for complex IV.

The proportion of fibres with different biochemical profiles is shown in Figure 3.11. The percentage of fibres negative for complex IV is generally smaller than for complex I, ranging from 0% (P3, biopsy 1) to 4.3% (P1, biopsy 2). Overall, there is no consistent change to the distribution of fibres across this group of patients. P3 and P5 show little to no change between biopsies. P1 and P6 show a reduction in the percentage of complex IV positive fibres alongside increases in intermediate and negative groups, whereas P2 and P4 show an increase in positive fibres with decreases in the remaining groups.

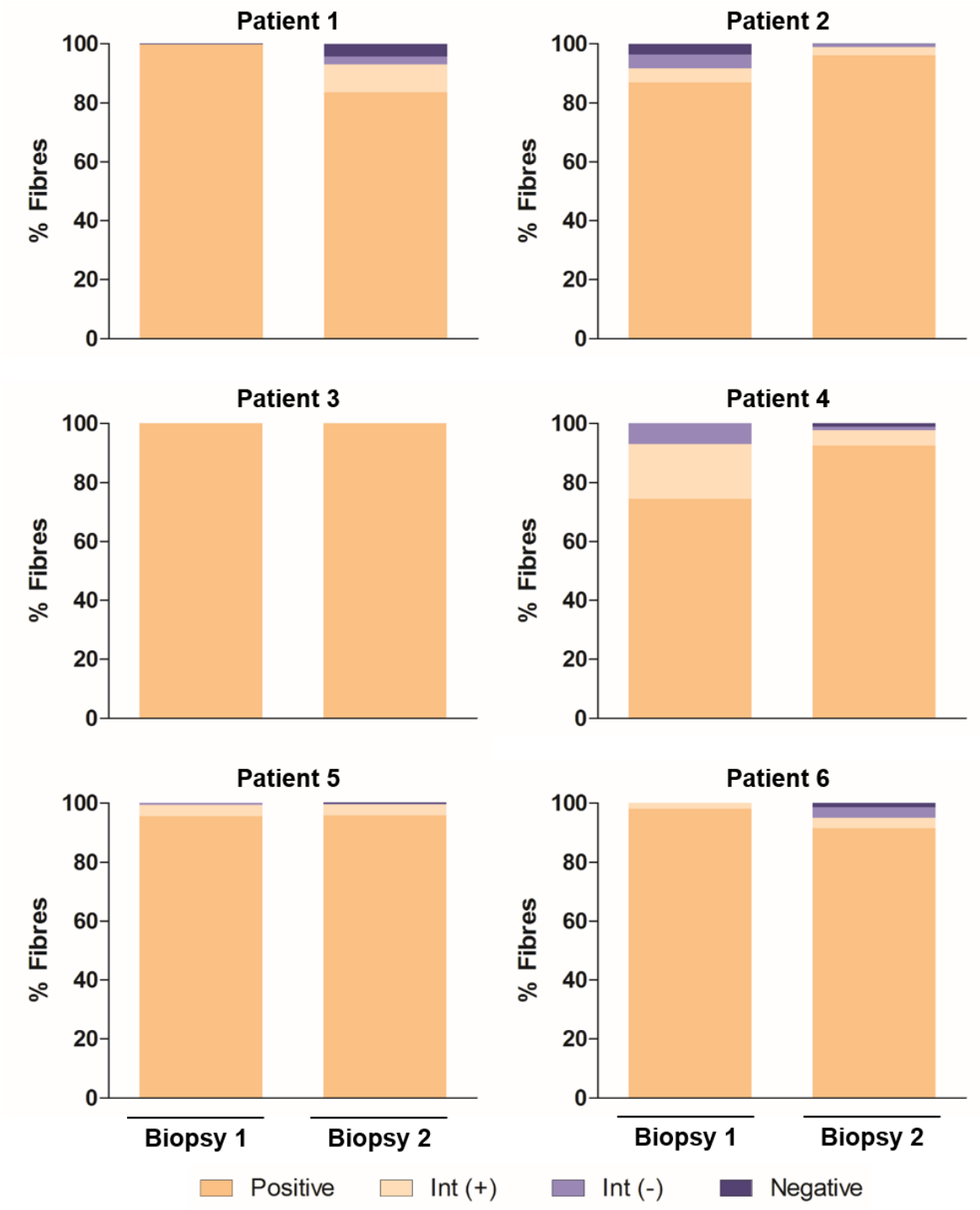

Figure 3.11: Distribution of fibres by biochemical profile for complex IV in serial biopsies from patients with m.3243A>G mutation. Fibres are classified as positive (z>-3, beige), intermediate positive (-3>z>-4.5, light beige), intermediate negative (-4.5>z>-6.0, light blue) or negative (z<-6, dark blue). The percentage of fibres of each class from biopsies one and two are displayed.

Changes to the percentage of fibres deficient for complex IV are also inconsistent across the group, with an increase observed in P1 and P6, a decrease in P2 and P4, and no change in P3 and P5 (Figure 3.12A). The rate at which the distribution of deficient fibres changes varies in terms of scale (Figure 3.12B).

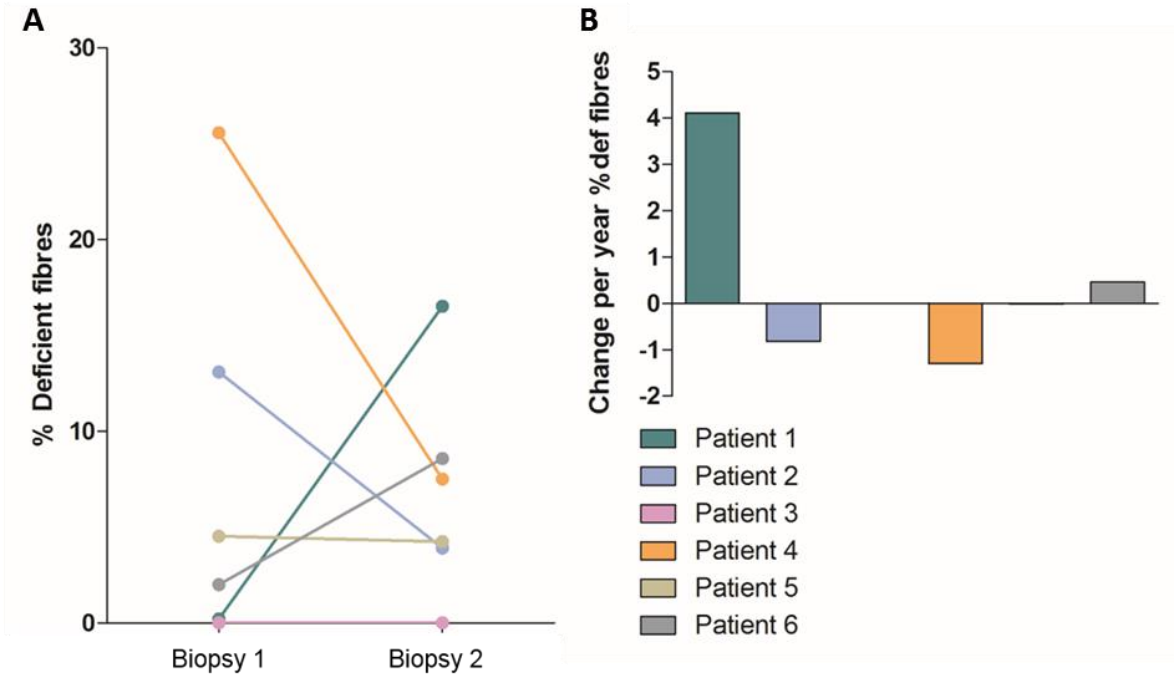

Figure 3.12: The proportion of complex IV deficient fibres in patients with m.3243A>G mutation. (A) Proportion of complex IV deficient fibres in biopsies one and two. **(B)** Change per year to proportion of complex IV deficient fibres in each patient.

3.4.5 Genetic changes: heteroplasmy level

Pyrosequencing was used to determine the heteroplasmy level of homogenate skeletal muscle DNA (section 3.3.7). Heteroplasmy levels from biopsies one and two from each patient are shown in Table 3.4. In the five patients presenting clinical symptoms, heteroplasmy levels range from 68.0-90.0% in the first biopsy to 62.2%-79.0% in the second. A significant correlation was observed between heteroplasmy level and median complex I level ($p<0.05$) but not with complex IV level.

P1 and P2 harbour significantly reduced heteroplasmy levels in biopsy two compared to biopsy one, whereas P4 and P6 show significant increases in heteroplasmy over time (paired t-test, $p<0.05$). P3 and P5 show negligible changes. The rate of change to heteroplasmy level

per year is also highly variable (Figure 3.13A). The most rapid change to heteroplasmy level is seen in P1, where mutation load decreases at 1.7% per year.

3.4.6 Genetic changes: mtDNA copy number

A real-time PCR assay for *MT-ND1* was used to quantify the number of mtDNA copies in a sample of homogenate skeletal muscle DNA. By comparing this to the number of copies of a *B2M*, single-copy nuclear gene marker, mtDNA copy number per nucleus was determined. Total mtDNA copy number per nucleus (Table 3.4) ranged from 1508-4224 in biopsy one, and 1243-4193 in biopsy two. Although P1, P2, P3 and P6 show changes to total mtDNA copy number between biopsies, there is no consistent change across the group with a decrease seen in P1 and P2, an increase in P3 and P6 and negligible changes in P4 and P5. The rate of change of total mtDNA copy number is presented as a compound percentage change as this best reflects the curvilinear nature of this change (Figure 3.13B). These rates vary across the group with P1 decreasing at 26.5% per year, representing the most rapid change to total mtDNA copy number.

Case	Heteroplasmy (%)		Total mtDNA copy number		Wild-type mtDNA copy number	
	Biopsy 1	Biopsy 2	Biopsy 1	Biopsy 2	Biopsy 1	Biopsy 2
P1	69.0(±0.3)	62.2(±0.3)	4224(±335)	1243(±150)	1309(±104)	470(±57)
P2	90.0(±0.3)	74.2(±0.2)	3236(±93)	2450(±162)	324(±9)	633(±42)
P3	4.5(±0.6)	3.3(±0.3)	2497(±107)	3027(±310)	2385(±102)	2926(±300)
P4	69.0(±0.3)	71.7(±0.2)	4158(±285)	4193(±494)	1289(±88)	1188(±140)
P5	78.7(±0.2)	79.0(±0.0)	2656(±173)	2779(±247)	567(±37)	584(±52)
P6	68.0(±0.6)	72.8(±0.4)	1508(±135)	1928(±128)	483(±43)	524(±35)

Table 3.4: Genetic analysis of skeletal muscle biopsies. Bx1=biopsy one; Bx2=biopsy two; Mean (±SEM) heteroplasmy was measured by quantitative pyrosequencing with samples loaded in triplicate on two replicate plates. Total mtDNA copy number was measured by real-time PCR with samples loaded in sextuplicate on at least six replicate plates.

Wild-type mtDNA copy number per cell is also shown in Table 3.4, and ranges from 324-2385 copies in biopsy one to 524-2926 copies in biopsy two. Only P1 and P2 show significant changes to wild-type mtDNA copy number, yet these changes occur in opposite directions. A slight increase is seen in P3 and P4, P5 and P6 show only negligible changes. As with total mtDNA copy number, the rate of change per year is presented as a compound percentage

change. Again, these rates vary across the group and P1 displays the most rapid change with a 22.7% decrease in wild-type mtDNA copy number per year (Figure 3.13C).

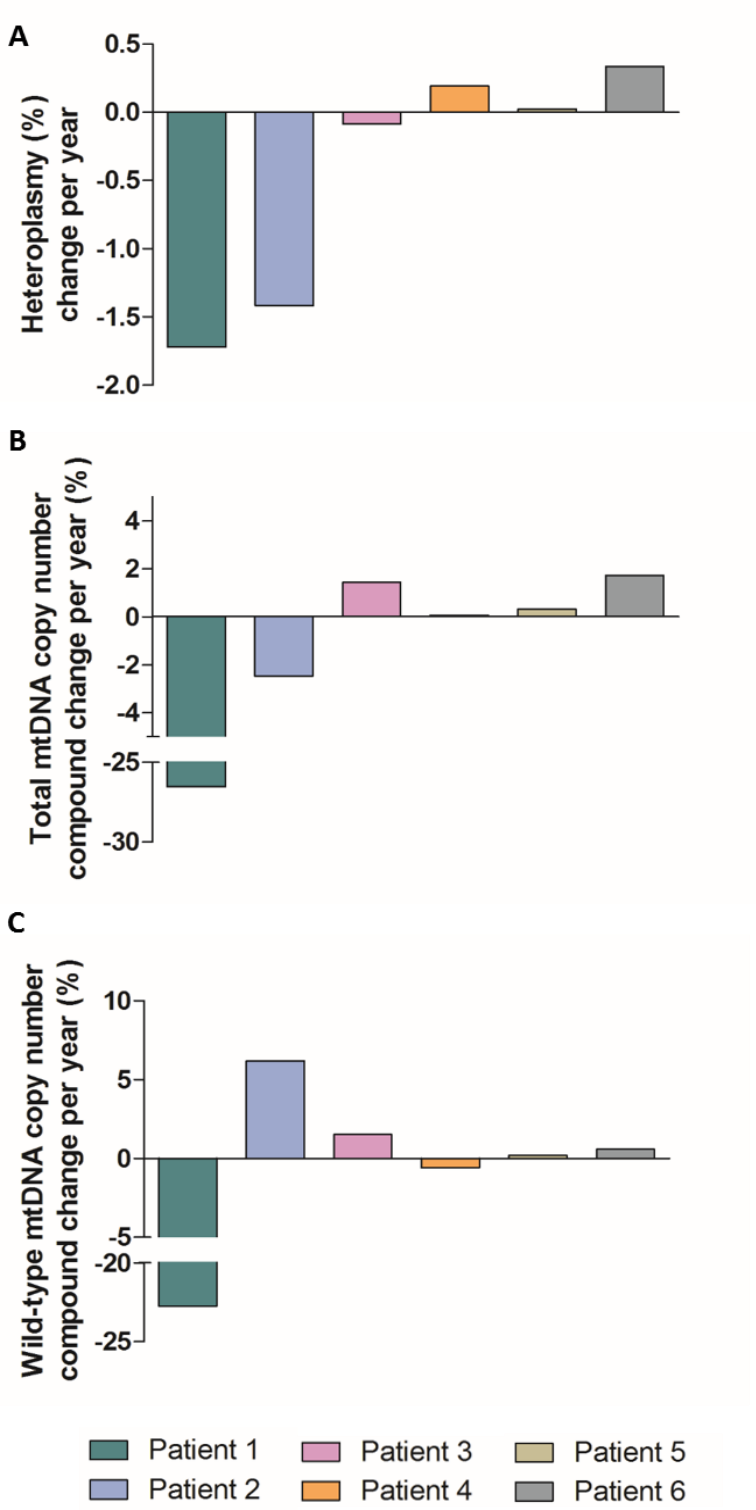

Figure 3.13: Genetic analysis of skeletal muscle biopsies from m.3243A>G patients. Change per year to (A) heteroplasmy levels, (B), total mtDNA copy number and (C) wild-type mtDNA copy number.

3.4.7 Genetic analysis of post-mortem tissue

The majority of patients featured in this study had serial muscle biopsies taken from the *quadriceps*, with one from the left side and one from the right. However, P1 and P4 have biopsies taken from two different muscles; biopsy one from the *gastrocnemius*, and biopsy two from the *quadriceps*. In order to evaluate whether differences observed between these biopsies could be attributable to the different biopsy sites, post-mortem samples were taken from multiple muscles of five patients with m.3243A>G for genetic analysis.

All five post-mortem cases showed variation in heteroplasmy levels between different muscles (Figure 3.14A) (Table 3.5). The largest range was seen in PM1 between *diaphragm* harbouring 48% heteroplasmy and *tibialis* with 82%, with a difference of 34% between these muscles. In the two cases where *gastrocnemius* and *quadriceps* were assessed, PM1 and PM2, significant differences in heteroplasmy were found (PM1 *gastrocnemius*=63%, *quadriceps*=76%, (t-test, $p<0.001$); PM2 *gastrocnemius*=89%, *quadriceps*=85% (t-test, $p<0.002$).

Muscle	PM1	PM2	PM3	PM4	PM5
Bicep	76%	84%	44%	71%	N/A
Diaphragm	48%	78%	N/A	N/A	85%
Gastrocnemeus	63%	89%	N/A	N/A	N/A
Paraspinal	N/A	87%	N/A	N/A	N/A
Psoas	81%	80%	54%	N/A	87%
Quadricep	76%	85%	55%	76%	N/A
Tibialis	82%	90%	N/A	N/A	N/A

Table 3.5: Heteroplasmy levels in multiple post-mortem muscle samples from patients with m.3243A>G. Mean heteroplasmy levels (%) were determined by quantitative pyrosequencing. PM1-PM5 = post mortem cases1-5; N/A = tissue not available.

Total mtDNA copy number was also measured in these five post-mortem cases (Figure 3.14B) (Table 3.6). Again, significant variation ($p<0.05$) was seen between different muscles in all cases but PM5 (PM1, PM2, PM3 each analysed by one-way ANOVA; P4 and P5 analysed by t-test). PM1 displayed the largest range in total mtDNA copy number from 565 in *gastrocnemius* to 6331 in *tibialis anterior*. Neither PM1 nor PM2 showed significant difference in mtDNA copy number between *gastrocnemius* and *quadriceps* however ($p>0.05$).

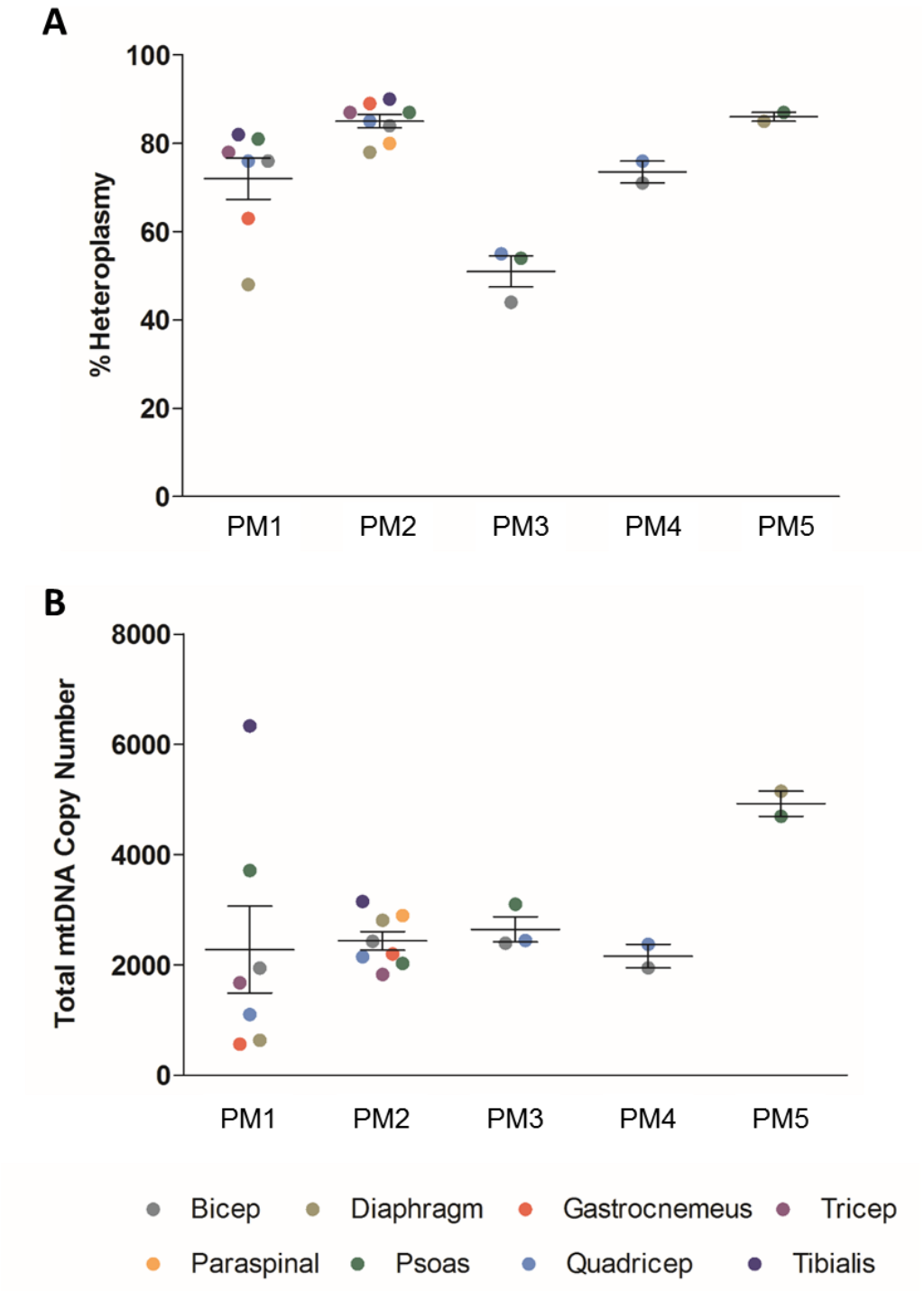

Figure 3.14: Genetic analysis of post-mortem skeletal muscle biopsies. Average (A) heteroplasmy levels and (B) total mtDNA copy numbers are shown for multiple muscles samples collected post-mortem from patients PM1-PM5. Error bars represent SEM where n=3 (% heteroplasmy) and n=2 (total mtDNA copy number).

Muscle	PM1	PM2	PM3	PM4	PM5
Bicep	1940	1778	2394	2371	N/A
Diaphragm	662	3046	N/A	N/A	5151
Gastrocnemeus	565	1945	N/A	N/A	N/A
Paraspinal	N/A	1861	N/A	N/A	N/A
Psoas	3710	2739	3102	N/A	4903
Quadricep	1100	1878	2441	1947	N/A
Tibialis	6331	2369	N/A	N/A	N/A

Table 3.6: Total mtDNA copy number in multiple post-mortem muscle samples from patients with m.3243A>G. Mean total mtDNA copy number was determined by real-time PCR and is presented as mtDNA copies per nuclear genome. PM1-PM5 = post mortem cases1-5; N/A = tissue not available.

3.5 Discussion

This study aimed to investigate molecular and cellular progressive changes over time in skeletal muscle from patients with m.3243A>G point mutation. Patients reflected the broad spectrum of m.3243A>G disease, and the majority showed progressive symptoms compatible with those within the large population of patients with m.3243A>G disease.

3.5.1 There is no consistent change to the respiratory defect over time

To date, there has been no longitudinal assessment of the respiratory chain defect in skeletal muscle of patients with m.3243A>G mutations reported in the literature. Whilst this study shows some variation in the degree of the respiratory defect over time, this group of patients showed no evidence of a marked deterioration of either complex I or complex IV level with time. This lack of significant change in the biochemical phenotype very much reflects the lack of changes in heteroplasmy or copy number. This is likely due to the absence of any severe or progressive muscle related-symptoms in this patient group.

Previous biochemical studies have observed a reduction in complex I and, to a lesser extent, complex IV activity in patients with m.3243A>G (Goto *et al.,* 1992; Mariotti *et al.,* 1995; Jeppesen *et al.,* 2006; Morgan-Hughes *et al.,* 1995). These findings do tally with the relatively low proportion of COX-deficient fibres seen in patient skeletal muscle, yet analysis of complex I deficiency in these patients is underrepresented in the literature. While the present study did not assess biochemical activity of respiratory chain complexes, it is the first to report complex I and complex IV levels for individual fibres using a recently developed

quadruple immunofluorescent technique. It is seen here, from the mtRC profiles generated by this technique, that patients with m.3243A>G mutation do have a predominant deficiency of complex I levels over complex IV in skeletal muscle biopsies, in concordance with the data from earlier biochemical studies.

Previous histochemical studies have not thoroughly evaluated heteroplasmy in the context of complex I levels in multiple patients, yet Mariotti *et al.* (1995) describe a correlation between mutation load and complex I activity. In the present study, a significant correlation was observed between heteroplasmy level and median complex I level indicating a possible relationship between genetic and biochemical factors, however this is difficult to evaluate due to the small group size.

3.5.2 There is no consistent change to heteroplasmy level over time

Diseases due to mtDNA mutations are particularly difficult to evaluate in terms of disease progression. In nuclear gene disorders the genetic defect will not change over time, however in mtDNA disease this is not necessarily the case. In post mitotic tissues such as skeletal muscle there is relaxed and continuous replication of the mitochondrial genome (Chinnery and Samuels, 1999). This has important implications, since it is possible for the mutation load to increase or decrease depending on selection pressures. An illustrative example of this is the mosaic pattern of deficiency observed in muscle biopsies with some fibres harbouring a much higher mutation load than others (Petruzzella *et al.,* 1994; Silvestri *et al*., 2000). There have also been documented reports of increasing levels of mtDNA point mutations over time in muscle (Weber *et al.,* 1997; Durham et al., 2006), but there has been no previous comprehensive assessment of the changes associated with the m.3243A>G mutation.

This study shows no evidence of a consistent change in mutation load over time in muscle. This is in contrast to the observation made in blood from patients with the m.3243A>G mutation where the mutation load has been shown to fall with age at a rate of 0.6-1.4% per year (T'Hart *et al.,* 1996; Rahman *et al*., 2001; Pyle *et al.,* 2007; Mehrazin *et al.,* 2009). Heteroplasmy levels in patient blood have consistently been shown to be lower than mutation loads in skeletal muscle (Hammans *et al.,* 1995; Silvestri *et al.,* 1997; Deschauer *et al.,* 2000), which was previously observed in patients with single, large-scale mtDNA

deletions (Moraes *et al.,* 1993). Perhaps the most disparate measurements of blood and skeletal muscle heteroplasmy were recorded by Chinnery *et al.* (1997), with levels of 4% in blood versus 85% in skeletal muscle needle biopsy. Hammans *et al.* (1995) also noted an inverse correlation between blood heteroplasmy level and age, leading to postulation that the level of m.3243A>G mutation declines throughout life in blood. The difference between muscle and blood is highly likely to be due to the proliferative nature of blood stem cells, which means that selection against those with a higher level of mutation can occur. In post-mitotic muscle this selection cannot occur (Sue *et al*., 1998; Mehrazin *et al.,* 2009).

Analysis of post-mortem skeletal muscle biopsies from patients with m.3243A>G mutation indicated that the level of heteroplasmy can vary between different muscles of the same patient. This is in agreement with post-mortem observations made by Shiraiwa *et al.* (1993), who observed a range in heteroplasmy levels across six muscles from approximately 60% in heart muscle to 85% in biceps brachii. Whilst most patients in the longitudinal study had serial biopsies taken from the quadriceps, biopsy one from P1 and P4 was sampled from the gastrocnemius. In the two post-mortem cases where both the quadriceps and gastrocnemius were assessed, a significant difference in heteroplasmy level was observed between the two muscles. Therefore any variation in the heteroplasmy level between serial biopsies from P1 and P4 may be attributable to biopsy site and rather than longitudinal change.

3.5.3 There is no consistent change to mtDNA copy number over time

Another change which could potentially modulate the effect of a pathogenic mtDNA mutation over time is the copy number of mtDNA. It has been shown that the vast majority of mtDNA mutations are functionally recessive (Sacconni *et al.,* 2008) and that the biochemical defect generally reflects the expression of the wild type molecules (Durham *et al.,* 2007). Single cell studies have proposed that respiratory chain deficiency occurs when the wild-type population declines to less than 15-20% of the total mtDNA population. This was based on observations of COX-normal fibres with mutation loads as high as 63.2±21.6% (Tokunaga *et al.,* 1994) and 56±21% (Petruzzella *et al.,* 1994). Therefore, if there was a significant decrease in total mtDNA copy number this could affect the biochemical phenotype, even in the absence of any change in heteroplasmy. However, no changes in this patient group were observed which could account for the progressive nature of their symptoms.

3.5.4 Limitations

This study provides a more comprehensive assessment of genetic and cellular changes occurring with clinical disease progression, however there are several limitations which need to be considered. First, although this study examines a larger group of patients than other longitudinal studies on skeletal muscle, the sample size is still too limited to draw statistically significant conclusions from the observed changes occurring over time. In addition, patients selected for this study had adult-onset disease and no major cognitive impairment, due to the difficulty in obtaining ethical consent for the collection of biopsies from these severely affected patients. Though only six patients were studied in detail, this study has shown that they did reflect the diversity in clinical severity and progression of other patients with m.3243A>G in the MRC Centre Mitochondrial Disease Patient Cohort.

Second, as the m.3243A>G mutation is associated with multisystem conditions, often with a neurological component, skeletal muscle may not be representative of the wider impact of the mutation. Whilst all affected patients did have some muscle related symptoms, in none was this severe nor did it progress markedly during the follow up period. This suggests that the observed disease progression is most probably due to other organ involvement, rather than a progression of the biochemical defect in muscle. Unfortunately it is not possible to biopsy other tissues such as cerebellum (for ataxia) or pancreas (for diabetes) from living patients for longitudinal study in order to understand how these tissues are affected by mitochondrial dysfunction over time. However, neuropathological studies on post-mortem tissue have shown extensive cell loss in the brains of patients with m.3243A>G disease, which may be reflected in the observed progression of the disease (Lax *et al*., 2012).

3.6 Conclusions

This is the most comprehensive longitudinal study of disease progression in patients with m.3243A>G, both in terms of the number of patients involved and the extent of the genetic and biochemical analysis performed. The findings of this study show that: (i) the majority of patients showed decreased levels of complex I and complex IV proteins in their biopsies relative to controls, but there was no evidence of a consistent change and limited evidence for a more severe defect with the second biopsy; (ii) there was no consistent change in the

level of heteroplasmy with time; (iii) there was no consistent change in copy number with time.

There is scope for further investigation, however. In this study, genetic analysis was performed on homogenate DNA from skeletal muscle, however performing this same analysis on laser micro-dissected muscle fibres would clarify the relationship between the genetic and biochemical defects observed. Furthermore, while no correlation between clinical disease progression and the genetic and biochemical defects in patient skeletal muscle biopsies was observed, the multisystem nature of the clinical phenotype associated with this mutation demands evaluation of these defects in additional tissues. The limitations of collecting such biopsies from living patients has already been discussed, and so further investigations could feature post-mortem biopsies of multiple tissues for comparison.

Chapter 4: Investigating disease progression in patients with single large scale mtDNA deletions

4.1 Introduction

4.1.1 Single, large-scale mtDNA deletions

Single, large-scale deletions of mitochondrial DNA (mtDNA) were the first class of mutations identified as a cause of mitochondrial diseases by Holt *et al.,* (1988) who identified the rearrangements in muscle from nine patients presenting with mitochondrial myopathy. Soon after, deletions of mtDNA were found in patients with Kearns-Sayre syndrome (KSS), ranging in size and location across the mitochondrial genome (Lestienne and Ponsot 1988; Zeviani *et al.,* 1988). Since these initial investigations, numerous single large-scale mtDNA deletions have been reported, with 149 recorded in MitoBreak (http://mitobreak.portugene.com) (Damas *et al*., 2014) at the time of writing (8th December 2016). These deletions vary in size (1.3-10kb (Pitceathly *et al.,* 2012)) and distribution within the mtDNA molecule (Damas *et al.,* 2012), although approximately 85% are located within the major arc between origins of light and heavy strand replication and are flanked by short repeat sequences (Bua *et al.,* 2006; Samuels *et al.,* 2004). A common deletion of 4977bp (nt.8470-13477 (rCRS), flanked by 13bp direct repeats) is found in one third of patients with single, large-scale mtDNA deletions (Pitceathly *et al.,* 2012) and removes genes encoding four complex I subunits, one complex IV subunit, two complex IV subunits and five tRNAs.

The mechanisms for deletion formation are presented in section 1.9.2. Single, large-scale mtDNA deletions occur sporadically with only one deletion species present in all affected cells of a patient (Chen *et al.,* 1995; Schaeffer *et al.,* 2008). Deletions are heteroplasmic and were shown to require lower pathological threshold (50-60% for the common deletion) to manifest dysfunction when compared to mtDNA point mutations (Hayashi *et al.,* 1991, Porteous *et al.,* 1998). The timing of deletion formation is unclear but heteroplasmic populations of mtDNA are present early in development (Zeviani *et al.,* 1990). Deletions were detected in numerous skeletal muscle and brain samples collected post mortem from a patient with CPEO, suggesting deletion formation occurred prior to the differentiation of embryonic layers (skeletal muscle = mesodermal, brain = ectodermal) (Marzuki *et al.,* 1997). Several studies have also observed single, large-scale mtDNA mutations in oocytes prior to fertilisation, suggesting formation during oogenesis (Chen *et al.,* 1995). The tissue-specific

phenotype of PEO possibly indicates the formation of deletions during differentiation of muscle pre-cursor cells, much later in development (Chinnery *et al.,* 2004).

The accumulation of single, large-scale mtDNA deletions during normal aging has been demonstrated in multiple tissues including skeletal muscle (Cortopassi and Arnheim 1990; Linnane *et al.,* 1990; Pallotti *et al.,* 1996), heart (Hattori *et al.,* 1991) and brain (Corral-Debrinski *et al.,* 1992; Bender *et al.,* 2006). Post-mitotic tissues are shown to have higher levels of deletion than mitotic tissues (Lui *et al.,* 1998), despite the low rate of cellular turnover. Generally, deletions are present at low levels but can accumulate to high enough levels to induce biochemical dysfunction with age (Bua *et al.,* 2006).

4.1.2 Epidemiology and clinical phenotypes

Collectively, patients with single, large-scale mtDNA deletions have an estimated prevalence of $1.5x10^{-5}$ in the population of North East England (Gorman *et al.,* 2015). Phenotypically, single, large-scale mtDNA deletions are associated with a number of clinical symptoms, most often categorised as either Kearns-Sayre syndrome (KSS) (Kearns & Sayre, 1958), Pearson Syndrome (PS) (Pearson *et al*., 1979) or chronic progressive external ophthalmoplegia (CPEO) (Moraes *et al.,* 1989). The mildest of the three syndromes associated with single, large-scale mtDNA deletions is CPEO, categorised as a slowly progressive bilateral ptosis and ophthalmoplegia. Additional features include dysphagia, exercise intolerance and proximal limb weakness.

KSS is a multisystem disorder classically defined as a combination of ophthalmoplegia, retinal pigmentary degradation and cardiomyopathy. However these criteria have since been adjusted (Rowland *et al.,* 1983) with the diagnosis of KSS now requiring a triad of PEO, pigmentary retinopathy and onset before 20 years of age in combination with either cardiac conduction block, cerebrospinal fluid protein >0.1g/L or cerebellar ataxia. Other common features seen in patients with KSS include broader myopathy, sensorineural hearing loss, renal tubular acidosis, dementia, seizures and short stature.

The most severe syndrome associated with single, large-scale mtDNA deletions is Pearson syndrome. This infantile-onset condition is often rapidly fatal and is characterised by sideroblastic anaemia and exocrine pancreatic dysfunction. One in three patients who

survive PS in infancy go on to develop a KSS phenotype (Simonsz *et al.,* 1992; Pitceathly *et al*., 2012).

Recent evaluations of large cohorts of patients with single mtDNA deletions have provided some useful data on the incidence of the various clinical phenotypes associated with these mutations. Across a cohort of 228 patients (Mancuso *et al.,* 2015), 57% had CPEO, 6.6% KSS and 2.6% PS. Common symptoms are shown in Table 4.1.

Clinical feature	N (%)
Ptosis	210 (92.1%)
PEO	192 (84.2%
Muscle weakness	106 (46.5%
Exercise intolerance	45 (19.7%)
Deafness	42 (18.4%)
Dysphagia	34 (14.9%)
Ataxia	28 (12.3%)
Retinopathy	24 (10.5%)
Short stature	22 (9.6%)

Table 4.1: Common clinical features associated with single, large-scale mtDNA deletions. PEO=progressive external ophthalmoplegia. Table adapted from Mancuso *et al.* (2015).

Although the majority of patients with single deletions can be assigned to one of the three main syndromes, a number of patients present with a collection of milder symptoms at onset. This complicates the diagnosis and determination of prognosis in patients with these mutations. Mancuso *et al.,* (2015) proposed an alternative criteria for the classification of KSS, termed 'KSS spectrum', in order to better categorise the phenotypes of their cohort. Here ptosis and ophthalmoplegia must be present in addition with at least one of either retinopathy, ataxia, cardiac conduction defects, hearing loss, short stature, cognitive impairment, tremor or cardiomyopathy. Using this new criteria, the authors were able to phenotypically classify 98.7% of their cohort, an improvement on the 66.2% classified using the traditional criteria. However, to date evaluating the prognosis of patients with single, large-scale mtDNA deletions remains challenging given the large amount of genetic and phenotypic heterogeneity associated with these mutations. This diversity has complicated investigations into the molecular and cellular mechanisms driving disease progression and it is not surprising that the yielded results are somewhat conflicting.

4.1.3 Correlating clinical phenotype, biochemical deficiency and genetics

The investigation of pathogenic mechanisms associated with single, large-scale mtDNA deletions is challenging due to the heterogeneity of the deletions themselves, which vary in size and location, and the vast array of clinical phenotypes seen in patients with these mutations. Early studies did not observe a correlation between clinical phenotype and location, size or level of the deletion (Moraes *et al.,* 1989; Holt *et al.,* 1989; Rotig *et al.,* 1995). More recent studies offer no further clarity on these relationships.

There are consistent reports of an inverse relationship between deletion size and heteroplasmy level (Lopez-Gallardo *et al.,* 2009; Grady *et al.,* 2014, Mancuso *et al.,* 2015), such that larger deletions do not accumulate to high levels, as smaller deletions do. Several studies have evaluated the role of heteroplasmy in disease severity and progression. While Mancuso *et al.* (2015) found no difference in mutation load between KSS and milder CPEO, others report heteroplasmy as a predictor of phenotype (Lopez-Gallardo *et al.,* 2009; Aure *et al.,* 2007). Multiple regression analyses by Grady *et al.* (2014) concluded that heteroplasmy level, deletion size and deletion of *MT-CYB* gene were significant predictors of disease progression.

The location of the deletion has been considered predictive of the clinical phenotype. Yamashita *et al.* (2008) observed earlier onset when the deletion encompassed genes encoding subunits of complex IV and V. However, Lopez-Gallardo *et al.* (2009) and Grady *et al.* (2014) concluded that the deletion of *MT-CYB*, encoding cytochrome b, was associated with a more severe clinical phenotype. However, the relationship between deletion size and phenotypic severity and progression is less clear, with conflicting reports identifying deletion size as a strong predictor of both clinical phenotype and age of onset (Yamashita *et al.,* 2008; Grady *et al*., 2014), either phenotype or age of onset (Mancuso *et al*., 2015; Lopez-Gallardo *et al*., 2009), or neither phenotype nor age of onset (Rotig *et al*., 1995; Sadikovic *et al*., 2010).

Somewhat clearer is the relationship between respiratory chain dysfunction and deletion level. Mita *et al.* (1989) reported the presence of single, large-scale mtDNA deletions in COX-deficient muscle fibres from a patient with KSS phenotype. A similar finding was later presented by Goto *et al.* (1990), where a higher proportion of COX-deficient fibres was

associated with an increased level of deletion in 22 CPEO patients. More recently, Schröder *et al.* (2000) observed a significant correlation between deletion level and the percentage of COX-negative fibres as well as normalised complex I and IV levels. Similar observations were made by Gellerich *et al.* (2002) who also noted a decline in the activities of complexes I, I+III, II+III, III and IV with increased deletion level. The deletion of *MT-CO* genes has been reported as predictive of the proportion of COX-deficient fibres (Grady *et al.,* 2014), however this was inconsistent with previous findings (Goto *et al.,* 1990; Oldfors *et al*., 1992).

Given the correlation between deletion size and level, and deletion level and respiratory chain deficiency, these studies together should indicate a relationship between the genetic and biochemical defects, such that smaller deletions are able to accumulate to higher heteroplasmy levels establishing a biochemical phenotype. However, as previously discussed, no direct correlation between deletion size and biochemical phenotype has been observed.

4.1.4 Disease progression with single, large-scale mtDNA deletions

A recent retrospective study of 228 patients noted ptosis, ophthalmoparesis, muscle weakness, exercise intolerance and hearing loss as the most common symptoms present at onset (Mancuso *et al.,* 2015). This group report an increase in the number of patients with these symptoms on follow-up, indicating that they can also be acquired at a later stage if not present at onset. The simultaneous progressive severity of established symptoms and the development of additional symptoms complicates the evaluation of clinical disease severity and estimates of prognosis.

Identifying the genetic and biochemical features which change over time in patients with clinically progressive disease could prove useful in providing markers for evaluating disease burden and prognosis. However, few longitudinal studies have been conducted using muscle biopsies from patients with single, large-scale mtDNA mutations, with some conflicting results. Heteroplasmy level has been shown to increase over time in muscle from KSS patients (Ishikawa *et al.,* 2000; Larsson *et al.,* 1990), however Durham *et al.* (2006) observed decreasing heteroplasmy levels in the muscle of patients with mitochondrial myopathy. Likewise, the distribution of COX-negative fibres has been shown to increase over time, yet also remain stable in some patients (Chinnery *et al.,* 2003; Durham *et al.,* 2006; Larsson *et*

al., 1990). Only one study has evaluated changes to mtDNA copy number over time (Durham *et al.,* 2006), postulating that a decline in wild-type mtDNA copy number, rather than the accumulation of mutant species, is the primary cause of observed COX-deficiency in mitochondrial myopathy.

4.2 Aims

Understanding the molecular and cellular mechanisms behind disease progression has important clinical implications regarding predicting prognosis, implementing treatment strategies and identifying suitable targets for therapeutic drug development. This longitudinal study uses serial skeletal muscle (SKM) biopsies, collected between 2-23 years, from patients (n=10) with single, large-scale mtDNA deletions, of various sizes, and progressive disease in order to evaluate changes to (i) the biochemical defect, (ii) deletion level and (iii) total mtDNA copy number over time, and determine whether these genetic and cellular characteristics play a role in clinical disease progression, as measured by validated Newcastle Mitochondrial Disease Adult Scale (NMDAS) scores (Schaefer *et al.,* 2006).

4.3 Methods

4.3.1 Patients and controls

Ten patients with single, large-scale mtDNA deletions and serial skeletal muscle biopsies were identified from the MRC Centre Mitochondrial Disease Patient Cohort (Table 4.2). Biopsies collected for diagnostic purposes were approved for research use by Newcastle and North Tyneside 1 committee (REC 2005/202). Additional skeletal muscle biopsies were collected under REC reference 11/NE/0337 (Newcastle and North Tyneside 2), with informed signed consent from all participants, and stored at the NHS Highly Specialised Rare Mitochondrial Disease Laboratory in Newcastle (REC 08/H0906/28+5). Skeletal muscle biopsies obtained from thee controls were used in this study (section 3.3.1).

Patient	Interval (years)	Biopsy one				Biopsy two			
		Age	Muscle	Symptoms	NMDAS	Age	Muscle	Symptoms	NMDAS
P1 (F)	2.6	42.7	LQ	Fatigue	*R	45.4	LQ	Dysphagia, myopathy	*R
P2 (M)	8.8	30.7	LQ	Ptosis, PEO	*R	39.5	LQ	Ptosis, PEO, myopathy, fatigue	*R
P3 (F)	9.4	30.8	N/A	Ptosis, fatigue, mild myopathy	*R	40.1	N/A	Ptosis, PEO, fatigue, myopathy, dysphagia, myalgia	*R
P4 (F)	12.4	43.8	LQ	Ptosis, PEO, myopathy, fatigue, migraine	*R	56.2	N/A	Ptosis, PEO, myopathy, migraine, ataxia, GI problems	31.0
P5 (F)	4.2	32.3	LQ	PEO, myopathy, ptosis, dysphagia	*R	36.5	RQ	PEO, ptosis, myopathy, dysphagia, migraine, GI problems, dysphonia, fatigue	*R
P6 (F)	6.1	15.0	N/A	Ptosis, heart conduction defects, PEO, retinal pigment changes	*R	21.1	RQ	Ptosis, PEO, myopathy, ataxia, heart conduction defects, cognition problems, short stature	21.0
P7 (M)	23.1	34.3	LQ	Ptosis, PEO	*R	57.4	RQ	Ptosis, PEO, dysphagia, myopathy, fatigue, dysphonia/dysarthria, hearing and vision problems	48.7
P8 (M)	6.8	50.0	LQ	Ptosis, PEO, diabetes	15.0	56.8	RQ	Ptosis, PEO, diabetes (insulin-dependent)	12.0
P9 M)	3.4	30.8	N/A	Ptosis, PEO	7.0	34.2	RQ	Ptosis, PEO, myopathy, ataxia	12.0
P10 (M)	9.8	33.1	RQ	Ptosis, dysphagia	*R	42.9	RQ	Ptosis, PEO, dysphagia, GI problems	14.0

Table 4.2: Patients with single, large-scale mtDNA deletions selected from the MRC Centre Mitochondrial Disease Patient Cohort. PEO= progressive external ophthalmoplegia; RQ=right quadriceps; LQ=left quadriceps; LG=left gastrocnemius; N/A = data not available; NMDAS=Newcastle Mitochondrial Disease Adult Scale; Scaled NMDAS scores are reported for the assessment nearest the biopsy date. Where patient biopsies were collected before 2005, no NMDAS data is available and so retrospective scoring is required (*R).

4.3.2 NMDAS

All available NMDAS data for the selected patients was used for the analysis of clinical disease progression as described in chapter three (section 3.3.3). Multiple NMDAS assessments were available for all patients.

4.3.3 Statistical modelling of disease progression

Modelling of clinical disease progression was carried out using the same method as described in section 3.3.4. Scaled total NMDAS scores were calculated using sections two and three of the NMDAS assessment, and transformed by square-rooting the data.

4.3.4 Immunofluorescent staining of cryosectioned skeletal muscle

Two serial 10µm sections were cut onto a single slide and left to dry before storing at -80°C. Prior to beginning the immunofluorescence protocol outlined in section 2.5.2, sections were removed from the freezer and left to dry at room temperature for up to one hour. Tiled fluorescent images were acquired at 20x magnification using a Zeiss Axioimager M1 microscope with Axiovision software (Carl Zeiss). Images were analysed using Imaris (Bitplane) and R script as described in sections 2.5.5 and 2.5.7.

4.3.5 Real time PCR assay for determination of mtDNA copy number

A 1:10 serial dilution of plasmid p.7D1.B2M was prepared for use as a standard curve. Dilutions 10^{-5} through 10^{-10} were loaded in triplicate onto each plate. Patient DNA samples were diluted to 1.0ng/µl in nuclease-free water. Each patient sample was loaded in sextuplicate onto six replicate plates, as suggested for a 10% mean detectable difference in mtDNA copy number (Grady *et al.,* 2014). This assay is further described in section 2.8.4.

4.3.6 Real time PCR assay for determination of deletion level

A standard curve was prepared as described in 4.3.5. Patient DNA samples diluted to 1ng/µl for use in the *B2M* assay for copy number were further diluted 1:100 in nuclease-free water. Each patient sample was loaded in sextuplicate onto six replicate plates, as suggested for a 1-2% mean detectable difference in deletion level by Grady *et al.,* (2014). This assay is further described in section 2.8.3.

4.3.7 Long-range PCR

To confirm the presence of a single, large-scale mtDNA deletion primers allowing for the amplification of an approximately 16kb region of mtDNA were selected. The PCR mastermix consisted of 10µl 5x PrimeSTAR GXL buffer, 4µl 2.5µM dNTPs, 1µl 10µM forward primer (nt. 122-150 (NC_012920.1) 5'- CAGTATCTGTCTTTGATTCCTGCCTCATC-3'), 1µl 10µM reverse primer (nt.16308-16281 (NC_012920.1) 5'- CTATGTACTGTTAAGGGTGGGTAGGTTTG-3') and 1µl PrimeSTAR GXL polymerase, made up to 49µl final volume with nuclease-free water. 1µl patient DNA, at 1ng/µl concentration, was added to 49µl mastermix per 0.2ml PCR tube. Tubes were pulse-vortexed for 15 seconds and centrifuged before being placed in a thermocycler pre-heated to 94°C. Cycling conditions were as follows: 35 cycles of 98°C for 10 seconds (denaturation), 68°C for 11 minutes (annealing and extension); hold at 4°C. PCR products were electrophoresed through a 0.7% agarose gel for approximately 45 minutes before imaging via a ChemiDoc system.

4.4 Results

4.4.1 Clinical progression of disease

Multiple NMDAS scores were available for all ten patients. Longitudinal modelling of scaled total NMDAS scores from these patients are shown alongside those from patients in the MRC Centre Mitochondrial Disease Patient Cohort in Figure 4.1. The average profile of progression across the cohort was highlighted for comparison with patients in this study. P2, P8, P9 and P10 were mildly affected, progressing below the cohort average. P1, P3, P4, P5 and P7 followed the expected progression profile. P6 was severely affected and progressed at a much faster rate than the cohort average.

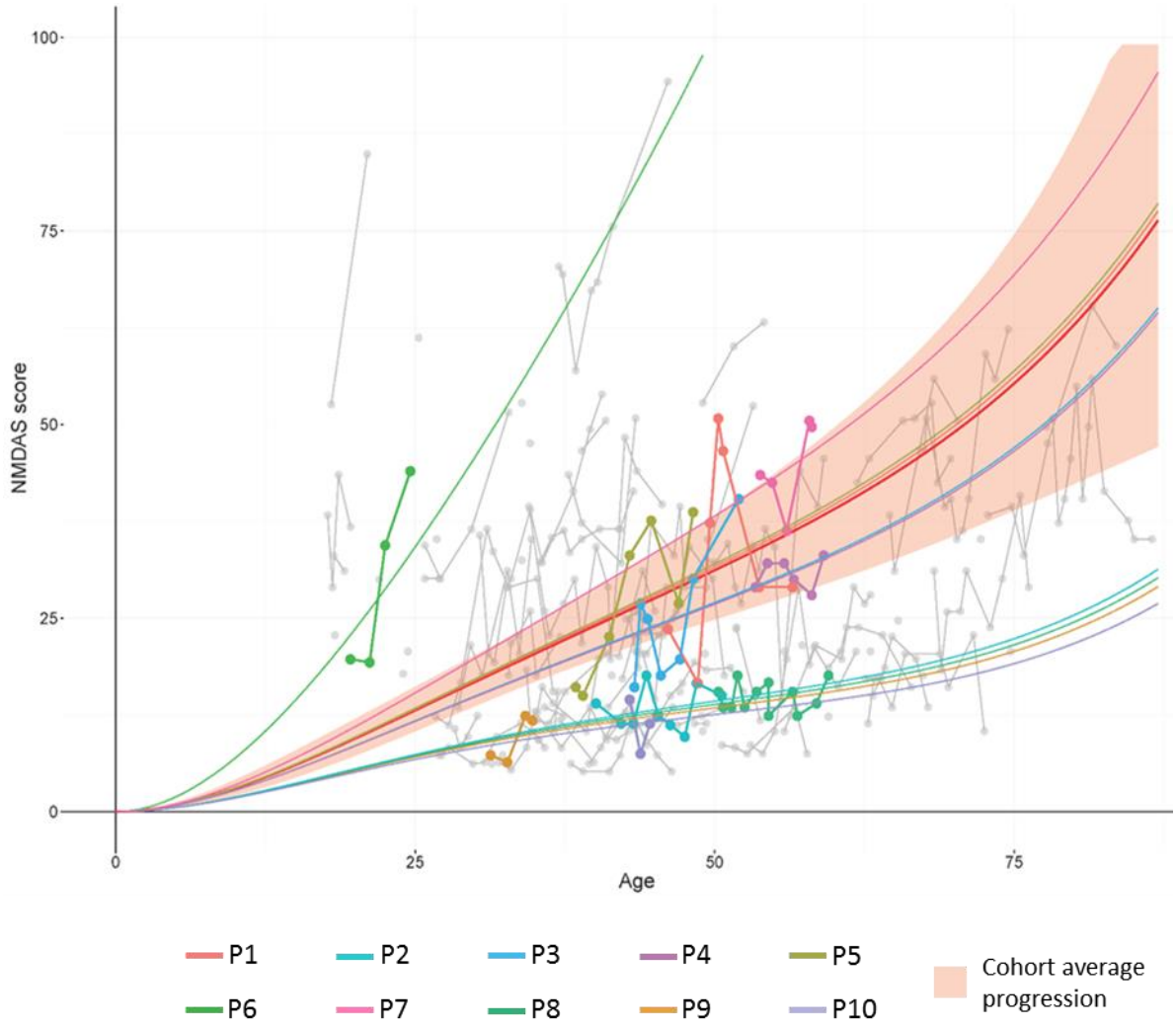

Figure 4.1: Total NMDAS scores for patients with single, large-scale mtDNA deletions. Total NMDAS scores were recorded and scaled (square-root transformed) for each patient in this study (n=6) and the MRC Centre Mitochondrial Disease Patient Cohort (n=104). Lines show the estimated disease progression from birth calculated from longitudinal mixed modelling for patients in this study (coloured) and those in the cohort (grey). The average progression for the cohort is shaded in red.

4.4.2 Characteristics of single, large-scale mtDNA deletions

Patients selected for this study harbour a variety of deletion species, ranging in size and location (Figure 4.2). The smallest deletion, removing only 2300 base pairs, is found in P8, whereas the largest deletion species was identified in P10 at 7595 base pairs. The 4977 bp common deletion was found in three patients in this group (P5, P6 and P7) (Table 4.3).

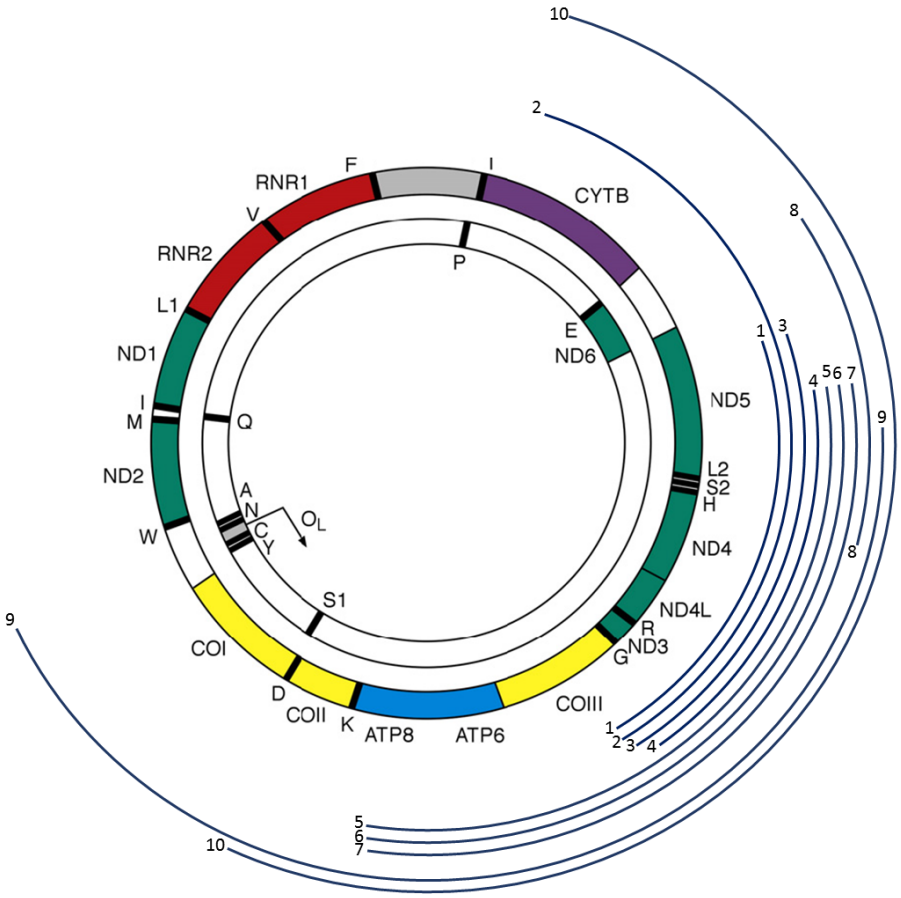

Figure 4.2: Size and location of single, large-scale mtDNA deletions. Deleted region of mtDNA is highlighted and numbered by patient.

	P1	P2	P3	P4	P5	P6	P7	P8	P9	P10
OLR										
tRNA cys									X	
tRNA tyr									X	
NC									X	
MT-COI									X	
tRNA ser1									X	
NC									X	
tRNA asp									X	
MT-COII									X	X
NC									X	X
tRNA lys									X	X
NC									X	X
MT-ATP8					X	X	X		X	X
MT-ATP6					X	X	X		X	X
MT-COIII	X	X	X	X	X	X	X		X	X
tRNA gly	X	X	X	X	X	X	X		X	X
MT-ND3	X	X	X	X	X	X	X		X	X
tRNA arg	X	X	X	X	X	X	X		X	X
MT-ND4L	X	X	X	X	X	X	X		X	X
MT-ND4	X	X	X	X	X	X	X	X	X	X
tRNA his	X	X	X	X	X	X	X	X	X	X
tRNA ser2	X	X	X	X	X	X	X	X	X	X
tRNA leu2	X	X	X	X	X	X	X	X	X	X
MT-ND5	X	X	X	X	X	X	X	X	X	X
MT-ND6		X						X		X
tRNA glu		X								X
NC		X								X
MT-CYB		X								X
Size (bp)	4241	5899	4237	3693	4977	4977	4977	2300	7144	7595
5' break	9498	9523	9486	9756	8482	8482	8482	12112	5772	7845
3' break	13739	15422	13723	13449	13460	13460	13460	14412	12916	15440
Genes deleted										
tRNAs	5	6	5	5	5	5	5	3	10	7
CI	4	5	4	4	4	4	4	3	4	5
CIII	0	1	0	0	0	0	0	0	0	1
CIV	1	1	1	1	1	1	1	0	3	2
CV	0	0	0	0	2	2	2	0	2	2

Table 4.3: Profiles of single large-scale deletions. Deleted genes are marked by 'X' for each patient. Deletion size is shown in base pairs (bp) alongside 5' and 3' breakpoints determined by Dr Georgia Campbell. The total number of tRNA and protein-encoding genes deleted are shown for each deletion species. OLR=origin of light strand replication; NC=non-coding nucleotides; CI-CV=complex I-V.

Eight patients (all except P3 and P10) had sufficient tissue from both biopsies to undergo the quadruple immunofluorescence protocol for quantitative analysis of respiratory chain dysfunction. The mtRC profiles, displaying the levels of complex I and complex IV deficiency in each muscle fibre, are shown in Figure 4.3. These profiles are consistent with those of single, large-scale deletion patients presented by Rocha *et al*. (2015). In biopsy one, most patients show an equal down-regulation of both complexes, with the exception of P8, who shows preferential complex I deficiency, and P9, who shows preferential complex IV deficiency. These profiles are similar in biopsy two although with the addition of fibres with greater levels of respiratory chain deficiency. Interestingly, these additional fibres highlight a preferential deficiency of complex IV in P2.

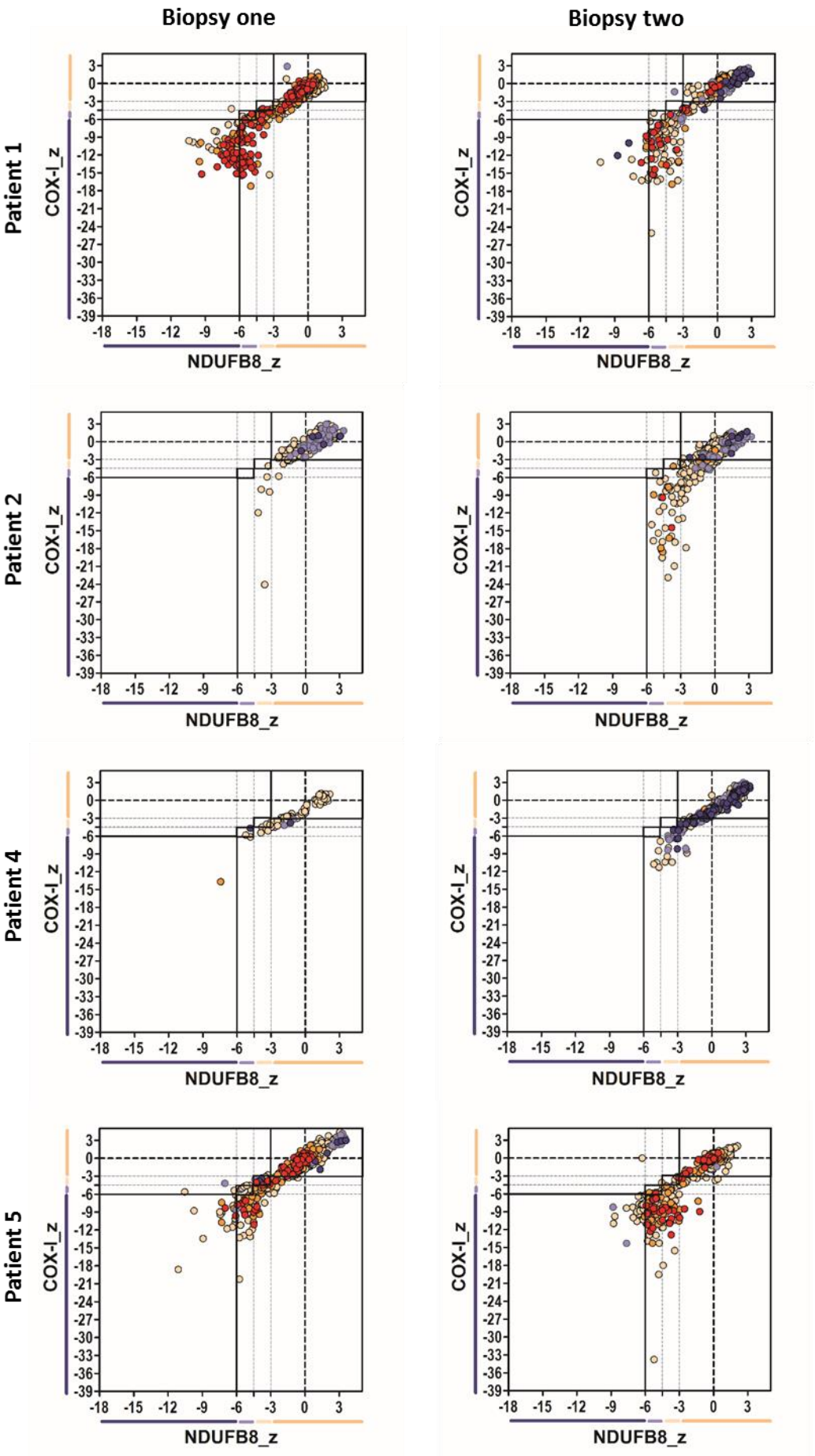
Biopsy one
Biopsy two
Patient 1
Patient 2
Patient 4
Patient 5
COX-I_z
NDUFB8_z
3 0 -3 -6 -9 -12 -15 -18 -21 -24 -27 -30 -33 -36 -39
-18 -15 -12 -9 -6 -3 0 3

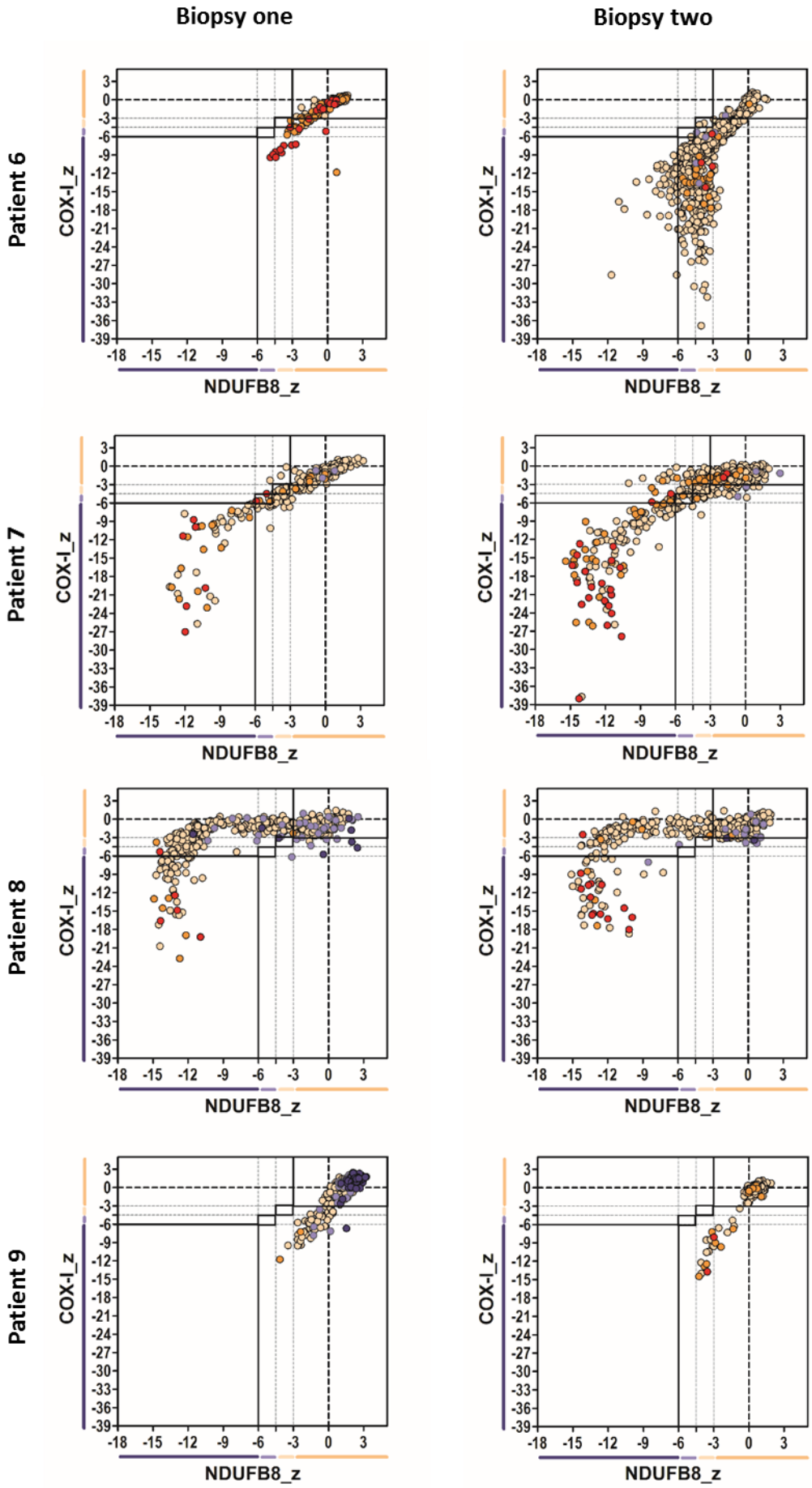
Biopsy one
Biopsy two
Patient 6
Patient 7
Patient 8
Patient 9
COX-I_z
NDUFB8_z
3 0 -3 -6 -9 -12 -15 -18 -21 -24 -27 -30 -33 -36 -39
-18 -15 -12 -9 -6 -3 0 3

Figure 4.3: Mitochondrial Respiratory Chain (mtRC) profiles for single, large-scale deletions. Z_scores for NDUFB8 (zCI) and COX-I (zCIV) are shown for each muscle fibre in two skeletal muscle biopsies from eight patients. There was not sufficient tissue available from P3 and P10 to perform the immunofluorescence protocol. Each dot represents an individual muscle fibre, colour coded according to porin level (dark blue=very low (z<-3SD), light blue=low (-3SD<z<-2SD), beige=normal (-2SD<z<+2SD), orange=high (+2SD<z<+3SD), red=very high (z>+3SD)). Fibres can be categorised based on zCI and zCIV as negative (dark blue y-axis (z<-6.0SD)), intermediate negative (light blue y-axis (-6.0SD<z<-4.5SD)), intermediate positive (light beige y axis (-4.5SD<z<-3.0SD)), or positive (dark beige y-axis (z>-3.0SD)) for complex I or complex IV respectively.

4.4.3 Respiratory chain deficiency: Complex I

Figure 4.4 shows the distribution of complex I levels across each biopsy with z_scores representing the levels of complex I in individual fibres from patient skeletal muscle biopsies. A Mann-Whitney U-test was performed to calculate the median level of complex I in each biopsy and determine the change in the distribution from biopsy one to biopsy two. Two patients (P3 and P10) had insufficient tissue for the immunofluorescent protocol to be carried out. Of the remaining eight patients, seven showed a notable change to the median level of complex I over time: P1 and P4 increased, whereas P2, P5, P6, P7 and P9 all decreased. P8 did not show any change to median complex I levels, however this patient already displayed marked complex I deficiency in biopsy one.

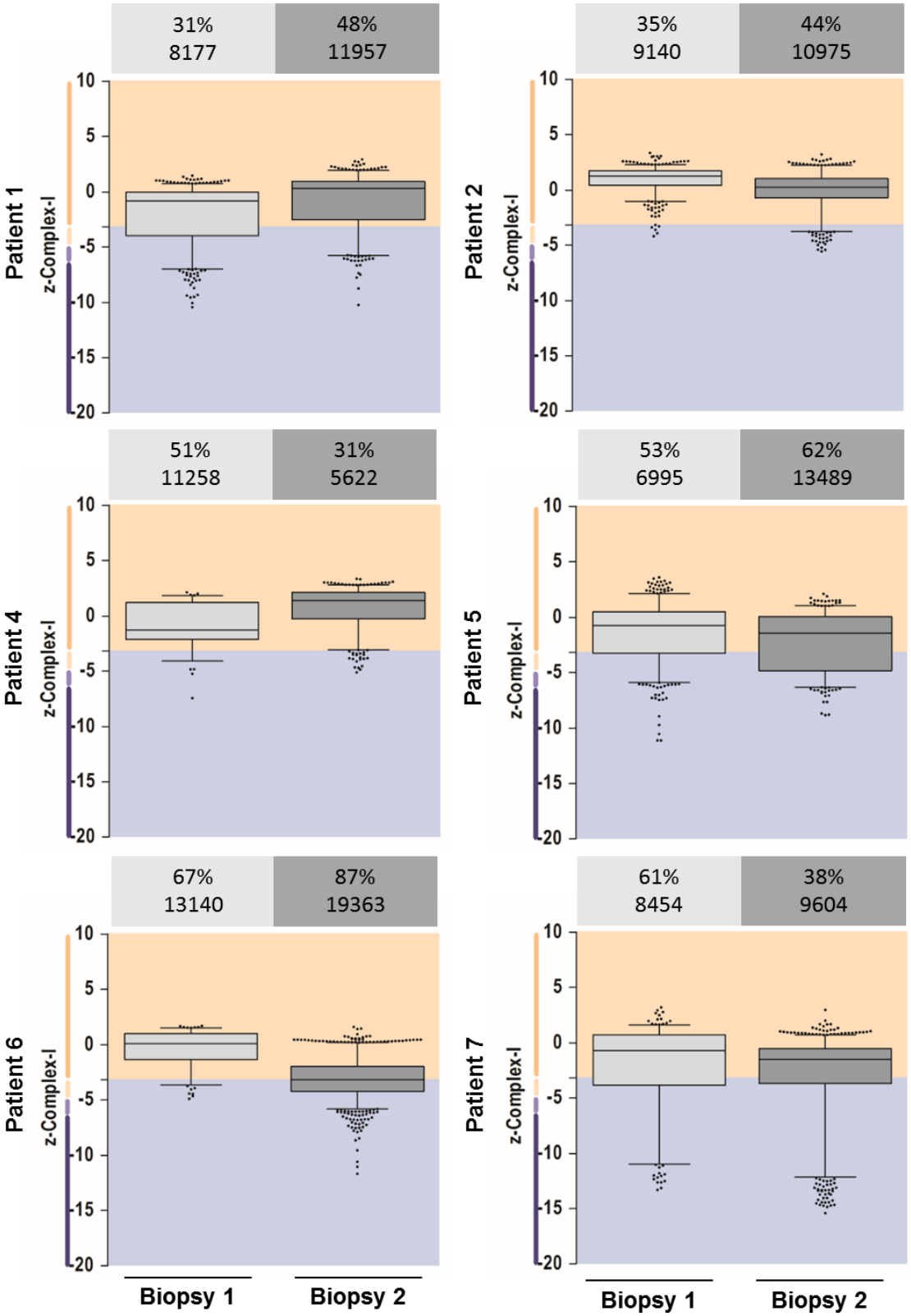
Patient 1
31%
8177
48%
11957
Patient 2
35%
9140
44%
10975
Patient 4
51%
11258
31%
5622
Patient 5
53%
6995
62%
13489
Patient 6
67%
13140
87%
19363
Patient 7
61%
8454
38%
9604
z-Complex-I
10
5
0
-5
-10
-15
-20
Biopsy 1
Biopsy 2

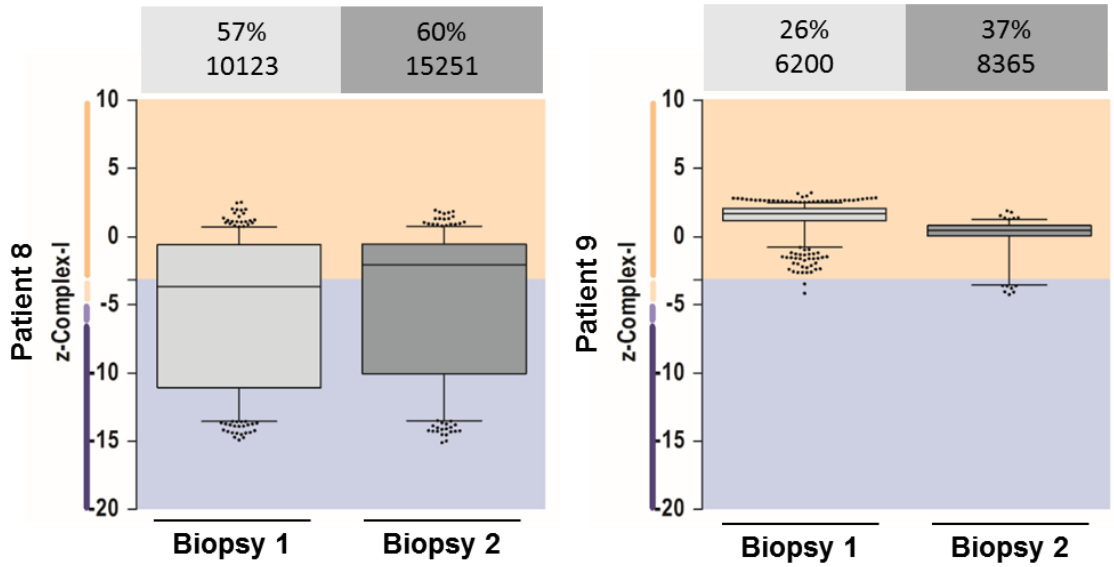

Figure 4.4: Distribution of complex I levels in serial biopsies from patients with single, large-scale deletions. z_scores for complex I (z_CI) are shown for biopsy one (light grey) and biopsy two (dark grey) for eight patients. Boxplots show the median and interquartile range of z_CI with whiskers extending to the 5-95th percentiles. Outliers are indicated by black dots. Fibres are categorised as positive (beige background) or deficient (blue background). Deficient fibres include those classified as intermediate positive (light beige y axis (-4.5SD<z<-3.0SD)), intermediate negative (light blue y-axis (-6.0SD<z<-4.5SD)) or negative (dark blue y-axis (z<-6.0SD)) for complex-I. Deletion level (%) and total mtDNA copy number are shown in the boxes above each graph (biopsy one=light grey; biopsy two=dark grey).

The total change to median complex I levels is shown in Figure 4.5A. The largest change is seen in P6 whose levels decline from 'normal' (z>-3SD) to 'deficient' (z<-3SD). The rate of change to median complex I levels over time was determined by dividing the overall change by the length of the interval between biopsies (Figure 4.5B). The most rapid change to complex I levels is observed in P6, with a decline of 0.47SD per year. In contrast, complex I levels in P8 decline at just 0.04SD per year, the slowest change in the group.

Accounting for the interval time over which a change is observed is important for the investigation of mechanisms contributing to this change. For example, P5 and P7 show similar levels of complex I in the first biopsy, declining to similar levels at biopsy two. However, the intervals over which these changes occur are substantially different, with 4.2 years between biopsies from P5 and 23.1 years between biopsies from P7. When interval is accounted for, it is evident that the rate of decline in P7 complex I levels is much slower than P5. Therefore, the rate of change is not related to the overall level of complex I.

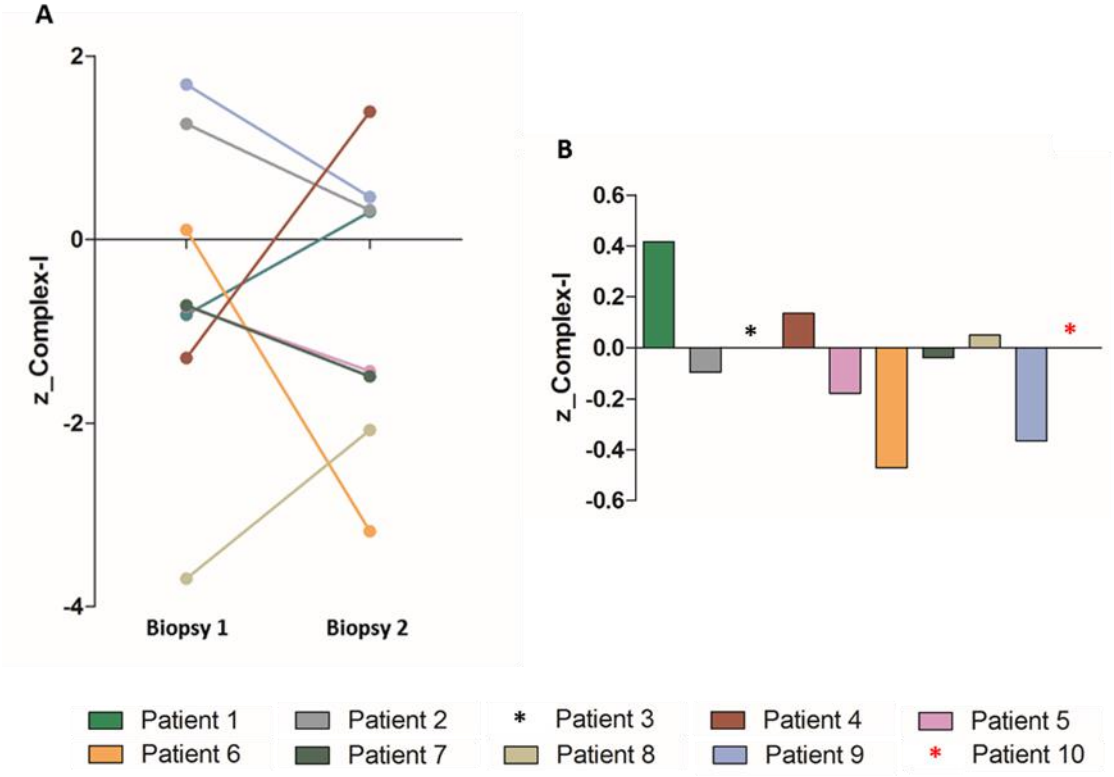

Figure 4.5: Complex I levels in patients with single, large-scale mtDNA deletions. (A) Median levels of complex I in biopsies one and two. (B) Change per year to median complex I levels.

In the majority of cases, the median level of complex I is classified as normal (z>-3SD), masking the extent of the respiratory chain defect seen across the tissue. In order to better evaluate deficiency, fibres were classified as either positive (z>-3SD) or deficient (z<-3SD) for complex I. As indicated by the median complex I levels, P1, P4 and P8 showed a decrease in the proportion of deficient fibres with the remaining patients showing an increase (Figure 4.6A). The rate of change to the proportion of complex I fibres is shown in Figure 4.6B, presented as the change per year over the biopsy interval. The most rapid change is seen in P6 where the proportion of complex I deficient fibres increases by 7.4% per year.

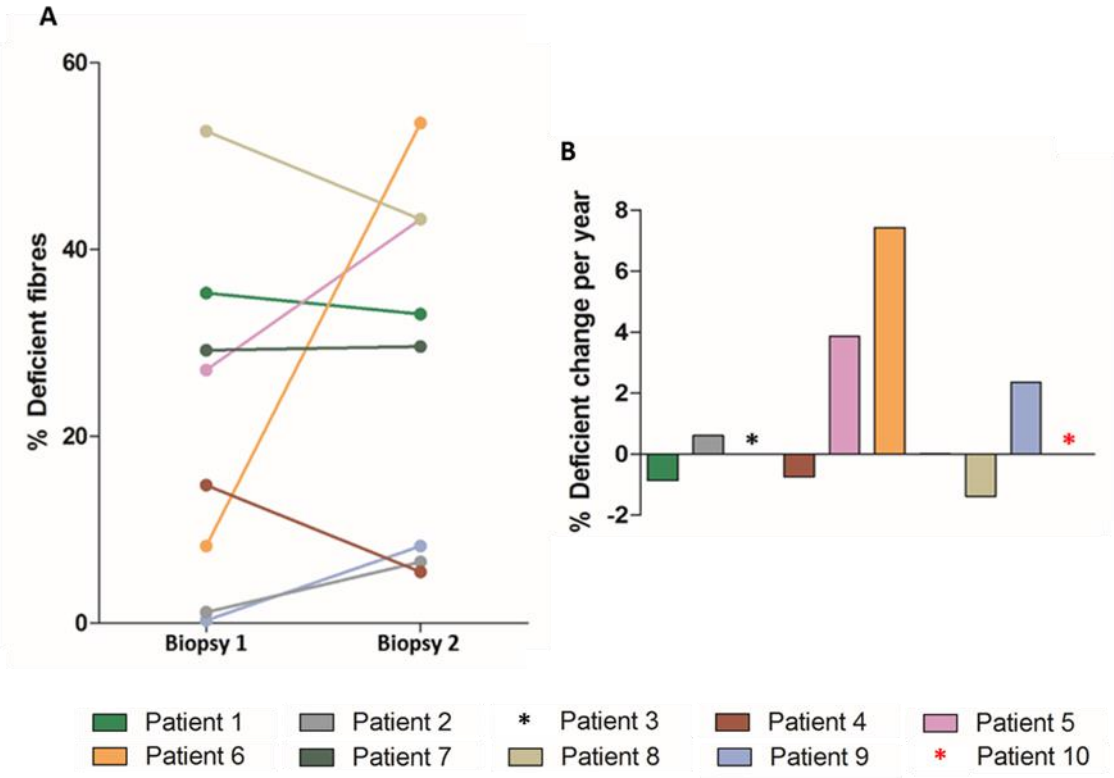

Figure 4.6: The proportion of complex I deficient fibres in patients with single, large-scale mtDNA deletions. (A) Percentage of complex I deficient fibres in biopsies one and two. (B) Change per year to the proportion of complex I deficient fibres.

To further evaluate the alteration to the respiratory chain defect over time, fibres were re-classified as normal (z>-3.0SD), intermediate positive (-3>z>-4.5sd), intermediate negative (-4.5>z>-6.0sd) or negative (z<-6.0sd) for complex I. Figure 4.7 shows the proportion of fibres in each category in biopsy one and two. The proportion of complex I negative fibres was generally low, with the highest seen in P8 at 38.3%. With the exception of P6, who showed a marked decrease in the proportion of complex I positive fibres over time, there were only mild changes to the distribution of complex I over time in these patients.

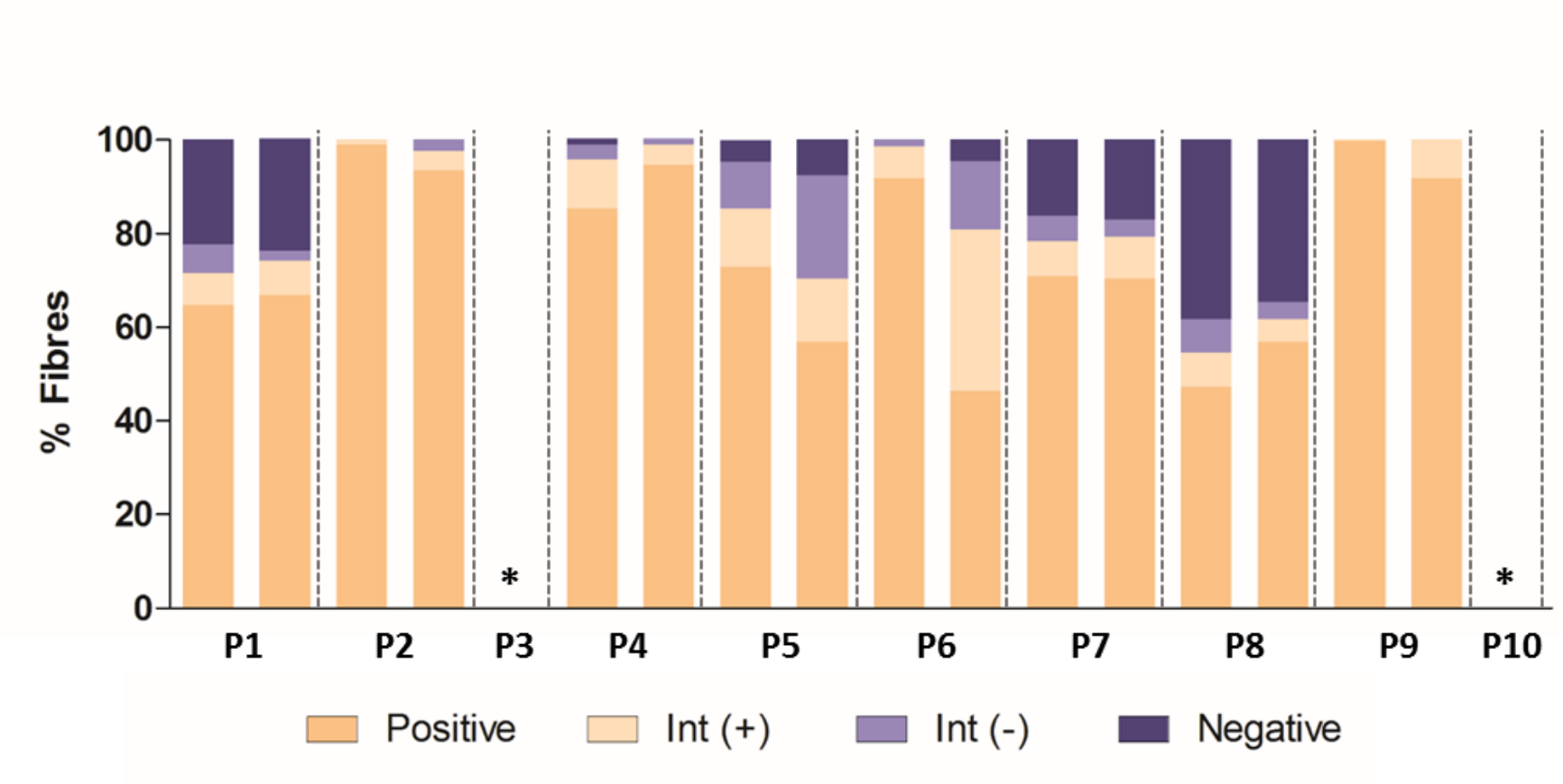

Figure 4.7: Classification of complex I deficiency in single, large-scale deletions. Fibres are categorised as negative (dark blue), intermediate negative (light blue), intermediate positive (light beige), or positive (dark beige) for complex I. The percentage of fibres belonging to each category is shown as a percentage of the total number of fibres in a biopsy for each patient (P1-P10, biopsy one = left bar, biopsy two = right bar).*=insufficient tissue for immunofluorescence protocol.

4.4.4 Respiratory chain defect: Complex IV

The distribution of complex IV levels across each biopsy is shown in Figure 4.8. A Mann-Whitney U-test was performed to determine the median levels of complex IV in each biopsy and calculate the change in distribution between biopsies. All but P8 showed notable changes to the median level of complex IV over time, with the majority of patients displaying a decrease in levels at the second biopsy (P2, P5, P6, P7 and P9). Only two patients showed an increase in complex IV levels (P1 and P4).

Median complex IV levels from each biopsy are shown in Figure 4.9A. As for complex I, the greatest change to complex IV levels is seen in P6 where levels decrease from -0.8SD to -6.9SD, crossing the threshold from normal ($z>-3$) to negative ($z<-6$). This patient also shows the most rapid change, with complex IV levels decreasing at 0.9SD per year (Figure 4.9B). In general the direction of change to complex IV levels mirrors that of complex I, with the exception of P8 where complex I levels increase and complex IV levels decrease.

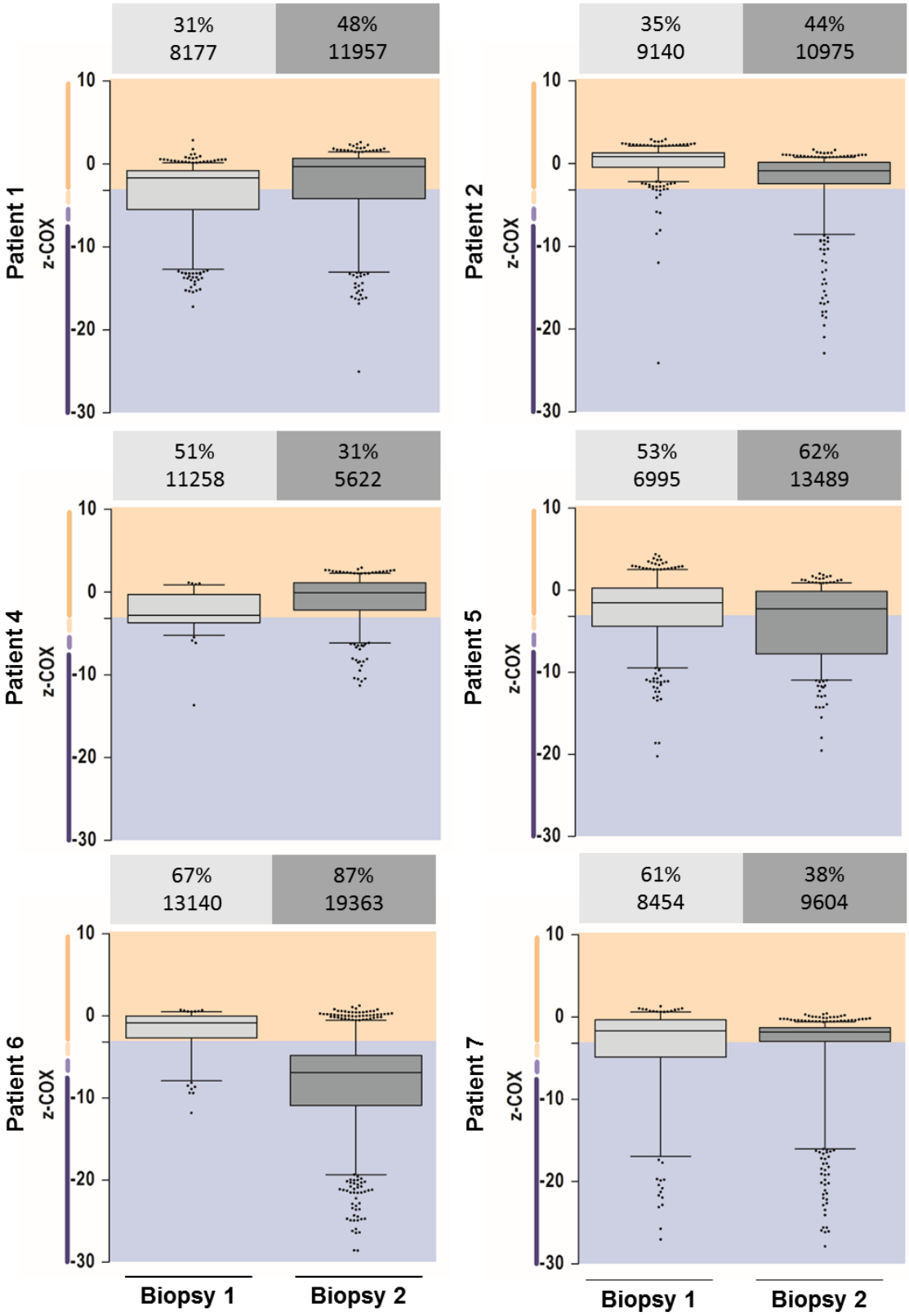
Patient 1
31%
8177
48%
11957
Patient 2
35%
9140
44%
10975
Patient 4
51%
11258
31%
5622
Patient 5
53%
6995
62%
13489
Patient 6
67%
13140
87%
19363
Patient 7
61%
8454
38%
9604
z-COX
10
0
-10
-20
-30
Biopsy 1
Biopsy 2

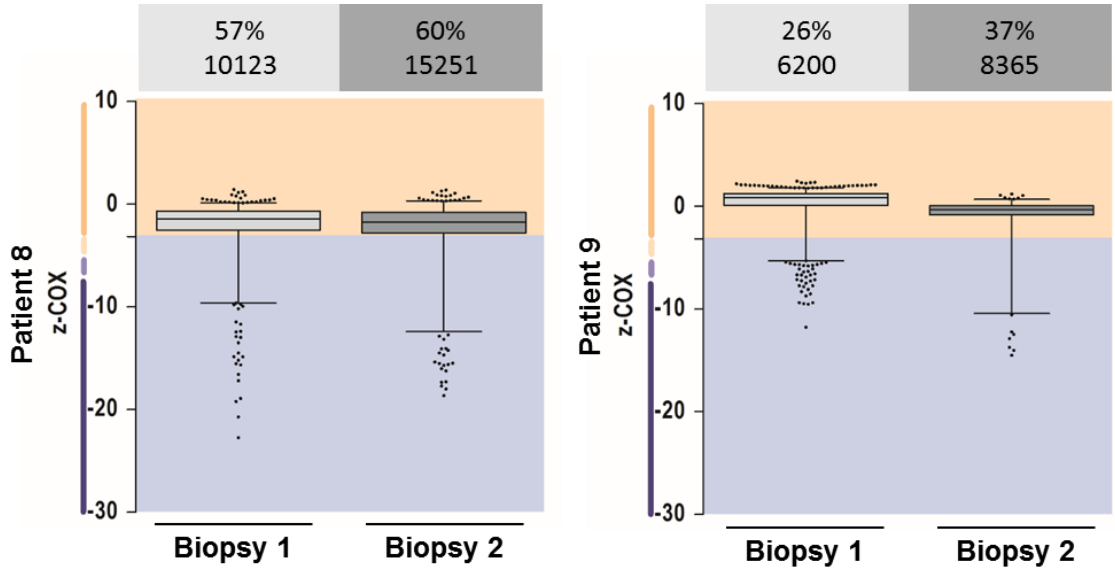

Figure 4.8: Distribution of complex IV levels in serial biopsies from patients with single, large-scale deletions. z_scores for complex IV (z_CIV) are shown for biopsy one (light grey) and biopsy two (dark grey) for eight patients. Boxplots show the median and interquartile range of z_CIV with whiskers extending to the 5-95th percentiles. Outliers are indicated by black dots. Fibres are categorised as positive (beige background) or deficient (blue background). Deficient fibres include those classified as intermediate positive (light beige y axis (-4.5SD<z<-3.0SD)), intermediate negative (light blue y-axis (-6.0SD<z<-4.5SD)) or negative (dark blue y-axis (z<-6.0SD)) for complex IV. Deletion level (%) and total mtDNA copy number is shown in the boxes above each graph (biopsy one=light grey; biopsy two=dark grey).

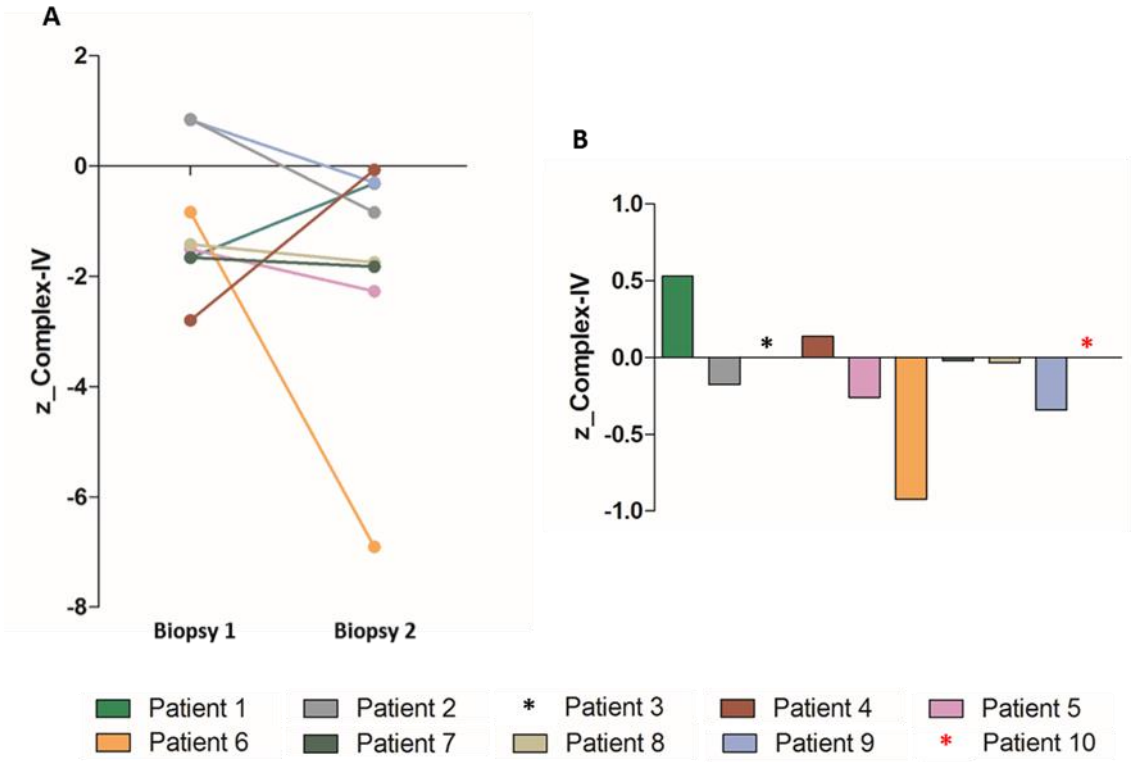

Figure 4.9: Complex IV levels in patients with single, large-scale mtDNA deletions. (A) Median levels of complex IV in biopsies one and two. (B) Change per year to median complex IV levels.

Fibres were classified as positive (z>-3SD) or deficient (z<-3SD) for complex IV to evaluate total deficiency across the biopsy. The proportion of complex IV deficient fibres ranged from 2.5% (P2) to 41.4% (P4) in biopsy one and 18.7% (P1) to 85.6% (P6) in biopsy two (Figure 4.10A). Three patients showed a decrease in the proportion of complex IV deficient fibres over time (P1, P4 and P7), while the remaining five patients showed an increase. The largest change to complex IV deficiency was seen in P6 where the proportion of deficient fibres increased from 20.5% in biopsy one to 85.9% in biopsy two. This patient also showed the most rapid change to complex IV deficiency with an increase of 10.7% deficient fibres per year. The slowest change to complex IV deficiency was seen in P8 where the proportion of complex IV deficient fibres increased by <0.1% per year (Figure 4.10B).

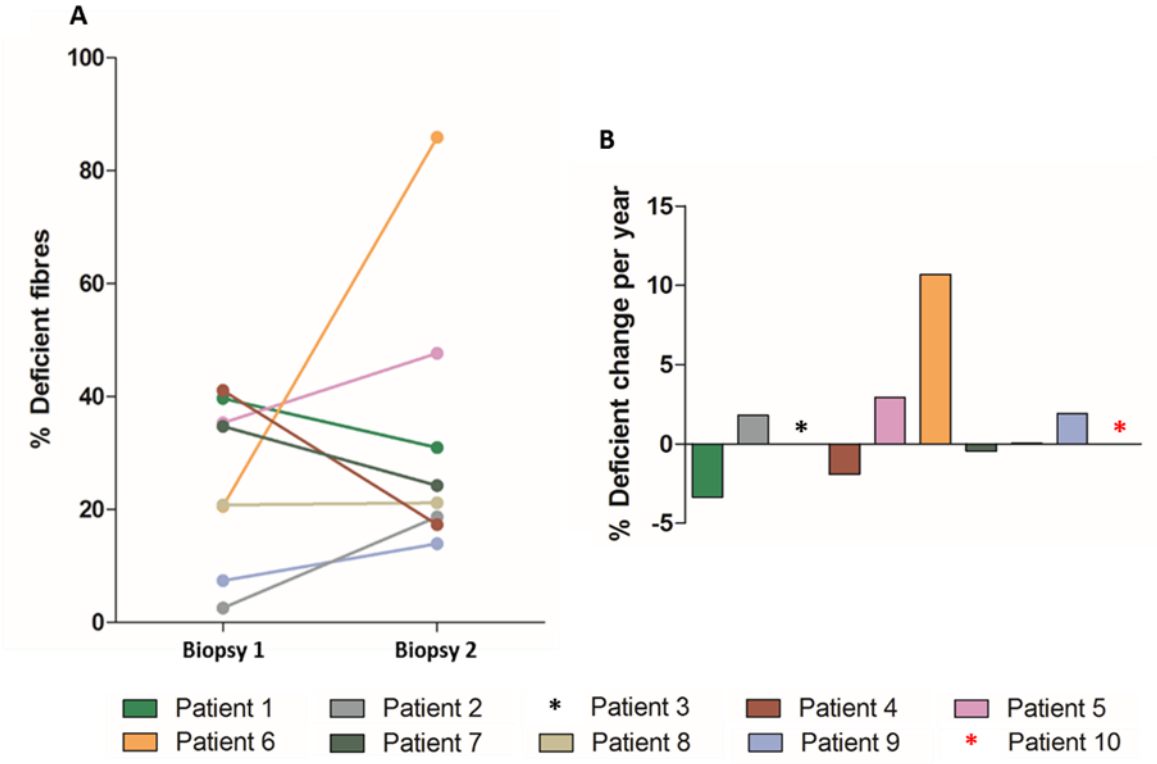

Figure 4.10: The proportion of complex IV deficient fibres in patients with single, large-scale mtDNA deletions. (A) Percentage of complex IV deficient fibres in biopsies one and two. (B) Change per year to the proportion of complex IV deficient fibres.

Figure 4.11 shows the proportion of fibres categorised either as positive (z>-3.0SD), intermediate positive (-3>z>-4.5sd), intermediate negative (-4.5>z>-6.0sd) or negative (z<-6.0sd) for complex IV. P2, P5, P6 and P9 all show an increase in the proportion of complex IV negative fibres over time, all accompanied by a reduction in complex IV positive fibres. In addition, P4 shows an increase in complex IV negative fibres alongside an increase in positive fibres. A decrease in the proportion of complex IV negative fibres is seen in P1 and P7, while P8 shows no change.

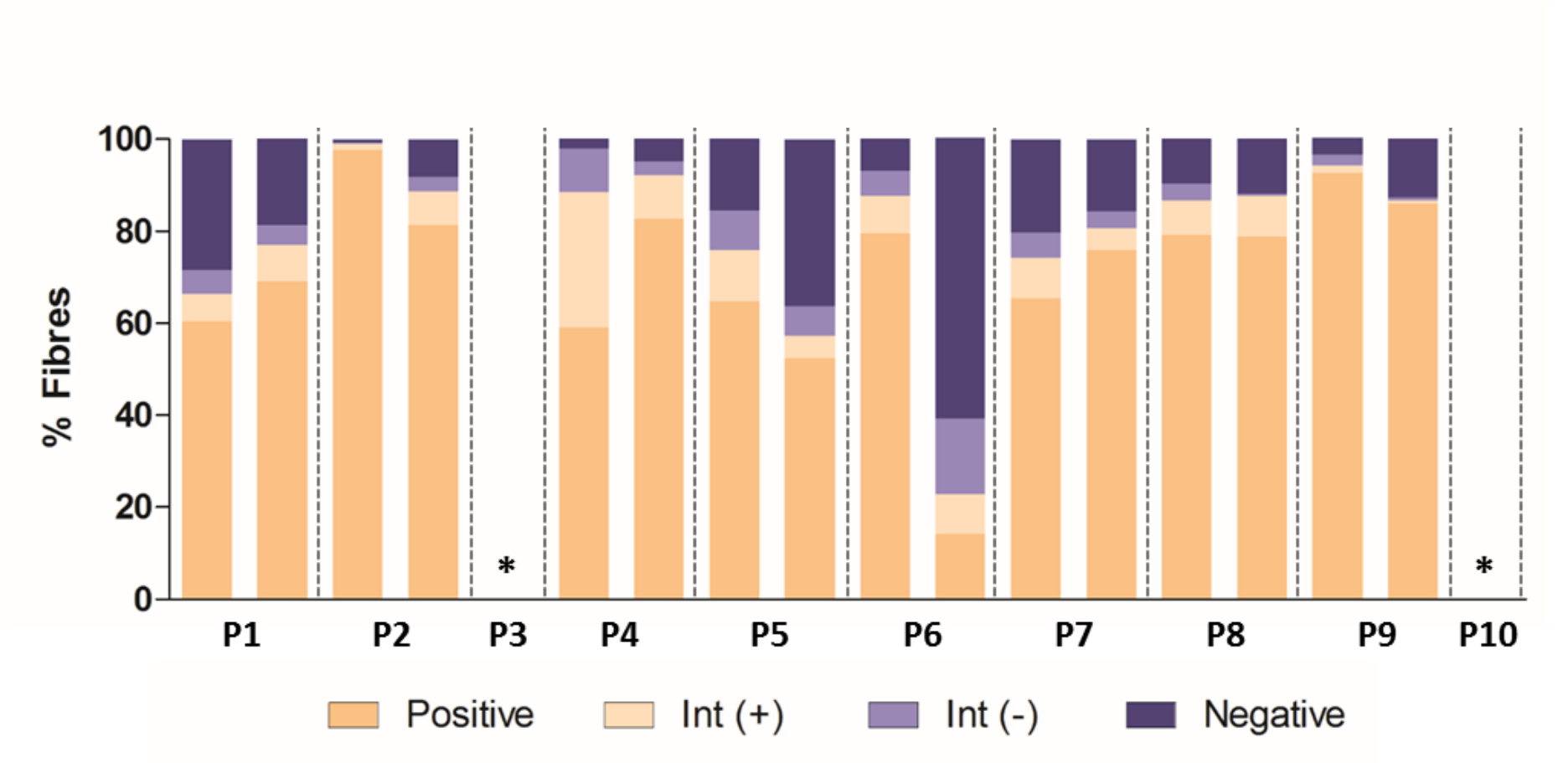

Figure 4.11: Classification of complex IV deficiency in single, large-scale deletions. Fibres are categorised as negative (dark blue), intermediate negative (light blue), intermediate positive (light beige), or positive (dark beige) for complex IV. The percentage of fibres belonging to each category is shown as a percentage of the total number of fibres in a biopsy for each patient (P1-P10, biopsy one = left bar, biopsy two = right bar). *=insufficient tissue for immunofluorescence protocol.

4.4.5 Genetic analysis: Deletion level

Deletion level in each skeletal muscle biopsy is shown in Table 4.4. All ten patients had sufficient tissue for genetic analyses. Deletion level was variable across the group of patients, ranging from 8.6% (P10) to 78.8% (P3) in biopsy one and 9.1% (P10) to 87.1% (P6) in biopsy two. All but two patients, P4 and P7, showed an increase in deletion level over time (Figure 4.12A), with the fastest accumulation seen in P1 at 6.5% per year. A long-rang PCR was performed confirming the presence of single, large-scale deletions in the second biopsies from P4 and P7 (Figure 4.12B). Therefore, the observed decrease in deletion level reflects genuine variation and was not due to the accumulation of additional deletion species.

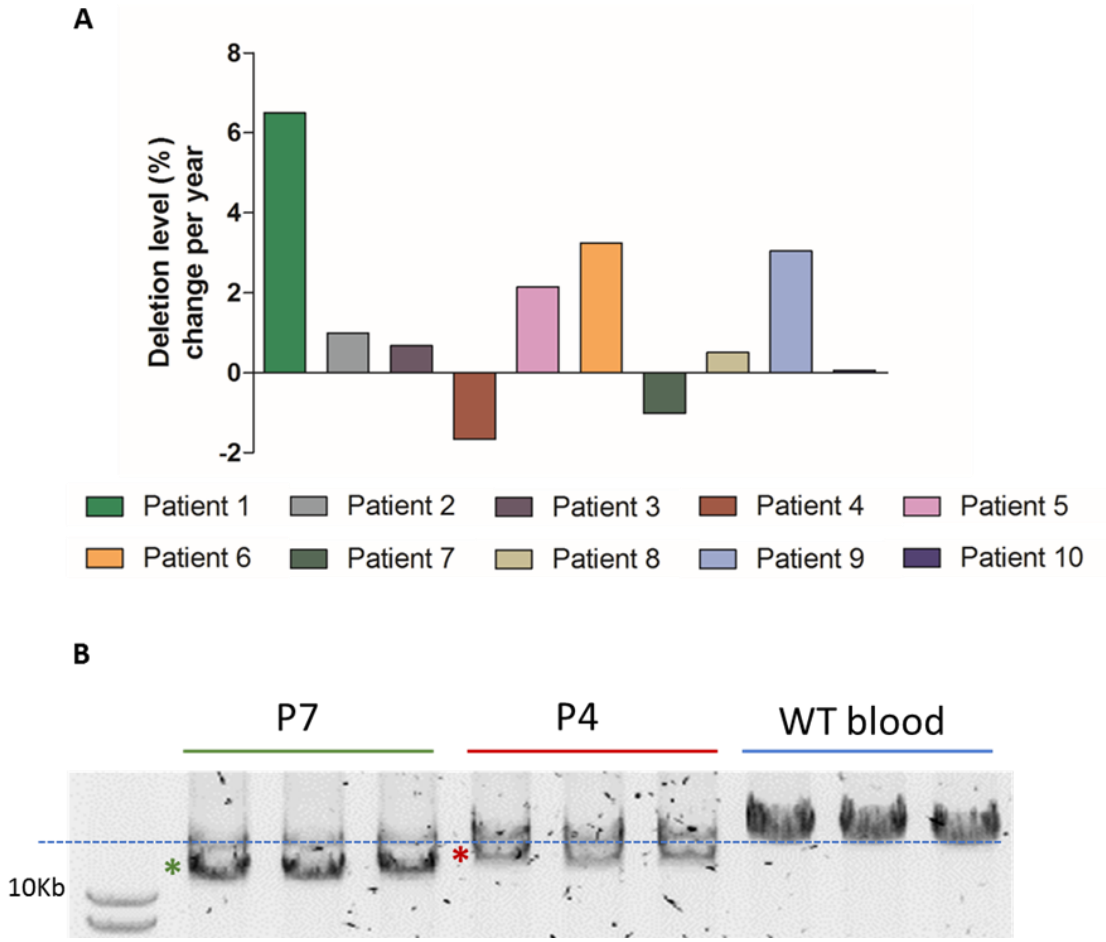

Figure 4.12: Assessing changes to deletion level over time. (A) Change per year to deletion level. (B) Long-range PCR to confirm the presence of single, large-scale mtDNA deletions in biopsy two from patient 7 (lanes 1-3) and patient 4 (lanes 4-6). The wild-type molecule, as indicated by wild-type blood homogenate (WT blood), is marked by a blue dotted line. Deletion species present in patients 7 and 4 are indicated by red and green asterisk, respectively.

Patient	Interval (years)	Deletion level (%)		Total mtDNA copy number		Wild-type mtDNA copy number	
		Bx1	Bx2	Bx1	Bx2	Bx1	Bx2
P1	2.6	31.2(±0.55)	48.1(±0.32)	8177(±594)	11957(±886)	5627(±409)	6202(±459)
P2	8.8	35.2(±0.66)	43.9(±0.55)	9140(±848)	10975(±154)	5923(±549)	6154(±86)
P3	9.4	78.8(±0.28)	85.2(±0.28)	13516(±978)	12576(±1003)	2863(±207)	1861(±149)
P4	12.4	51.4(±0.35)	30.7(±0.45)	11258(±2074)	5622(±199)	5476(±1009)	3898(±138)
P5	4.2	53.4(±0.69)	62.4(±0.82)	6995(±576)	13489(±827)	3260(±268)	5079(±311)
P6	6.1	67.4(±0.39)	87.1(±0.20)	13140(±575)	19363(±1042)	4289(±188)	2488(±134)
P7	23.1	61.2(±0.34)	37.7(±0.52)	8454(±560)	9604(±848)	3276(±217)	5979(±528)
P8	6.8	56.8(±0.56)	60.3(±0.64)	10123(±886)	15251(±1292)	4375(±383)	6062(±513)
P9	3.4	26.2(±0.69)	36.5(±0.56)	6200(±432)	8365(±644)	4573(±318)	5311(±467)
P10	9.8	8.6(±0.33)	9.1(±0.48)	4353(±156)	8420(±368)	3979(±142)	7650(±334)

Table 4.4: Molecular genetic analysis of skeletal muscle from patients with single, large-scale mtDNA deletions. Mean deletion level, total mtDNA copy number and wild-type mtDNA copy number are shown with ±SEM for biopsy one (Bx1) and biopsy two (Bx2).

The relationship between deletion size and deletion level is shown in Figure 4.13. A significant correlation is present in biopsy one ($p=0.036$, $r^2=0.4399$), but not biopsy two ($p=0.148$, $r^2=0.2423$).

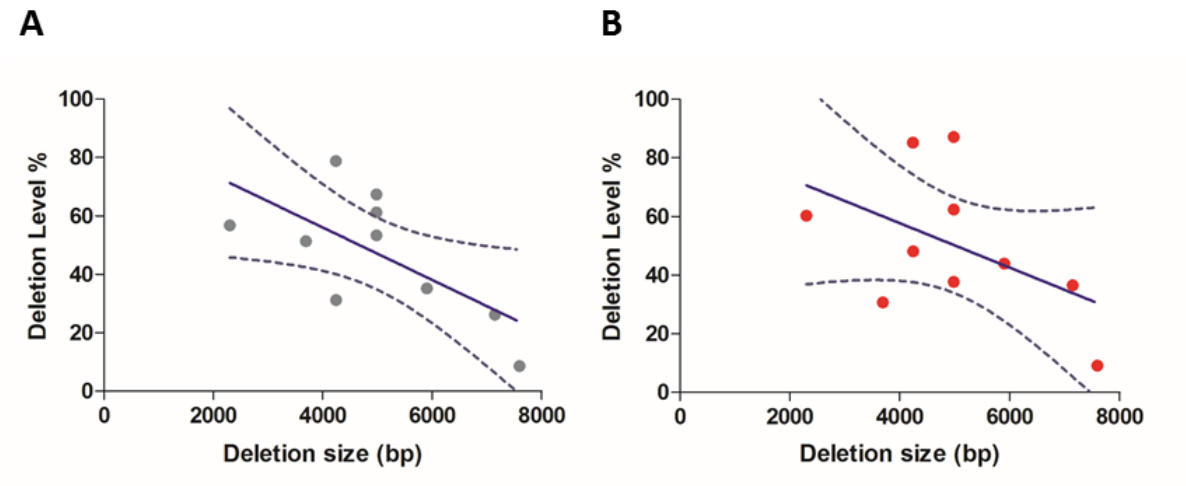

Figure 4.13: Correlation between deletion size and level in skeletal muscle. Deletion level measured in biopsy one (A) and biopsy two (B) is plotted against deletion size (bp). Linear regression analysis of the datasets (solid blue line) is shown with 95% confidence intervals (dotted dark blue lines).

4.4.6 Genetic analysis: mtDNA copy number

Table 4.4 shows the total mtDNA copy number for each biopsy, presented as the number of copies of mtDNA per nucleus. Total mtDNA copy number ranges from 4353 copies (P10) to 13516 copies (P3) in biopsy one and 5622 copies (P4) to 19362 copies (P6) in biopsy two. Eight patients showed an increase in total mtDNA copy number over time while two (P3 and P4) showed decreases. P5 showed the most rapid change to total mtDNA copy number with a compound increase of 17.0% per year, while P8 displayed the slowest change of just 0.6% compound increase per year (Figure 4.14A).

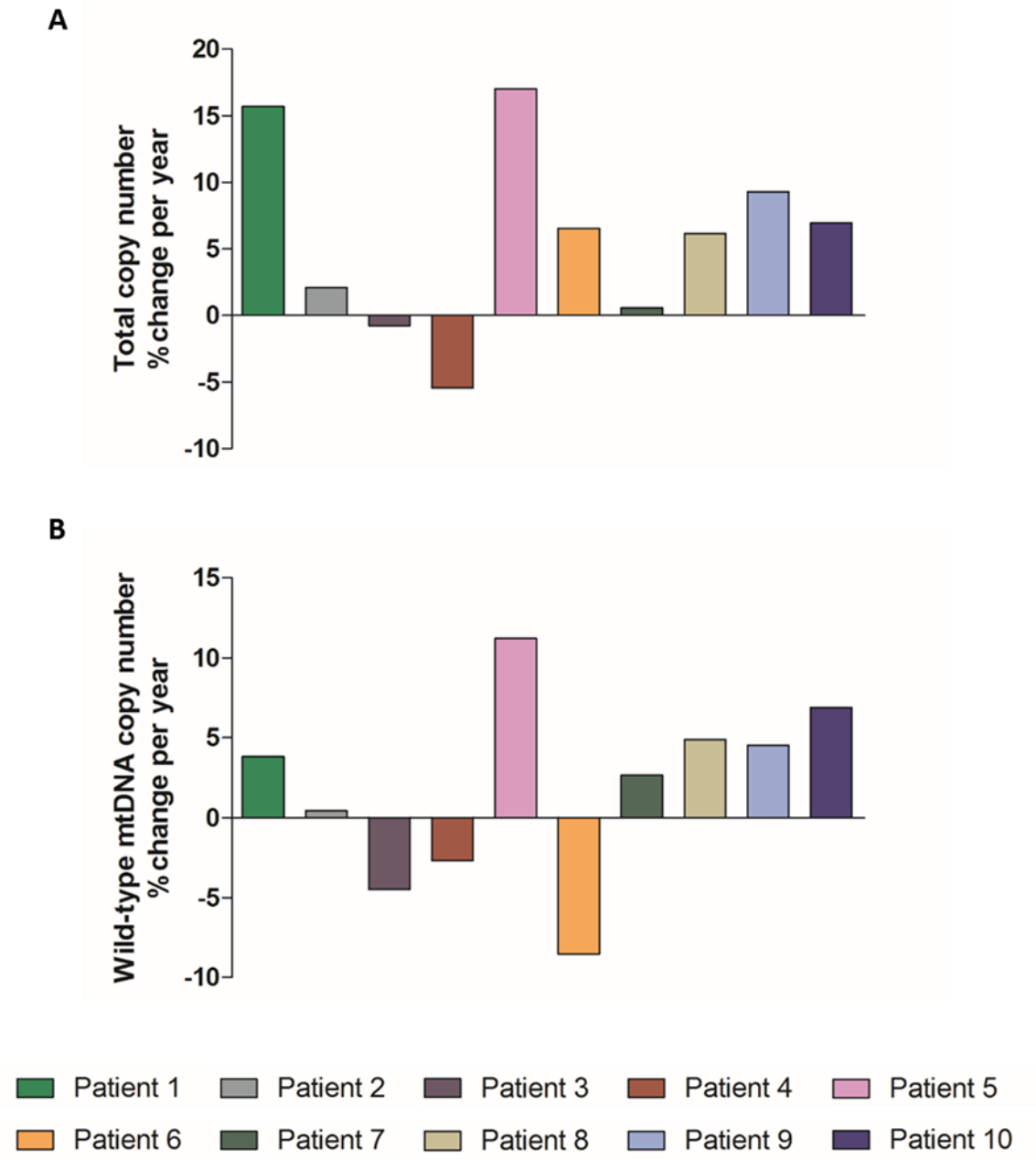

Figure 4.14 mtDNA copy number changes in patients with single, large-scale mtDNA deletions. (A) Change per year to total mtDNA copy number and (B) change per year to wild-type mtDNA copy number are shown as a compound percentage change.

Wild-type mtDNA copy number was calculated by applying the deletion level to the total mtDNA copy number in each biopsy. Wildtype copy number ranges from 2863 copies (P3) to 5923 copies (P2) in biopsy one and 1861 copies (P3) to 7650 copies (P10) in biopsy two (Table 4.4) . Three patients (P3, P4 and P6) showed decreases in wild-type mtDNA copy number over time, while the remaining seven patients all showed an increase. As seen for

total mtDNA copy number, the most rapid change to the proportion of wild-type mtDNA species was seen in P5 with a compound increase of 11.7% per year (Figure 4.14B).

Figure 4.15 shows the relationship between total mtDNA copy number and deletion level. A significant correlation was seen in both biopsies one ($p=0.0022$, $r^2=0.7107$) and two ($p=0.0039$, $r^2=0.6670$). Furthermore, the rate of change in deletion level correlated with the rate of change of total mtDNA copy number ($p=0.0085$, $r2=0.6003$). No such relationships were observed between deletion level and wild-type mtDNA copy number.

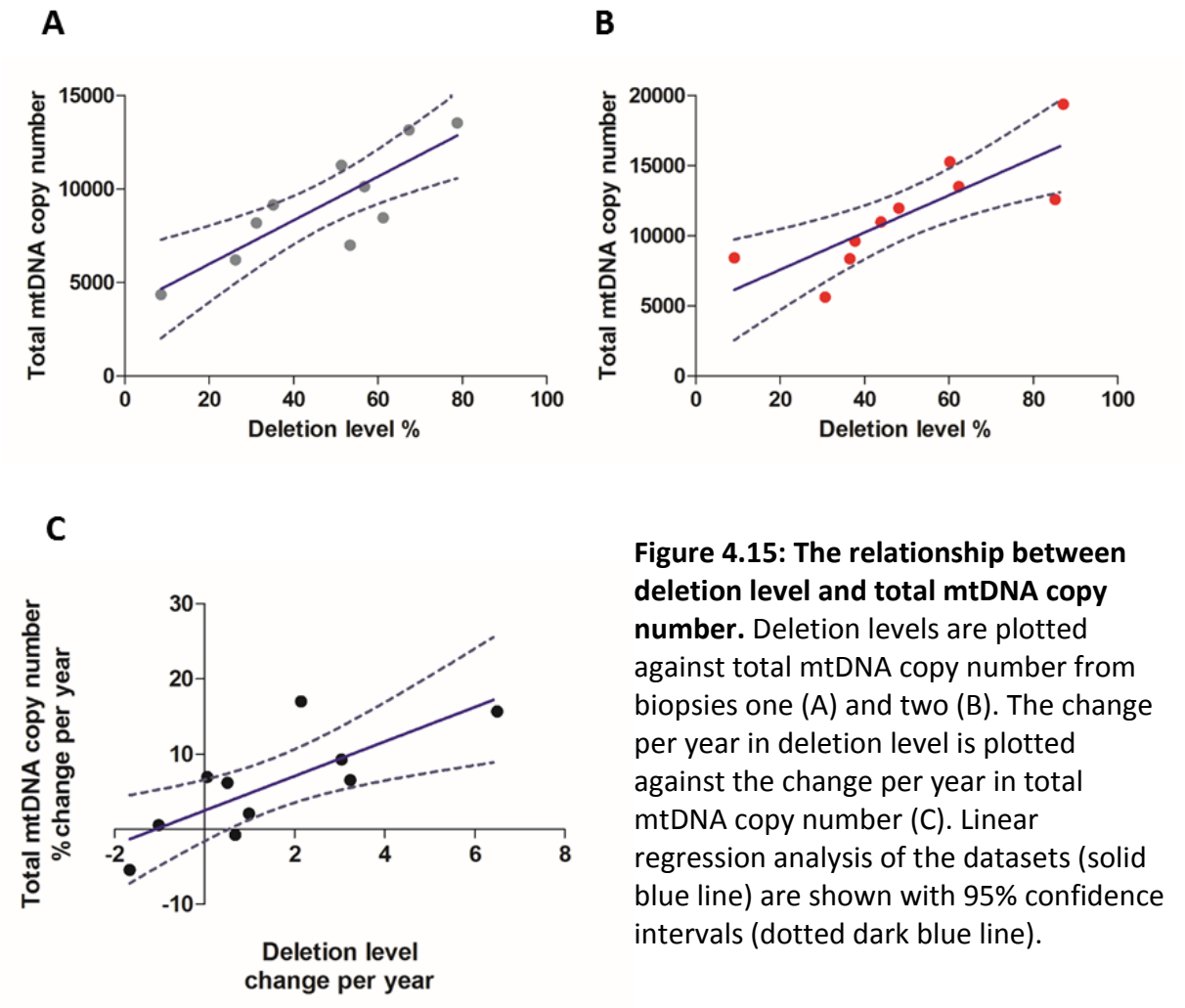

Figure 4.15: The relationship between deletion level and total mtDNA copy number. Deletion levels are plotted against total mtDNA copy number from biopsies one (A) and two (B). The change per year in deletion level is plotted against the change per year in total mtDNA copy number (C). Linear regression analysis of the datasets (solid blue line) are shown with 95% confidence intervals (dotted dark blue line).

4.5 Discussion

Identifying the molecular and cellular mechanisms behind the progressive symptoms associated with mitochondrial disease is challenging due to the genetic and phenotypic nature of these conditions. Understanding the relationship between these biological and clinical components could have important implications for prognosis, management and treatment of mitochondrial diseases. To investigate this in further detail, this longitudinal study examined two serial skeletal muscle biopsies from 10 patients with single, large-scale mtDNA deletions taken over two to 23 years. Their clinical disease progression was quantified using the validated NMDAS rating system. To our knowledge, this is the largest such study to date.

4.5.1 Deletion size correlates with deletion level, but is not related to clinical severity

Previous reports have consistently indicated that deletion size is inversely related to deletion level, such that smaller deletions are typically found at higher levels than larger deletions (Lopez-Gallardo *et al.,* 2009; Grady *et al.,* 2014; Mancuso *et al.,* 2015). This trend is also apparent in this study, although the strength of this association declines over time suggesting more prominent factors impacting on deletion level emerge. It is important to note, however, that the statistical analysis is somewhat compromised by the small sample size.

There have been inconsistent reports of the reliability of deletion size as an independent predictor of disease severity and progression (Yamashita *et al*., 2008; Grady *et al*., 2014; Mancuso *et al*., 2015; Rotig *et al*., 1995; Sadikovic *et al*., 2010). Although the number of patients in this study is small, they are representative of the larger MRC Mitochondrial Disease Patient Cohort. P8 and P10 are both classed as showing mild clinical phenotypes and below the average rate of progression and yet they harbour the smallest (2300bp) and largest (7595bp) deletions, respectively. Therefore, deletion size alone does not appear to predict severity or progression in these patients. Work by Grady *et al.,* (2014) on the same cohort has shown that deletion size can be a good predictor of disease progression when deletion level and *MT-CYB* deletion are also accounted for. It is difficult to compare these findings with those of the current study as only two patients, P2 and P10, harbour deletions removing *MT-CYB.* The size and level of deletion is variable in these two patients (P2=5899 at

35-44%, P10=7595 at 9%), and statistical modelling of NMDAS scores indicated fairly mild rates of clinical progression, similar to those of P3 and P9, where *MT-CYB* is in-tact. Therefore, the size of deletion does not seem to be a predictor of progression even when deletion level and removal of *MT-CYB* is considered, however this would need to be evaluated in a much larger group to form a sound conclusion.

A range of deletion species have been investigated in the literature, often resulting in conflicting observations. However this larger study is able to compare three patients with the same deletion – the common 4977bp deletion (P5-P7). Despite harbouring the same deletion species, there is no consistent change to heteroplasmy level or the respiratory chain defect, whereas total mtDNA copy number consistently increases across the group. Clinically, these patients present with different phenotypes which vary in severity and multisystem involvement. Patient age at onset, age at biopsy and heteroplasmy level also differ, which may contribute to the lack of coherence between the genetic, cellular and clinical observations.

4.5.2 Deletion level and mtDNA copy number change over time

This study has shown that deletion level in skeletal muscle does change over time in patients with mitochondrial disease. However, the magnitude and rates of these changes varies. It is possible that this could be due to obtaining biopsies from different muscles. For most patients, the location of the biopsy is given as either the left or right quadriceps, however the specific muscle is not noted.

Although deletion level was shown to increase in the majority of patients, P4 and P7 showed a decline in deletion level of 20.7% and 23.5% over 12.4 and 23.1 years respectively. These patients were the oldest at the time of second biopsy (P4=56 and P7=57) and so initial concerns were that additional age-related deletion species may have interfered with the real-time PCR assay for determination of deletion level by removing one of the target genes. A long-range PCR showed no additional deletions in the second biopsy for either patient and so this was ruled out as a possible cause for the declining mutation load. Of interest, P1 was found to have been re-biopsied as part of an exercise trial two years after the date of the second biopsy used in this study. In the first two biopsies, P1 showed an increase in deletion level from 31.2-48.1% over a 2.6 year interval. Deletion level determined in the third biopsy

was 39%, showing a decrease of 10% after a similar time period, raising speculation that deletion level may periodically fluctuate, which may explain the decline in levels seen in P4 and P7. This is only based on observations from one patient, and so further investigations with additional serial biopsies would be required to evaluate this as a hypothesis.

The effect of changes to deletion level over time may be modulated by changes to total mtDNA copy number. In this group of patients, total mtDNA copy number is significantly correlated with deletion level, such that a higher deletion load is associated with an increase in copy number. Interestingly, the rate at which the deletion level changes over time correlates with the rate of change to mtDNA copy number, so patients accumulating deletions at a faster rate see a more rapid increase in copy number than those where deletion load increases more slowly. This could be interpreted as a compensatory mechanism implemented in an attempt to increase the wild-type mtDNA population to neutralise any functional effects of the increasing mutation load.

Interestingly, total mtDNA copy number is much higher in patients with single large-scale mtDNA deletions than was seen in patients with the m.3243A>G point mutation (Chapter 3). While this could be an artefact of skeletal muscle being more clinically involved in patients with single, large scale mtDNA deletions, it could also indicate a replicative advantage for the smaller mtDNA molecules harbouring the deletion resulting in a gross increase in copy number. In addition, the overall level of respiratory chain deficiency was greater in skeletal muscle harbouring single, large-scale mtDNA deletions compared to that with m.3243A>G, for both complex I and complex IV. This could also be reflective of the muscle-based symptoms seen more predominantly with this mutation.

It has been previously suggested by Durham *et al.,* (2006) that a reduction in wild-type mtDNA copy number, rather than the accumulation of deletion species, could result in COX-deficiency based on observations in skeletal muscle biopsies from patients with mitochondrial myopathy. Although wild-type mtDNA copy number did increase in the majority of patients with single, large-scale mtDNA deletions, there was no relationship between the number of wild-type mtDNA species and the proportion of COX, or complex I, deficiency.

4.5.3 Inconsistent changes to the extent of complex I and complex IV deficiency

The proportion of COX-negative muscle fibres in patients with single, large-scale mtDNA deletions has been assessed longitudinally in a few studies concluding that this population increases over time (Chinnery *et al.,* 2003; Durham *et al.,* 2006; Larsson *et al.,* 1990) in some patients, yet remains stable in others (Durham *et al.,* 2006; Larsson *et al.,* 1990). The COX-histochemistry method used to identify COX-negative fibres in these studies has been superseded by an immunofluorescence assay in this study allowing for the quantification of COX and complex I levels, normalised to the level of porin, in individual fibres. This provides a more accurate and in-depth analysis of the extent of the respiratory chain defect in muscle fibres. Using this method, the median level of COX was determined, as well as quantification of the proportion of COX-negative and COX-deficient (negative and intermediate) fibres, across a biopsy. The majority of patients show a decline in the levels of COX, alongside an increase in the proportion of deficient and negative fibres. However, there are a few cases where the level of COX is shown to increase over time and the proportion of COX-negative and COX-deficient fibres decreases, something which has not been shown in the literature to date. This could be due to a number of genetic or environmental factors such as the deletion heterogeneity or these patients having a more active lifestyle. Alternatively, this could be an artefact of the different muscles biopsied in these patients.

As with COX, the extent of complex I deficiency was shown to change over time in an inconsistent manner across this group of patients. However, most patients did show a decline in complex I levels with an increase in the proportion of complex I-negative and deficient fibres. Generally, the scale of COX deficiency was greater than that of complex I in these patients, while changes to these complexes tended to occur in the same direction (i.e. an increase in COX-negative fibres was associated with an increase in complex I-negative fibres). Such longitudinal analysis of complex I deficiency in skeletal muscle of patients with single, large-scale mtDNA deletions is not reported in the current literature and is therefore a novel feature of this study.

4.5.4 Respiratory chain deficiency and genetic defects

Understanding the relationships between biochemical and genetic factors associated with disease could help determine the mechanisms of pathogenesis and progression. The relationship between deletion level and the proportion of COX-deficient fibres is well

established in the literature (Mita et al 1989; Goto et al 1990), however this is difficult to evaluate in the current study due to small sample size. Although the highest proportion of COX-deficiency is seen in biopsy two of P6, which has the highest deletion level, there is no consistent trend among the remaining biopsies. Similarly no relationship between deletion level and the proportion of complex I deficient fibres is observed, although previous studies have identified a correlation between complex I activity and deletion level (Schröder et al 2000; Gellerich et al 2002).

Grady et al (2014) reported that removal of *MT-CO* genes, encoding structural subunits of complex IV, was predictive of COX deficiency. Only one patient (P8) in the current study harbours a deletion which does not encompass these *MT-CO* genes, and interestingly displays marked preferential complex I deficiency in the mtRC profile. Furthermore, P9 who has all three *MT-CO* genes deleted shows a preferential complex IV deficiency in the mtRC profile. These findings seem to corroborate those of Grady et al (2014), although inconsistent with others (Goto *et al.,* 1990; Oldfors *et al*., 1992). A more detailed discussion on the role of deleted genes in the pathogenesis of mitochondrial dysfunction is presented in chapter 5.

4.5.5 Limitations

This study provides a more comprehensive evaluation of the genetic and biochemical changes associated with disease progression in patients with single, large scale mtDNA deletions, however there are a few limitations to consider. First, although this study is larger than any in the current literature, the ability to draw statistically significant conclusions from our ten patients is limited by the genetic variability of single large scale mtDNA deletions and the spectrum of associated clinical phenotypes. This variability is amplified by the different biopsy sites in patients.

Furthermore, although all patients present a predominantly muscle-related phenotype, multisystem conditions are not uncommon in this group, with several patients presenting a neurological component. The impact of these symptoms on clinical disease severity and progression may not be well represented by the skeletal muscle biopsies used for the genetic and cellular analysis.

Despite being unable to evaluate the significance of the relationships between genetic and respiratory chain factors in these patients, the observed trends do warrant further investigation. Deletion level and mtDNA copy number were determined using DNA extracted from homogenate patient skeletal muscle and therefore represent an average measurement across multiple fibres within a biopsy. The respiratory chain defect, on the other hand, is measured for each individual fibre. In order to better understand the relationship between the genetic and biochemical defects a single-fibre approach should be implemented.

4.6 Conclusion

Through the use of improved quantitative techniques for the determination of deletion level, mtDNA copy number and respiratory chain deficiency, this study present the most comprehensive longitudinal analysis of single, large-scale mtDNA deletions in patient skeletal muscle. In addition, this work presents the first longitudinal analysis of complex I deficiency in skeletal muscle of patients with single, large-scale mtDNA deletions. The findings of this longitudinal study show that (i) these patients reflect the clinical spectrum of patients in the MRC Mitochondrial Disease Patient Cohort in terms of disease severity and progression, (ii) there was no consistent change to the levels of complex I and complex IV proteins across this group of patients, however the direction of change is related, (iii) the majority of patients showed an increase in deletion level over time, (iv) total mtDNA copy number increased over time in the majority of patients As mentioned in the limitations, the relationship between genetic and respiratory chain defects may be best assessed at the single fibre level, rather than across the whole biopsy section. This is addressed using a single fibre approach in the next chapter.

Chapter 5: A single fibre approach to investigating pathogenic mechanisms associated with single, large-scale mtDNA deletions.

5.1 Introduction

5.1.1 Single, large-scale mtDNA deletions: Genotype and respiratory chain deficiency

As discussed in the chapter four, elucidating the pathogenic mechanisms associated with single, large-scale mtDNA deletions is challenging due to the genetic heterogeneity of these mutations and the spectrum of clinical phenotypes. While the previous longitudinal study did not show any consistent changes to deletion level, mtDNA copy number or levels of complex I or IV, it did corroborate previous reports of a relationship between these genetic features and the associated respiratory chain deficiency in patient skeletal muscle biopsies.

The relationship between the size and location of the deletion and the biochemical phenotype presented by patients with single, large-scale mtDNA deletions has been further investigated in our group by Dr Mariana Rocha (Wellcome Trust Centre for Mitochondrial Research, Newcastle University). In this unpublished work, the quadruple immunofluorescence assay, described in section 2.5.2, was performed on skeletal muscle biopsies from 23 genetically-characterised patients (Table 5.1), producing three distinct profiles of respiratory chain deficiency (mtRC profiles). Individual mtRC profiles are shown in appendix II. On this basis patients could be assigned to one of three classes: class I with equal and simultaneous down-regulation of both complex I and complex IV; class II with an early and more pronounced loss of complex I over complex IV; and class III with slightly earlier involvement of complex IV deficiency (Figure 5.1). Deletion level varied across the whole group of patients regardless of the class, suggesting that the shape of the mtRC profile is not influenced by the proportion of mutated mtDNA species.

Patient (sex)	Age	Clinical information	5' break point	3' break point	Deletion size	Deletion level
Class I: both complexes equally down-regulated						
P1 (F)	21	CPEO, ptosis, myopathy, ataxia, short stature	8482	13460	4977	87%
P2 (F)	22	CPEO	8543	15672	7128	7%
P3 (M)	25	Ptosis, CPEO, fatigue	8569	14603	6033	78%
P4 (F)	29	CPEO and bilateral ptosis	8929	13301	4371	53%
P5 (F)	36	CPEO, myopathy	8577	12983	4405	78%
P6 (F)	43	CPEO, myopathy	8482	13460	4977	73%
P7 (F)	44	CPEO, myopathy	9486	13723	4236	81%
P8 (F)	48	CPEO, myopathy	9498	13739	4240	39%
Class II: complex I more affected						
P9 (F)	25	CPEO	13039	15661	2621	66%
P10 (F)	26	CPEO, myopathy	10747	15598	4850	71%
P11 (F)	26	CPEO, myopathy, deafness	10946	15587	4640	83%
P12 (M)	39	CPEO, myopathy	11262	15375	4112	81%
P13 (F)	40	CPEO, myopathy, retinal pigment changes	12113	14421	2307	90%
P14 (F)	47	Ptosis, CPEO	12112	14412	2299	70%
P15 (M)	56	Ptosis, CPEO, diabetes	12112	14412	2299	59%
P16 (F)	59	CPEO	12211	15556	3344	38%
Class III: complex IV more affected						
P17 (F)	28	CPEO, myopathy	6341	13989	7647	33%
P18 (M)	34	Ptosis, CPEO, myopathy, ataxia	5772	12916	7143	36%
P19 (F)	39	CPEO, diplopia	7130	14628	7497	28%
P20 (F)	41	CPEO, myopathy	6742	13223	6480	19%
P21 (M)	59	N/A	6002	11221	5218	N/A
P22 (M)	63	Ptosis, CPEO	7128	13992	6863	35%
P23 (F)	74	CPEO	7205	12090	4884	34%

Table 5.1: Patients with single, large-scale mtDNA deletions. 23 patients assessed for respiratory chain deficiency by Dr Mariana Rocha in previous, unpublished work. Patients are classed according to their mtRC profile of deficiency. Age at biopsy is shown in years. Deletion size is shown in base pairs. Deletion level was measured from skeletal muscle homogenate. CPEO=chronic progressive external ophthalmoplegia; N/A=data not available.

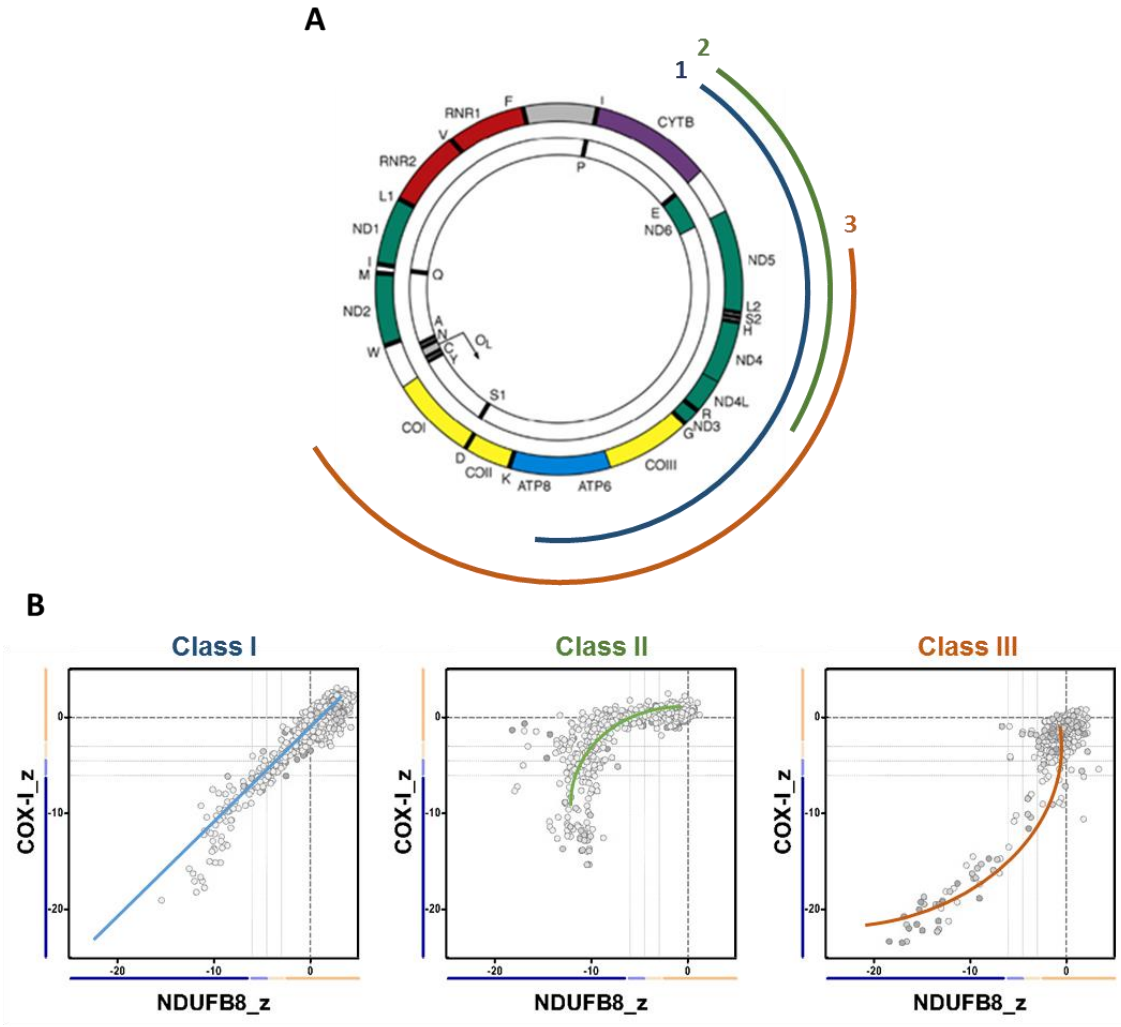

C

Genes deleted	Class I	Class II	Class III
Average size (kb)	5.1	3.3	6.8
tRNA	5-6	3-4	5-10
Complex I	4-5	3-4	3-5
Complex III	0-1	0-1	0
Complex IV	1	0	2-3
Complex V	0-2	0	2

Figure 5.1: mtRC profiles present three distinct patterns of deficiency with single, large-scale mtDNA deletions. (A) The average site of deletions in class I (blue), class II (green) and class III (orange), (B) representative mtRC profiles for each deletion class, where class I shows equal complex I and IV deficiency, class II shows predominant complex I deficiency and class III shows predominant complex IV deficiency, (C) the mtRC profiles relate to the deletion size and the number of complex I and IV genes removed by the deletion.

Interestingly, the different classes were related to the size and location of the deletion. Class I deletions, where equal degrees of complex I and IV deficiency were observed, removed 4-5 complex I genes and one complex IV gene. In class II deletions, all complex IV genes were preserved, potentially explaining the predominant complex I deficiency seen in this class. Conversely, all complex IV genes were removed in class III deletions, where complex IV deficiency was predominant over complex I. These observations highlight the role of protein-encoding genes in the pathogenesis of single, large-scale mtDNA deletions as there is a very clear link between the deletion of genes encoding sub-units for complexes I and IV and the respiratory chain dysfunction at the cellular and tissue level.

The work presented and discussed in this chapter was conducted in collaboration with Dr. Mariana Rocha to further investigate the pathogenic mechanisms alluded to by the work described above (contributions are specified for particular protocols in the methods section). In this study, a single fibre approach was taken to better understand the interplay between (i) the deletion size, location and level, (ii) the mtDNA copy number and (iii) the respiratory chain deficiency at the cellular level.

5.1.2 Single fibre studies in the literature

The study of single fibres from skeletal muscle biopsies taken from patients with single, large-scale mtDNA deletions has contributed to the understanding of the intricate relationship between the genetic defect and the nature of the biochemical phenotype. In the first such study on a patient with KSS phenotype, Mita *et al.*, (1989) observed that COX-deficient fibres, especially ragged red fibres (RRF) harboured higher levels of deletion than COX-normal fibres. This has also been described by a number of subsequent studies (Collins *et al.,* 1990; *Moraes et al*., 1992) with reports of accumulated mutant transcripts in these deficient fibres (Shoubridge *et al.,* 1990; Oldfors *et al.,* 1992). There have, however, been conflicting reports of the proportion of mutant mtDNA genomes in COX-normal fibres. Shoubridge *et al.,* (1990) found no deleted mtDNA species in biochemically normal fibres from two patients with mitochondrial myopathy and CPEO. In contrast, Sciacco *et al.,* (1994) determined the mean level of deletion in COX-normal fibres to range from 15-77%, reaching 90% in one case. More recently, He *et al.,* (2012) reported an average deletion level of 21%

in COX-normal fibres, in line with findings from Sciacco *et al.,* (1994), although the highest level of deletion in these fibres was approximately 50%.

The wild-type mtDNA copy number has also been measured in single fibres from patients with single, large-scale mtDNA deletions although reports are inconsistent. A decrease in the level of wild-type mtDNA (Mita *et al.,* 1989; Sciacco *et al.,* 1994) and associated transcripts (Oldfors *et al.,* 1992) has been observed in COX-deficient fibres. Collins *et al.,* (1991) report a comparable finding in one patient, but normal or increased levels of wild-type mtDNA were seen in COX-negative fibres in two other patients. Similar, contradictory observations between patients were made by Moraes *et al.,* (1992).

A more recent study by Durham *et al.,* (2007) found the wild-type mtDNA copy number to be relatively stable in COX-positive muscle fibres, despite varying levels of the common 4977bp deletion. An increase in deletion level was associated with a decline in wild-type mtDNA copy number and COX-deficiency. This later work reflects the *in silico* predictions made by Chinnery and Samuels (1999) who postulated wild-type mtDNA copy number is maintained at a high level by non-specific proliferation of mtDNA to compensate for the presence of the mutant species, until a critical threshold is reached and relaxed replication results in an abrupt decline in wild-type mtDNA copy number. This process allows for the gradual accumulation of a deletion in a cell over time, accounting for the levels in post-mitotic tissues and the late presentation of clinical symptoms. Furthermore, it may offer explanation for the conflicting reports regarding levels of wild-type mtDNA in single fibres discussed above. Fibres with deletion level below the threshold will have a normal wild-type mtDNA copy number, and those above the threshold level will present much lower copy number counts. However, cells in the stage of transition across the threshold level would show a dramatic change in wild-type mtDNA copy number alongside only a minor alteration in deletion level.

Studying the relationship between genotype and biochemical phenotype on a single cell level is useful for determining threshold levels for respiratory chain deficiency. The detection of mutant mtDNA species in COX-positive muscle fibres from patients with various single,

large-scale mtDNA deletions places the threshold level around 70-80% (Sciacco *et al.,* 1994), much higher than estimates of 50-60% from studies using *trans*mitochondrial cybrids (Hayashi *et al.,* 1991; Porteous *et al.,* 1998). Given the genetic heterogeneity of single, large-scale mtDNA deletions as a group, it is possible that the threshold level varies depending on the size and location of the deletion, however this is yet to be comprehensively evaluated.

5.1.3 Pathogenic mechanisms associated with single, large-scale mtDNA deletions.

The pathogenic mechanisms associated with single, large-scale mtDNA deletions are not yet fully understood. In a study of 123 patients with mtDNA deletions, Moraes *et al.,* (1989) reported decreased activity of complexes I, III and IV, regardless of deletion size or location. This lack of coherence between the biochemical phenotype and the mitochondrial genetics led to the suggestion that the deletion of mt-tRNA genes, not protein-encoding genes, was imperative to pathogenesis. Nakase *et al.,* (1990) reported disrupted translation of mtDNA-encoded proteins in patient fibroblasts, attributed to insufficient mt-tRNAs as a result of the deletion of these genes. In some agreement, Hayashi *et al.,* (1991) observed a decrease in overall translation in HeLa cells only after the proportion of deleted mtDNA species reached over 60%. This indicated a complementation effect whereby wild-type mtDNA genomes were able to compensate for the loss of mt-tRNAs resulting from the mutant species. More recently, biochemical analysis of muscle biopsies from 16 patients with single, large-scale mtDNA deletions reported no obvious relationship between the size of the deletion and citrate synthase (CS) activity, normalised COX activity and the rates of normalised respiration, concluding that impairment of mitochondrial function is dependent only on deletion level and not size or location (Gellerich *et al.,* 2002). As such, the deletion of mt-tRNA genes is still considered a likely pathogenic mechanism for single, large-scale mtDNA deletions (Schon *et al.,* 2012).

Single-fibre studies have also provided an insight into the pathogenic mechanisms behind single, large-scale mtDNA deletions. In a study of 23 patients with mitochondrial myopathy and single, large-scale mtDNA deletions, Hammans *et al.,* (1992) grouped patients based on the location of their deletion. Group one had COX-genes deleted, whereas group two had COX-genes present. A significant difference in the ratio of COX-negative:RRF was reported between groups, with COX-negative fibres much more common in group one patients,

where COX-genes were removed by the deletion. Furthermore, four patients in group two, who had only complex I genes removed, presented with isolated complex-I deficiency. These findings suggested a relationship between the location of the deletion and the biochemical phenotype. Supporting evidence was found by re-analysing data from Goto *et al.,* (1990), where a similar trend was observed in 21 patients, leading the authors to conclude that the loss of protein-encoding genes has a role in the pathogenesis of disorders associated with single, large-scale mtDNA deletions (Hammans *et al.,* 1992). A similar finding was reported by Moraes *et al.* (1992) in a study of seven patients with KSS phenotype showing a significantly lower ratio of COX-negative:RRF in patients with deletions not encompassing COX-genes.

5.2 Aims

As discussed in the chapter four, elucidating the pathogenic mechanisms associated with single, large-scale mtDNA deletions could have important implications for the clinical management of these conditions, by informing treatment regimens, improving the prediction of prognosis and highlighting potential targets for therapeutic intervention. The use of homogenate DNA has its limitations, particularly concerning the evaluation of the complex relationship between genetic and biochemical defects occurring within individual cells. This is especially pertinent given the mosaic nature of the cellular phenotype in skeletal muscle. As such, this study takes a single fibre approach, using skeletal muscle biopsies from six patients with previously characterised single, large-scale mtDNA deletions. Laser microdissected muscle fibres will be assessed for OXPHOS deficiency, fibre type, deletion level and mtDNA copy number to better understand the complex relationship between the genetic defect and the resulting respiratory chain deficiency. In particular, this study aims to investigate whether (i) deletion level affects the extent of respiratory chain deficiency, (ii) the deletion size and location contribute to the biochemical threshold level, (iii) the threshold level of deficiency is different for complex I and IV, (iv) mtDNA copy number is involved in regulating deletion level and respiratory chain deficiency and (v) muscle fibre types are affected differently by mtDNA deletions.

5.3 Methods

5.3.1 Patient and control tissue

Muscle biopsies were collected from six patients with genetically characterised single, large-scale mtDNA deletions (Table 5.2) Break points had been previously determined and the genes removed are highlighted in Table 5.3. Ethical approval was granted by the Newcastle and North Tyneside Local Research Ethics Committees (reference 09/H0906/75), and written informed consent was received from patients prior to inclusion in the study. The experiments were carried out in accordance with the approved guidelines.

Patient	Sex	Age	Clinical information	Break-points	Deletion level
Class I: complexes I and IV equally down-regulated					
P1 *(P2)*	F	22y	CPEO	8543-15672	7%
P2 *(P8)*	F	48y	CPEO, myopathy	9498-13739	39%
Class II: complex I more affected					
P3 *(P13)*	F	40y	CPEO, muscle atrophy, weakness, retinal pigmentary changes	12113-14421	90%
P4 *(P15)*	M	56	CPEO, diabetes, ptosis	12112-14412	59%
Class III: complex IV slightly more affected					
P5 *(P17)*	F	28y	CPEO, mild myopathy	6341-13989	33%
P6 *(P18)*	M	34y	CPEO, ptosis, myopathy and ataxia	5772-12916	36%
Control	M	34y	-	-	-

Table 5.2: Patients with single, large-scale mtDNA deletions selected for the single fibre study. F=female; M-male; Age is presented in years at the time of biopsy. Deletion level was measured previously from skeletal muscle homogenate.

	Class I		Class II		Class III	
	P1	P2	P3	P4	P5	P6
MT-OLR						X
MT-TC						X
MT-TY						X
NC nucleotides						X
MT-COI					X	X
tRNA serine 1					X	X
NC nucleotides					X	X
tRNA aspartic acid					X	X
MT-COII					X	X
NC nucleotides					X	X
tRNA lysine					X	X
NC nucleotides					X	X
MT-ATP8	X				X	X
MT-ATP6	X				X	X
MT-COIII	X	X			X	X
tRNA glycine	X	X			X	X
MT-ND3	X	X			X	X
tRNA arginine	X	X			X	X
MT-ND4L	X	X			X	X
MT-ND4	X	X	X	X	X	X
tRNA histidine	X	X	X	X	X	X
tRNA serine2	X	X	X	X	X	X
tRNA leucine2	X	X	X	X	X	X
MT-ND5	X	X	X	X	X	X
MT-ND6	X		X	X		
tRNA glutamic acid	X					
NC nucleotides	X					
MT-CYB	X					
Deletion size	7.1kb	4.2kb	2.3kb	2.3kb	7.6kb	7.1kb
tRNAs removed	6	5	3	3	8	10
CI genes removed	5	4	3	3	4	4
CIV genes removed	1	1	-	-	3	3
CIII genes removed	1	-	-	-	-	-
CV genes removed	2	-	-	-	2	2

Table 5.3: Genes deleted in patients 1-6. X marks a deleted gene in this patient. The total size of the deletion is presented in kilo bases and the number of tRNA and individual complex genes is tallied.

5.3.2 Cryosectioning of skeletal muscle

Serial sections of skeletal muscle were cryosectioned (as described in section 2.5.1) for OXPHOS and fibre typing immunofluorescence protocols (Figure 5.2). Two serial 10µm sections were cut onto the same slide and designated as no primary control (NPC) (section 1) and OXPHOS1 (section 2). A serial section of 20µm thickness was cut onto another slide for use in the fibre typing protocol (section 3). Finally, another serial 10µm section was cut as OXPHOS2 (section 4). Cryosections were left to dry at room temperature for one hour before storing at -80°C.

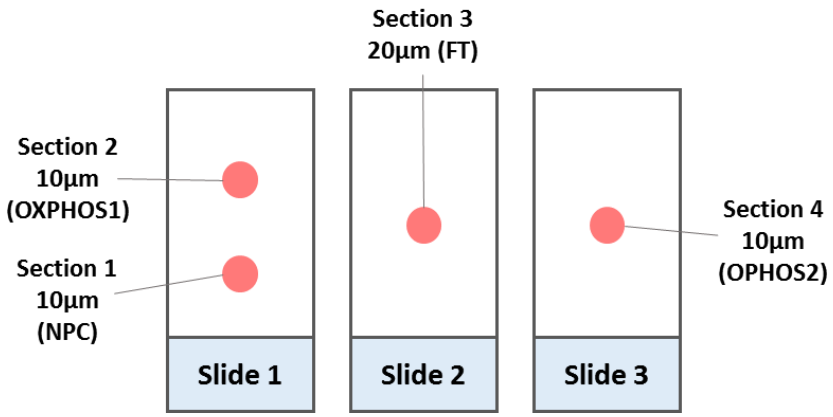

Figure 5.2: Serial cryosections of skeletal muscle biopsies for immunofluorescence protocols. Two serial sections of 10µm thickness were cut onto slide one for the OXPHOS immunofluorescence assay. Section 2, of 20µm thickness, was cut onto a different slide for fibre typing. A final serial section of 10µm thickness was also cut for use in the OXPHOS immunofluorescence assay. NPC=no primary control; FT=fibre type.

5.3.3 Immunofluorescent staining of cryosectioned muscle for the detection of OXPHOS subunits

OXPHOS quadruple immunofluorescence was carried out on 10µm transverse muscle sections 1, 2 and 4 from each patient as described in section 2.5.2. Briefly, sections were fixed in paraformaldehyde, permeabilised in a methanol gradient and blocked firstly with 10% normal goat serum (NGS) and further with an avidin/biotin blocking kit (Vector Laboratories). OXPHOS sections 2 and 4 were incubated with a cocktail of primary antibodies for MTCO1, VDAC1, NDUFB8 and laminin. NPC section 1 was incubated with laminin antibody only. All sections were then incubated with a secondary antibody cocktail (Alexa Fluor 488, 546, 750 and IgG1– Biotin-XX conjugate) and subsequently with streptavidin 647.

The sections were washed, mounted in Prolong Gold (Sigma) and stored at -20°C until imaging. This protocol was performed by both myself and Dr Mariana Rocha.

5.3.4 Fibre typing IF

Muscle fibre types were determined using an immunofluorescence protocol described in section 2.5.3. 20µm transverse muscle sections (serial section 3) were blocked in 10% NGS before incubation with primary antibodies for BA-F8 (type I), SC-71 (type IIa), 6H1 (type IIx) and laminin. Sections were incubated with the secondary antibody cocktail (Alexa Fluor 488, 546, 647 and 750) and mounted in Prolong Gold (Sigma). As these sections were to be used for the laser microdissection of single muscle fibres, they were stored at 4°C before and following imaging to preserve mtDNA. This was performed by both myself and Dr Mariana Rocha.

5.3.5 Image acquisition and analysis

Fluorescent images were acquired as described in section 2.5.4. Stitched image files for the OXPHOS immunofluorescence assay were analysed using the ImmunoAnalyser software (section 2.5.6). Stitched images for the fibre typing protocol were analysed by visual classification of type I, type IIa and type IIx fibres. Muscle fibres on serial sections 2 (OXPHOS1) and 3 (fibre typing) were manually matched so that a profile of respiratory chain deficiency and fibre type was available for each individual muscle fibre on biopsy section 3. Image acquisition and analysis was performed by both myself and Dr Mariana Rocha.

5.3.6 Selection and isolation of single muscle fibres for molecular genetic analysis

Muscle fibres were categorised first into OXPHOS groups, representing their levels of complex I and complex IV deficiency (Figure 5.3). From each OXPHOS group, equal numbers (minimum of 10 where possible) of type I, type IIa and type IIx fibres were randomly selected. Single cell laser microdissection was carried out for selected fibres as described in section 2.6, after which single cell lysates were stored at -20°C until molecular genetic analysis. The selection criteria were determined jointly by myself and Dr Mariana Rocha. Single fibre laser microdissection and subsequent molecular genetic analyses was performed by myself only.

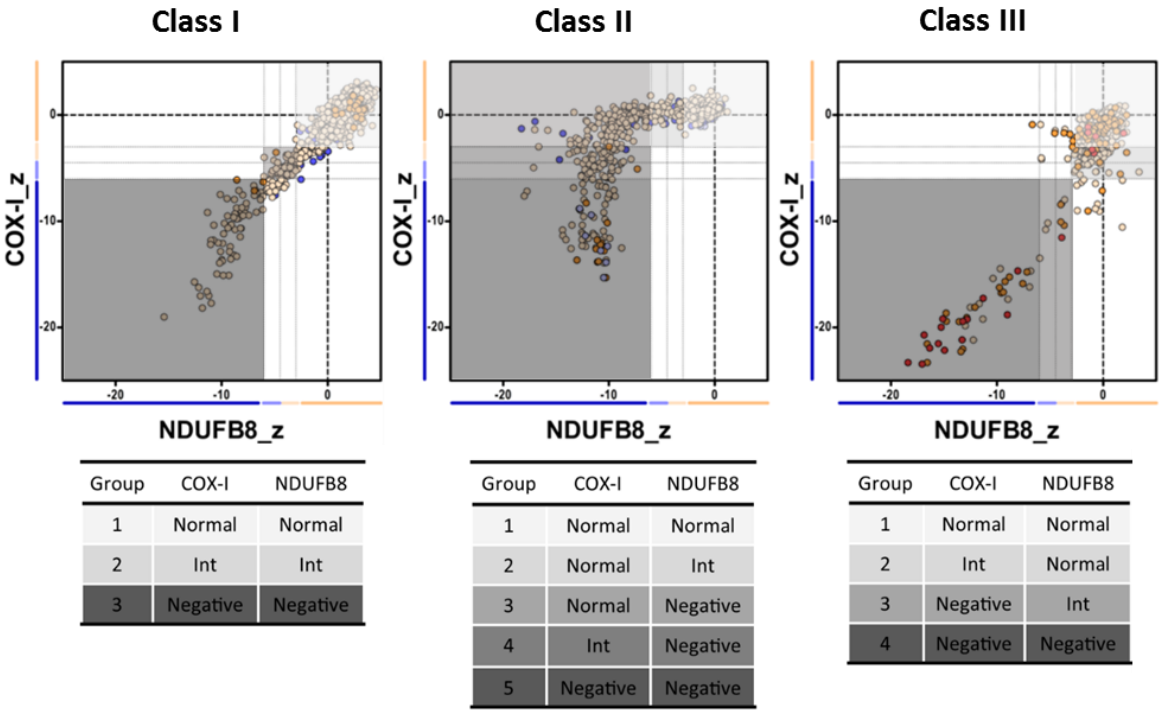

Group	COX-I	NDUFB8
1	Normal	Normal
2	Int	Int
3	Negative	Negative

Group	COX-I	NDUFB8
1	Normal	Normal
2	Normal	Int
3	Normal	Negative
4	Int	Negative
5	Negative	Negative

Group	COX-I	NDUFB8
1	Normal	Normal
2	Int	Normal
3	Negative	Int
4	Negative	Negative

Figure 5.3: Selection of fibres for single cell laser microdissection. Fibres were selected based on the extent of OXPHOS deficiency, as indicated by the grey shading. Each class of deletion had different OXPHOS categories due to the shape of the mtRC profile.

5.3.7 Real-time PCR for the determination of mtDNA deletion level and copy number

The deletion level was determined using a duplex *MT-ND1*/*MT-ND4* TaqMan realtime PCR assay, as previously described in chapter four (section 4.3.6). Single fibre lysate stocks were diluted 1:5 in nuclease free water and also loaded in triplicate onto three replicate plates. Absolute copy numbers of *MT-ND4* and *MT-ND1* were determined by comparing the average sample Cq against the standard curve. Deletion level was calculated as the [1-(*MT-ND4*: *MT-ND1*)*100]. The total mtDNA copy number was represented by the *MT-ND1* copy number, whereas wild-type mtDNA copy number was represented by *MT-ND4* copy number. MtDNA copy number was then normalised to cell area to give total, or wild-type, mtDNA copy number per μm^2.

5.3.8 Statistical analysis

OXPHOS statistical analyses were carried out using a newly-developed website (http://iah-rdevext.ncl.ac.uk/immuno/) (developed by Dr John Grady) and GraphPad Prism software. All

data are presented as percentage (%) of the total number of myofibres, with n corresponding to the number of muscle fibres analysed.

5.4 Results

5.4.1 Deletion level and respiratory chain deficiency

In all six patients, deletion level was increased in fibres with higher levels of respiratory chain deficiency (Figure 5.4, quantified Table 5.4). Fibres positive for both complex I and complex IV (OXPHOS group 1), deemed respiratory-'normal', harboured variable deletion levels ranging from 0% (observed in all patients) to a maximum of 93% (P2). The level of deletion in this group of fibres showed vast variability within individual patients, as indicated by the coefficient of variation. In contrast, fibres classed as negative for both complex-I and complex-IV consistently showed the highest deletion levels and a much narrower range (Table 5.4). A number of patients showed fibres with high levels of respiratory chain deficiency harbouring levels of deletion as low as 8.8% in a fibre from P5. There was relatively little variation in this proportion between deletion classes (class I mean=86.8%; class II mean=93.7%; class III mean=91.8%), however, the mean deletion level of complex I and complex IV negative fibres was generally lower in class I deletions than class II or III.

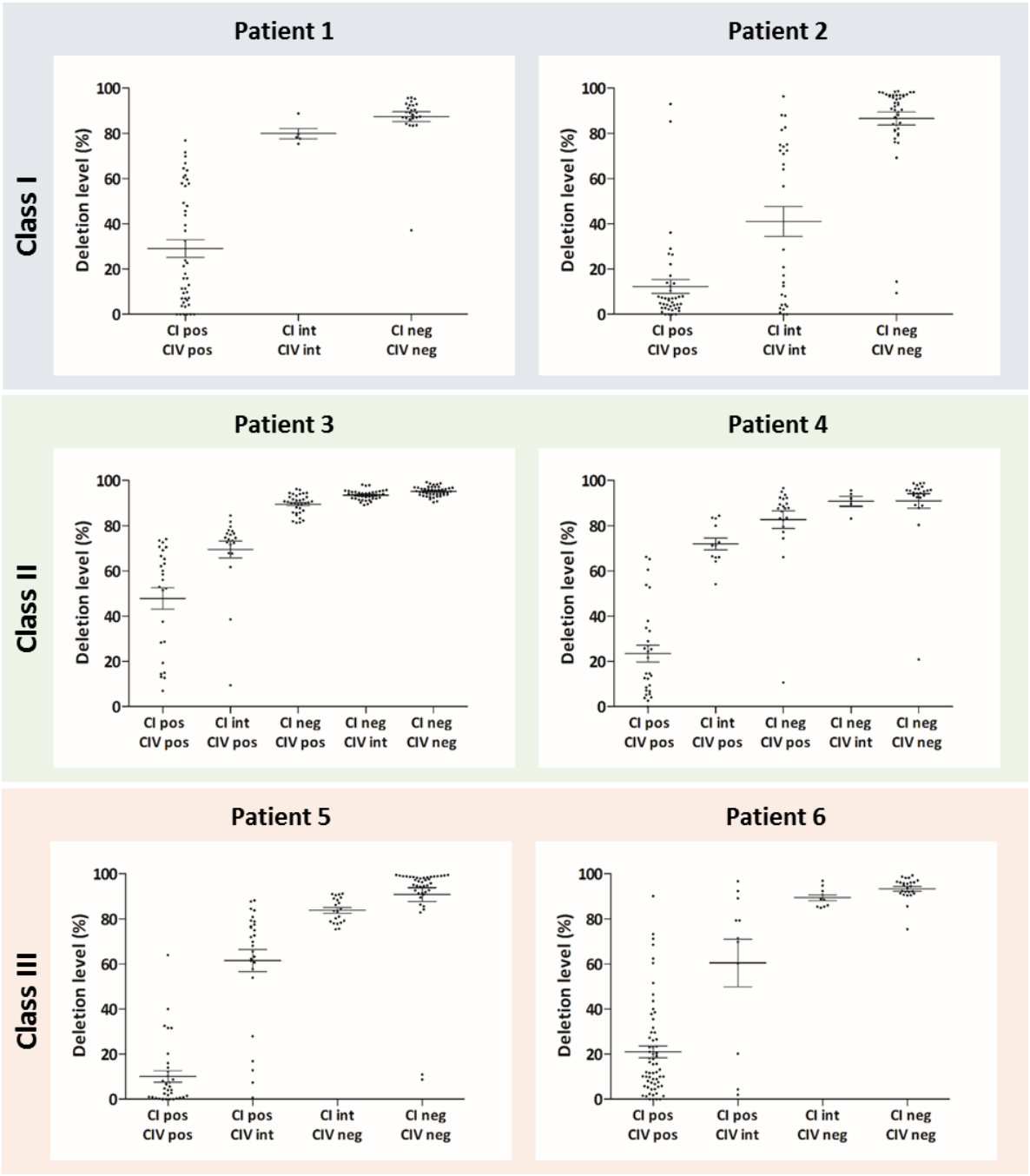

Figure 5.4: Deletion level increases with respiratory chain deficiency. Individual fibres were grouped according to the level of OXPHOS deficiency. Each dot represents the deletion level for each fibre. Mean deletion level per group is shown with bars denoting SEM (standard error of the mean) above and below.

Patient		Deletion level		
		Positive	*Intermediate	Negative
P1	Mean	29.1±3.9%	79.9±2.3%	87.4±2.1%;
	CV	88.7%	6.5%	12.5%
	n=	44	5	26
P2	Mean	12.3±3.1%	41.1±6.6%	86.5±2.9%
	CV	159.2%	86.6%	21.5%
	n=	41	29	42
P3	Mean	47.8±4.6%	86.9±1.3%	95.1±0.3%
	CV	48.5%	14.2%	2.2%
	n=	25	95	44
P4	Mean	23.4±3.7%	80.3±2.5%	91.0±3.2%
	CV	84.8%	19.5%	17.0%
	n=	29	38	24
P5	Mean	10.1±2.4%	71.2±3.2%	90.9±3.1%
	CV	143.0%	31.2%	21.3%
	n=	34	48	40
P6	Mean	21.0±2.6%	74.2±6.3%	93.4±1.0
	CV	98.8%	39.1%	5.3%
	n=	63	21	25

Table 5.4: Deletion levels for individual fibres categorised by OXPHOS deficiency. The mean deletion level for n fibres is shown alongside the coefficient of variance (CV) for each OXPHOS group. *Intermediate groups contain fibres which are neither positive for both complex I and IV, nor negative for complexes I and IV.

The remaining fibres not falling into the above categories were grouped as intermediate fibres. These fibres harboured mean deletion levels between those observed for normal and negative groups (Table 5.4, “intermediate”), increasing with higher levels of OXPHOS deficiency. The range of deletion levels in these fibres is large as they encompass fibres with slight biochemical deficiency (e.g. complex I intermediate and complex IV negative) to more severe deficiency (e.g. complex I negative and complex IV intermediate). As such, deletion levels as low as 0% and up to 98.1% were recorded in these fibres. These fibres represent those in transition from ‘healthy’ to fully deficient and, therefore, offer valuable insight into the changing genetic and biochemical status of fibres over this period.

5.4.2 Threshold for complex I and complex IV deficiency

To further investigate the relationship between the deletion level and the extent of complex I and complex IV deficiency, inverted z_scores of COX-I and NDUFB8 from each muscle fibre were plotted against its associated mutation load. This data transformation was essential to fit a logarithmic regression and model the data. Threshold levels for complex I and IV were measured by determining deletion level at z_CI=-3SD and z_COXI =-3SD using the logarithmic regression model. As illustrated in Figure 5.5, and quantified in Table 5.5, the thresholds for complex I and IV deficiency were variable according to the class of deletion. In patients harbouring class I deletions (P1 and P2), where complex I and IV were equally affected, threshold levels for complex I and IV deficiency were not pointedly different. However in patients with class II deletions (P3 and P4), where complex I deficiency is predominant, a lower threshold for deficiency is measured for complex I than complex IV (Table 5.5). In patients harbouring class III deletions (P5 and P6), who present predominant complex IV deficiency, the opposite was observed whereby complex IV showed a lower threshold for deficiency (Table 5.5).

Patient		Threshold level for deficiency		n=
		Complex I	Complex IV	
P1	Mean (95% CI inf;sup)	74.5% (61.1; 85.6)	71.0% (48.6; 87.9)	75
P2	Mean (95% CI inf;sup)	55.5% (31.4; 74.5)	56.8% (21.4; 82.6)	112
P3	Mean (95% CI inf;sup)	62.7% (47.3; 75.6)	90.6% (84.0; 95.8)	164
P4	Mean (95% CI inf;sup)	67.2% (42.2; 85.0)	91.7% (88.0; 94.7)	91
P5	Mean (95% CI inf;sup)	81.9% (74.4; 88.0)	74.1% (68.1; 79.4)	122
P6	Mean (95% CI inf;sup)	78.9% (71.3; 85.3)	69.8% (61.3; 76.93)	109

Table 5.5: Threshold level for complex I and complex IV deficiency. Mean threshold level determined by non-linear regression is shown alongside the 95% inferior (inf) and superior (sup) confidence intervals (CI). n= the total number of fibres assessed for each patient.

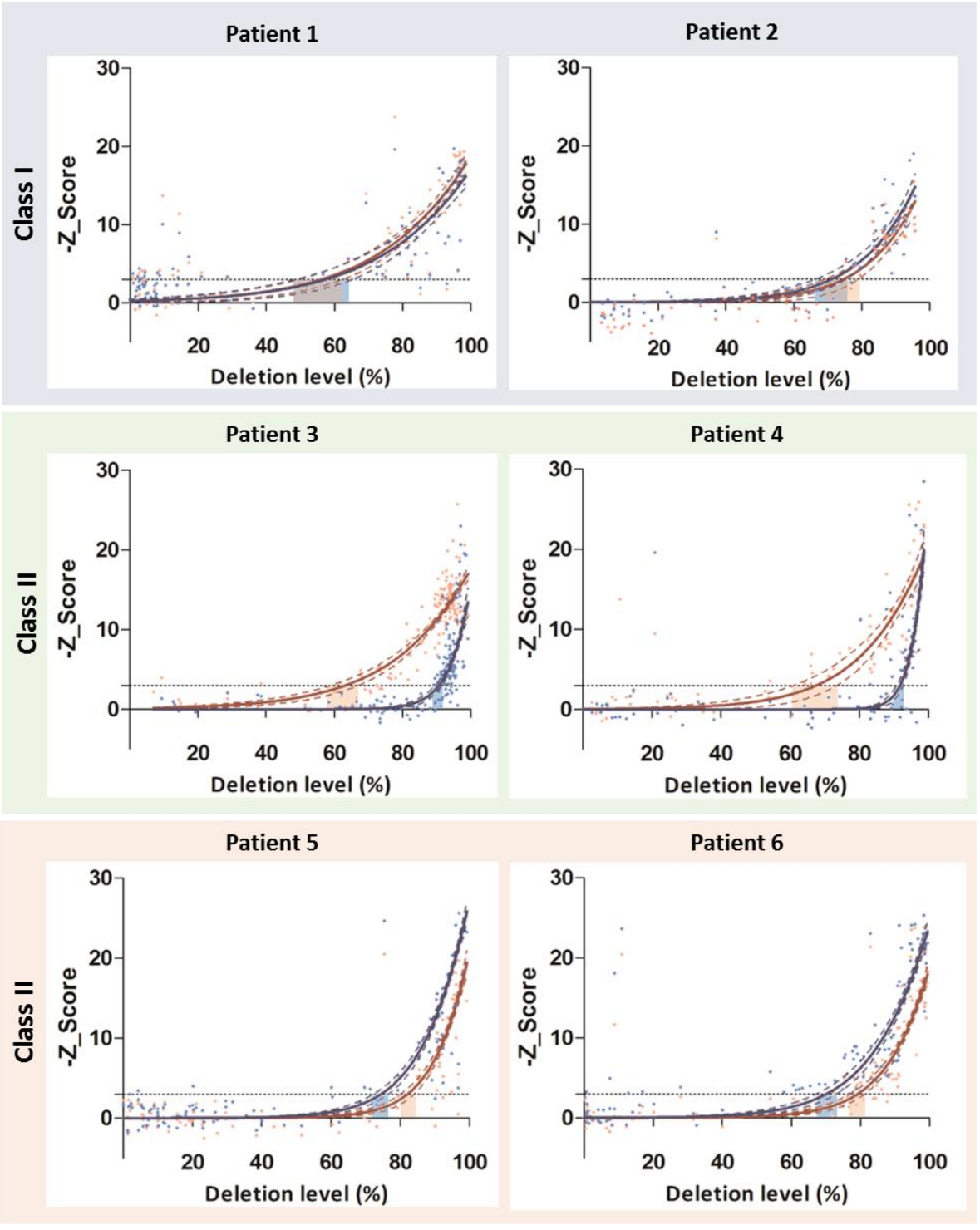

Figure 5.5: Threshold levels for complex I and complex IV deficiency is dependent on the size and location of the deletion (class). Each dot represents the deletion level for each fibre plotted against the inverted z-score for NDUFB8 (red) and COX-I (blue). A logarithmic exponential growth curve was fitted for NDUFB8 (red curve) and COX-I (blue curve) data. Dashed lines indicate the 95% confidence interval of the fitted curves. Black dashed line (-y= 3) indicates the threshold for deficiency. Shaded red and blue areas indicate the threshold levels for complex I and IV deficiency, respectively.

5.4.3 MtDNA copy number and respiratory chain deficiency

MtDNA copy number, presented as copies per μm^2, was determined using real-time PCR. As for analysis of the deletion level, fibres were grouped according to the extent of complex I and complex IV deficiency. Average total mtDNA copy number for each patient was not related to deletion class. Total mtDNA copy number did increase with greater levels of OXPHOS deficiency in all patients (Figure 5.6) (Table 5.6), with the exception of P1 who showed minimal differences in total mtDNA copy number across the OXPHOS groups. In patients with normal levels of complex I and complex IV, total mtDNA copy number was variable between fibres (as shown by the coefficient of variation (CV)) and between patients, with no relation to deletion class. Mean total mtDNA copy number in fibres negative for complex I and complex IV was significantly greater than was seen in normal fibres ($p<0.05$, t-test; except P1), however the CV reflects a larger degree of variation within this group of fibres in most patients. Negative fibres with class III deletions had higher mean total mtDNA copy numbers compared to those with class I and II deletions.

Wild-type mtDNA copy number was shown to decrease with increased levels of OXPHOS deficiency in all patients (Figure 5.7). A significant decline in wild-type mtDNA copy number was seen from normal fibres to those negative for complex I and IV ($p<0.05$, t-test) in all patients. As with total mtDNA copy number, there was a large variation between fibres in each group of deficiency and between patients (Table 5.6). There was no apparent correlation between the wild-type mtDNA copy number and deletion class.

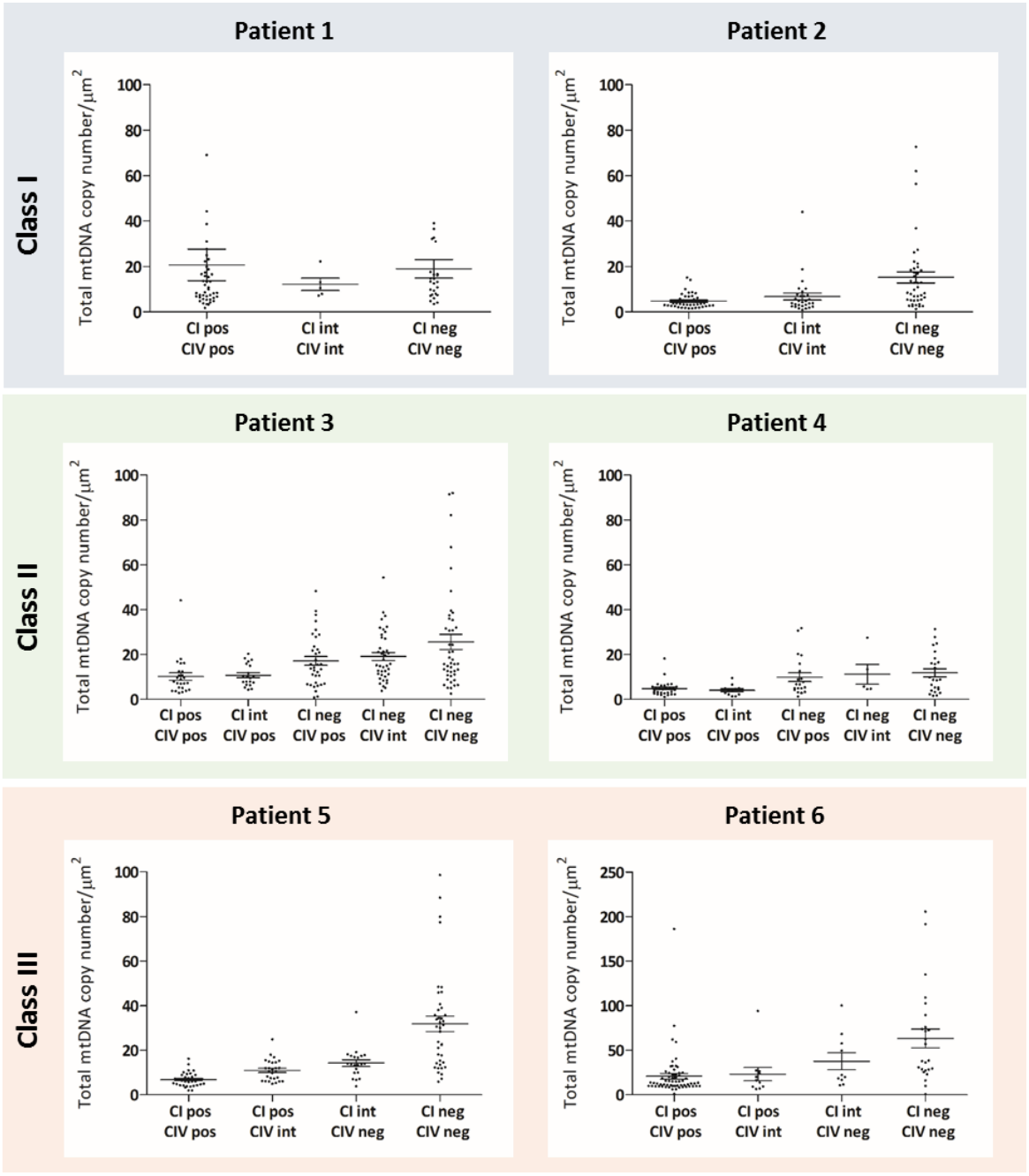

Figure 5.6: Total mtDNA copy number changes with respiratory chain deficiency. Individual fibres were grouped according to the level of OXPHOS deficiency. Each dot represents the total mtDNA copy number per µm^2 for each fibre. Mean total mtDNA copy number is shown with bars denoting SEM (standard error of the mean) above and below. Mean total mtDNA copy number is shown with bars denoting SEM (standard error of the mean) above and below.

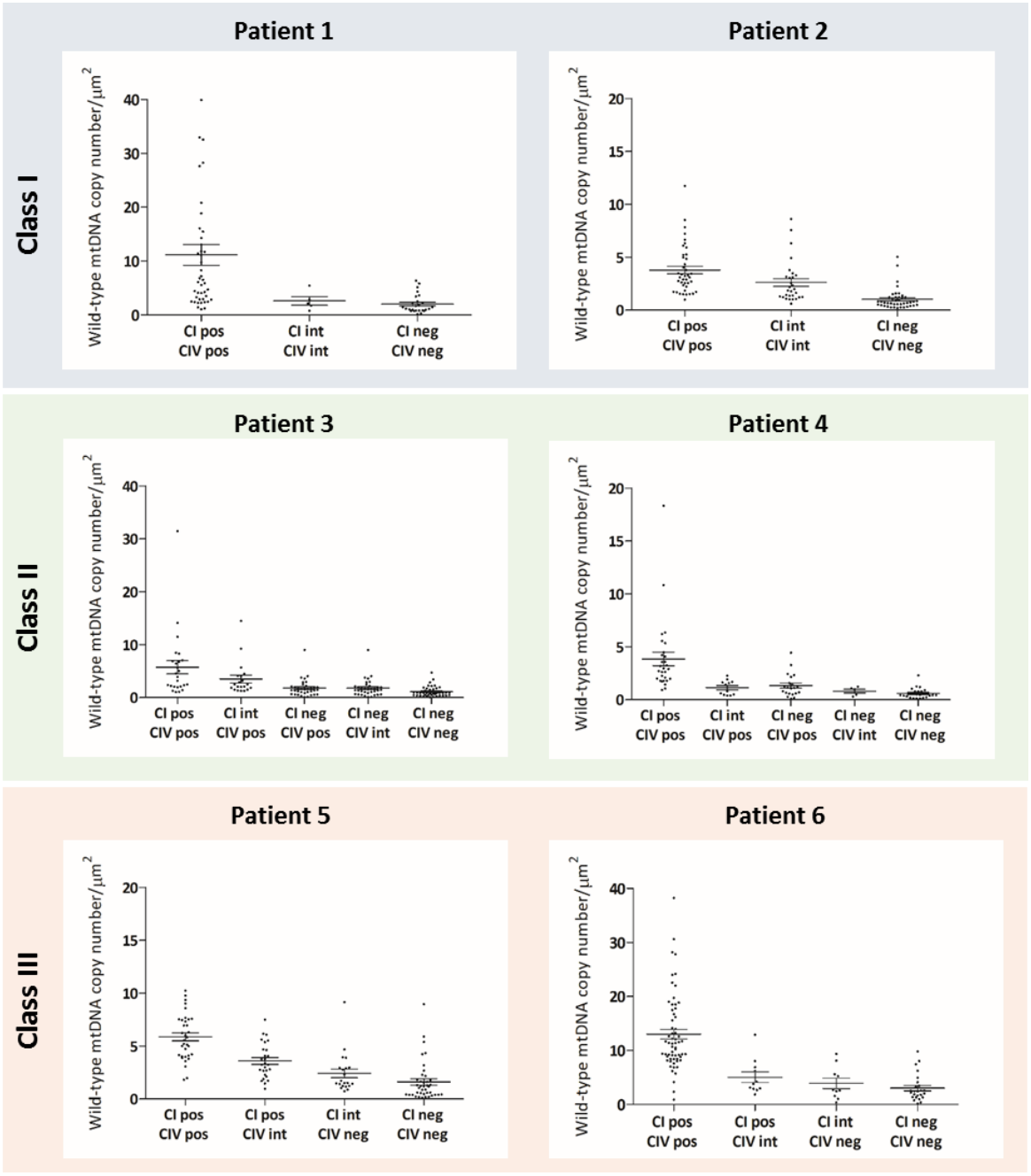

Figure 5.7: Wild-type mtDNA copy number decreases with respiratory chain deficiency. Individual fibres were grouped according to the level of OXPHOS deficiency. Each dot represents the wild-type mtDNA copy number per µm^2 for each fibre. Mean wild-type mtDNA copy number is shown with bars denoting SEM (standard error of the mean) above and below.

Patient		Total mtDNA copy number			Wild-type mtDNA copy number		
		Positive	*Int	Negative	Positive	*Int	Negative
P1	Mean	20.7±6.9	12.2±2.7	19.0±4.1	11.2±1.9	2.6±0.8	2.0±0.3
	CV	221.4%	49.9%	27.4%	112.7%	67.8%	85.7%
	n=	44	5	26	44	5	26
P2	Mean	4.7±0.5	6.8±1.5	15.2 ±2.4	3.8±0.4	2.6±0.4	1.0±0.2
	CV	67.5%	121.1%	104.5%	60.7%	76.5%	95.3%
	n=	41	29	42	41	29	42
P3	Mean	10.2±1.7	16.7±1.1	25.6±3.4	5.7±1.3	2.2±0.2	1.1±0.1
	CV	81.99%	64.3%	87.8%	110.4%	100.5%	83.8%
	n=	25	95	44	25	95	44
P4	Mean	4.9±0.6%	8.3±1.3	11.9±1.8	3.9±0.6	1.2±0.1	0.6±0.1
	CV	68.2%	95.7%	76.0%	89.9%	75.8%	49.8%
	n=	29	38	24	29	38	24
P5	Mean	6.8±0.5	12.4±0.9	31.9±3.5	5.9±0.4	3.1±0.3	1.6±0.3
	CV	46.3%	47.7%	69.3%	36.9%	59.6%	114.8%
	n=	34	48	40	34	48	40
P6	Mean	20.9±3.2	30.0±6.1	63.2±10.5	13.0±0.9	4.5±0.7	3.0±0.5
	CV	12.35%	92.4%	83.3%	53.9%	70.0%	81.6%
	n=	63	21	25	63	21	25

Table 5.6: Total and wild-type mtDNA copy number grouped by OXPHOS deficiency. The mean mtDNA copy number is presented for each OXPHOS group alongside the coefficient of variance (CV) and the total number of fibres in that group (n=). *Int denotes intermediate fibres which are neither positive for both complexes I and IV, nor negative for both complexes I and IV.

5.4.4 mtDNA deletion level and copy number

The mtDNA deletion level and total copy number were plotted for each muscle fibre (Figure 5.8). When deletion level approached the previously determined biochemical threshold for the first affected complex, total mtDNA copy number showed little change and remained relatively stable. However, as the level of deletion increased towards and above the biochemical threshold for the second affected complex, total mtDNA copy number began to increase exponentially. This trend was observed in all patients, except P1 who showed consistent mtDNA copy number regardless of deletion level.

A similar approach was taken to assess wild-type mtDNA copy number and deletion level (Figure 5.9). Again, wild-type mtDNA copy number remained stable at lower levels of deletion, declining slowly as the deletion level neared that of the first biochemical threshold. Once the second threshold level had been reached, wild-type mtDNA copy number decreased further. This trend was apparent in all six patients.

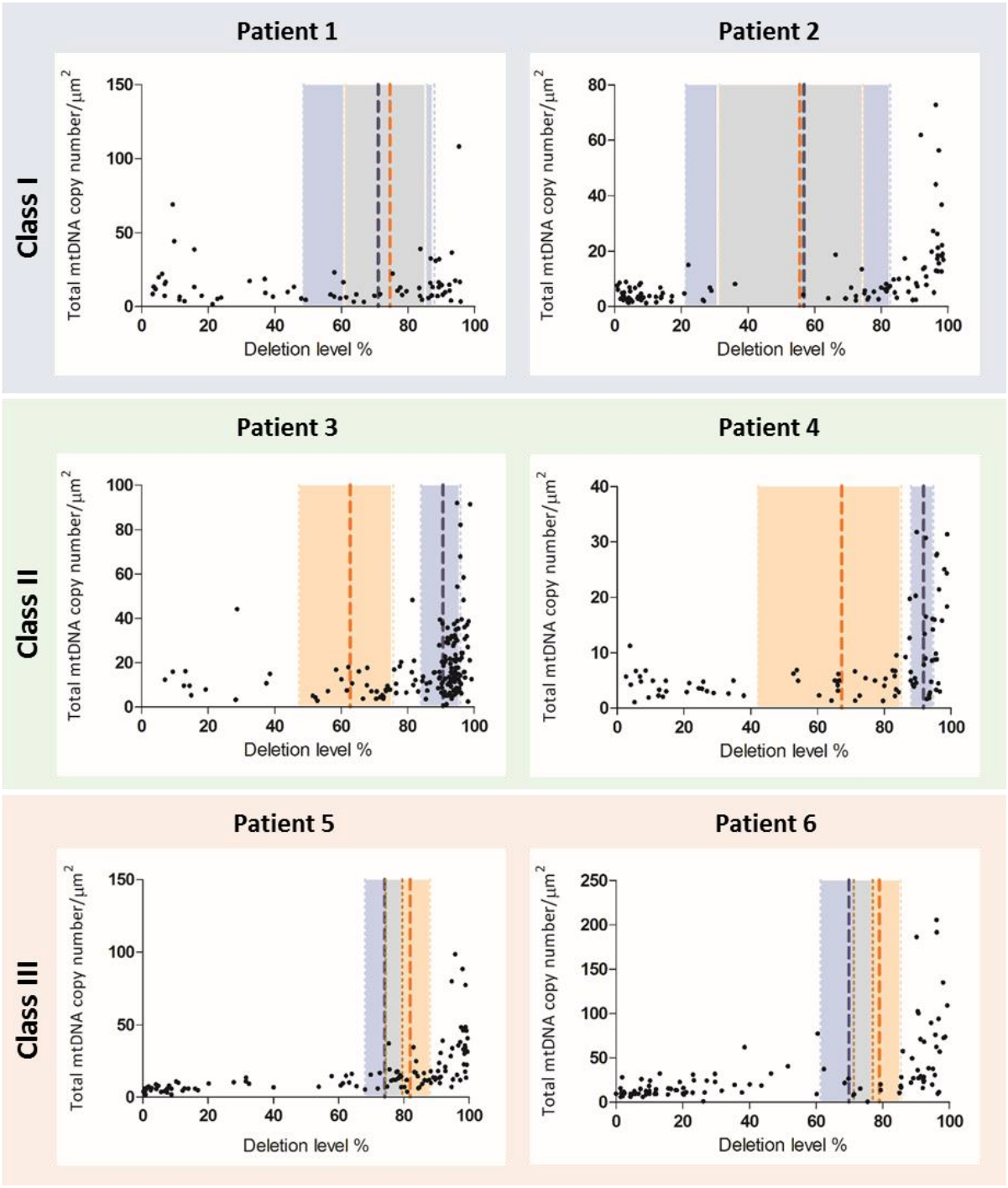

Figure 5.8: Total mtDNA copy number increases after the biochemical threshold has been reached: Deletion level and total mtDNA copy number were plotted for each fibre. Each black dot represents one fibre. The previously determined biochemical threshold levels for complex I and IV are shown as red and blue dashed lines, respectively. Shaded red and blue areas correspond to the upper and lower 95% confidence intervals for the threshold levels determined by the logarithmic regression model.

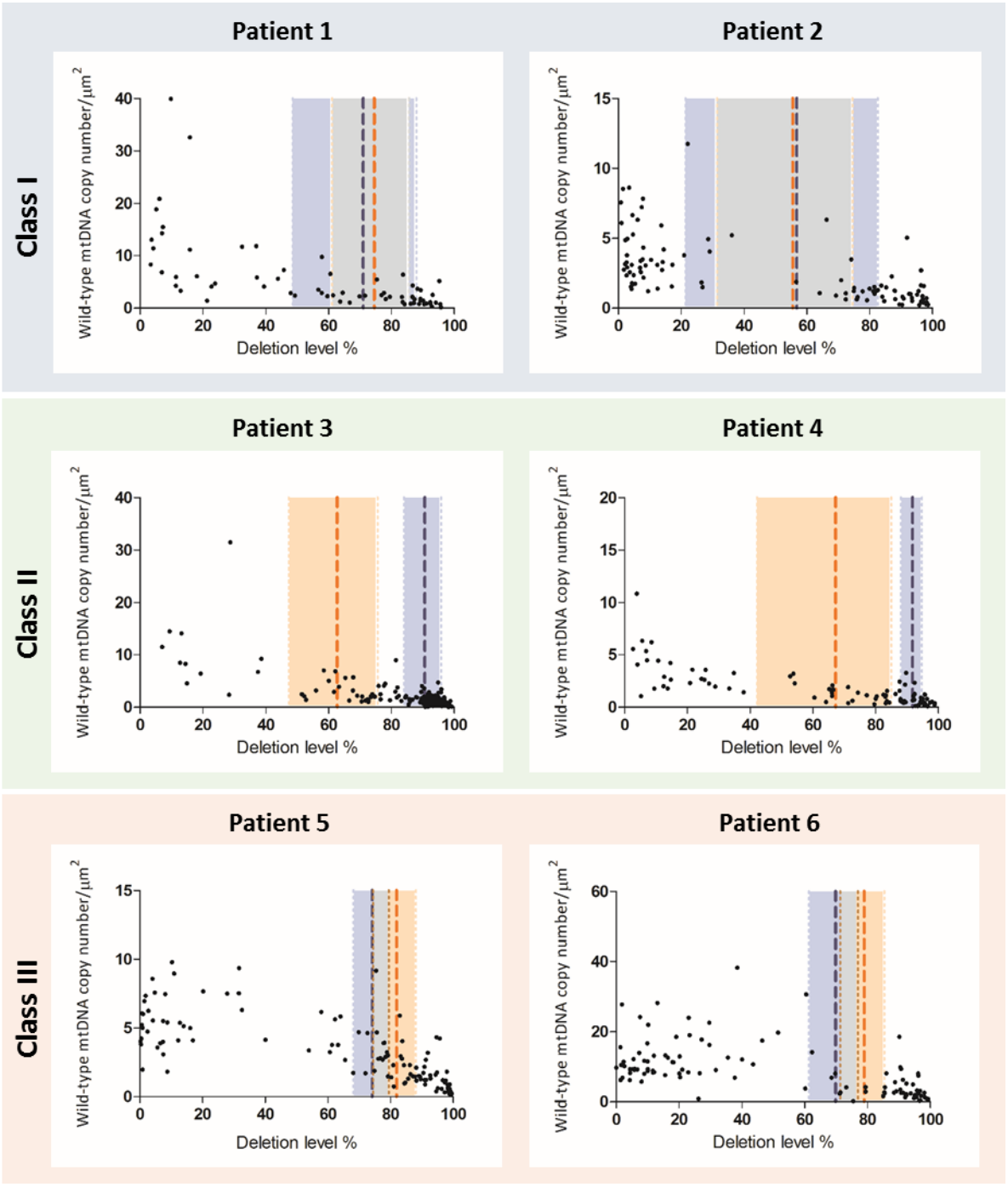

Figure 5.9: Wild-type mtDNA copy number decreases after the biochemical threshold has been reached: Deletion level and wild-type mtDNA copy number were plotted for each fibre. Each black dot represents one fibre. The previously determined biochemical threshold levels for complex I and IV are shown as red and blue dashed lines, respectively. Shaded red and blue areas correspond to the upper and lower 95% confidence intervals for the threshold levels determined by the logarithmic regression model.

5.4.5 Muscle fibre types: preliminary work

Preliminary work indicated some differences in the genetic and biochemical defects between different muscle fibre types. In these early investigations, immunofluorescent protocols were performed to determine the OXPHOS and fibre type profile of individual fibres from one control and one patient biopsy (P4 in the final study). Small numbers of fibres were selected for laser microdissection and subsequent molecular genetic analyses.

Figure 5.10 shows the respiratory chain deficiency seen in patient tissue. A total number of 2224 fibres were analysed (162 type I and 2062 type II fibres) revealing a greater proportion of complex I and complex IV deficient fibres in the type II population compared to type I, thereby suggesting a potential difference in susceptibility to mitochondrial dysfunction between fibre types.

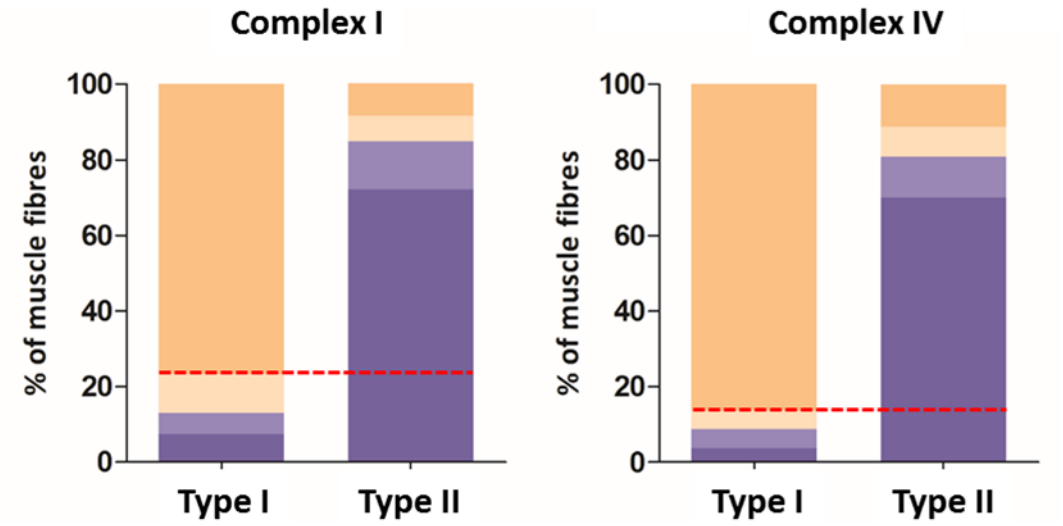

Figure 5.10: Preliminary evaluation of the biochemical defect in different muscle fibre types. Bar graphs show the proportion of fibres categorised as positive (beige), intermediate positive (light beige), intermediate negative (light blue) and negative (blue) for complex I and complex IV, in type I and type II fibres from one patient biopsy. The dotted red line indicates the percentage of deficient (positive, intermediate positive and intermediate negative) type I fibres.

Genetic analysis of single fibres from the control and patient biopsies showed a difference in total mtDNA copy number between fibres types (Figure 5.11A and B). However. No difference was seen in deletion level between fibres types in patient tissue (Figure 5.11C). Only a small number of fibres were analysed as part of these preliminary experiments, however the results highlighted the importance of considering fibre type when evaluating genetic and biochemical defects in future investigations.

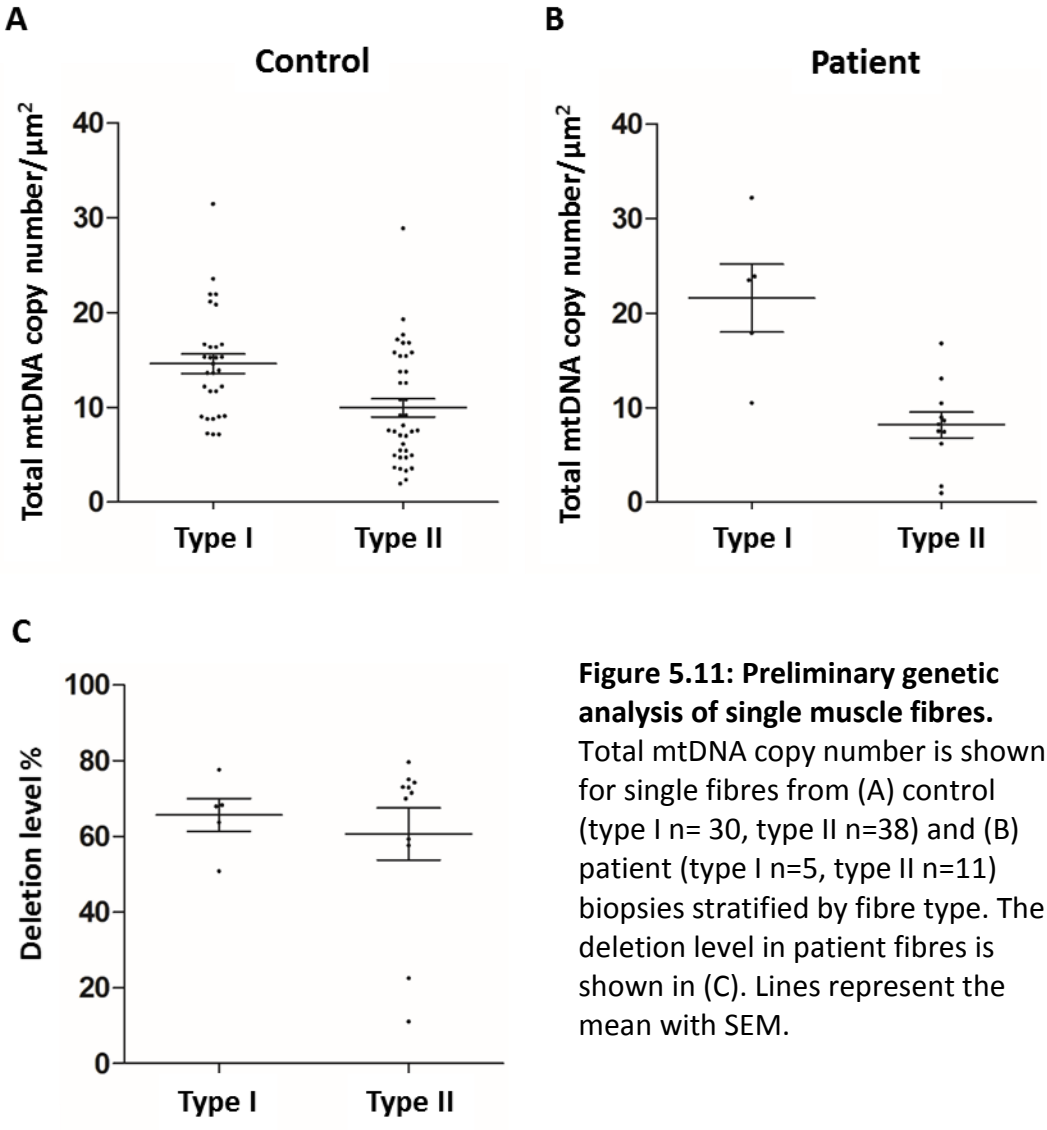

Figure 5.11: Preliminary genetic analysis of single muscle fibres. Total mtDNA copy number is shown for single fibres from (A) control (type I n= 30, type II n=38) and (B) patient (type I n=5, type II n=11) biopsies stratified by fibre type. The deletion level in patient fibres is shown in (C). Lines represent the mean with SEM.

5.4.6 Muscle fibre types and respiratory chain deficiency

Muscle sections stained for OXPHOS subunits (section 2) were manually aligned with the fibre typed sections (section 3) to create a profile of respiratory chain deficiency and fibre type for most fibres.

Table 5.7 shows the total number of fibres profiled, stratified by fibre type as either type I or type II (consisting of type IIa and IIx fibres). There was no consistent predominance of one fibre type over the other in these sections, with P1, P2 and P5 showing a larger proportion of type I fibres, whereas P3, P4 and P6 showed a majority of type II fibres. Fibre typing was also carried out on one control which showed predominantly type II fibres (65%). There was no association between deletion class and the distribution of fibre types (Figure 5.12). Typically, type I fibres consisted of a higher proportion of complex I and complex IV positive fibres, compared with type II, with the exception of P6. Conversely, most complex I and complex IV negative fibres were found to be type II in patients P1-P5. Finally, it is noteworthy that the differences in complex I and IV deficiencies characteristic of the different deletion classes were maintained within fibre types, for example the predominant complex I deficiency associated with deletion class II was evident in both type I and type II fibres.

Patient	Total fibres	Type I				Type II			
		n (%total)	Positive (%)	Int (%)	Negative (%)	n (%Total)	Positive (%)	Int (%)	Negative (%)
P1	470	352 (74.9%)	336 (95.5%)	11 (3.1%)	5 (1.4%)	118 (25.1%)	65 (55.1%)	32 (27.1%)	21 (17.8%)
P2	771	494 (64.1%)	405 (82.0%)	39 (7.9%)	50 (10.1%)	277 (35.9%)	150 (54.2%)	71 (25.6%)	56 (20.2%)
P3	252	89 (35.3%)	65 (73.0%)	20 (22.5%)	4 (4.5%)	163 (64.7%)	72 (44.2%)	68 (41.7%)	23 (14.1%)
P4	654	324 (49.5%)	33 (10.2%)	252 (77.8%)	39 (12.0%)	330 (50.5%)	30 (9.1%)	183 (55.5%)	117 (35.5%)
P5	719	464 (64.5%)	332 (71.6%)	37 (8.0%)	95 (20.5%)	255 (35.5%)	179 (70.2%)	22 (8.6%)	54 (21.2%)
P6	213	37 (17.4%)	16 (43.2%)	8 (21.6%)	13 (35.1%)	176 (82.6%)	146 (83.0%)	14 (8.0%)	16 (9.1%)
Control	270	104 (38.5%)	104 (100%)	-	-	166 (61.5%)	166 (100%)	-	-

Table 5.7: The number of muscle fibres profiled for OXPHOS deficiency and fibre type. The total number of fibres for each patient (P1-6) and control is stratified by fibre type, as type I or type II. The number of fibres belonging to each fibre type is shown (n) as a percentage of the total number of fibre profiled (%). For each fibre type, the number of fibres belonging to the different OXPHOS groups is shown as a count and a percentage of the total number of type I or type II fibres.

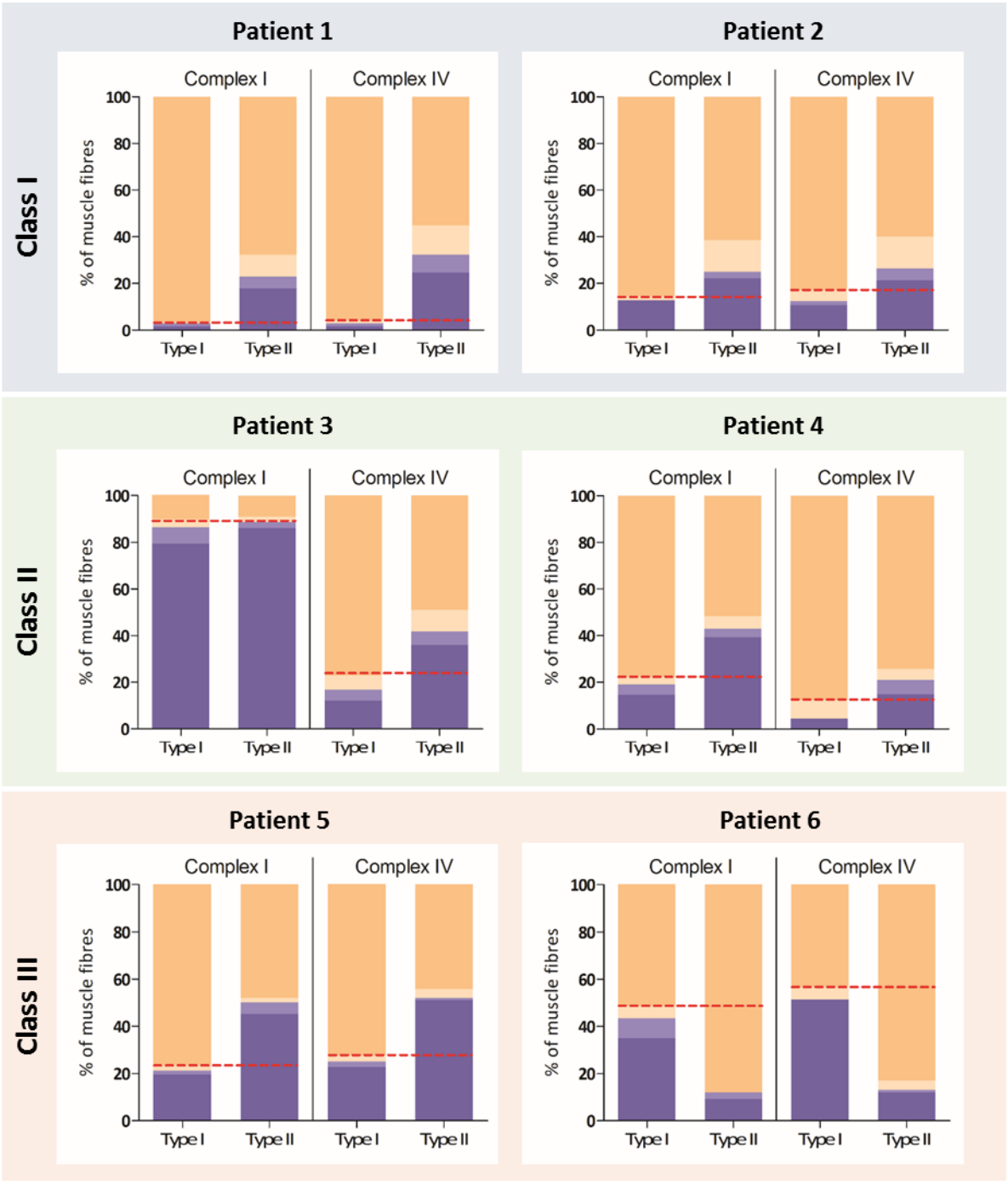

Figure 5.12: OXPHOS deficiency in type I and type II muscle fibres. Bar graphs show the percentage of fibres with normal (beige), intermediate positive (light beige), intermediate negative (light blue), and negative (blue) levels of complex I and complex IV, in type I and type II fibres. Type II fibres comprise type IIa and type IIx. The red dotted line indicates the proportion of deficient (intermediate positive, intermediate negative and negative) fibres in type I fibres.

5.4.7 Muscle fibre types and deletion level

Laser microdissected fibres were grouped firstly by fibre type (type I or type II) and then by respiratory chain deficiency (positive, intermediate or negative for complex I and IV) (Table 5.8). The small number of fibres in some groups was due either to (i) underrepresentation of these fibres across the muscle section, (ii) fibres not matching across serial sections, or (iii) fibres lost during processing of the section for single cell laser microdissection. Due to this unequal weighting of the OXPHOS groups between fibre types, deletion level was compared between fibres with the same degree of respiratory chain deficiency (positive, intermediate or negative). This allowed for direct comparison of the level of deletion in the different fibre types, independent of fibre selection bias.

Both type I and type II fibres displayed the trend of increasing deletion level with higher levels of respiratory chain deficiency described earlier in this chapter (Figure 5.13). There was no consistent trend between deletion level and fibre type within OXPHOS group or deletion class. In OXPHOS positive fibres, P1, P2 and P5 showed higher levels of deletion in type I fibres whereas P3, P4 and P6 showed higher levels in type II fibres. Deletion level in OXPHOS negative fibres was similar in type I and type II fibres in P1, P3, P5 and P6, yet unevenly distributed in P2 and P4.

Patient	n=	Type I				Type II			
		Positive	Int	Negative	Total	Positive	Int	Negative	Total
P1	75	19	2	5	26	25	3	21	49
P2	112	12	5	20	37	29	24	22	75
P3	164	11	47	18	76	14	48	26	88
P4	91	17	15	4	36	12	23	20	55
P5	122	15	27	23	65	19	21	17	57
P6	109	11	7	9	27	52	14	16	82
CN	30	10	-	-	10	20	-	-	20

Table 5.8: The number of type I and type II laser microdissected fibres grouped by OXPHOS deficiency. CN= control; n= shows the total number of fibres isolated for each patient or control; Int = intermediate OXPHOS deficiency group

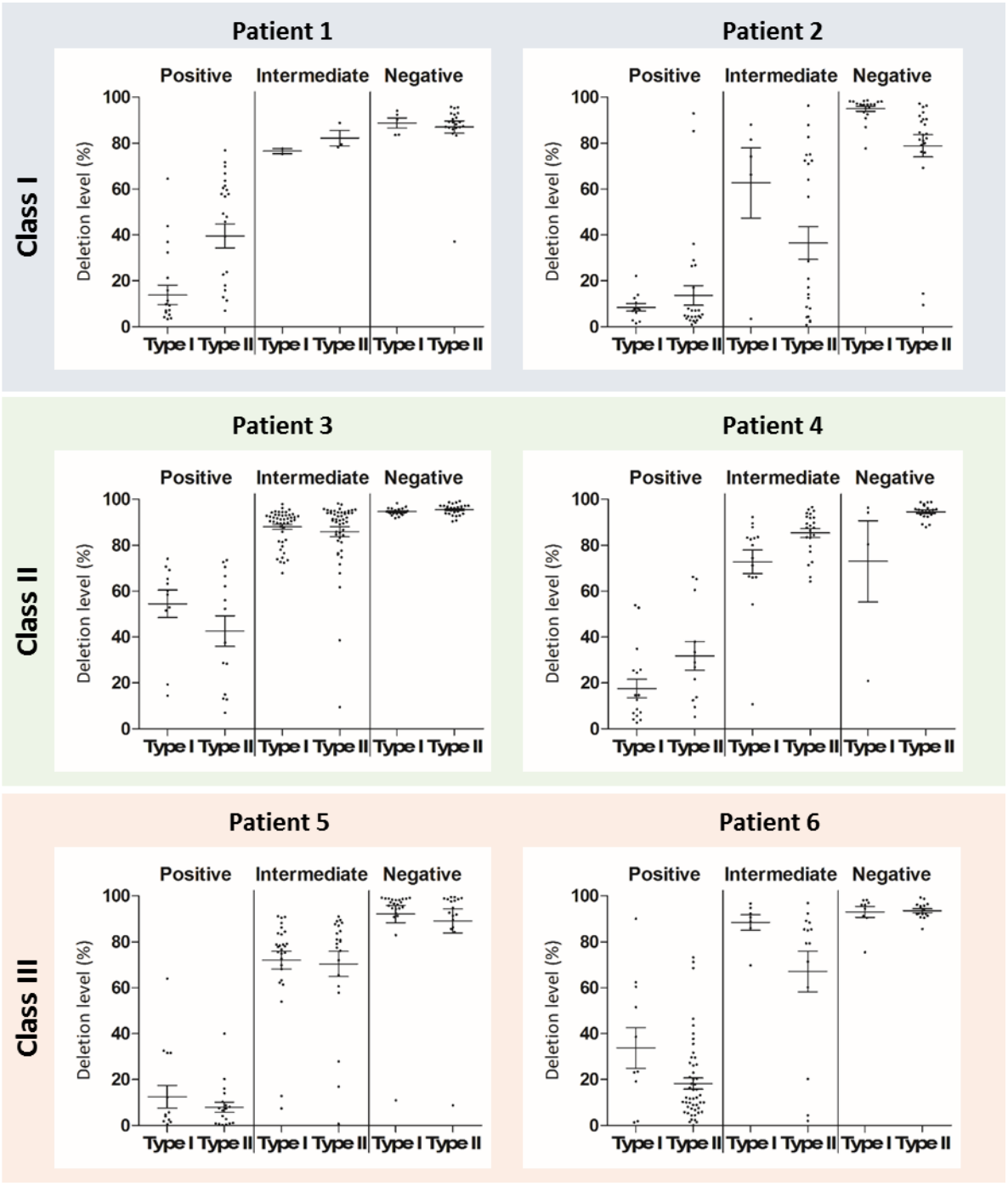

Figure 5.13: Deletion level for different muscle fibre types grouped by OXPHOS deficiency. Each dot represents the deletion level of one fibre. Type I and type II fibres are grouped to compare deletion level independent of the extent of OXPHOS deficiency. Mean deletion level is shown with SEM (standard error of the mean) above and below.

5.4.8 Muscle fibre types and mtDNA copy number

Using the same grouping as described for deletion level, total mtDNA copy number was compared between type I and type II fibres (Figure 5.14). There was no significant difference between fibre types observed in the control, although the lowest total mtDNA copy numbers were seen in type II fibres. In comparable OXPHOS normal fibres from patients, type I fibres harboured higher total mtDNA copy number than type II in P1, P4, P5 and P6, while no difference was seen between fibre types in patients P2 and P3. As with the control, lower copy number was generally seen in type II fibres. With the onset of respiratory chain deficiency, all patients (with the exception of P1) showed an increase in total mtDNA copy number in type I and type II fibres.

In OXPHOS positive fibres, wild-type mtDNA copy number was higher in type I compared to type II fibres for all patients except P3. Both fibre types showed a decline in wild-type mtDNA copy number with OXPHOS deficiency in all patients (Figure 5.15).

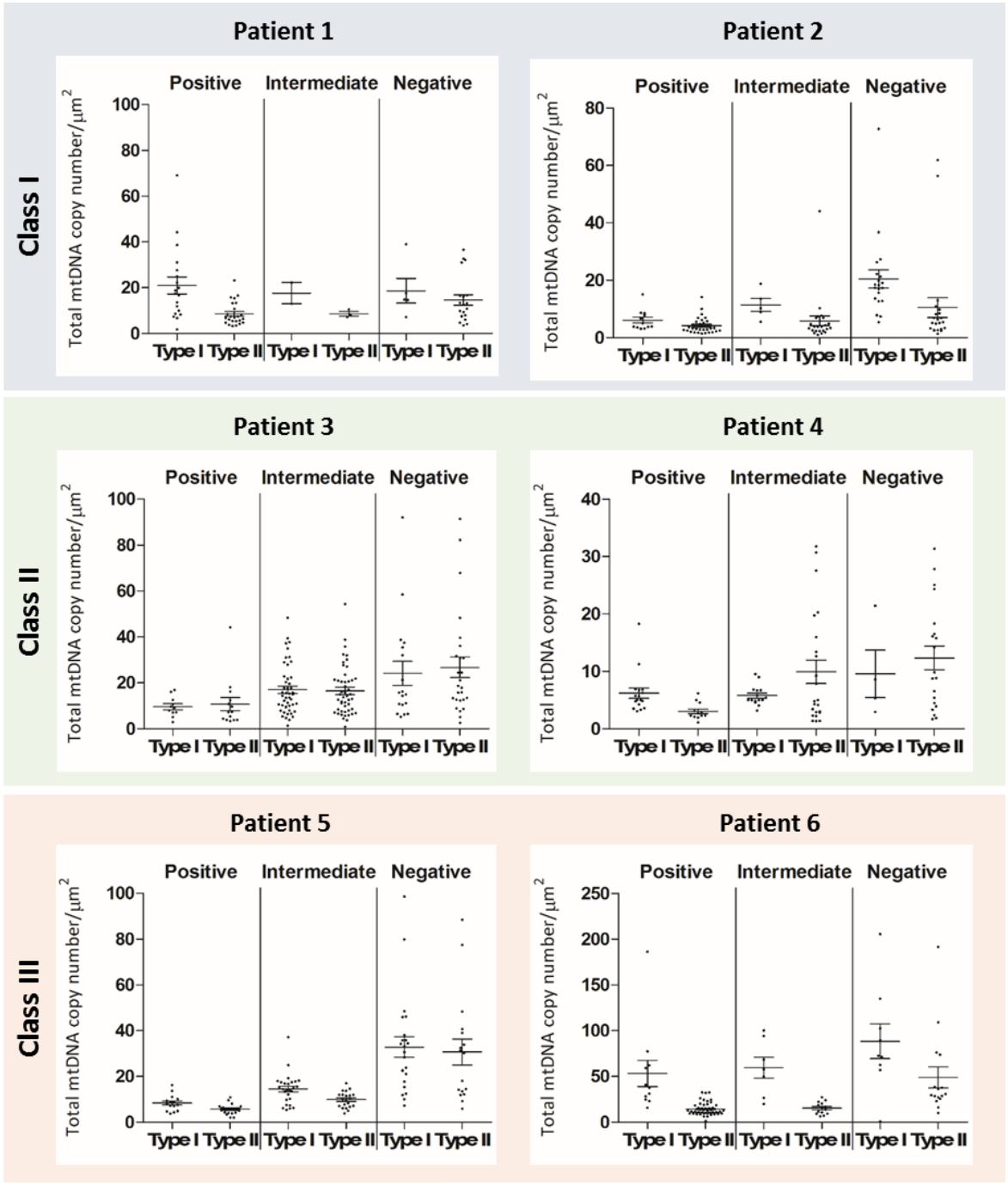

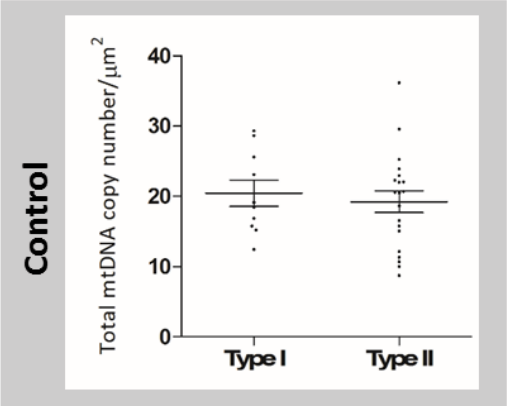

Figure 5.14: Total mtDNA copy number for different muscle fibre types grouped by OXPHOS deficiency. Each dot represents the total mtDNA copy number of one fibre. Type I and type II fibres are grouped to compare copy number independent of the extent of OXPHOS deficiency. Total mtDNA copy number is also shown for type I and II fibres in the control, all of which are OXPHOS positive. Mean total mtDNA copy number is shown with SEM (standard error of the mean) above and below.

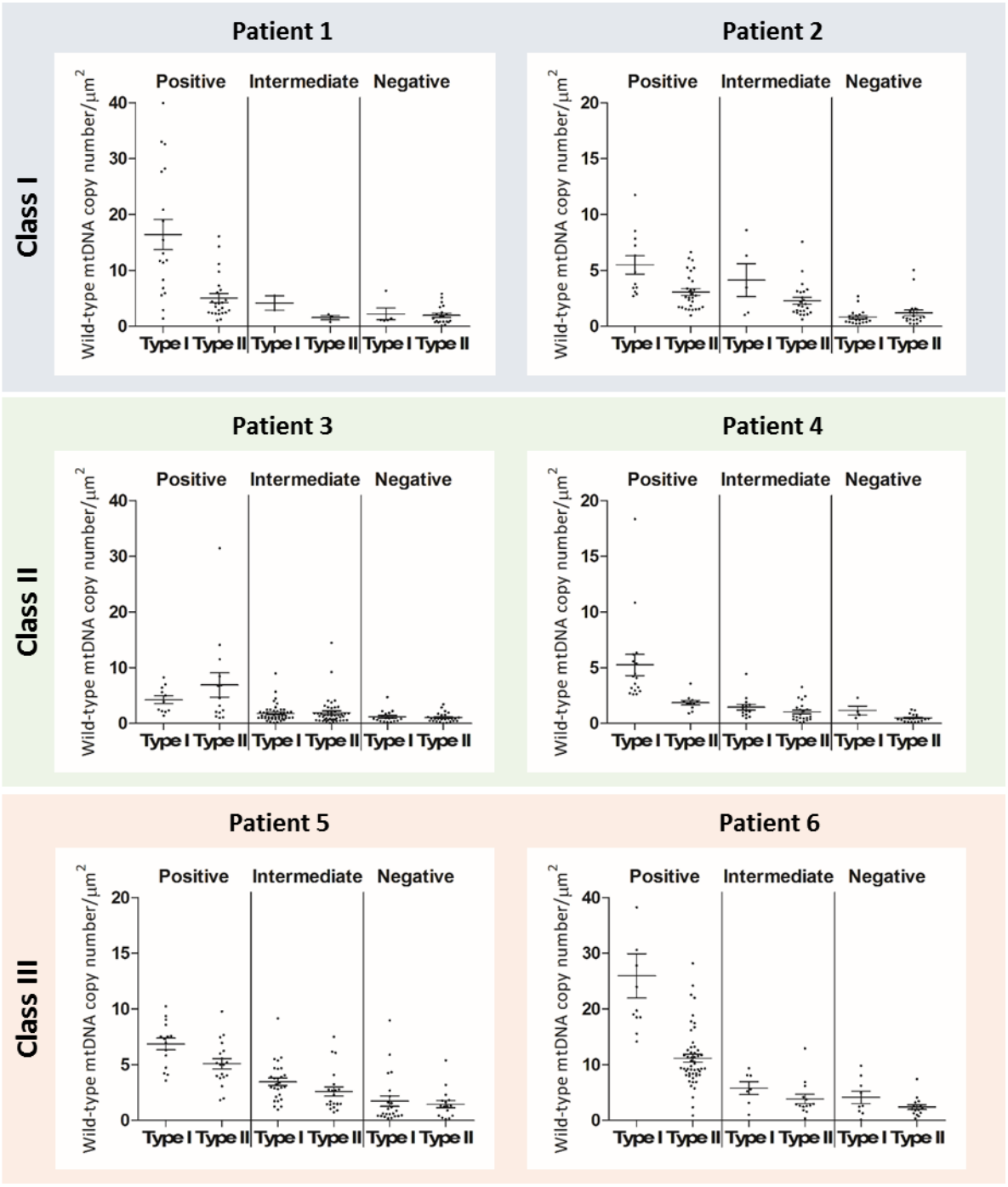

Figure 5.15: Wild-type mtDNA copy number for different muscle fibre types grouped by OXPHOS deficiency. Each dot represents the wild-type mtDNA copy number of one fibre. Type I and type II fibres are grouped to compare copy number independent of the extent of OXPHOS deficiency. Mean deletion level is shown with SEM (standard error of the mean) above and below.

5.5 Discussion

Elucidating pathogenic mechanisms associated with single, large-scale mtDNA deletions is challenging due to the genetic heterogeneity and the spectrum of clinical symptoms presented by patients. As such, there are conflicting reports regarding the relationship between the genetic defect, in terms of the size, location and level of the deletion, and the resulting biochemical deficiency (as discussed in chapter four). In this study, a single fibre approach was taken to more precisely explore this relationship on a cellular level, with the aim of determining the molecular mechanisms driving pathogenesis. Skeletal muscle biopsies from six patients with single, large-scale mtDNA deletions, classed based on the size and location of the deletion, were subjected to immunofluorescence assays to provide OXPHOS and fibre type profiles for individual muscle fibres. Single fibres were isolated by laser microdissection for molecular genetic analysis of deletion level and mtDNA copy number. This is the largest single fibre study using skeletal muscle biopsies obtained from patients with single, large-scale mtDNA deletions.

5.5.1 Deletion level is higher in fibres with greater levels of respiratory chain deficiency

It has long been established that higher levels of deletion are present in COX-deficient fibres in patients with single, large-scale mtDNA deletions (Mita *et al.,* 1989; Collins *et al.,* 1990; Moraes *et al.,* 1992). Using a recently developed immunofluorescence protocol, the current study has been able to more accurately quantify the extent of COX-deficiency as well as evaluating complex I deficiency in the same fibre (Rocha *et al.,* 2015). Furthermore, use of a duplex real-time PCR assay allowed for improved precision in the determination of deletion level in single laser-microdissected muscle fibres, compared to the semi-quantitative techniques used previously. In concordance with the previous findings, this work has shown that deletion level increases with higher degrees of respiratory chain deficiency across a total of 673 fibres from six patients.

There are conflicting reports in the literature regarding the level of deletion in fibres which maintain normal respiratory function. Across all six patients in this study, 236 fibres designated OXPHOS positive (displaying normal levels of complex I and IV) were shown to harbour a mean deletion level of 22.6% (SD=23.4%), ranging from 0-93%. This reflects the observations made by Sciacco *et al.* (1994), who record levels of deletion reaching 90% in

biochemically normal fibres, and He *et al.* (2002) who report a similar average of 21% deletion level. However, Shoubridge *et al*. (1990) did not detect deletion species in normal fibres, a finding somewhat represented in the present study, as 11% (n=26) of normal fibres showed deletion levels of less than 1%. This earlier study used a Southern blotting technique on PCR amplified DNA from only seven samples, and so the observation could be an artefact of the semi-quantitative analysis or a genuine result from a limited sample size. This highlights the importance of analysing large numbers of fibres when investigating such a heterogeneous group of mutations.

Chapter four discussed the relationship between deletion size and level, reporting that larger deletions were typically present at lower levels than smaller deletions, in-line with observations in the literature (Lopez-Gallardo *et al.,* 2009; Grady *et al.,* 2014; Mancuso *et al.,* 2015). The three classes of deletion used to group patients in this chapter differ in average deletion size (class I =5.1kb; class II=3.3kb; class III=6.7kb), although no difference in the average deletion level was seen between classes in this single fibre study. This is likely due to an artefact of uneven sampling of fibres with different degrees of OXPHOS deficiency in each patient. For example, only 25 positive fibres were laser-microdissected from P3 (15% of the total fibres cut) compared with 63 fibres from patient 6 (58% of total fibres). As these fibres typically harboured lower levels of deletion, the average deletion level for P6 would be drastically lowered due to the higher proportion of positive fibres sampled. When deletion level was analysed in skeletal muscle homogenate from 23 patients, as part of the previous work by Dr. Mariana Rocha, a noticeable difference in average deletion level was observed between deletion classes, following the trend discussed above: class I=52%; class II=74%; class III=36%.

5.5.2 The class (size and location) of the deletion determines the biochemical threshold

The pathogenic mechanisms associated with single, large-scale mtDNA deletions have been long debated in the literature. Novel findings of the current study indicate that the threshold level of deletion, required for the onset of respiratory chain deficiency, is different for complex I and complex IV, and is variable depending on the deletion class. For class I deletions, where complex I and IV are equally affected, the threshold levels for these complexes are similar. However, for class II deletions, the threshold level for complex I is

considerably lower than for complex IV. This may explain the predominant complex I deficiency associated with these deletions. Likewise, for class III deletions complex IV deficiency arises at a lower level of deletion than complex I deficiency.

Reports from Moraes *et al.* (1992) and Hammans *et al.* (1992) indicated the pathogenic mechanism associated with single, large-scale mtDNA deletions related to the deletion of protein-encoding genes. These studies observed higher proportions of COX-deficient fibres in patients with deletions encompassing complex IV genes, compared to those where the deletion was elsewhere located. The findings of the work presented in this chapter support these observations. The clearest demonstration of this is the different threshold levels for complex I and IV deficiency in class II deletions. These deletions removed three complex I (*MT-ND4*, *MT-ND5* and *MT-ND6*) and three mt-tRNA genes (*MT-TH*, *MT-TS2* and *MT-TL2*), leaving all complex IV genes intact. This resulted in a threshold level of 63-67% for complex I deficiency and 91-92% for complex IV deficiency, directly linking the location of the deletion to the biochemical defect.

Further support for this is provided by the other deletion classes. In class III deletions, all mitochondrial complex IV genes are deleted, while four of the seven complex I genes were also removed. This resulted in a lower threshold level for complex IV deficiency (70-74%) compared to complex I (79-82%). Although these thresholds are much closer than those for class II deletions, possibly due to the additional removal of complex I genes in class III, there still remains a preferential deficiency of complex IV directly correlated with the location of the deletion. An alternative theory based on work in *trans*mitochondrial cybrids suggested the deletion of tRNA genes to be the primary driver of pathogenesis (Nakase *et al.,* 1990; Hayashi *et al.,* 1991). It is possible that the different threshold levels seen in class II deletions could be, in part, attributed to the complex-specific requirements for the tRNAs deleted. The mtRC profile of deficiency associated with these deletions is also seen in patients with m.3243A>G point mutation in the *MT-TL1* gene encoding mitochondrial $tRNA^{Leu(UUR)}$ resulting in a predominant complex I deficiency.

Hayashi *et al.* (1991) described a complementation effect whereby wild-type mtDNA is able to compensate for the deleted mt-tRNAs up until a deletion level of 60%. It might be expected that the removal of a greater number of mt-tRNA genes would have an impact on the threshold level, possibly causing respiratory chain deficiency to occur at a lower deletion level due to insufficient complementation capabilities. However, in the current study class III deletions removed 8-10 mt-tRNA genes and showed a higher threshold level for complex I deficiency than was observed for class II deletions, where only three mt-tRNA genes were deleted.

It is clear that the involvement of tRNA and protein-encoding genes in the pathogenesis of single, large-scale mtDNA deletions is complex. Work presented in this chapter indicates a more prominent role for deleted genes encoding subunits of the mitochondrial respiratory chain in the pathogenic mechanism due to the strong correlation between deletion size, location and biochemical threshold level. However, only six patients feature in this study and the investigation of additional patients with a wider range of deletions would be required to further elucidate these mechanisms.

5.5.3 mtDNA copy number is related to the biochemical threshold

The longitudinal study of patients with single, large-scale mtDNA deletions presented in the previous chapter reports a correlation between deletion level and total mtDNA copy number in skeletal muscle homogenate, such that higher levels of deletion were associated with increased total mtDNA copy number. In this single fibre study, deletion level and total copy number (per μm^2) were plotted against each other to reveal a comparable relationship: fibres with high levels of deletion typically harboured more mtDNA copies. This appeared to be a threshold-dependent occurrence as copy number was relatively stable through lower levels of deletion and even approaching the threshold level of the first affected complex, before increasing exponentially once the second threshold level had been surpassed.

Curiously, a similar yet inverted trend was seen regarding wild-type mtDNA copy number and deletion level. Here, the number of wild-type mtDNA copies dropped rapidly after the deletion level moved beyond the second threshold level. This is in agreement with observations made by Durham *et al.* (2007) who reported a decline in wild-type copy

number related to higher deletion levels and COX-deficiency in skeletal muscle fibres. Like the work presented by Durham *et al.* (2007), the current study supports the *in silico* predictions of Chinnery and Samuels (1999), who postulated an increase in mtDNA proliferation occurs in order to maintain a wild-type mtDNA copy number as close to 'normal' as possible. This continues until a critical point, after which a steep decline in wild-type mtDNA copy number is observed leading to the accumulation of deleted mtDNA species. The current study did not see a notable increase in total mtDNA copy number prior to alteration of the wild-type proportion, however this may be due to an insufficient number of fibres with the required deletion levels to place them in this transitional phase.

5.5.4 Respiratory chain deficiency varies between fibre types

Muscle fibre type was determined in the present study using an immunofluorescence assay to detect myosin heavy chains. There was no clear predominance of type I or type II fibres across patients, however this may be due to the various muscle biopsy sites. Of note, however, was the observation of increased respiratory chain deficiency in type II fibres over type I, as was indicated by the preliminary investigations. Previous studies have suggested a loss of type II fibres with age (Lexell *et al.,* 1995), possibly due to an increased susceptibility to mitochondrial dysfunction (Conley *et al.,* 2007). The underlying mechanisms behind this are not currently fully understood. Data presented in this chapter does not offer much clarification on the matter, as type II fibres did not consistently show higher deletion levels than type I fibres, and although lower total mtDNA copy numbers were seen in type II fibres, overall there was little difference compared with type I fibres. While the single fibre genetic analysis did not reveal the mechanisms behind the fibre type specific susceptibility to respiratory chain deficiency, it is important to consider that this was performed on a small number of biopsies and that larger sample sizes will be required to better evaluate this relationship.

5.5.5 Limitations

This study is the largest investigation of single muscle fibres from patients with single, large-scale mtDNA deletions. Although the combination of quantitative molecular genetic and immunofluorescent techniques has improved the analyses of the genetic and respiratory chain defects, there are some limitations to consider. First, although this study analyses 673

fibres in total, only six patients were represented. Given the labour-intensive and time-consuming nature of the experimental protocol, a limited number of patients could be included in the single fibre portion of the study. These patients were grouped according to the size and location of their deletions, so that each deletion class comprised two patients. The deletion classes formed an important aspect of this study, and having only two patients per class could not provide significant conclusions. Therefore, further work should continue to evaluate additional patients to confirm the conclusions drawn in this study.

Second, the clinical features of the patients involved in the single fibre study were not investigated in relation to the genetic and biochemical findings. This was mainly due to the focus on the cellular mechanisms and the relationship between the mtDNA and cellular dysfunction, rather than the association with clinical phenotypes. Attempting to correlate the findings of this study with the clinical symptoms of the patients involved could prove difficult due to the small size of the group (n=6), particularly considering the heterogeneity of this group of mutations at the genetic and clinical levels.

Finally, the analysis of muscle fibre type is limited by the grouping of type II fibres. Not all biopsies contained fibres of type I, IIa and IIx, and so during analysis type II fibres were grouped to allow for comparison with type I fibres. However, type IIa fibres have been shown to rely on both glycolytic and oxidative metabolism, whereas type IIx fibres rely predominantly on glycolysis. The grouping of these fibres into one class of 'type II' could explain some of the variation in this fibre type and the lack of consistent observations with regards to the comparisons with type I fibres.

5.6 Conclusion

The findings of the work presented in this chapter show that (i) the extent of respiratory chain deficiency correlates with deletion level, (ii) the size and location of the deletion dictates the biochemical threshold level, (iii) deletion of mitochondrial genes encoding sub-units of the respiratory chain complexes plays a key role in the pathogenic mechanisms of single, large-scale deletions, (iv) mtDNA copy number may be regulated by the level of deletion and the biochemical threshold and (v) type II muscle fibres are more susceptible to

respiratory chain deficiency than type I fibres. Overall, the study contributes valuable, novel observations to the ongoing research into the relationship between genetic and biochemical defects at the cellular level, in an effort to better understand the pathogenic mechanisms associated with single, large-scale mtDNA deletions.

Chapter 6: Optimisation of a an new assay for the determination of mtDNA copy number

6.1 Introduction

6.1.1 mtDNA copy number

The balance between wild-type and mutant mtDNA has been shown to affect normal respiratory chain function in skeletal muscle from patients with mtDNA mutations. Durham *et al.* (2007) reported a clear relationship between high levels of mutant mtDNA, decreased wild-type mtDNA copy number and COX-deficiency in single muscle fibres with a 5.0kb deletion and the m.10010T>C *MT-TG* mutation. These observations are consistent with in-silico predictions made by Chinnery and Samuels (1999), that conclude a non-selective proliferation of the entire mtDNA population of a cell occurs in the presence of high levels of mutated mtDNA, in order to restore the wild-type mtDNA copy number. Previous work presented in this thesis has also shown that mtDNA copy number changes over time in skeletal muscle of patient with single, large-scale mtDNA deletions (chapter four) and has indicated that the balance between wild-type and total mtDNA copy number may play a role in the pathogenesis of these mutations (chapter five). Therefore, accurately determining mtDNA copy number in human tissues is of high importance to the investigation of pathogenic molecular mechanisms driving cellular dysfunction in the presence of mtDNA mutations.

6.1.2 Quantifying mtDNA copy number

Historically, the quantification of mtDNA copy number was studied by Southern blotting, a technique devised by Edward Southern in 1975 (Southern, 1975). This technique first involves preparation of DNA by restriction digest, followed by gel electrophoresis and denaturation of DNA in a strong alkaline solution. This results in linearised, single-stranded DNA fragments separated by size in a gel matrix. The blotting process transfers these DNA fragments to a more stable nitrocellulose or nylon membrane, so that they may be detected by target-specific radio-labelled probes. Although this technique easily permits the detection of multiple mtDNA deletion species, there are several limitations. First, a large amount of total DNA (approximately 2-3µg) is required for the analysis. This is of particular concern when using human tissue biopsies, a valuable and limited resource, and is not suitable for analysis of single muscle fibres. Second, densitometric analysis is semi-quantitative and can

be misleading due to oversaturation of bands or normalisation to an unsuitable control. Finally, the entire protocol can take days to complete and is relatively labour-intensive. As such, it has since been succeeded by quantitative real-time PCR, which is more efficient in terms of time and tissue usage, as well as providing fully quantitative data.

There are two commonly used real time PCR fluorescent chemistries employed for the quantification of total mtDNA copy number. SYBR Green dye-based assays quantify target DNA amplification using a fluorescent dye which binds to double-stranded DNA. As this binding is non-specific, these assays do not allow for quantification of multiple gene targets in a single reaction (multiplexing), the benefits of which are discussed later. Real-time PCR assays using TaqMan chemistry utilise fluorogenic-labelled probes to detect specific amplification products. These probes are target-specific and therefore facilitate multiplexing whilst improving the sensitivity, specificity and reproducibility of the assay beyond that of SYBR Green capabilities. It is for these reasons that this is the preferred approach for assay development later in this chapter.

A number of gene targets have been used for the quantification of mtDNA copy number using real-time PCR methods (Table 6.1). Commonly, a highly conserved region of *MT-ND1* is used as a marker for the mitochondrial genome (Balakrishnan *et al.,* 2010; Thyagarajan *et al.,* 2012; Zhang *et al.,* 2013; Spendiff *et al.,* 2013; Huang *et al.,* 2014; Shen *et al.,* 2016; Stiles *et al*., 2016) as it lies in the minor arc, where mtDNA deletions are less likely to occur. It also features in an assay for determination of mtDNA deletion level and so both protocols can be used in tandem for genetic investigation of single, large-scale mtDNA deletions (He *et al.,* 2002).

In order to be fully quantitative, mtDNA copy number must be normalised to a nuclear gene marker, providing a figure for the relative mtDNA copy number per cell. There are several nuclear gene targets used in the literature, in combination with the mitochondrial gene markers described above (Table 6.1). All of these genes are deemed suitable reference genes as they are required by all nucleated cells for survival (Pfaffl, 2004). However, pseudogenes of *ACTB* and *GAPDH* are known to exist in the human genome (Sun *et al.,* 2012) and so careful consideration to primer/probe design is required to ensure these are not amplified to give false-positives in the final assay quantification. The *RNA18S* gene is present as

numerous repeat units on multiple chromosomes so this gene is usually used to determine mtDNA depletion rather than an accurate total mtDNA copy number count. Single-copy genes, like *β2M*, are perhaps the most regularly used reference genes as only one copy is present per haploid genome and so there is only one potential target for primers and probes.

Authors	Mitochondrial gene target	Nuclear gene target
TaqMan chemistry		
Wong *et al.,* 2003	*tRNA$^{Leu(UUR)}$, D-loop*	*β2M*
Bai & Wong, 2005	*tRNA$^{Leu(UUR)}$, MT-ND4, MT-ATP8, D-loop*	*AIB1, β2M, ACTB*
Marcuello *et al.,* 2005	*MT-RNR1*	*RNaseP* control kit
Thyagarajan, 2012	*MT-ND1*	*RNA18S*
Sabatino *et al.,* 2013	*MT-COI*	*ACTB*
Spendiff *et al.,* 2013	*MT-ND1*	*RNA18S*
Zhang *et al.,* 2013	*MT-ND1*	*ACTB*
Grady *et al.,* 2014	*MT-ND1*	*β2M*
Phillips *et al.,* 2014	*MT-ND4, D-loop*	*β2M*
Huang *et al.,* 2016	*MT-ND1*	*HBB*
SYBR Green chemistry		
Bai & Wong, 2005	*tRNALeu, MT-ND4, MT-ATP8, D-loop*	*AIB1, β2M, ACTB*
Pejznochova *et al.,* 2008	*MT-RNR2*	*GAPDH*
Balakrishnan *et al.,* 2010	*MT-ND1*	*LPL*
Venegas & Halberg, 2012	*tRNA$^{Leu(UUR}$, MT-RNR2*	*β2M*
Stiles *et al.,* 2016	*MT-ND1*	*β2M*

Table 6.1: Mitochondrial and nuclear gene targets used in real-time PCR assays for the quantification of mtDNA copy number. *AIB1*= nuclear receptor co-activator 3; ACTB = β-actin; RNA18S = 18S rRNA; HBB=human β-globin; GAPDH= glyceraldehyde-3-phosphate dehydrogenase.

To date, relatively few of the published assays have been systematically validated for specificity and sensitivity. In 2014, Grady *et al.* performed a thorough evaluation of the sensitivity of a TaqMan-based real-time PCR assay for mtDNA copy number determination using *MT-ND1* and *β2M* gene targets. This study concluded that assay precision was affected by sample DNA concentration, as suggested by Sochivko *et al*. (2013), and proposed guidelines for the number of well and plate replicates required for the preferred detectable difference in mtDNA copy number. This assay has featured in previous chapters of this thesis (chapters three and four), and is performed regularly at the Wellcome Trust Centre for Mitochondrial Research in a variety of human and animal tissues.

These guidelines highlight the difficulty in accurately and precisely quantifying mtDNA copy number and reinforce the importance of planning experiments involving these assays. For example, in order to detect a copy number difference of 10% between DNA samples at high concentrations (0.6ng/µl), five replicate plates are required each with six sample replicates. As the *ß2M* and *MT-ND1* assays are performed as singleplex reactions, the total number of plates required is actually doubled. This assay, therefore, can be costly in terms of the reagents and tissue used, and the time required to complete these experiments. Therefore, it has been suggested by our group that the assay be modified with the addition of another nuclear gene marker, the multicopy *RNA18S* gene, such that two multiplex reactions for *MT-ND1*/*RNA18S* and *RNA18S*/*ß2M* are performed for each sample. With an estimated 200 copies per nuclear genome, *RNA18S* acts as an intermediate measure between *ß2M* (one copy) and *MT-ND1* (ranging up to 100,000s copies), thereby reducing the fold-change in copy number between targets, improving quantitative accuracy and reducing the number of replicate plates required.

6.1.3 RNA18S as a target in mtDNA copy number assay

RNA18S(1-5) genes encode 18S rRNA, a component of the catalytic portion of the small subunit of the ribosome. 18S rRNA is produced by the post-transcriptional processing of the polycistronic precursor 45S rRNA (*RNA45S*), comprised of 5.8S, 18S and 28S rRNA (Lodish *et al*., 2000b). *RNA45S* is organised as a series of tandem repeat sequences of 44kb (Wellauer and Dawid, 1979) arranged at the p12 loci of chromosomes 13, 14, 15, 21 and 22 (Henderson *et al*., 1972).

A number of studies have attempted to quantify *RNA18S* copy number in humans with estimates ranging from 50 to 200 copies per haploid genome (Bross and Krone, 1972; Schmickel *et al.,* 1973; Gaubatz *et al.,* 1976; Young *et al.,* 1976). This level of variation may be due to the various techniques employed by these studies. Copy number determined using labelled rRNA samples was consistently reported at 160-200 (Bross and Krone 1972; Schmickel *et al*., 1973; Gaubatz *et al*., 1976), whereas analysis using cDNA concluded only 50 copies per haploid genome (Young *et al.,* 1976).

Despite no comprehensive study reporting *RNA18S* copy number in the normal population, this target is frequently used in real-time PCR assays for the determination of mtDNA

depletion (Thyagarajan *et al.,* 2012 and 2013) where the ratio of *RNA18S:ND1* is used as a marker for mtDNA copy number depletion. However, *RNA18S* could be a potentially useful target for more quantitative assessments of mtDNA copy number. Currently, the single-copy nuclear gene, *β2M*, is analysed alongside the multiple copies of mtDNA, represented by *MT-ND1,* to derive the number of mtDNA copies per cell. However, the fold-difference in the copy number of these two genes is vast, with the number of mtDNA per cell reaching 100,000 in oocytes. This contributes to the variation seen between measurements using this assay. By establishing ratios of *MT-ND1*:*RNA18S* and *RNA18S:β2M* using separate multiplex real-time PCR assays, and combining these to calculate the ratio of *MT-ND1*:*β2M*, this margin of error should be reduced.

6.1.4 Multiplexing real-time PCR assays

Multiplex real-time PCR allows for the simultaneous amplification of multiple target sequences in a single reaction. This is facilitated by the use of specific probes with unique fluorescent dyes assigned to different target sequences. There are several advantages to multiplexing real-time PCR assays. As mentioned, multiple targets can be assessed at once, reducing the number of reactions required for the quantification of a target. This not only lessens the costs associated with reagents and equipment, but also requires a reduced quantity of sample overall. This is particularly pertinent when using DNA from samples with limited availability, such as patient tissue biopsies. Furthermore, the ability to run multiple assays at once increases throughput, allowing for more samples to be analysed in a given time period. There is also a benefit to the reliability when real-time PCR assays are multiplexed as targets are normalised to the same endogenous control and face the same reaction conditions. In addition, pipetting error, which can contribute to variation when quantifying targets with singleplex reactions, is equal for both targets in the multiplex assay.

6.2 Aims

This chapter details the optimisation of a new assay for the determination of mtDNA copy number, more sensitive and less variable than the existing *MT-ND1/β2M* assay, which may be used in the evaluation of individual cells or small amount of tissue. In particular, this study aims to (i) optimise conditions for a multiplex real-time PCR protocol using *RNA18S* and *β2M* targets, (ii) apply the optimised protocol to control tissue samples to evaluate the suitability of this method in the investigation of patient samples (iii) validate the accuracy of

existing targets *MT-ND1* and *β2M* using *MT-RNR2* and *GAPDH* as alternative mitochondrial and nuclear markers.

6.3 Methods

6.3.1 Cloning and transformation part 1 – plasmid p.MTCN1

In order to determine *RNA18S* copy number, a plasmid was engineered to contain a portion of this gene. The standard protocol for cloning and transformation is outlined in section 2.10). Primers were designed to amplify a locus of interest on *RNA18S5* (22p12) (GenBank accession number: NT_167214.1 (GRCh38.p7); forward 5'-GCCGCTAGAGGTGAAATTCTTG-3' (nt.110026-110047); reverse 5'-CATTCTTGGCAAATGCTTTCG-3' (nt.110091-110071)) by standard PCR using control human blood homogenate DNA, introducing *EcoR*V restriction sites at the 5'- and 3'- ends. Products were resolved by gel electrophoresis to confirm amplification of the 240bp fragment before DNA clean-up and polishing as described in sections 2.10.3 and 2.10.4 respectively. The vector, plasmid p.7D1.B2M (section 2.8.2), underwent restriction digest by *EcoR*V and was ligated with the *RNA18S* insert using T4 ligase (section 2.10.5) (Figure 6.1A). Competent JM109 cells were transformed and plated as described in 2.10.7. Standard PCR (using the primers above) and Sanger sequencing protocols were used to confirm successful insertion of the *RNA18S* fragment into the vector p.7D1.B2M. A glycerol stock of plasmid p.MTCN1 was prepared for long-term storage (section 2.10.10). DNA was extracted from bacterial cultures (section 2.10.11) and stored in 5µl aliquots at -20°C.

6.3.2 Cloning and transformation part 2 – plasmid p.MTCN2

A second plasmid, p.MTCN2, was constructed to allow for measurement of *GAPDH* and *MT-RNR2* copy number. Primers were designed to amplify regions of *GAPDH* and *MT-RNR2*, and introduce restriction sites (Table 6.2). Gel electrophoresis was used to confirm the size of the amplicons before clean-up and quantification by Nanodrop. Amplicons were digested with *EcoR*1, according to the manufacturer's guidelines, and ligated overnight at 4°C using T4 ligase. Standard PCR using *GAPDH*_F and *MT-RNR2*_R primers was performed to confirm the construction of the intermediate fragment.

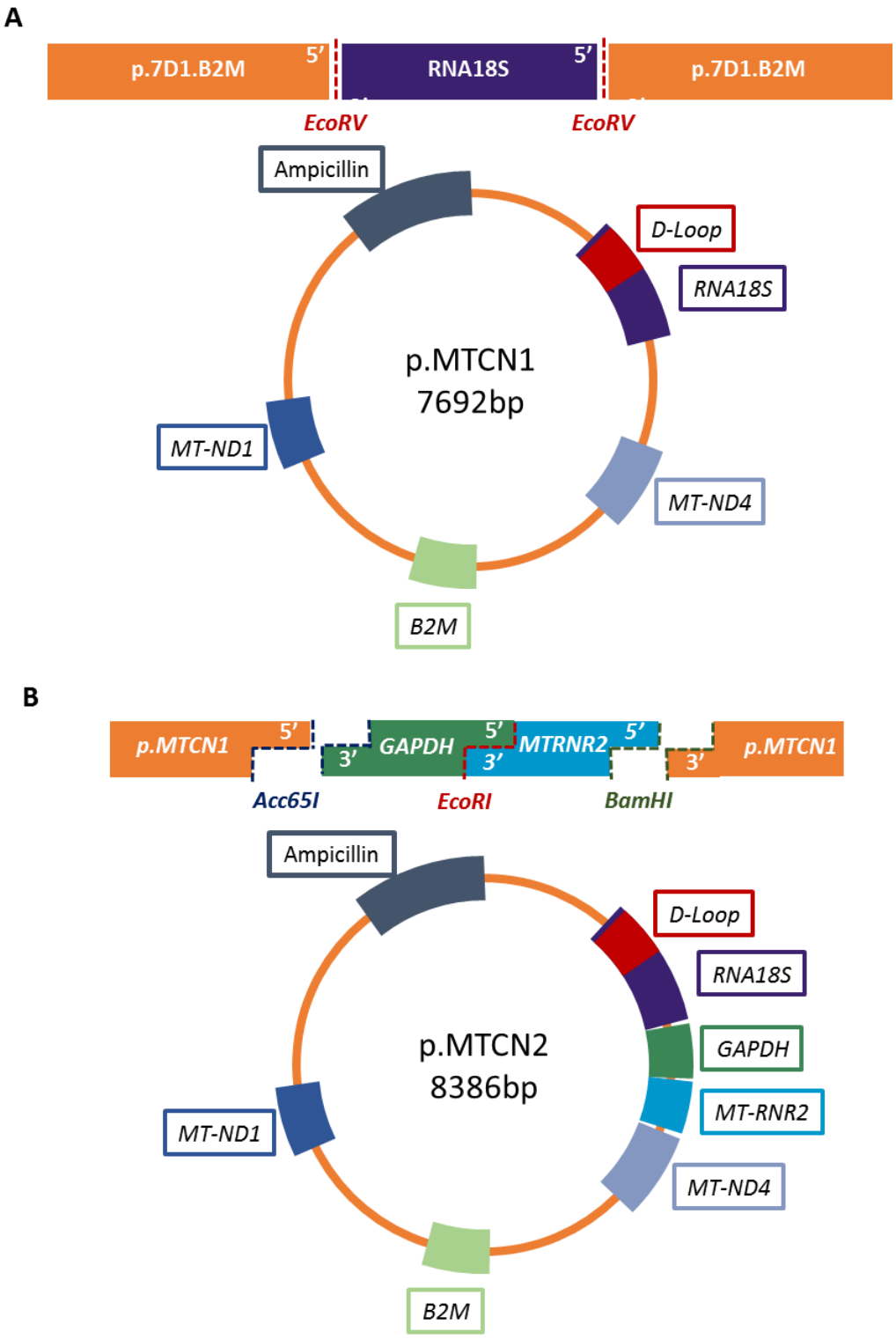

Figure 6.1: Construction of plasmid p.MTCN2. (A) Locus of *RNA18S5* gene was inserted into plasmid p.7D1.B2M by blunt-ended ligation using *EcoR*V to create plasmid p.MTCN1. (B) An intermediate fragment constructed of *GAPDH* and *MT-RNR2* loci was inserted into plasmid p.MTCN1 using *Acc65*I and *BamH*I restriction sites.

Primer	Location	RE	Sequence
*GAPDH*_F	nt.6264-6282	*Acc65*I	5'-CT***GGTACC***CCTTCTCCCCATTCCGTCTT-3'
*GAPDH*_R	nt. 6563-6544	*EcoR*I	5'-AC***GAATTC***AGCCCACCCCTTCTCTAAGT-3'
*MT-RNR2*_F	nt.2835-2854*	*EcoR*I	5'-AG***GAATTC***CCAACCTCCGAGCAGTACAT-3'
*MT-RNR2*_R	nt.3092-3072*	*BamH*I	*5'*-AT***GGATCC***ACCTGGATTACTCCGGTCTGA-3'

Table 6.2: Primers for amplification of *GAPDH* and *MT-RNR2* target loci. GenBank accession numbers: *GAPDH* = NG_007073.2, *MT-RNR2* = NC_012920.1; nt=nucleotide position (*Revised Cambridge Reference Sequence (rCRS)); F= forward; R=reverse;; RE = restriction endonuclease. RE sites introduced using primers are underlined in the sequences.

The intermediate fragment and plasmid p.MTCN1 underwent a double digest with *Acc65*I and *BamH*I (Figure 6.1B). The reaction mixture was incubated at 37°C for one hour before heating to 65°C for 20 minutes to inactivate *Acc65*I. Subsequent DNA clean-up removed *BamH*I. Insert and vector DNA were quantified for ligation with T4 ligase, as previously described (section 2.10.5) to produce plasmid pMTCN2.

Transformation of competent JM109 cells and subsequent culture of bacterial cells was carried out as described in section 2.10.7. Confirmation of the insertion of *GAPDH* and *MT-RNR2* gene loci was provided by PCR and Sanger sequencing protocols (section 2.10.9). A glycerol stock was prepared for long-term storage of p.MTCN2. For more immediate use, DNA was extracted from bacterial cultures using Qiagen Miniprep kit, and stored in 5µl aliquots at -20°C

6.3.3 Real-time PCR

The standard method for determining total mtDNA copy number is discussed in section 2.8.4. Briefly, the assay consists of two singleplex reactions for MT-ND1 and *β2M*. For the *MT-ND1* assay, 5µl of sample DNA is added to 15µl of mastermix, consisting of 300nM *MT-ND1* forward and reverse primers, 100nM *MT-ND1* probe, 10µl TaqMan Universal Mastermix and 3.4µl dH_2O (to make up to volume). The same mastermix is used for the *β2M* reaction, but with the addition of 3mM MgCl2. Sample DNA was diluted to the specified concentration for *β2M* and *GAPDH* reactions, and then diluted 100-fold for *MT-ND1*, *MT-RNR2* and *RNA18S* reactions. Real-time PCR was carried out under cycling conditions: 50°C for two minutes (one

cycle); 95°C for 10 minutes (one cycle); 95°C for 15 seconds and 60°C for one minute (40 cycles).

This study presents an alternative method using an *RNA18S* assay in addition to the *ß2M* and *MT-ND1* assays commonly used. Optimisation of this protocol is described throughout this chapter. Standard conditions referred to in this chapter are as described for the *MT-ND1* assay above. A four-point standard curve consisting of a 10-fold serial dilution of plasmid p.MTCN1, unless otherwise stated, was loaded in triplicate onto each plate. Sample DNA was also loaded in triplicate.

Primers and probes for the various targets featured are shown in Table 6.3 and Table 6.4, respectively. *ß2M* and *MT-ND1* primer/probe sets were previously designed and optimised for their respective assays (He *et al.,* 2002; Grady *et al*., 2014). The design of primers and probes for additional targets, such as *RNA18S*, *GAPDH* and *MT-RNR2*, was carried out using Primer Express® (Applied Biosystems). Primer pairs were selected based on their Tm (melting temperature), %GC content (between 40-60%) and length, while also avoiding any internal secondary structures. Suggested primer/probe combinations were screened for suitability using the online tool SNPCheck3 (last accessed 03/12/16) to confirm specificity and verify that no SNPs were present in the primer and probe binding regions.

Target	F/R	Position	Sequence	Tm (°C)	Length (nt)	%GC	Annealing (°C)	Amplicon length (nt)
MT-RNR2	F	nt.2941-2964*	5'- GCGCAATCCTATTCTAGAGTCCAT-3'	57.5	24	46	52.8	32
	R	nt.3015-2996*	5'- ACCATCGGGATGTCCTGATC-3'	57.6	20	55		
RNA18S	F	nt.110026- 110047	5'-GCCGCTAGAGGTGAAATTCTTG-3'	57.3	22	50	48.7	24
	R	nt.110091-110071	5'-CATTCTTGGCAAATGCTTTCG-3'	53.7	21	43		
β2M	F	nt.8969-8990	5'-CCAGCAGAGAATGGAAAGTCAA -3'	55.8	22	45	53.5	68
	R	nt.9064-9037	5'-TCTCTCTCCATTCTTCAGTAAGTCAACT-3'	57.4	28	40		
GAPDH	F	nt.6385- 6405	5'- CCCCACACACATGCACTTACC-3'	59.6	21	57	50.8	37
	R	nt.6462- 6442	5'- TTGCCAAGTTGCCTGTCCTT-3'	58.2	20	50		
MT-ND1	F	nt.3485-3504*	5'-CCCTAAAACCCGCCACATCT-3'	58.5	20	55	53.2	28
	R	nt.3553-3532*	5'-GAGCGATGGTGAGAGCTAAGGT-3'	60.0	22	55		

Table 6.3: Primers for real-time PCR copy number assays. GenBank accession numbers: *MT-RNR2*/*MT-ND1* = NC_012920.1; *RNA18S* = NT_167214.1 (GRCh38.p7); *β2M* = NG_012920.1; *GAPDH* = NG_007073.2; F=forward primer; R=reverse primer; nt=nucleotide position (*rCRS); Tm=melting temperature.

Target	Position	Sequence	5'- Dye	Tm (°C)	Length (nt)	%GC
MT-RNR2	nt.2966-2987*	5'-TCAACAATAGGGTTTACGACCT-3'	VIC	52.6	22	41
RNA18S	nt.110050-110069	5'-CCGGCGCAAGACGGACCAGA-3'	NED	65.5	20	70
β2M	nt.9006-9032	5'-ATGTGTCTGGGTTTCATCCATCCGACA-3'	FAM	61.7	27	48
GAPDH	nt. 6420-6437	5'-TGATTTCTGGAAAAGAGC-3'	FAM	45.7	18	39
MT-ND1	nt.3506-3529*	5'-CCATCACCCTCTACATCACCGCCC-3'	VIC	64.2	24	62.5

Table 6.4: Fluorogenic probes for real-time PCR copy number assays.
GenBank accession numbers: *MT-RNR2*/*MT-ND1* = NC_012920.1; *RNA18S* = NT_167214.1 (GRCh38.p7); *β2M* = NC_000015.10; *GAPDH* = NG_007073.2; nt=nucleotide position (*rCRS); Tm=melting temperature.

A number of characteristics were assessed to determine whether the optimisation condition was successful. First, the reaction efficiency was calculated using the standard curve. If the reaction is running at 100% efficiency, the sample DNA doubles with every cycle, equating to a difference of 3.33 Cq between 10-fold serially diluted samples. Reaction efficiencies ranging from 90-110% were considered within the acceptable range for these optimisation experiments. Second, the shape of the amplification curves was used to indicate the successful target amplification. The curve consists of a baseline region, exponential phase and a plateau, as shown in Figure 6.2. Abnormal curves can indicate a number of experimental errors, ranging from pipetting errors, incorrect primer/probe concentrations and poor instrument calibration. In the following optimisation experiments, amplification curves were also used to evaluate the efficiency of reactions in patient or control samples. This was done by visual comparison of the exponential phase gradient in sample profiles against that of the standard curve.

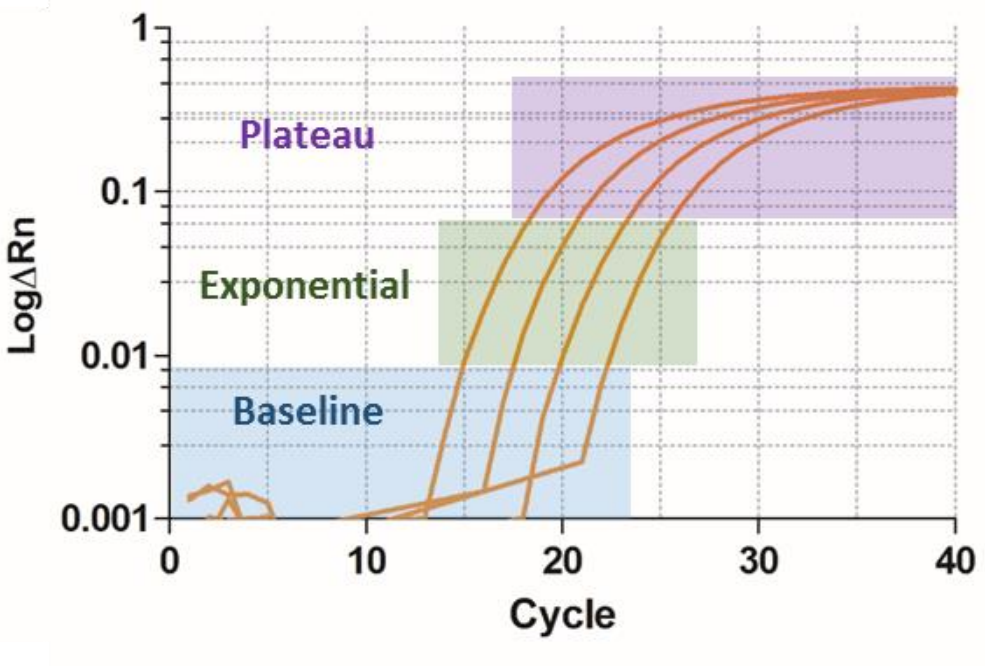

Figure 6.2: Real-time PCR amplification curve. LogΔRN (log of relative fluorescence units) quantifies the fluorescent signal emitted by a sample (orange) over 40 cycles of amplification by real-time PCR. There are three distinct phases to the amplification curve; baseline (blue), exponential growth (green) and plateau (purple).

6.4 Results

6.4.1 Optimisation of RNA18S singleplex assay

Optimisation of the singleplex *RNA18S* real-time PCR assay was performed using a standard curve to evaluate reaction efficiency. The standard protocol (section 6.3.3) was performed with increasing concentrations of *RNA18S* forward and reverse primers: 50nM, 300nM, 600nM and 900nM. All reactions were carried out on the same plate. The amplification graphs for these reactions (Figure 6.3A) were of a good shape with well-defined exponential phases. The most efficient reactions were seen with *RNA18S* primer concentrations of 300nM and 600nM (Table 6.5). An increase in sample Cq was noted between the reactions containing 300nM and 50nM primer, indicating 300nM was the minimum concentration of primer required for the amplification of the *RNA18S* target in a singleplex reaction.

Primer concentration	50nM	300nM	600nM	900nM
Reaction efficiency	90%	96%	96%	95%
S1 Cq	17.93	16.27	16.10	16.10
S2 Cq	20.52	18.66	18.57	18.69
S3 Cq	22.97	21.08	21.11	20.95
S4 Cq	25.46	23.46	23.23	23.40

Table 6.5: Optimisation of RNA18S singleplex assay primer concentrations.
S1-4=standard curve samples 1-4 of a 10-fold serial dilution; Cq=cycle quantification:

In future applications, *RNA18S* would ideally be measured in a multiplex reaction with *β2M*. The *β2M* singleplex assay requires the addition of 3mM $MgCl_2$ to improve reaction efficiency. In order to determine whether the addition of $MgCl_2$ affected the efficiency of the reaction in the *RNA18S* singleplex assay, a four-point standard curve was loaded in triplicate into mastermixes containing 300nM *RNA18S* primers (as determined above) with either 0mM or 3mM $MgCl_2$. The addition of $MgCl_2$ to the reaction reduced the peak fluorescence (logΔRN) of the amplification curve (Figure 6.3B) and caused a slight decrease in reaction efficiency across the standard curve. The difference in sample Cq between conditions is minimal, so the addition of $MgCl_2$ to this reaction can be tolerated (Table 6.6).

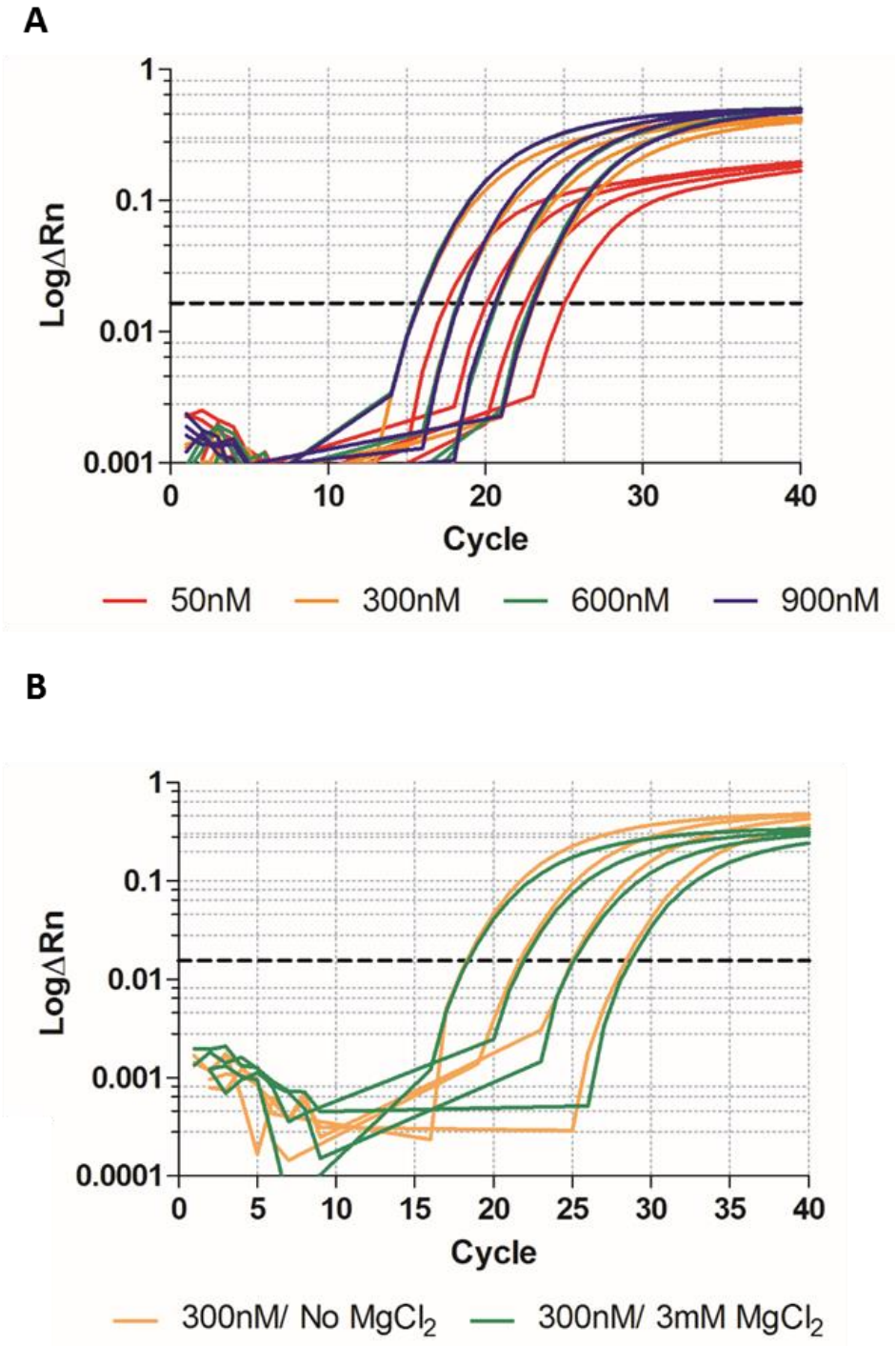

Figure 6.3: Amplification curves for *RNA18S* target for singleplex assay optimisation. (A) Primer concentrations of 50nM (red), 300nM (yellow), 600nM (green) and 900nM (blue) were each tested with the same standard curve. (B) With primer concentration at 300nM, the standard curve was loaded in the absence of $MgCl_2$ (yellow) or with 3mM $MgCl_2$ (green). The black dotted line indicates the automatic threshold level for the determination of sample Cq.

$MgCl_2$ concentration	0mM	3mM
Reaction efficiency	98%	96%
S1 Cq	15.49	15.63
S2 Cq	18.11	18.26
S3 Cq	20.44	20.52
S4 Cq	22.65	22.81

Table 6.6: Optimisation of $MgCl_2$ concentration in *RNA18S* singleplex assay.
S1-4=standard curve samples 1-4 of a 10-fold serial dilution; Cq=cycle quantification:

6.4.2 Optimisation of RNA18S/β2M multiplex assay

The composition of the mastermix for the multiplex reaction was based on that used for the individual singleplex reactions. 5µl standard curve DNA was added to 15µl mastermix containing 300nM forward and reverse primers for *RNA18S* and *β2M* , 10µl TaqMan Universal Mastermix , 3mM $MgCl_2$ and 100nM probes, made up to volume with dH_2O. This reaction was carried out alongside the *RNA18S* and *β2M* singleplex reactions on the same plate, using the same standard curve DNA for comparison.

The height of the amplification curve is commonly affected by multiplexing a target, usually appearing lower than is seen in the singleplex reaction. This was evident in both the *RNA18S* and *β2M* reactions (Figure 6.4). Although the efficiencies of the multiplex reaction were improved for both targets, the change in Cqs for the standard curve points was particularly evident in the B2M reactions (Table 6.7).

Target	***RNA18S***		***β2M***	
Reaction type	Singleplex	Multiplex	Singleplex	Multiplex
Reaction efficiency	96%	99%	91%	99%
S1 Cq	18.92	18.25	21.50	17.25
S2 Cq	22.34	21.61	24.80	20.77
S3 Cq	25.47	25.16	27.96	24.52
S4 Cq	29.06	28.46	31.63	27.86

Table 6.7: Comparison of singleplex and multiplex assays for RNA18S and β2M targets.
S1-4=standard curve samples 1-4 of a 10-fold serial dilution; Cq=cycle quantification

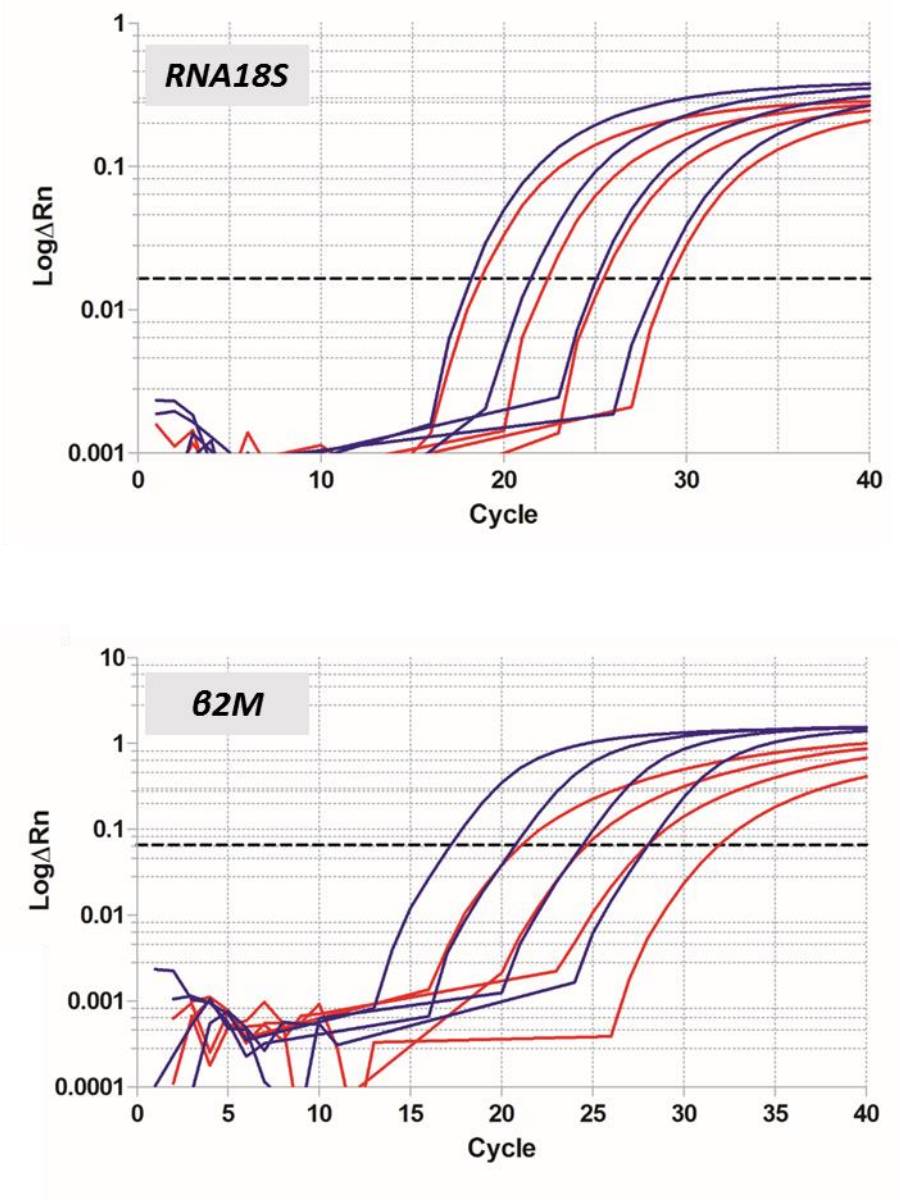

Figure 6.4: Comparison of amplification curves from *RNA18S* and *β2M* singleplex and multiplex reactions. Amplification curves for *RNA18S* (top) and *β2M* (bottom) targets in singleplex (red) and multiplex (blue) assays. The black dotted line indicates the threshold level set for the individual singleplex assays.

In order to further optimise the multiplex reactions, a number of different primer concentrations were tested for each target, using a three-point standard curve to determine reaction efficiency (Figure 6.5). Increasing *β2M* primer concentration to 600nM, with *RNA18S* primers kept at 300nM, did not allow the *β2M* reaction to plateau before the 40 cycle limit. The same was observed when primer concentrations were reversed (Figure 6.5B-C). Increasing the concentration of both sets of primers to 600nM caused poor amplification of the *β2M* target such that the reaction efficiency could not be determined (Figure 6.5D). Extreme primer concentrations of 900nM *β2M* alongside 100nM *RNA18S* compromised

amplification of *β2M*. Reversing these concentrations did allow for amplification of both targets, with good reaction efficiencies (Figure 6.5E-F).

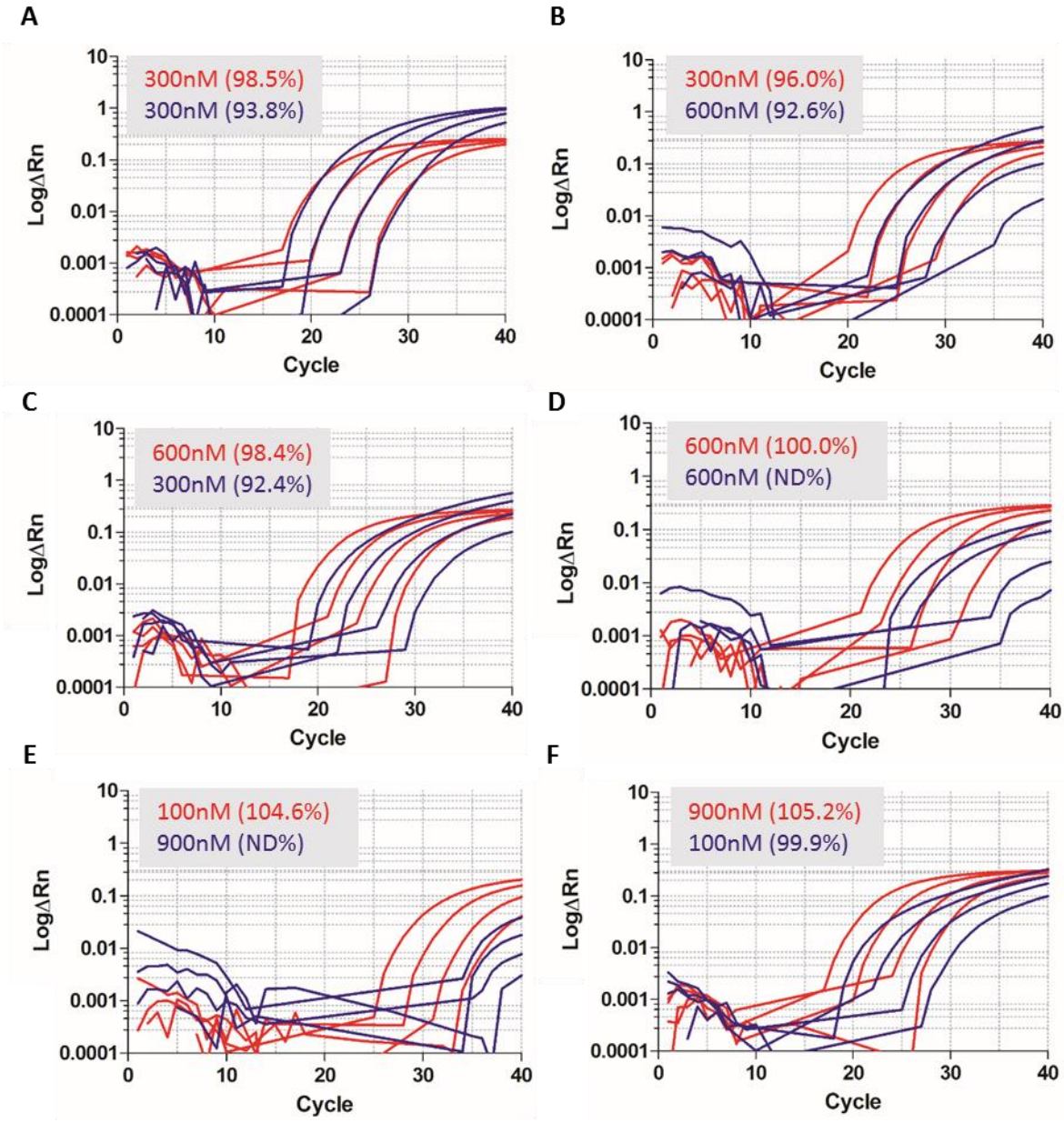

Figure 6.5: Optimisation of *RNA18S* and *β2M* primer concentrations for multiplex assay. Amplification curves for *RNA18S* (red) and *β2M* (blue) for each set of primer combinations tested on a four-point standard curve. Reaction efficiencies for each target are shown alongside the primer concentrations (grey boxes). ND% (not determined) is attributed when *β2M* is not sufficiently amplified to allow calculation of the reaction efficiency.

The concentration of $MgCl_2$ in the mastermix can impact the efficiency with which a target is amplified so, using primer concentrations of 100nM *β2M* and 900nM *RNA18S*, a range of $MgCl_2$ concentrations were tested (Figure 6.6A-E) to see if *β2M* reaction efficiency improved. Increasing $MgCl_2$ concentration to 5mM resulted in no amplification of B2M. Gradually reducing $MgCl_2$ in the mastermix, however, improved the reaction efficiency and amplification curves of the *β2M* and *RNA18S* reactions. Completely removing $MgCl_2$ proved to be optimal for both targets.

Using such a high concentration of *RNA18S* (900nM) may not prove cost-effective with future use of the assay and so the standard primer concentrations of 300nM (for both targets) were tried without $MgCl_2$ in the mastermix (Figure 6.6F). In this case, the reaction efficiencies improved again, and so the mastermix used for further optimisation experiments contained 300nM primers and 0mM $MgCl_2$ in addition to the standard Taqman Universal Mastermix and probe concentrations.

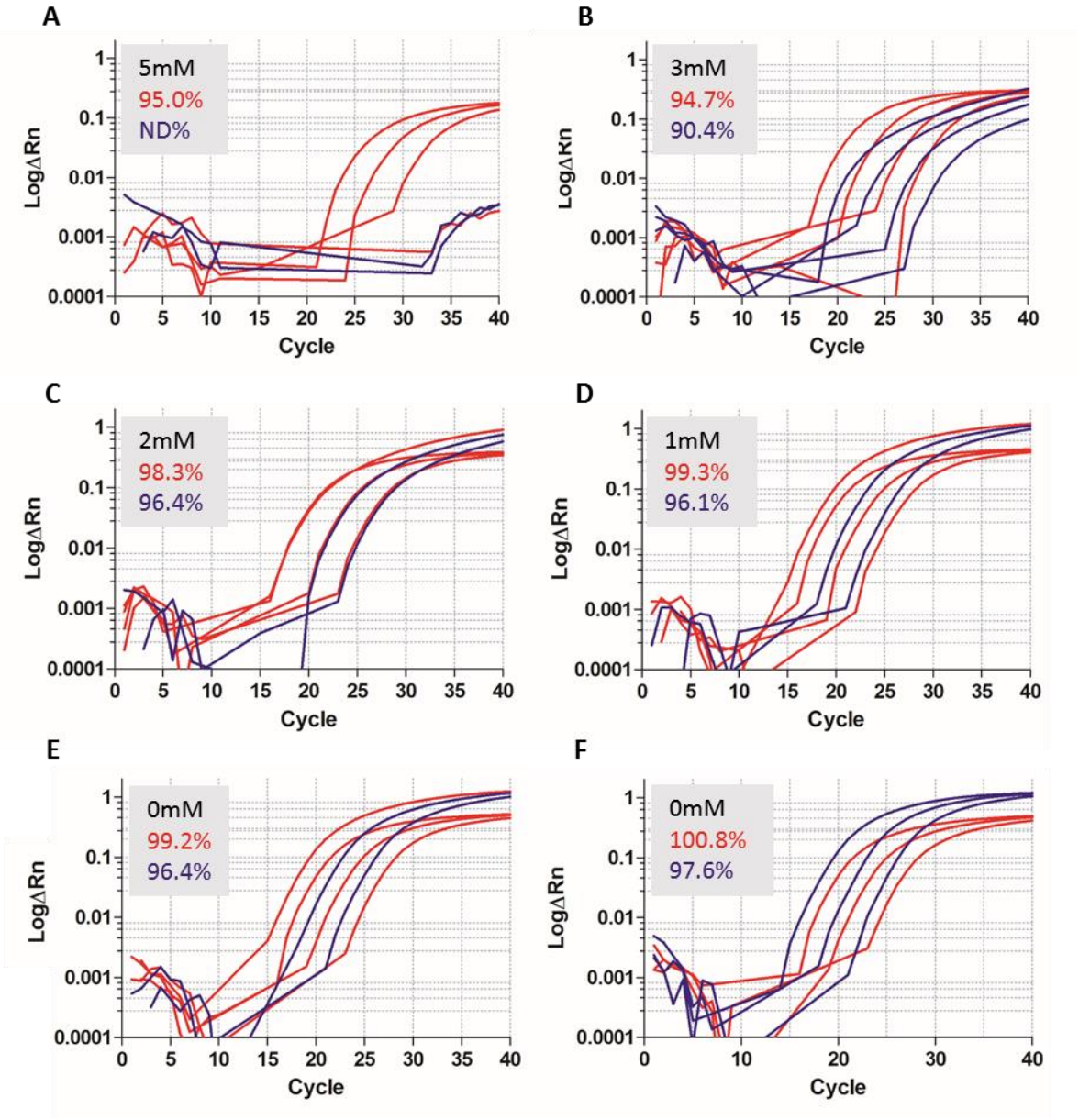

Figure 6.6: Optimisation of $MgCl_2$ concentration for multiplex assay. Amplification curves for *RNA18S* (red) and *β2M* (blue) for $MgCl_2$ concentrations (A) 5mM, (B) 3mM, (C) 2mM, (D) 1mM (E) 0mM, with 900nM *RNA18S* primers and 100nM *β2M* primers tested on a four-point standard curve. (F) 0mM $MgCl_2$ concentration with 300nM *RNA18S* and *β2M* primers tested on a three-point standard curve. Reaction efficiencies for each target are shown alongside the $MgCl_2$ concentrations (grey boxes). ND% is attributed when *β2M* is not sufficiently amplified to allow calculation of the reaction efficiency. Standard curve points were removed from A, C, D and E due to insufficient amplification of the target gene.

6.4.3 RNA18S/β2M multiplex reaction with samples

The optimised multiplex reaction was first tested using patient neutrophil DNA. A five-point standard curve was loaded alongside five patient DNA samples (1ng/µl concentration), each in triplicate on the same plate. 5µl DNA were added to 15µl optimised mastermix described above. The *RNA18S* and *β2M* singleplex reactions were carried out on a different plate using the same standard curve and sample DNA for comparison.

Reaction efficiencies for the amplification of both targets, as determined by the standard curve, were slightly lowered in the multiplex reaction. There was minimal change to sample and standard curve Cqs between singleplex and multiplex reactions. The ratio of *RNA18S: β2M* (Table 6.8) was slightly higher for the multiplex reaction than for the singleplex reaction, in most cases.

Target	***RNA18S***		***β2M***		**Ratio *RNA18S*: *β2M***		
Reaction	Single	Multi	Single	Multi	Single	Multi	Change
Efficiency	100.1%	99.7%	97.5%	95.6%	-	-	-
P1 Cq	25.70	25.66	30.50	30.25	24.19	23.88	0.31 (1.3%)
P2 Cq	25.44	25.24	29.44	29.36	14.15	17.32	-3.17 (22.4%)
P3 Cq	25.47	25.35	30.32	30.28	25.07	30.18	-5.11 (20.4%)
P4 Cq	26.12	26.04	30.98	30.84	24.92	27.45	-2.53 (10.2%)
P5 Cq	24.87	24.90	30.04	30.08	31.53	36.03	-4.5 (14.3%)

Table 6.8: Singleplex and multiplex assays for *RNA18S* and *β2M* using patient neutrophils. Reaction efficiency is calculated using the standard curve. Change to *RNA18S: β2M* was calculated as singleplex Cq-mulitplex Cq. Percentage change is shown in brackets. P1-P5 = patient 1-5; Cq =cycle quantification; single=singleplex reaction; multi=multiplex reaction

Upon further inspection, it was apparent that the *β2M* target in the sample DNA was being amplified with a lower efficiency than that of the standard curve, as indicated by the exponential phase gradient on the amplification curves (Figure 6.7). Sample Cq and the Cq of a standard curve point were measured at the automatic threshold level, and the difference between them calculated (ΔSCq1 value). The same was done at an alternative threshold level (ΔSCq2 value). When sample and standard curve targets are amplified with the same efficiency, the difference between ΔSCq1 and ΔSCq2 (ΔΔSCq) is small, increasing when efficiencies become dissimilar (Table 6.9). As the threshold level is automatically set for each plate to account for any background signal present, inter-plate variability in the measurement of *β2M* copy number would be greatly increased.

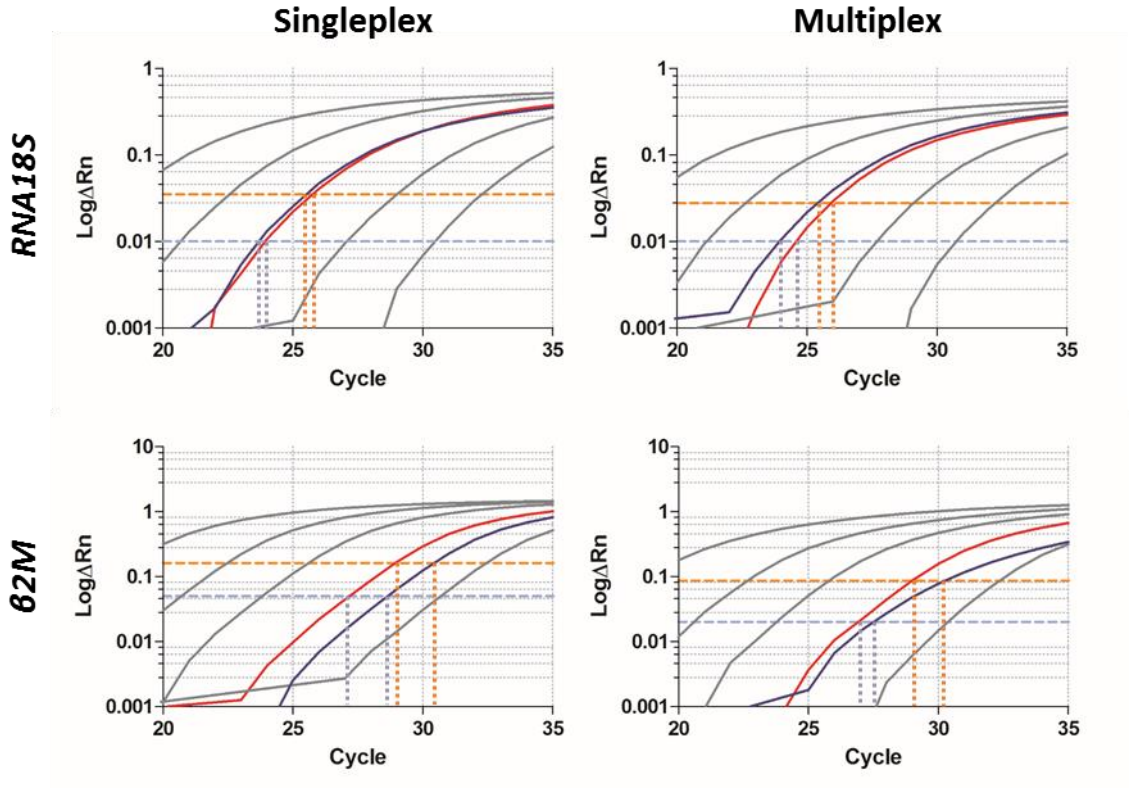

.

Figure 6.7: Amplification efficiency of the *β2M* target is altered by the multiplex assay in patient blood samples. Amplification curves are shown for *RNA18S* and *β2M* reactions in a patient blood sample (P3). Standard curve points are coloured grey, with the nearest point to the patient (blue) sample shown in red. Cq values are indicated for the patient sample and nearest standard curve point at the automatic (orange, ΔSCq1) and alternative (light blue, ΔSCq2) threshold levels.

Sample	*β2M* ΔΔSCq		*RNA18S* ΔΔSCq	
	Singleplex	Multiplex	Singleplex	Multiplex
P1	0.00	3.99	0.01	0.07
P2	0.09	3.86	0.01	0.05
P3	0.04	4.06	0.01	0.05
P4	0.01	4.05	0.02	0.02
P5	0.03	0.93	0.01	0.01

Table 6.9: ΔΔSCq values for *β2M* and *RNA18S* targets in single- and multiplex reactions using patient neutrophils. ΔΔSCq is calculated as ΔSCq1 (automatic threshold) - ΔSCq2 (alternative threshold)

The compromise in *β2M* reaction efficiency in patient samples relative to the plasmid DNA could be due to a common artefact of the multiplexing process which occurs when one target is more abundant than another within a sample. When initially optimising the

reaction, a serial dilution of p.MTCN1 was used, which contained the *RNA18S* and *β2M* targets in a 1:1 ratio and so both could be amplified with equal efficiency. In patient sample DNA however, the ratio of *β2M* to *RNA18S* is estimated at 1:200 copies per nuclear genome. The greater abundance of the *RNA18S* gene in the sample DNA results in this target being more readily amplified early on, consuming the dNTPs and saturating the Taq polymerase. This effectively starves the *β2M* assay of reagents and suppresses the amplification of the *β2M* target, explaining the reduced reaction efficiency seen for this target in this experiment.

In light of this primer concentrations were re-optimised, as limiting the concentration of primers for the more abundant target (*RNA18S*) causes this reaction to plateau earlier, leaving adequate reagents for the amplification of the other target (*β2M*). DNA extracted from human skeletal muscle was diluted to 1ng/µl and loaded in triplicate alongside a five-point standard curve. While maintaining the *β2M* primer concentration at 300nM, the *RNA18S* primer concentrations were reduced to 100nM and 50nM (Figure 6.8A). The lower *RNA18S* primer concentrations did improve the efficiency of the *β2M* amplification, as measured using the standard curve. This does not appear to compromise the efficiency of the *RNA18S* amplification (Table 6.10). Both these *RNA18S* primer concentrations were then tested with increased levels of Taqman added to the mastermix (Figure 6.8B). The optimum conditions were 100nM *RNA18S* primer concentration with 12.5µl Taqman based on the reaction efficiencies for both targets.

Conditions	Reaction efficiency %	
	RNA18S	***β2M***
Primer limiting		
RNA18S 300nM	97.9%	94.7%
RNA18S 100nM	98.5%	98.8%
RNA18S 50nM	100.1%	101.4%
TaqMan Universal Mastermix		
RNA18S 100nM/ 12.5µl TaqMan	100.1%	98.5%
RNA18S 50nM/ 12.5µl TaqMan	96.6%	100.5%
RNA18S 100nM/ 15µl TaqMan	102.5%	98.9%
RNA18S 50nM/ 15µl TaqMan	115.1%	102.7%

Table 6.10: Optimisation of multiplex assay by primer limiting and altered TaqMan Mastermix concentration. Reaction efficiency was calculated using the standard curve for each set of conditions.

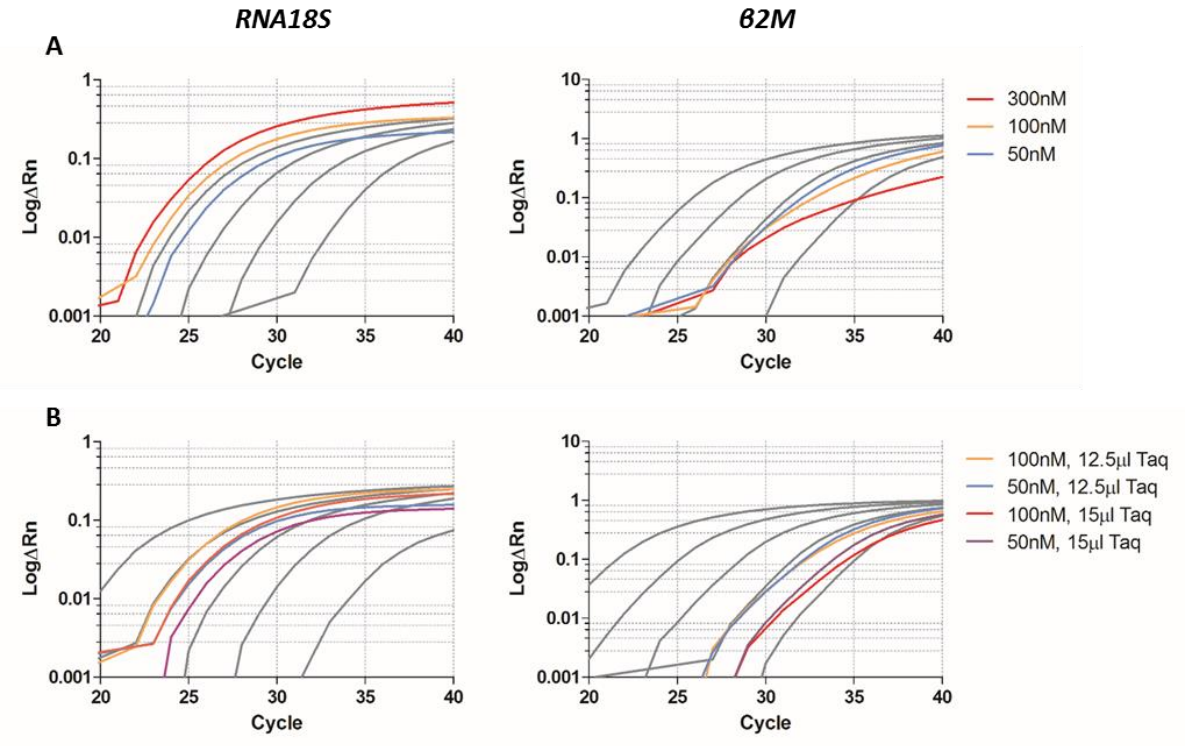

Figure 6.8: Amplification curves for primer limiting and TaqMan concentration optimisation of the multiplex assay. Amplification curves for *RNA18S* (left) and *β2M* (right) targets in the multiplex assay. (A) *RNA18S* primer limiting to 300nM (red), 100nM (yellow) and 50nM (blue), while *β2M* primer concentration was maintained at 300nM. (B) Increased TaqMan Universal Mastermix added to reactions with 100nM *RNA18S* primers (12.5µl = yellow, 15µl = red) or 50nM *RNA18S* primers (12.5µl = blue, 15µl = purple). A representative standard curve is shown in grey (average across conditions for (A) and (B) separately).

6.4.4 Verifying sample DNA concentration

Thus far, DNA samples obtained from whole blood and skeletal muscle homogenates have been used in the optimisation of the *RNA18S*/*β2M* multiplex assay. Although they have not been assessed under the same reaction conditions, the different tissues indicated very different ratios of *RNA18S:β2M* (Table 6.11).

Tissue type	*RNA18S:β2M*
Blood (P1)	23.88
Blood (P2)	17.32
Blood (P3)	30.18
Blood (P4)	27.45
Blood (P5)	36.03
Skeletal muscle (P6)	107.1

Table 6.11: Ratio of *RNA18S:β2M* calculated from tissues used in optimisation experiments. P1-6 = patient 1-6 used thus far in experiments for the optimisation of the multiplex assay.

In order to determine whether this was an artefact of the various reaction conditions, the optimised multiplex reaction (section 6.4.3) was performed using DNA extracted from neutrophils, white blood cells, whole blood homogenate, skeletal muscle and brain (occipital lobe), each collected from a different individual. DNA samples were diluted to 10ng/µl, 5ng/µl, 2ng/µl and 1ng/µl to evaluate the effect of altering DNA concentration on reaction efficiency and to determine the optimum concentration for DNA samples in future experiments.

The ratio of *RNA18S*:*β2M* in each sample is shown in Table 6.12. Fairly low variance was observed for the whole blood homogenate and neutrophil DNA samples across different concentrations. In the white blood cell sample, there was a progressive decline in *RNA18S:β2M* ratio with reduced DNA concentration. Although SKM and brain samples showed relatively high variance, the ratios at the highest and lowest sample concentrations are very similar and so this is likely a result of pipetting error or sample handling. There was no consistent evidence that the DNA concentration affected the RNA18S:β2M ratio as the final outcome of this reaction.

Sample	Concentration				Mean (SEM)	CoV (%)
	10ng/µl	5 ng/µl	2 ng/µl	1 ng/µl		
Whole blood	23.9	23.4	23.0	22.9	23.3 (±0.2)	2.03
Neutrophils	16.0	15.9	16.0	16.2	16.0 (±0.3)	0.82
White blood cells	17.6	16.7	15.4	14.4	16.0 (±0.7)	8.87
SKM	115.6	105.4	101.9	115.2	109.5 (±3.5)	6.35
Brain	67.9	61.4	73.6	69.4	68.1 (±02.5)	7.44

Table 6.12: *RNA18S:ß2M* ratio in patient samples at different concentrations. The mean ratio was calculated across three sample replicates. SEM=standard error of the mean. CoV=coefficient of variance (shown as a percentage).

The ratio of *RNA18S*: *ß2M* was varied between different tissue samples, with relatively low levels seen in the various blood fractions compared to skeletal muscle and brain, as seen in previous optimisation experiments. To verify these results further, singleplex *RNA18S* and *ß2M* assays were conducted using the same standard curve and DNA samples as the previous multiplex reaction. Sample DNA was diluted to a 2ng/µl to minimise depletion of precious patient samples.

The ratio of *RNA18S*: *ß2M* as determined by singleplex assays for these targets is quite dissimilar to that calculated using the multiplex reaction (Table 6.13). Using both assays, a much lower ratio was seen in the blood samples compared to the brain and skeletal muscle. As there is very little published data on *RNA18S* copy number in human tissues it is difficult to conclude that these results reflect a genuine tissue-specific distribution of the gene. These samples are not from the same individual and so it seems more likely that the variation between tissues is attributable to the different nuclear backgrounds of the patients.

Sample	Ratio *RNA18S*: *ß2M*		
	Singleplex	Multiplex	Difference
Whole blood	17.7	23.0	5.3 (29.9%)
Neutrophils	12.0	16.0	4.0 (33.3%)
White blood cells	9.5	15.4	5.9 (62.11%)
SKM	112.4	101.9	-16.5 (9.3%)
Brain	41.2	73.6	32.4 (78.6%)

Table 6.13: Ratio of *RNA18S: ß2M* calculated by singleplex and multiplex assays. Ratios shown are means calculated from three sample replicates.

The gradient of the exponential phase of *RNA18S* and *β2M* amplification curves again indicated that multiplexing the assays impacted the amplification efficiency of targets in the sample DNA, particularly *β2M*. Figure 6.9 shows portions of the amplification profiles for the *β2M* target recorded for whole blood homogenate (A), skeletal muscle (B) and brain (C) samples using the singleplex and multiplex assays. ΔΔSCq was calculated as explained previously. Table 6.14 shows relatively low ΔΔSCq for the singleplex reactions. However, an increase in ΔΔSCq was seen when targets were measured using the multiplex assay, suggesting sample DNA was amplified with less efficiency than standard curve DNA in these reactions. This was particularly evident for the *β2M* target. Furthermore, each tissue was affected to a different degree indicating that the multiplex reaction would require different conditions, optimised for individual tissue types. It was therefore decided that *RNA18S* and *β2M* singleplex assays would be used in future experiments to quantify these targets.

Sample	*β2M* ΔΔSCq		*RNA18S* ΔΔSCq	
	Singleplex	**Multiplex**	**Singleplex**	**Multiplex**
Whole blood	0.04	1.03	0.13	0.83
Skeletal muscle	0.01	1.21	0.06	0.85
Brain	0.11	1.11	0.12	0.73

Table 6.14: ΔΔSCq values for *β2M* and *RNA18S* targets in single- and multiplex reactions. ΔΔSCq is calculated as ΔSCq1- ΔSCq2

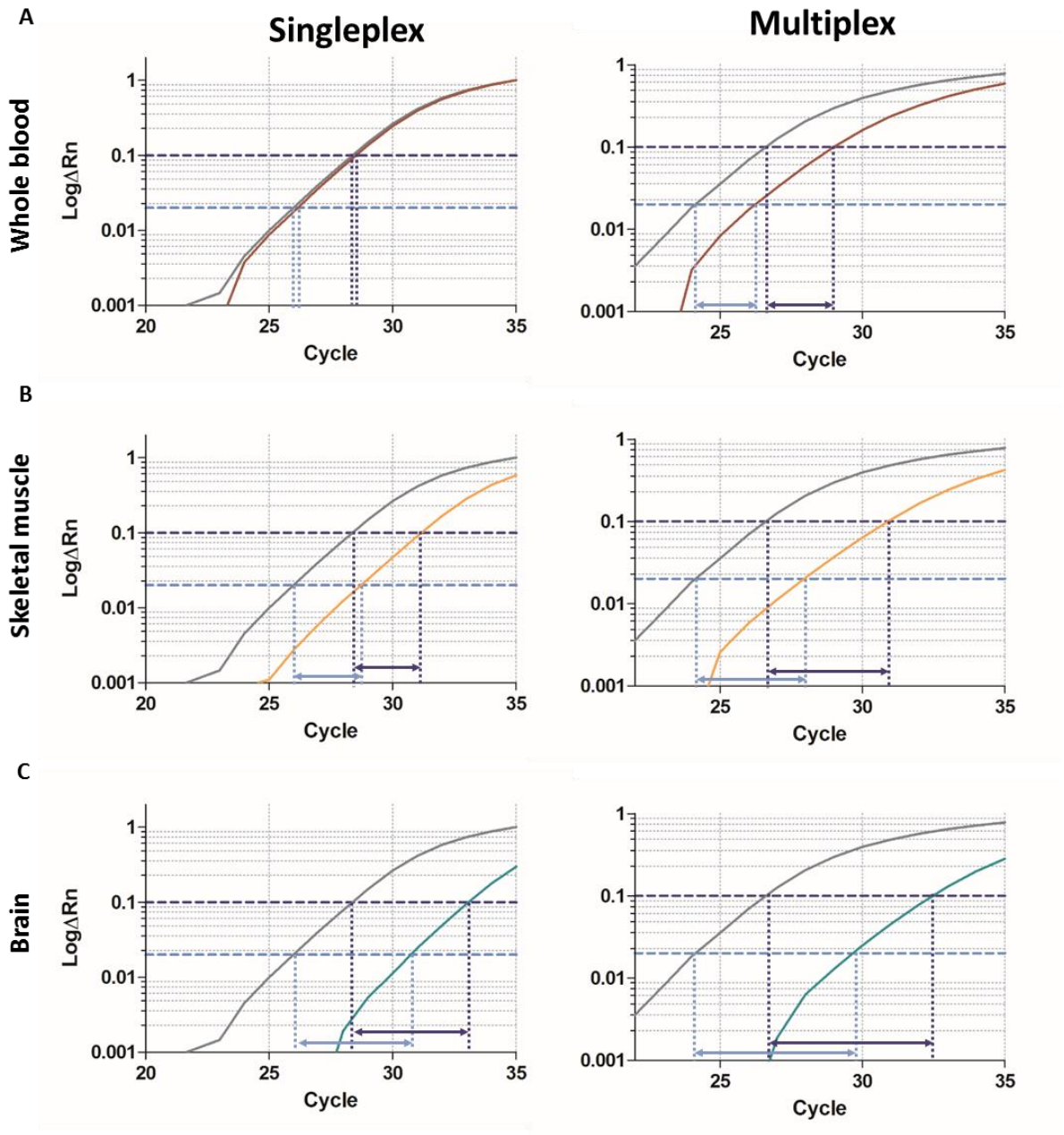

Figure 6.9: Inefficient amplification of the *β2M* target in multiple tissues using the multiplex reactions. A portion of the amplification curve for the *β2M* target in (A) whole blood homogenate, (B) skeletal muscle and (C) brain samples using singleplex (left) and multiplex (right) reactions. Difference in Cq between sample and standard, indicated by a double-headed arrow, was measured at the automatically assigned threshold level (light blue dotted line; ΔSCq1) and a higher threshold level (dark blue dotted line; ΔSCq2) set within the exponential phase of the amplification curve.

6.4.5 Measuring mtDNA copy number in multiple tissues from the same individual

A common observation throughout the optimisation process was the variation in *RNA18S*: *ß2M* copy number across different tissues. Although this was validated using singleplex and multiplex reactions for each target, DNA samples were not available for multiple tissues from the same individual. Therefore, this range in *RNA18S*: *ß2M* ratio could have been the result of sampling from different patients rather than a genuine difference between tissue types. To investigate this further, multiple tissues (whole blood, urinary epithelium, hair and buccal mucosa) were collected from six healthy controls (REC reference 12/NE/0395). DNA was extracted as described in section 2.7, quantified by Nanodrop and aliquoted for storage at -80°C until use. A five-point standard curve of p.MTCN2 was loaded alongside sample DNA in triplicate. Singleplex assays for *RNA18S*, *ß2M, MT-ND1, GAPDH* and *MT-RNR2* were performed on different plates, with three replicate plates for each target.

The ratio of *RNA18S*: *ß2M* was calculated for each sample using singleplex assays for these targets (Table 6.15). DNA extracts from hair samples were at very low concentrations and the *ß2M* target was often undetectable. Therefore results obtained from these samples were removed from the final analysis. Across the three remaining tissues, a significant difference in *RNA18S*:*ß2M* ratio was determined for all cases, except C6 (one-way ANOVA; $p<0.05$). *RNA18S*:*ß2M* ratio was consistently lower in whole blood homogenate than other tissues, with a mean of 22.8 compared to 127.8 for buccal and 475.0 for urine.

Control	Sample Type	*RNA18S:ß2M* ratio	
		Mean (±SEM)	CoV(%)
C1	Blood	17.7 (±0.66)	3.24
	Buccal	160.7 (±4.94)	1.83
	Urine	160.6 (±9.57)	2.96
C2	Blood	19.0 (±1.11)	5.96
	Buccal	153.2 (±8.95)	3.41
	Urine	162.2 (±14.78)	4.59
C3	Blood	32.8 (±1.25)	3.32
	Buccal	94.9 (±5.73)	3.25
	Urine	366.9 (±32.10)	3.67
C4	Blood	19.4 (±1.56)	7.89
	Buccal	110.8 (±5.54)	3.15
	Urine	564.1 (±12.62)	0.86
C5	Blood	14.3 (±0.47)	3.81
	Buccal	119.1 (±5.92)	3.29
	Urine	87.3 (±10.14)	7.87
C6	Blood	21.9 (±0.83)	3.60
	Buccal	144.8 (±8.76)	3.47
	Urine	342.5 (±85.19)	16.70

Table 6.15: *RNA18S:ß2M* ratio in multiple tissues from each control case. Mean *RNA18S:ß2M* with standard error (SEM) measured in whole blood homogenate, buccal mucosa and urinary epithelium from six controls (C1-C6). CoV% = coefficient of variance.

Conventionally, total mtDNA copy number is indicated by the ratio of *MT-ND1*: *β2M*. To evaluate total mtDNA copy number using the additional *RNA18S* marker, *MT-ND1:RNA18S* ratios were multiplied by *RNA18S: β2M* ratios (Table 6.16). Both methods for determining total mtDNA copy number provide very similar estimates. However, the *MT-ND1:RNA18S: β2M* ratio was associated with increased variability when compared to the *MT-ND1: β2M* ratio measured in the same sample. As this new assay requires an additional singleplex reaction, consuming reagents and samples, it does not seem cost-effective to employ this protocol when the standard method can produce almost identical results.

Control	Sample Type	*MT-ND1: β2M*		*MT-ND1:RNA18S: β2M*	
		Mean (±SEM)	CoV(%)	Mean (±SEM)	CoV(%)
C1	Blood	83.2 (±7.7)	5.9	87.1 (±24.4)	16.2
	Buccal	186.3 (±5.3)	1.6	184.5 (±5.3)	1.6
	Urine	327.2 (±39.7)	7.0	472.8 (±99.9)	13.1
C2	Blood	63.1 (±4.4)	5.1	64.9 (±5.3)	6.0
	Buccal	103.4 (±6.3)	3.8	101.9 (±9.8)	5.8
	Urine	163.7 (±31.1)	13.5	168.0 (±34.5)	13.8
C3	Blood	45.4 (±1.6)	2.9	45.2 (±2.3)	3.9
	Buccal	44.4 (±10.6)	44.3	124.0 (±50.7)	55.1
	Urine	4708.9 (±1504.9)	11.7	4767.8 (±1509.3)	11.3
C4	Blood	35.0 (±6.8)	24.8	46.0 (±8.4)	28.0
	Buccal	128.7 (±6.8)	3.4	141.0 (±12.5)	5.3
	Urine	4887.6 (±320.4)	2.5	5003.0 (±392.1)	3.0
C5	Blood	67.5 (±1.5)	1.6	67.8 (±3.0)	3.2
	Buccal	73.3 (±6.1)	6.5	82.0 (±8.2)	8.5
	Urine	1111.8 (±103.8)	4.2	1105.1 (±188.5)	7.7
C6	Blood	80.9 (±3.2)	2.6	80.9 (±4.1)	3.5
	Buccal	104.2 (±8.7)	5.5	113.6 (±12.1)	6.5
	Urine	337.7 (±90.8)	19.8	303.0 (±108.0)	26.9

Table 6.16: Total mtDNA copy number represented by *MT-ND1: β2M* and *MT-ND1:RNA18S: β2M* ratios. Mean ratios of *MT-ND1: β2M* and *MT-ND1:RNA18S: β2M,* with standard error (SEM), measured in whole blood homogenate, buccal mucosa and urinary epithelium from six controls (C1-C6). Assay variability is represented by the coefficient of variance (CoV%).

6.4.6 Validation of MT-ND1 and β2M as targets for mtDNA copy number quantification

Validation of the suitability of *MT-ND1* and *β2M* as targets in the determination of mtDNA copy number was assessed by comparison with *MT-RNR2* and *GAPDH* respectively. Singleplex assays for the additional targets were tested using the standard conditions described in section 6.3.3 to ensure efficient target amplification across three replicate plates. These conditions were deemed suitable for use in further experiments.

An estimate of total mtDNA copy number was obtained by calculating the *MT-ND1:β2M* and *MT-RNR2*:*GAPDH* ratios for each sample (Table 6.17). Although there is some discrepancy in the total mtDNA copy number indicated by these ratios, the difference is small in most control cases. However, C5 showed a large disparity in the two ratios.

Control	Sample Type	*MT-ND1:β2M*	*MT-RNR2*:*GAPDH*
C1	Blood	83.2 (±7.7)	77.3 (±4.7)
	Buccal	186.3 (±5.3)	180.9 (±9.2)
	Urine	327.2 (±39.7)	322.3 (±34.1)
C2	Blood	63.1 (±4.4)	41.4 (±10.8)
	Buccal	103.4 (±6.3)	101.0 (±5.6)
	Urine	163.7 (±31.1)	N/A
C3	Blood	45.4 (±1.6)	48.1 (±2.2)
	Buccal	44.4 (±10.6)	64.9 (±2.7)
	Urine	4708.9 (±1504.9)	5102.2 (±1628.8)
C4	Blood	35.0 (±6.8)	35.2 (±6.3)
	Buccal	128.7 (±6.8)	119.0 (±3.6)
	Urine	4887.6 (±320.4)	4688.5 (±306.3)
C5	Blood	67.5 (±1.5)	25.3 (±0.7)
	Buccal	73.3 (±6.1)	26.4 (±1.2)
	Urine	1111.8 (±103.8)	415.8 (±38.5)
C6	Blood	80.9 (±3.2)	73.6 (±4.0)
	Buccal	104.2 (±8.7)	93.2 (±7.0)
	Urine	337.7 (±90.8)	461.0 (±130.9)

Table 6.17: Calculation of total mtDNA copy number using alternative markers for the nuclear and mitochondrial genomes. Mean ratios of *MT-ND1:β2M* and *MT-RNR2:GAPDH* are shown with standard error (SEM) for whole blood homogenate, buccal mucosa and urinary epithelium from six controls (C1-6).

In order to investigate this further, the mitochondrial and nuclear markers were compared separately. The proportion of *β2M* to *GAPDH* in a sample should be equal, as the same number of copies are present within each nucleus. The average *GAPDH*:*β2M* ratio in most samples was similar to the expected ratio of one (Table 6.18). Similarly, the ratio of *MT-RNR2:MT-ND1* should be one, as both genes are present in one copy per wild-type mitochondrial genome. In most controls this was the case, with *MT-RNR2:MT-ND1*, however this ratio was dramatically lower in C5, reaching a mean of 0.38 across the three tissues (Table 6.18).

Control	Sample Type	*GAPDH:β2M*	*MT-RNR2:MT-ND1*
C1	Blood	1.18 (±0.04)	0.98 (±0.09)
	Buccal	1.52 (±0.06)	0.97 (±0.05)
	Urine	1.80 (±0.09)	0.86 (±0.11)
C2	Blood	1.34 (±0.08)	1.00 (±0.06)
	Buccal	1.68 (±0.09)	0.98 (±0.03)
	Urine	0.93 (±0.10)	1.21 (±N/A)
C3	Blood	1.11 (±0.04)	1.06 (±0.04)
	Buccal	0.99 (±0.18)	1.01 (±0.05)
	Urine	2.69 (±0.22)	1.09 (±0.03)
C4	Blood	1.44 (±0.10)	0.98 (±0.01)
	Buccal	1.17 (±0.03)	0.95 (±0.06)
	Urine	4.01 (±0.28)	0.96 (±0.02)
C5	Blood	1.14 (±0.03)	0.38 (±0.01)
	Buccal	1.41 (±0.03)	0.38 (±0.04)
	Urine	1.42 (±0.16)	0.38 (±0.03)
C6	Blood	1.35 (±0.05)	0.91 (±0.04)
	Buccal	1.48 (±0.09)	0.92 (±0.07)
	Urine	2.72 (±0.63)	1.11 (±0.28)

Table 6.18: Validation of *β2M* and *MT-ND1* as nuclear and mitochondrial DNA markers. The ratios of *GAPDH:β2M* and *MT-RNR2:MT-ND1* (mean and standard error (SEM)) for whole blood homogenate, buccal mucosa and urinary epithelium from six controls (C1-C6).

6.5 Discussion

This work aimed to optimise a new real-time PCR assay for the quantification of mtDNA copy number to be used with control and patient tissue samples. The current preferred protocol, using *MT-ND1* and *β2M* gene targets, is subject to high levels of inter-plate variability requiring several repeat plates and high sample concentrations to detect small changes in mtDNA copy number. The addition of *RNA18S* as a gene target in multiplex reactions with

MT-ND1 and *β2M* was suggested to reduce this variability and the associated usage of tissue and reagents. Once optimised, this protocol could be used to determine mtDNA copy number in future studies of multiple control and patient tissues.

6.5.1 Optimisation of RNA18S/β2M multiplex reaction required tissue-specific conditions

The multiplex *RNA18S*/ *β2M* reaction was optimised successfully for use with plasmid p.MTCN1. However, the addition of patient samples to the assay highlighted a problem with reaction efficiency due to the greater abundance of *RNA18S* relative to *β2M*. Whereas plasmid p.MTCN1 had only one copy of each gene, the targets could be amplified with equal efficiency. In human tissue samples, *RNA18S* copy number is 50-200 times that of *β2M* and so the preferential amplification of this target early in the multiplex reaction effectively starved the *β2M* assay of reagents, leading to less efficient amplification.
Throughout the optimisation process, DNA samples from human blood, skeletal muscle and brain were used. These indicated that *RNA18S*: *β2M* ratio was highly variable between tissue, which would require optimisation of the multiplex reaction for each tissue type. Given the range of human tissue samples intended for analysis by this assay, namely blood, skeletal muscle and urinary epithelium, this could prove costly.

In addition, there was no apparent benefit to including *RNA18S* as a target in a panel of singleplex reactions for the determination of mtDNA copy number. The ratio *of MT-ND1:RNA18S: β2M* was frequently shown to be more variable than that of *MT-ND1: β2M*. This is likely due to the additional singleplex reaction introducing plate variability, which could be reduced by multiplexing *MT-ND1/RNA18S* and *RNA18S/β2M*. As previously discussed, this is not a feasible option with concerns over the time and amount of reagents required to optimise these assays.

6.5.2 RNA18S copy number varied between tissues from the same person

As there has been no systematic evaluation of the range of *RNA18S* copy number in the control population, variation between individuals is not well characterised. Based on previous accounts, however, it can be inferred that some differences are present and likely contribute to the large range in reported copy numbers. In this study, the same tissues from six control cases did show variable *RNA18S* copy number, particularly across the urinary sediment samples. Although evaluating different tissue types, Gaubatz *et al.,* (1976) also

report person-person differences in *RNA18S* copy number, ranging from 142-289 copies in haploid genomes. This was attributed to potential unequal crossover, a process during meiosis where homologous chromosomes break at different loci and reconnect resulting in gene duplications or deletions.

An intriguing observation made during this study is the variation in *RNA18S* copy number between different tissues of the same individual. While this has been previously observed in brain and liver tissue samples (Gaubatz *et al.,* 1976), the largest difference was 55 copies (liver = 142, brain = 197). A much higher degree of variation was seen between tissues of controls used in this study where the lowest copy number was frequently measured in whole blood, increasing in buccal cells and highest in urinary epithelium. This would suggest *RNA18S* has a tissue-specific copy number, although this has never been investigated fully.

6.5.3 The MT-ND1/B2M assay was validated using alternative targets

Although the *MT-ND1*/*β2M* copy number assay is regularly used within our group, these targets have never been validated against other nuclear or mitochondrial gene targets. In this chapter, *MT-RNR2* and *GAPDH* were used for comparison against *MT-ND1* and *β2M* respectively. Both of these alternative targets have previously been used to assess mtDNA copy number by Pejznochova *et al.* (2008). Like *β2M*, *GAPDH* is a single-copy nuclear gene and would be measured to validate the *β2M* copy number quantification. Similarly, *MT-RNR2* was selected as an additional mtDNA marker to validate the *MT-ND1* copy number count. *GAPDH* is commonly used in real-time PCR assays, as discussed in section 6.1.2. *MT-RNR2* was suggested by Dr. Gavin Hudson (Institute of Genetic Medicine, Newcastle University) due to the low frequency of variants in a particular region of the gene.

Although the ratio of *GAPDH*:*β2M* should be one, it reached up to 4.01 in C6. It is possible that this is due to the presence of *GAPDH* pseudogenes, which could be amplified alongside the intended target sequence and producing false positive signals. The ratio of *MT-RNR2*:*MT-ND1* should also be 1, as both are present in single copies in the mitochondrial genome. For the majority of cases this was true, however C5 consistently showed a ratio of 0.38 across all tissues, indicating that *MT-RNR2* is present at a third of the quantity of *MT-ND1*. This could be due to a deletion in *MT-RNR2*, however this gene is located in the minor arc where single deletions are uncommon. It is possible that multiple, smaller deletions are

present in these samples, and so further investigation into this control case is warranted. It is also not unfeasible that this individual harbours a rare polymorphism which could affect the binding of the primer/probe specific to *MT-RNR2*, in which case the low ratio would be attributable to experimental design.

6.5.4 Limitations of this chapter

The main limitation of the work presented in this chapter is the lack of replicate plates performed during the optimisation experiments. While this would have provided a more accurate evaluation of the performance of the assays under the various experimental conditions, the cost of running replicate plates for each experiment would have been substantial. Furthermore, human tissue for use in the optimisation experiments was limited and needed to be conserved. In the later work, using control tissues, three replicate plates were performed for each singleplex assay as these samples were more readily available.

6.6 Conclusion

The use of *RNA18S* as an additional gene marker in an assay for the determination of mtDNA copy number offers no improvement to the standard *MT-ND1*/*β2M* real-time PCR assay as (i) multiplexing the assay would require tissue-specific conditions, (ii) performing three singleplex assays increases the variability of the calculated copy number compared to the standard protocol and (iii) the *MT-ND1*/*β2M* assay has been validated by the use of additional nuclear and mitochondrial gene targets. It is therefore, recommended that the *MT-ND1*/*β2M*continue to be used for the quantification of mtDNA copy number.

Chapter 7: Final discussion

The vast clinical and genetic heterogeneity associated with mitochondrial disease presents challenges to diagnosis and patient management, regarding treatment and evaluation of prognosis. Such heterogeneity also complicates research into the genetic and cellular mechanisms behind mitochondrial dysfunction. However, elucidating the pathogenic mechanisms driving the onset and progression of mitochondrial dysfunction could improve understanding of clinical prognosis and provide potential targets for the development of therapeutic interventions. Therefore, the aim of the work presented in this thesis was to improve understanding of the potential mechanisms of pathogenesis in skeletal muscle, and evaluate the genetic and biochemical changes occurring in this tissue over time.

7.1 Genetic and molecular mechanisms behind disease progression

In order to evaluate the potential molecular mechanisms driving disease progression, longitudinal studies were performed using skeletal muscle biopsies from patients with m.3243A>G point mutation or single, large-scale mtDNA deletions. These mutations represent the largest groups in the MRC Centre Mitochondrial Disease Cohort, affecting 46% of patients (m.3243A>G = 33%, single, large-scale mtDNA deletions = 13%). Despite being common mutations associated with mitochondrial disease, there are relatively few longitudinal studies evaluating genetic and biochemical changes in patient tissues over time, particularly in skeletal muscle. Indeed, longitudinal assessment of respiratory chain deficiency in skeletal muscle of patients with m.3243A>G, as presented in chapter three, is not documented in the current literature.

The longitudinal study of six patients with m.3243A>G (chapter three) presents novel data regarding changes to the deficiency of complex I and complex IV in skeletal muscle over time, reporting no marked fluctuations. This was reflected by small changes in heteroplasmy level and mtDNA copy number, which have also not been comprehensively assessed over time in this tissue. Although heteroplasmy of other point mutations has been previously shown to increase in muscle (Weber *et al*., 1997; Durham *et al*., 2006), this was only seen in two patients in this study, with two others showing a decrease and two remaining stable. This study concluded no consistent changes to heteroplasmy level, mtDNA copy number or

respiratory chain deficiency occurred over time in these patients. However, despite being the most comprehensive assessment of genetic and cellular changes to date, the sample size (six patients) is too limited to draw any statistically significant conclusions. Furthermore, these patients lacked any progressive muscle-related symptoms, and so skeletal muscle biopsies may not be representative of the multisystem conditions associated with m.3243A<G. Unfortunately, addressing these limitations is challenging as the sample size is restricted by the number of patients with multiple skeletal muscle biopsies, and collecting multiple biopsies from other affected tissues, such as brain and pancreas, is not possible.

Unlike m.3243A>G, previous longitudinal studies have been conducted in skeletal muscle from patients with single, large-scale mtDNA deletions. While these have evaluated deletion level (Ishikawa *et al*., 1999; Larson *et al*., 1990; Durham *et al*., 2006), mtDNA copy number (Durham *et al*., 2006) and COX-deficiency (Chinnery *et al*., 2003; Larsson *et al*., 1990; Durham *et al*., 2006), none have quantified complex I deficiency and so the findings reported in chapter four are novel. Furthermore, this longitudinal study features 10 patients, a much larger sample size than previous longitudinal studies.

The study of single, large-scale mtDNA deletions revealed an increase in deletion level over time in the majority of patients, which is in line with previous reports (Ishikawa *et al*., 1999; Larsson *et al*., 1990). Wild-type mtDNA copy number was also shown to increase in most patients, however this is in disagreement with findings made by Durham et al 2006 who conclude that a decrease in wild-type mtDNA copy number over time may drive pathogenesis. It is possible that these conflicting results may be due to the analysis of homogenate DNA, whereas a longitudinal assessment of wild-type copy number at the single fibre level may resolve this.

Previous longitudinal studies report either stationary or increasing proportions of COX-deficient fibres in skeletal muscle biopsies from patients with single, large-scale mtDNA deletions (Chinnery *et al*., 2003; Durham *et al*., 2006; Larsson *et al*., 1990). While the current study reports a general increase in the proportion of COX-deficient fibres, some patients show a decrease over time, representing a novel finding likely due to the larger sample size.

The proportion of complex I deficient fibres also changes inconsistently across the group, although always in the same direction as complex IV deficiency. The inconsistent changes in the biochemical defects between patients could be due to the different deletion species present, i.e. the size and location of the deletion, which is shown to have an impact on the extent of respiratory chain deficiency in chapter five.

7.2 A single fibre approach to elucidating pathogenic mechanisms

Previous studies into the pathogenic mechanisms associated with single, large-scale mtDNA deletions have evaluated the relationship between deletion level, mtDNA copy number and respiratory chain deficiency. While it has long been established that the deletion level is greater in COX-deficient fibres (Mita *et al*., 1989), there are conflicting reports surrounding the level of deletion in biochemically normal fibres. The work presented in chapter five corroborates the findings of He *et al*. (2012) and Sciacco *et al*. (1994), detecting high levels of deletion in fibres with normal complex I and complex IV levels. Wild-type mtDNA copy number is also inconsistently reported in COX deficient fibres, with this study reporting a decline in wild-type mtDNA copy number with increasing levels of respiratory chain deficiency, as seen by Mita *et al*. (1989) and Sciacco *et al*. (1994).

Further to contributing to previous findings, the work presented in chapter five also presents novel data. The use of more accurate quantitative techniques, such as real-time PCR assays for deletion level and mtDNA copy number determination and a recently developed immunofluorescence assay for quantification of complex I and IV levels, allowed for estimation of the threshold levels for complex I and complex IV deficiency in six patients. Previous estimates place the threshold level in muscle at 70-90% heteroplasmy (Sciacco *et al*., 1994), however levels determined in chapter five are slightly lower, ranging from 55.5% to 81.9% for complex I and 56.8% to 91.7% for complex IV. The work presented in this thesis is the first to show that the biochemical threshold level is variable depending on the size and location of the deletion. Furthermore, the threshold levels for complexes I and IV differ, correlating with the number of complex-specific protein-encoding genes encompassed by the deletion. These findings are highly relevant to the continued discussion surrounding the pathogenic mechanisms associated with single, large-scale mtDNA deletions. There is much debate over whether the mitochondrial dysfunction arises due to the deletion of tRNA

genes, based on work in cell transmitochondrial cybrids (Nakase *et al*., 1990; Hayashi *et al*., 1991), or protein-encoding genes (Hammans *et al*., 1995), with the results of the current study supportive of a prominent role for deleted genes encoding respiratory chain subunits. However, only six patients were analysed in this study and so analysis of a larger group with additional, more diverse deletion species is required to better understand the intricacies of this complex mechanism.

Another key finding relating to the pathogenic mechanisms of single, large-sale mtDNA deletions was the relationship between mtDNA copy number and biochemical threshold. This work reports a steady level of total mtDNA copy number with increasing deletion level, until the second threshold level (i.e. the level for the complex affected second), after which total mtDNA copy number increases exponentially. A similar, yet inverted trend was observed for wild-type mtDNA copy number which decreased after the second threshold level was reached. This is in concordance with observations made in skeletal muscle by Durham *et al*., (2007), and supports the in silico predictions made by Chinnery and Samuels (1999) who suggest the wild-type mtDNA copy number is maintained at normal levels by a proliferation of all mtDNA.

7.3 Further work

Although the longitudinal studies present novel findings, the pathogenic mechanisms behind disease progression are yet to be elucidated. Further investigation of the genetic and cellular longitudinal changes occurring in patents with m.3243A>G mutation or single, large-scale mtDNA deletions could involve a single fibre approach similar to that outlined in chapter five. Here, sections from the two patient biopsies would be subjected to immunofluorescence protocols to determine the OXPHOS and fibre type profile of individual fibres, which would then be laser microdissected for further molecular genetic analyses to determine heteroplasmy level and mtDNA copy number. This would allow for in-depth evaluation of changes at the cellular level, for example assessing changes to the wild-type mtDNA copy number in respiratory chain normal and deficient fibres over time.

The single-fibre analysis of single deletion patients did allude to potential mechanisms of pathogenesis, however a larger group of patients with a more diverse range of deletion sizes and locations is required to better understand these findings. In addition, it would be interesting to evaluate the genetic and cellular data in the context of the clinical phenotypes, particularly those involving muscle, i.e. myopathy, to see if there is a relationship between the genetic and biochemical defects and the extent of the clinical symptoms. This same approach could prove useful for other mtDNA mutations and could be adapted for use with other tissues.

7.4 Concluding remarks

The work presented in this thesis aimed to improve understanding of the complex molecular mechanisms behind pathogenesis of mitochondrial dysfunction in skeletal muscle. Longitudinal studies revealed inconsistent changes to heteroplasmy level, mtDNA copy number and respiratory chain deficiency in patients with m.3243A>G mutation, whilst these genetic and biochemical defects were more consistently affected in patients with single, large-scale mtDNA deletions. A single fibre study determined that biochemical thresholds are dictated by the size and location of single, large-scale mtDNA deletions, indicating that the removal of protein –encoding genes plays a key role in the pathogenesis of the mutation. Overall, this body of work has contributed to the current literature with novel findings, however there is still much work to be done to better understand the pathogenic mechanisms behind mitochondrial dysfunction in skeletal muscle.

Appendices

Appendix I – The NMDAS assessment (sections I-III)

THE NEWCASTLE
MITOCHONDRIAL DISEASE ADULT SCALE
(NMDAS)

Name: _____

Date of birth: _____

Age at assessment: _____

date of assessment: _____

Checklist – please tick off when completed.

- ❑ **Height:** _____
- ❑ **FVC - 1st attempt** _____
- ❑ **FVC - 2nd attempt** _____
- ❑ **FVC - 3rd attempt** _____ **% Predicted** _____

	Raw Score	Scaled Score	Centile
❑ **SF-12v2 self completion questionnaire**	_____	_____	_____
❑ **WTAR reading test (1 minute)**	_____	_____	_____
❑ **Symbol Search (2 minutes)**	_____	_____	_____
❑ **Speed of comprehension test (2 minutes)**	_____	_____	_____

Disease score (sections I-III)_____

SF-12v2 Quality of Life score (section IV)_____

Section I- Current Function

Rate function over the preceding **4 week period, according to patient and/or caregiver** interview only. The clinician's subjective judgement of functional ability should **not** be taken into account.

1. **Vision** with usual glasses or contact lenses

0. Normal.
1. No functional impairment but aware of worsened acuities.
2. Mild - difficulty with small print or text on television.
3. Moderate - difficulty outside the home (eg bus numbers, road signs or shopping).
4. Severe - difficulty recognising faces.
5. Unable to navigate without help (eg carer, dog, cane).

2. **Hearing** with or without hearing aid

0. Normal.
1. No communication problems but aware of tinnitus **or** deterioration from prior 'normal' hearing.
2. Mild deafness (eg missing words in presence of background noise). **Fully** corrected with hearing aid.
3. Moderate deafness (eg regularly requiring repetition). **Not fully** corrected with hearing aid.
4. Severe deafness - poor hearing even with aid (see 3 above).
5. End stage - virtually no hearing despite aid. Relies heavily on non-verbal communication (eg lip reading) **or** has cochlear implant.

3. **Speech**

0. Normal.
1. Communication unaffected but patient or others aware of changes in speech patterns or quality.
2. Mild difficulties - usually understood and **rarely** asked to repeat things.
3. Moderate difficulties - poorly understood by strangers and **frequently** asked to repeat things.
4. Severe difficulties - poorly understood by family or friends.
5. Not understood by family or friends. Requires communication aid.

4. **Swallowing**

0. Normal.
1. Mild - sensation of solids 'sticking' (occasional).
2. Sensation of solids 'sticking' (most meals) **or** need to modify diet (eg avoidance of steak/salad).
3. Difficulty swallowing solids - affecting meal size or duration. Coughing, choking **or** nasal regurgitation infrequent (1 to 4 times per month) but more than peers.
4. Requires adapted diet - regular coughing, choking, **or** nasal regurgitation (more than once per week).
5. Requiring enteral feeding (eg PEG).

5. **Handwriting**

0. Normal.
1. Writing speed unaffected but aware of increasing untidiness.
2. Mild – Has to write slower to maintain tidiness/legibility.
3. Moderate – Handwriting takes at least twice as long **or** resorts to printing (must previously have used joined writing).
4. Severe – Handwriting mostly illegible. Printing very slow and untidy (eg 'THE BLACK CAT' takes in excess of 30 seconds).
5. Unable to write. No legible words.

6. **Cutting food and handling utensils** (irrespective of contributory factors – eg weakness, coordination, cognitive function etc. This is also true for questions 7-10)

0. Normal.
1. Slightly slow and/or clumsy but **minimal** effect on meal duration.
2. Slow and/or clumsy with extended meal duration, but no help required.
3. Difficulty cutting up food and inaccuracy of transfer pronounced. Can manage alone but avoids problem foods (eg peas) or carer typically offers minor assistance (eg cutting up steak).
4. Unable to cut up food. Can pass food to mouth with great effort or inaccuracy. Resultant intake minimal. Requires major assistance.
5. Needs to be fed.

7. **Dressing**

0. Normal.
1. Occasional difficulties (eg shoe laces, buttons etc) but no real impact on time or effort taken to dress.
2. Mild – Dressing takes longer and requires more effort than expected at the patient's age. No help required.
3. Moderate - Can dress unaided but takes at least twice as long and is a major effort. Carer typically helps with difficult tasks such as shoe laces or buttons.
4. Severe – Unable to dress without help but some tasks completed unaided.
5. Needs to be dressed.

8. **Hygiene**

0. Normal.
1. Occasional difficulties only but no real impact on time or effort required.
2. Mild – hygienic care takes longer but quality unaffected.
3. Moderate - bathes and showers alone with difficulty **or** needs bath chair / modifications. Dextrous tasks (eg brushing teeth, combing hair) performed poorly.
4. Severe - unable to bathe or shower without help. Major difficulty using toilet alone. Dextrous tasks require help.
5. Dependent upon carers to wash, bathe, and toilet.

9. **Exercise Tolerance**

0. Normal.
1. Unlimited on flat - symptomatic on inclines or stairs.
2. Able to walk < 1000m on the flat. Restricted on inclines or stairs - rest needed after 1 flight (12 steps).
3. Able to walk < 500m on the flat. Rest needed after 8 steps on stairs.
4. Able to walk < 100m on the flat. Rest needed after 4 steps on stairs.
5. Able to walk < 25m on the flat. Unable to do stairs alone.

10. **Gait stability**

0. Normal.
1. Normal gait - occasional difficulties on turns, uneven ground, or if required to balance on narrow base.
2. Gait reasonably steady. Aware of impaired balance. **Occasionally** off balance when walking.
3. Unsteady gait. **Always** off balance when walking. **Occasional** falls. Gait steady with support of stick or person.
4. Gait grossly unsteady without support. **High likelihood** of falls. Can only walk short distances (< 10m) without support.
5. Unable to walk without support. Falls on standing.

Section II – System Specific Involvement

Rate function according to patient and/or caregiver interview and consultation with the medical notes. Each inquiry should take into account the situation for the preceding **12 month period** only, unless otherwise stated in the question.

1. **Psychiatric**

0. None.
1. Mild & transient (eg reactive depression) - lasting **less** than 3 months.
2. Mild & persistent (lasting **more** than 3 months) **or** recurrent. Patient has consulted GP.
3. Moderate & warranting specialist treatment (e.g. from a psychiatrist) - eg. bipolar disorder or depression with vegetative symptoms (insomnia, anorexia, abulia etc).
4. Severe (eg self harm - psychosis etc).
5. Institutionalised or suicide attempt.

2. **Migraine Headaches** During **the last 3 months**, how many days have headaches prevented the patient from functioning normally at school, work, or in the home?

0. No past history.
1. Asymptomatic but past history of migraines.
2. One day per month.
3. Two days per month.
4. Three days per month.
5. Four days per month or more.

3. **Seizures**

0. No past history.
1. Asymptomatic but past history of epilepsy.
2. Myoclonic or simple partial seizures only.
3. Multiple absence, complex partial, or myoclonic seizures affecting function **or** single generalised seizure.
4. Multiple generalised seizures.
5. Status epilepticus.

4. **Stroke-like episodes** (exclude focal deficits felt to be of vascular aetiology)

0. None.
1. Transient focal sensory symptoms only (**less** than 24 hours).
2. Transient focal motor symptoms only (**less** than 24 hours).
3. Single stroke-like episode affecting one hemisphere (**more** than 24 hours).
4. Single stroke-like episode affecting both hemispheres (**more** than 24 hours).
5. Multiple stroke-like episodes (**more** than 24 hours each).

5. **Encephalopathic Episodes**

0. No past history.
1. Asymptomatic **but** past history of encephalopathy.
2. Mild - single episode of personality or behavioural change but retaining orientation in time/place/person.
3. Moderate - single episode of confusion or disorientation in time, place or person.
4. Severe – multiple moderate episodes (as above) **or** emergency hospital admission due to encephalopathy **without** associated seizures or stroke-like episodes.
5. Very severe - in association with seizures, strokes or gross lactic acidaemia.

6. **Gastro-intestinal symptoms**

0. None.
1. Mild constipation only **or** past history of bowel resection for dysmotility.
2. Occasional symptoms of 'irritable bowel' (pain, bloating or diarrhoea) with long spells of normality.
3. Frequent symptoms (as above) most weeks **or** severe constipation with bowels open less than once/week **or** need for daily medications.
4. Dysmotility requiring admission **or** persistent and/or recurrent anorexia/vomiting/weight loss.
5. Surgical procedures **or** resections for gastrointestinal dysmotility.

7. **Diabetes mellitus**

0. None.
1. Past history of gestational diabetes or transient glucose intolerance related to intercurrent illness.
2. Impaired glucose tolerance (in absence of intercurrent illness).
3. NIDDM (diet).
4. NIDDM (tablets).
5. DM requiring insulin (irrespective of treatment at onset).

8. **Respiratory muscle weakness**

0. FVC normal (≥ 85% predicted).
1. FVC < 85% predicted.
2. FVC < 75% predicted.
3. FVC < 65% predicted.
4. FVC < 55% predicted.
5. FVC < 45% predicted **or** ventilatory support for over 6 hours per 24 hr period (**not** for OSA alone).

9. **Cardiovascular system**

0. None.
1. Asymptomatic ECG change.
2. Asymptomatic LVH on echo **or** non-sustained brady/tachyarrhythmia on ECG.
3. Sustained or **symptomatic** arrhythmia, LVH **or** cardiomyopathy. Dilated chambers **or** reduced function on echo. Mobitz II AV block or greater.
4. Requires pacemaker, defibrillator, arrhythmia ablation, **or** LVEF < 35% on echocardiogram.
5. Symptoms of left ventricular failure **with** clinical and/or x-ray evidence of pulmonary oedema **or** LVEF < 30% on echocardiogram.

Section III – Current Clinical Assessment

Rate current status according to examination performed at **the time of** assessment

1. **Visual acuity** with usual glasses, contact lenses or pinhole.

0. CSD ≤ **12** (ie normal vision - 6/6, 6/6 or better).
1. CSD **≤ 18** (eg 6/9, 6/9).
2. CSD **≤ 36** (eg 6/12, 6/24).
3. CSD **≤ 60** (eg 6/24, 6/36).
4. CSD **≤ 96** (eg 6/60, 6/36).
5. CSD **≥ 120** (eg 6/60, 6/60 **or worse**).

2. **Ptosis**

0. None.
1. Mild ptosis - not obscuring **either** pupil.
2. Unilateral ptosis obscuring **<** 1/3 of pupil.
3. Bilateral ptosis obscuring **<** 1/3 **or** unilateral ptosis obscuring **>** 1/3 of pupil **or** prior unilateral surgery.
4. Bilateral ptosis obscuring > 1/3 of pupils **or** prior bilateral surgery.
5. Bilateral ptosis obscuring >2/3 of pupils **or** >1/3 of pupils **despite** prior bilateral surgery.

3. **Chronic Progressive External Ophthalmoplegia**

0. None.
1. Some restriction of eye movement (any direction). Abduction complete.
2. Abduction of worst eye incomplete.
3. Abduction of worst eye below 60% of normal.
4. Abduction of worst eye below 30% of normal.
5. Abduction of worst eye minimal (flicker).

4. **Dysphonia/Dysarthria**

0. None.
1. Minimal - noted on examination only.
2. Mild – clear impairment but easily understood.
3. Moderate – some words poorly understood and infrequent repetition needed.
4. Severe – many words poorly understood and frequent repetition needed.
5. Not understood. Requires communication aid.

5**. Myopathy**

0. Normal.
1. Minimal reduction in hip flexion and/or shoulder abduction **only** (eg MRC 4+/5).
2. Mild but clear proximal weakness in hip flexion and shoulder abduction (MRC 4/5). Minimal weakness in elbow flexion and knee extension (MRC 4+/5 - both examined with joint at 90 degrees).
3. Moderate proximal weakness including elbow flexion & knee extension (MRC 4/5 or 4 -/5) **or difficulty** rising from a 90 degree squat.
4. Waddling gait. **Unable** to rise from a 90 degree squat (=a chair) unaided.
5. Wheelchair dependent **primarily** due to proximal weakness.

6. **Cerebellar ataxia**

0. None.
1. Normal gait but hesitant heel-toe.
2. Gait reasonably steady. Unable to maintain heel-toe walking **or** mild UL dysmetria.
3. Ataxic gait (but walks unaided) **or** UL intention tremor & past-pointing. Unable to walk heel-toe - falls immediately.
4. Severe - gait grossly unsteady without support **or** UL ataxia sufficient to affect feeding.
5. Wheelchair dependent **primarily** due to ataxia **or** UL ataxia **prevents** feeding.

7**. Neuropathy**

0. None.
1. Subtle sensory symptoms **or** areflexia.
2. Sensory impairment only (eg glove & stocking sensory loss).
3. Motor impairment (distal weakness) **or** sensory ataxia.
4. Sensory ataxia **or** motor effects severely limit ambulation.
5. Wheelchair bound **primarily** due to sensory ataxia or neurogenic weakness.

8. **Pyramidal Involvement**

0. None.
1. Focal or generalised increase in tone or reflexes only.
2. Mild **focal** weakness, sensory loss or fine motor impairment (eg cortical hand).
3. Moderate hemiplegia allowing unaided ambulation **or** dense UL monoplegia.
4. Severe hemiplegia allowing ambulation with aids **or** moderate tetraplegia (ambulant).
5. Wheelchair dependant **primarily** due to hemiplegia or tetraplegia.

9. **Extrapyramidal**

0. Normal.
1. Mild and unilateral. Not disabling (H&Y stage 1).
2. Mild and bilateral. Minimal disability. Gait affected (H&Y stage 2).
3. Moderate. Significant slowing of body movements (H&Y stage 3)
4. Severe. Rigidity and bradykinesia. Unable to live alone. Can walk to limited extent (H&Y stage 4).
5. Cannot walk or stand unaided. Requires constant nursing care (H&Y stage 5).

10. **Cognitition**

Patients undergo testing using WTAR, Symbol Search and Speed of Comprehension Test.

0. Combined centiles **100 or more.**
1. Combined centiles **60 - 99**
2. Combined centiles **30 - 59**
3. Combined centiles **15 - 29**
4. Combined centiles **5 - 14**
5. Combined centiles **4 or below.**

Appendix II – mtRC profiles for single, large-scale mtDNA deletion patients

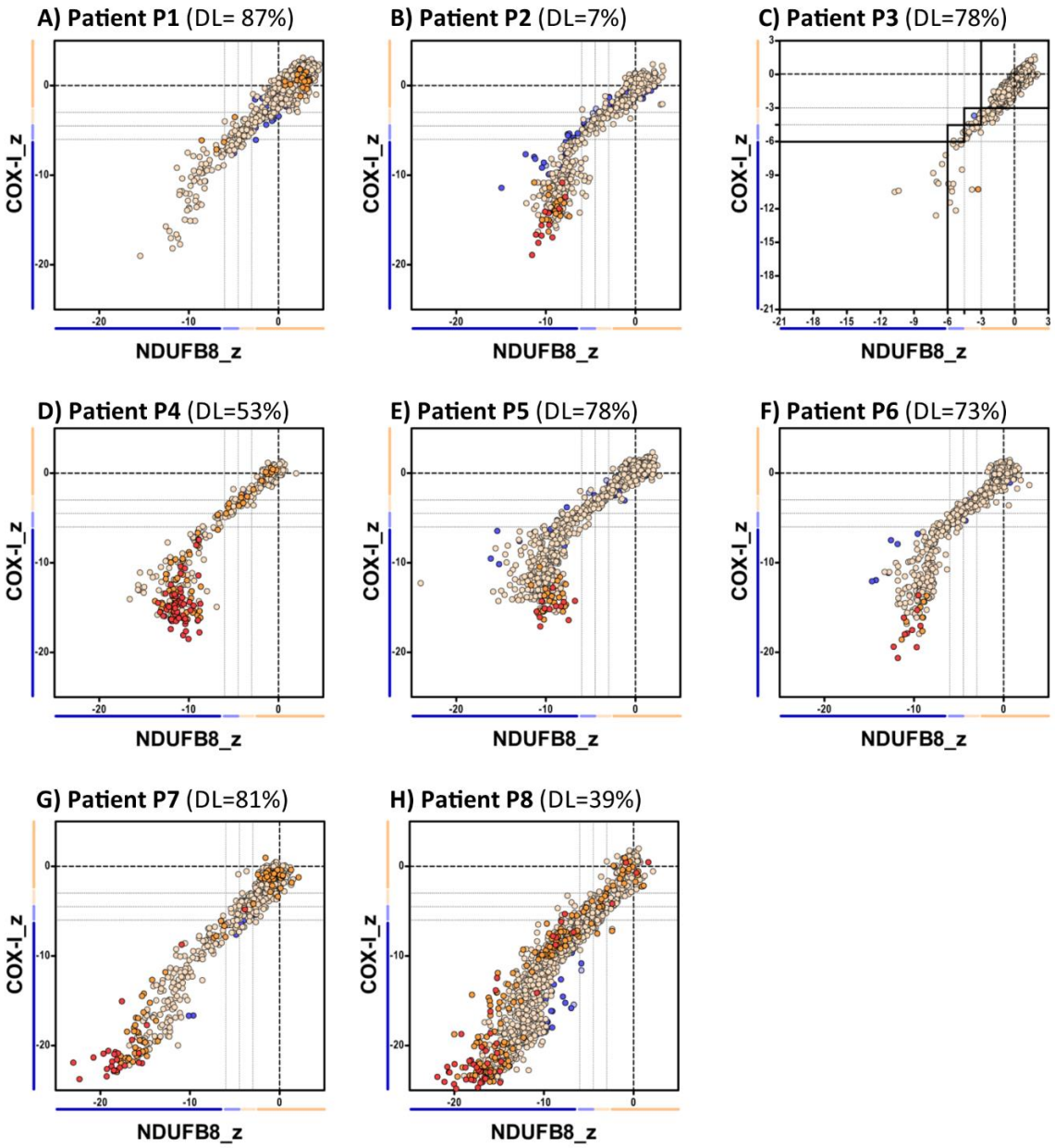

Figure A.1: mtRC profiles from patients grouped in class 1 – showing both complexes I and IV equally affected**.** mtRC graphs show complex I and IV expression profile from (A) P1 (n = 1448 fibres analysed), (B) P2 (n = 1261), (C) P3 (n = 631), (D) P4 (n = 1228), (E) P5 (n = 388), (F) P6 (n = 853), (G) P7 (n = 609) and (H) P8 (n = 1309). Each dot represents an individual muscle fibre colour coded according to its mitochondrial mass (very low: blue, low: light blue, normal: beige, high: orange and very high: red). DL indicates the deletion level (proportion of deleted over wild-type mtDNA) determined in muscle homogenates.

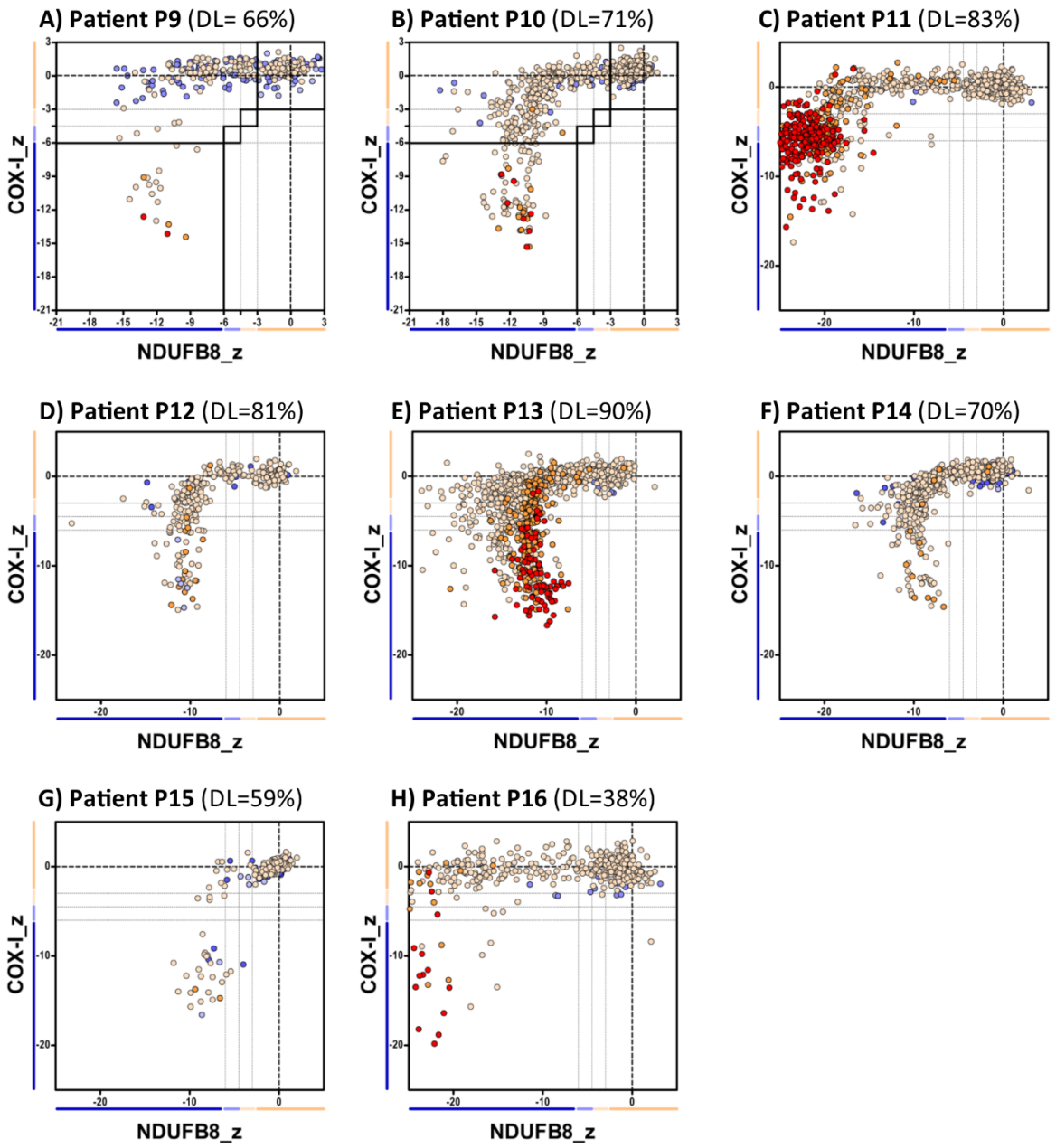

Figure A.2: mtRC profiles from patients grouped in class 2 – showing a more pronounced involvement of complex I over complex IV. mtRC graphs show complex I and IV expression profile from (A) P9 (n = 322 fibres analysed), (B) P10 (n = 579), (C) P11 (n = 1804), (D) P12 (n = 272), (E) P13 (n = 737), (F) P14 (n = 606), (G) P15 (n = 546) and (H) P16 (n = 283). Each dot represents an individual muscle fibre colour coded according to its mitochondrial mass (very low: blue, low: light blue, normal: beige, high: orange and very high: red). DL indicates the deletion level (proportion of deleted over wild-type mtDNA) determined in muscle homogenates.

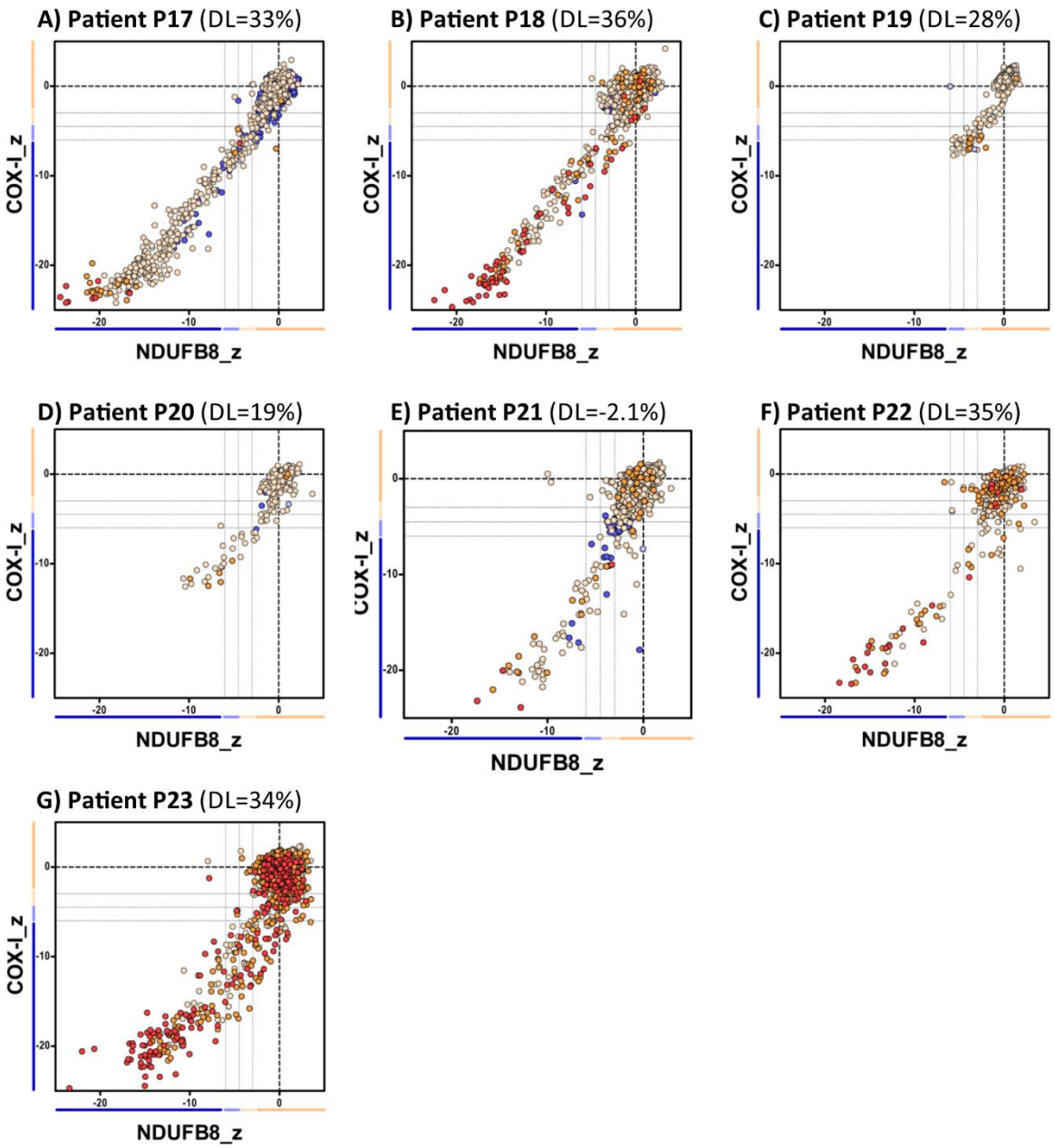

Figure A.3: mtRC profiles from patients grouped in class 3 – showing a more pronounced involvement of complex VI over complex I. mtRC graphs show complex I and IV expression profile from (A) P17 (n = 1400 fibres analysed), (B) P18 (n = 764), (C) P19 (n = 841), (D) P20 (n = 283), (E) P21 (n = 1333), (F) P22 (n = 730) and (G) P23 (n = 1579). Each dot represents an individual muscle fibre colour coded according to its mitochondrial mass (very low: blue, low: light blue, normal: beige, high: orange and very high: red). DL indicates the deletion level (proportion of deleted over wild-type mtDNA) determined in muscle homogenates.

Chapter Eight: Bibliography

Abrahams, J.P., Leslie, A.G., Lutter, R. and Walker, J.E. (1994) 'Structure at 2.8 A resolution of F1-ATPase from bovine heart mitochondria', *Nature*, 370(6491), pp. 621-8.

Adhihetty, P.J., Ljubicic, V., Menzies, K.J. and Hood, D.A. (2005) 'Differential susceptibility of subsarcolemmal and intermyofibrillar mitochondria to apoptotic stimuli', *Am J Physiol Cell Physiol*, 289(4), pp. C994-c1001.

Agar, J.N., Krebs, C., Frazzon, J., Huynh, B.H., Dean, D.R. and Johnson, M.K. (2000) 'IscU as a Scaffold for Iron−Sulfur Cluster Biosynthesis: Sequential Assembly of [2Fe-2S] and [4Fe-4S] Clusters in IscU', *Biochemistry*, 39(27), pp. 7856-7862.

Ahmed, A.U. and Fisher, P.R. (2009) 'Import of nuclear-encoded mitochondrial proteins: a cotranslational perspective', *Int Rev Cell Mol Biol*, 273, pp. 49-68.

Al Rawi, S., Louvet-Vallee, S., Djeddi, A., Sachse, M., Culetto, E., Hajjar, C., Boyd, L., Legouis, R. and Galy, V. (2011) 'Postfertilization autophagy of sperm organelles prevents paternal mitochondrial DNA transmission', *Science*, 334(6059), pp. 1144-7.

Albring, M., Griffith, J. and Attardi, G. (1977) 'Association of a protein structure of probable membrane derivation with HeLa cell mitochondrial DNA near its origin of replication', *Proc Natl Acad Sci U S A*, 74(4), pp. 1348-52.

Alston, C.L., Davison, J.E., Meloni, F., van der Westhuizen, F.H., He, L., Hornig-Do, H.T., Peet, A.C., Gissen, P., Goffrini, P., Ferrero, I., Wassmer, E., McFarland, R. and Taylor, R.W. (2012) 'Recessive germline SDHA and SDHB mutations causing leukodystrophy and isolated mitochondrial complex II deficiency', *J Med Genet*, 49(9), pp. 569-77.

Anderson, S., Bankier, A.T., Barrell, B.G., de Bruijn, M.H., Coulson, A.R., Drouin, J., Eperon, I.C., Nierlich, D.P., Roe, B.A., Sanger, F., Schreier, P.H., Smith, A.J., Staden, R. and Young, I.G. (1981) 'Sequence and organization of the human mitochondrial genome', *Nature*, 290(5806), pp. 457-65.

Andersson, S.G. and Kurland, C.G. (1999) 'Origins of mitochondria and hydrogenosomes', *Curr Opin Microbiol*, 2(5), pp. 535-41.

Andersson, S.G.E., Zomorodipour, A., Andersson, J.O., Sicheritz-Ponten, T., Alsmark, U.C.M., Podowski, R.M., Naslund, A.K., Eriksson, A.-S., Winkler, H.H. and Kurland, C.G. (1998) 'The genome sequence of Rickettsia prowazekii and the origin of mitochondria', *Nature*, 396(6707), pp. 133-140.

Andrews, R.M., Kubacka, I., Chinnery, P.F., Lightowlers, R.N., Turnbull, D.M. and Howell, N. (1999) 'Reanalysis and revision of the Cambridge reference sequence for human mitochondrial DNA', *Nat Genet*, 23(2), pp. 147-147.

Arnberg, A., van Bruggen, E.F. and Borst, P. (1971) 'The presence of DNA molecules with a displacement loop in standard mitochondrial DNA preparations', *Biochim Biophys Acta*, 246(2), pp. 353-7.

Auré, K., Ogier de Baulny, H., Laforêt, P., Jardel, C., Eymard, B. and Lombès, A. (2007) 'Chronic progressive ophthalmoplegia with large-scale mtDNA rearrangement: can we predict progression?', *Brain*, 130(6), pp. 1516-1524.

Bai, R.K. and Wong, L.J. (2005) 'Simultaneous detection and quantification of mitochondrial DNA deletion(s), depletion, and over-replication in patients with mitochondrial disease', *J Mol Diagn*, 7(5), pp. 613-22.

Balakrishnan, V.S., Rao, M., Menon, V., Gordon, P.L., Pilichowska, M., Castaneda, F. and Castaneda-Sceppa, C. (2010) 'Resistance training increases muscle mitochondrial biogenesis in patients with chronic kidney disease', *Clin J Am Soc Nephrol*, 5(6), pp. 996-1002.

Barrell, B.G., Anderson, S., Bankier, A.T., de Bruijn, M.H., Chen, E., Coulson, A.R., Drouin, J., Eperon, I.C., Nierlich, D.P., Roe, B.A., Sanger, F., Schreier, P.H., Smith, A.J., Staden, R. and Young, I.G. (1980) 'Different pattern of codon recognition by mammalian mitochondrial tRNAs', *Proc Natl Acad Sci U S A*, 77(6), pp. 3164-6.

Barupala, D.P., Dzul, S.P., Riggs-Gelasco, P.J. and Stemmler, T.L. (2016) 'Synthesis, delivery and regulation of eukaryotic heme and Fe–S cluster cofactors', *Archives of Biochemistry and Biophysics*, 592, pp. 60-75.

Bencze, K.Z., Kondapalli, K.C., Cook, J.D., McMahon, S., Millán-Pacheco, C., Pastor, N. and Stemmler, T.L. (2006) 'The Structure and Function of Frataxin', *Critical Reviews in Biochemistry and Molecular Biology*, 41(5), pp. 269-291.

Bender, A., Krishnan, K.J., Morris, C.M., Taylor, G.A., Reeve, A.K., Perry, R.H., Jaros, E., Hersheson, J.S., Betts, J., Klopstock, T., Taylor, R.W. and Turnbull, D.M. (2006) 'High levels of mitochondrial DNA deletions in substantia nigra neurons in aging and Parkinson disease', *Nat Genet*, 38(5), pp. 515-7.

Bereiter-Hahn, J. and Voth, M. (1994) 'Dynamics of mitochondria in living cells: shape changes, dislocations, fusion, and fission of mitochondria', *Microsc Res Tech*, 27(3), pp. 198-219.

Berg, J., Tymoczko, J. and Stryer, L. (2012a) *Biochemsitry 7th edition. Glycolysis and gluconeogenesis.* New York: W.H. Freeman and Company.

Berg, J., Tymoczko, J. and Stryer, L. (2012b) *Biochemsitry 7th edition. The citric acid cycle.* New York: W.H. Freeman and Company.

Berg, J., Tymoczko, J. and Stryer, L. (2012c) *Biochemsitry 7th edition. Oxidative phosphorylation.* New York: W.H. Freeman and Company.

Berry, E.A. and Trumpower, B.L. (1985) 'Isolation of ubiquinol oxidase from Paracoccus denitrificans and resolution into cytochrome bc1 and cytochrome c-aa3 complexes', *Journal of Biological Chemistry*, 260(4), pp. 2458-2467.

Bleazard, W., McCaffery, J.M., King, E.J., Bale, S., Mozdy, A., Tieu, Q., Nunnari, J. and Shaw, J.M. (1999) 'The dynamin-related GTPase Dnm1 regulates mitochondrial fission in yeast', *Nat Cell Biol*, 1(5), pp. 298-304.

Boesch, P., Weber-Lotfi, F., Ibrahim, N., Tarasenko, V., Cosset, A., Paulus, F., Lightowlers, R.N. and Dietrich, A. (2011) 'DNA repair in organelles: Pathways, organization, regulation, relevance in disease and aging', *Biochim Biophys Acta*, 1813(1), pp. 186-200.

Bogenhagen, D. and Clayton, D.A. (1974) 'The Number of Mitochondrial Deoxyribonucleic Acid Genomes in Mouse L and Human HeLa Cells: quantitative isolation of mitochondrial deoxyribonucleic acid', *Journal of Biological Chemistry*, 249(24), pp. 7991-7995.

Bogenhagen, D. and Clayton, D.A. (1977) 'Mouse L cell mitochondrial DNA molecules are selected randomly for replication throughout the cell cycle', *Cell*, 11(4), pp. 719-27.

Börner, G.V., Zeviani, M., Tiranti, V., Carrara, F., Hoffmann, S., Gerbitz, K.D., Lochmüller, H., Pongratz, D., Klopstock, T., Melberg, A., Holme, E. and Pääbo, S. (2000) 'Decreased aminoacylation of mutant tRNAs in MELAS but not in MERRF patients', *Human Molecular Genetics*, 9(4), pp. 467-475.

Bourgeois, J.M. and Tarnopolsky, M.A. (2004) 'Pathology of skeletal muscle in mitochondrial disorders', *Mitochondrion*, 4(5-6), pp. 441-52.

Boveris, A., Oshino, N. and Chance, B. (1972) 'The cellular production of hydrogen peroxide', *Biochemical Journal*, 128(3), pp. 617-630.

Bowmaker, M., Yang, M.Y., Yasukawa, T., Reyes, A., Jacobs, H.T., Huberman, J.A. and Holt, I.J. (2003) 'Mammalian mitochondrial DNA replicates bidirectionally from an initiation zone', *J Biol Chem*, 278(51), pp. 50961-9.

Box, G.E.P. and Cox, D.R. (1964) 'An Analysis of Transformations', *Journal of the Royal Statistical Society. Series B (Methodological)*, 26(2), pp. 211-252.

Boyman, L., Williams, G.S.B., Khananshvili, D., Sekler, I. and Lederer, W.J. (2013) 'NCLX: The Mitochondrial Sodium Calcium Exchanger', *Journal of molecular and cellular cardiology*, 59, pp. 205-213.

Brandt, U. (2006) 'Energy converting NADH:quinone oxidoreductase (complex I)', *Annu Rev Biochem*, 75, pp. 69-92.

Brooke, M.H. and Kaiser, K.K. (1970) 'Muscle fiber types: how many and what kind?', *Arch Neurol*, 23(4), pp. 369-79.

Bross, K. and Krone, W. (1972) 'On the number of ribosomal RNA genes in man', *Humangenetik*, 14(2), pp. 137-41.

Brown, D.T., Samuels, D.C., Michael, E.M., Turnbull, D.M. and Chinnery, P.F. (2001) 'Random Genetic Drift Determines the Level of Mutant mtDNA in Human Primary Oocytes', *American Journal of Human Genetics*, 68(2), pp. 533-536.

Brown, G.C. and Borutaite, V. (2012) 'There is no evidence that mitochondria are the main source of reactive oxygen species in mammalian cells', *Mitochondrion*, 12(1), pp. 1-4.

Brown, M.D., Voljavec, A.S., Lott, M.T., Torroni, A., Yang, C.C. and Wallace, D.C. (1992) 'Mitochondrial DNA complex I and III mutations associated with Leber's hereditary optic neuropathy', *Genetics*, 130(1), pp. 163-73.

Brown, T.A., Tkachuk, A.N., Shtengel, G., Kopek, B.G., Bogenhagen, D.F., Hess, H.F. and Clayton, D.A. (2011) 'Superresolution Fluorescence Imaging of Mitochondrial Nucleoids Reveals Their Spatial Range, Limits, and Membrane Interaction', *Molecular and Cellular Biology*, 31(24), pp. 4994-5010.

Brown, W.M., George, M. and Wilson, A.C. (1979) 'Rapid evolution of animal mitochondrial DNA', *Proceedings of the National Academy of Sciences*, 76(4), pp. 1967-1971.

Bua, E., Johnson, J., Herbst, A., Delong, B., McKenzie, D., Salamat, S. and Aiken, J.M. (2006) 'Mitochondrial DNA–Deletion Mutations Accumulate Intracellularly to Detrimental Levels in Aged Human Skeletal Muscle Fibers', *The American Journal of Human Genetics*, 79(3), pp. 469-480.

Buller, A.J., Eccles, J.C. and Eccles, R.M. (1960) 'Interactions between motoneurones and muscles in respect of the characteristic speeds of their responses', *The Journal of Physiology*, 150(2), pp. 417-439.

Campbell, G., Krishnan, K.J., Deschauer, M., Taylor, R.W. and Turnbull, D.M. (2014) 'Dissecting the mechanisms underlying the accumulation of mitochondrial DNA deletions in human skeletal muscle', *Human Molecular Genetics*, 23(17), pp. 4612-4620.

Carroll, J., Fearnley, I.M., Skehel, J.M., Shannon, R.J., Hirst, J. and Walker, J.E. (2006) 'Bovine Complex I Is a Complex of 45 Different Subunits', *Journal of Biological Chemistry*, 281(43), pp. 32724-32727.

Carrozzo, R., Tessa, A., Vazquez-Memije, M.E., Piemonte, F., Patrono, C., Malandrini, A., Dionisi-Vici, C., Vilarinho, L., Villanova, M., Schagger, H., Federico, A., Bertini, E. and Santorelli, F.M. (2001) 'The T9176G mtDNA mutation severely affects ATP production and results in Leigh syndrome', *Neurology*, 56(5), pp. 687-90.

Chang, D.D. and Clayton, D.A. (1984) 'Precise identification of individual promoters for transcription of each strand of human mitochondrial DNA', *Cell*, 36(3), pp. 635-43.

Chen, H. and Chan, D.C. (2004) 'Mitochondrial dynamics in mammals', *Curr Top Dev Biol*, 59, pp. 119-44.

Chen, X., Prosser, R., Simonetti, S., Sadlock, J., Jagiello, G. and Schon, E.A. (1995) 'Rearranged mitochondrial genomes are present in human oocytes', *American Journal of Human Genetics*, 57(2), pp. 239-247.

Chen, X.J. and Butow, R.A. (2005) 'The organization and inheritance of the mitochondrial genome', *Nat Rev Genet*, 6(11), pp. 815-825.

Chinnery, P.F., DiMauro, S., Shanske, S., Schon, E.A., Zeviani, M., Mariotti, C., Carrara, F., Lombes, A., Laforet, P., Ogier, H., Jaksch, M., Lochmuller, H., Horvath, R., Deschauer, M., Thorburn, D.R., Bindoff, L.A., Poulton, J., Taylor, R.W., Matthews, J.N. and Turnbull, D.M. (2004) 'Risk of developing a mitochondrial DNA deletion disorder', *Lancet*, 364(9434), pp. 592-6.

Chinnery, P.F., Howel, D., Turnbull, D.M. and Johnson, M.A. (2003) 'Clinical progression of mitochondrial myopathy is associated with the random accumulation of cytochrome c oxidase negative skeletal muscle fibres', *Journal of the Neurological Sciences*, 211(1–2), pp. 63-66.

Chinnery, P.F., Howell, N., Lightowlers, R.N. and Turnbull, D.M. (1997) 'Molecular pathology of MELAS and MERRF. The relationship between mutation load and clinical phenotypes', *Brain*, 120 (Pt 10), pp. 1713-21.

Chinnery, P.F. and Samuels, D.C. (1999) 'Relaxed replication of mtDNA: A model with implications for the expression of disease', *Am J Hum Genet*, 64(4), pp. 1158-65.

Chomyn, A., Martinuzzi, A., Yoneda, M., Daga, A., Hurko, O., Johns, D., Lai, S.T., Nonaka, I., Angelini, C. and Attardi, G. (1992) 'MELAS mutation in mtDNA binding site for transcription termination factor causes defects in protein synthesis and in respiration but no change in levels of upstream and downstream mature transcripts', *Proc Natl Acad Sci U S A*, 89(10), pp. 4221-5.

Chomyn, A., Meola, G., Bresolin, N., Lai, S.T., Scarlato, G. and Attardi, G. (1991) 'In vitro genetic transfer of protein synthesis and respiration defects to mitochondrial DNA-less cells with myopathy-patient mitochondria', *Mol Cell Biol*, 11(4), pp. 2236-44.

Ciafaloni, E., Ricci, E., Servidei, S., Shanske, S., Silvestri, G., Manfredi, G., Schon, E.A. and DiMauro, S. (1991) 'Widespread tissue distribution of a tRNALeu(UUR) mutation in the mitochondrial DNA of a patient with MELAS syndrome', *Neurology*, 41(10), pp. 1663-4.

Ciafaloni, E., Ricci, E., Shanske, S., Moraes, C.T., Silvestri, G., Hirano, M., Simonetti, S., Angelini, C., Donati, M.A., Garcia, C. and et al. (1992) 'MELAS: clinical features, biochemistry, and molecular genetics', *Ann Neurol*, 31(4), pp. 391-8.

Cipolat, S., de Brito, O.M., Dal Zilio, B. and Scorrano, L. (2004) 'OPA1 requires mitofusin 1 to promote mitochondrial fusion', *Proceedings of the National Academy of Sciences of the United States of America*, 101(45), pp. 15927-15932.

Clay Montier, L.L., Deng, J. and Bai, Y. (2009) 'Number matters: control of mammalian mitochondrial DNA copy number', *Journal of genetics and genomics = Yi chuan xue bao*, 36(3), pp. 125-131.

Clayton, D.A. (1982) 'Replication of animal mitochondrial DNA', *Cell*, 28(4), pp. 693-705.

Cogliati, S., Enriquez, J.A. and Scorrano, L. 'Mitochondrial Cristae: Where Beauty Meets Functionality', *Trends in Biochemical Sciences*, 41(3), pp. 261-273.

Collins, S., Rudduck, C., Marzuki, S., Dennett, X. and Byrne, E. (1991) 'Mitochondrial genome distribution in histochemically cytochrome c oxidase-negative muscle fibres in patients with a mixture of deleted and wild type mitochondrial DNA', *Biochimica et Biophysica Acta (BBA) - Molecular Basis of Disease*, 1097(4), pp. 309-317.

Conley, K.E., Amara, C.E., Jubrias, S.A. and Marcinek, D.J. (2007) 'Mitochondrial function, fibre types and ageing: new insights from human muscle in vivo', *Experimental Physiology*, 92(2), pp. 333-339.

Corral-Debrinski, M., Horton, T., Lott, M.T., Shoffner, J.M., Beal, M.F. and Wallace, D.C. (1992) 'Mitochondrial DNA deletions in human brain: regional variability and increase with advanced age', *Nat Genet*, 2(4), pp. 324-9.

Cortopassi, G.A. and Arnheim, N. (1990) 'Detection of a specific mitochondrial DNA deletion in tissues of older humans', *Nucleic Acids Research*, 18(23), pp. 6927-6933.

Cortopassi, G.A., Shibata, D., Soong, N.W. and Arnheim, N. (1992) 'A pattern of accumulation of a somatic deletion of mitochondrial DNA in aging human tissues', *Proceedings of the National Academy of Sciences of the United States of America*, 89(16), pp. 7370-7374.

Cree, L.M., Samuels, D.C., de Sousa Lopes, S.C., Rajasimha, H.K., Wonnapinij, P., Mann, J.R., Dahl, H.-H.M. and Chinnery, P.F. (2008) 'A reduction of mitochondrial DNA molecules during embryogenesis explains the rapid segregation of genotypes', *Nat Genet*, 40(2), pp. 249-254.

Curth, U., Urbanke, C., Greipel, J., Gerberding, H., Tiranti, V. and Zeviani, M. (1994) 'Single-stranded-DNA-binding proteins from human mitochondria and Escherichia coli have analogous physicochemical properties', *Eur J Biochem*, 221(1), pp. 435-43.

Dairaghi, D.J., Shadel, G.S. and Clayton, D.A. (1995) 'Addition of a 29 residue carboxyl-terminal tail converts a simple HMG box-containing protein into a transcriptional activator', *J Mol Biol*, 249(1), pp. 11-28.

Damas, J., Carneiro, J., Amorim, A. and Pereira, F. (2014) 'MitoBreak: the mitochondrial DNA breakpoints database', *Nucleic Acids Research*, 42(D1), pp. D1261-D1268.

Damas, J., Carneiro, J., Gonçalves, J., Stewart, J.B., Samuels, D.C., Amorim, A. and Pereira, F. (2012) 'Mitochondrial DNA deletions are associated with non-B DNA conformations', *Nucleic Acids Research*.

Davidzon, G., Mancuso, M., Ferraris, S., Quinzii, C., Hirano, M., Peters, H.L., Kirby, D., Thorburn, D.R. and DiMauro, S. (2005) 'POLG mutations and Alpers syndrome', *Ann Neurol*, 57(6), pp. 921-3.

De Grey, A.D.N.J. (1997) 'A proposed refinement of the mitochondrial free radical theory of aging', *BioEssays*, 19(2), pp. 161-166.

Delettre, C., Griffoin, J.M., Kaplan, J., Dollfus, H., Lorenz, B., Faivre, L., Lenaers, G., Belenguer, P. and Hamel, C.P. (2001) 'Mutation spectrum and splicing variants in the OPA1 gene', *Hum Genet*, 109(6), pp. 584-91.

Denton, R.M., McCormack, J.G. and Edgell, N.J. (1980) 'Role of calcium ions in the regulation of intramitochondrial metabolism. Effects of Na+/Mg2+ and ruthenium red on the Ca²⁺-stimulated oxidation of oxoglutarate and on pyruvate dehydrogenase activity in intact rat heart mitochondria', *Biochemical Journal*, 190(1), pp. 107-117.

Deschauer, M., Neudecker, S., Müller, T., Gellerich, F.-N. and Zierz, S. (2000) 'Higher Proportion of Mitochondrial A3243G Mutation in Blood Than in Skeletal Muscle in a Patient with Cardiomyopathy and Hearing Loss', *Molecular Genetics and Metabolism*, 70(3), pp. 235-237.

DeVay, R.M., Dominguez-Ramirez, L., Lackner, L.L., Hoppins, S., Stahlberg, H. and Nunnari, J. (2009) 'Coassembly of Mgm1 isoforms requires cardiolipin and mediates mitochondrial inner membrane fusion', *J Cell Biol*, 186(6), pp. 793-803.

Diaz, F. (2010) 'Cytochrome c oxidase deficiency: patients and animal models', *Biochim Biophys Acta*, 1802(1), pp. 100-10.

Diaz, F., Bayona-Bafaluy, M.P., Rana, M., Mora, M., Hao, H. and Moraes, C.T. (2002) 'Human mitochondrial DNA with large deletions repopulates organelles faster than full-length genomes under relaxed copy number control', *Nucleic Acids Research*, 30(21), pp. 4626-4633.

Dubowitz, V. and Sewry, C.A. (2007) *Muscle biopsy: A practical approach*. Third edition edn. Saunders Elsevier

Durham, S.E., Brown, D.T., Turnbull, D.M. and Chinnery, P.F. (2006) 'Progressive depletion of mtDNA in mitochondrial myopathy', *Neurology*, 67(3), pp. 502-4.

Durham, S.E., Samuels, D.C., Cree, L.M. and Chinnery, P.F. (2007) 'Normal Levels of Wild-Type Mitochondrial DNA Maintain Cytochrome c Oxidase Activity for Two Pathogenic Mitochondrial DNA Mutations but Not for m.3243A→G', *American Journal of Human Genetics*, 81(1), pp. 189-195.

Duvezin-Caubet, S., Jagasia, R., Wagener, J., Hofmann, S., Trifunovic, A., Hansson, A., Chomyn, A., Bauer, M.F., Attardi, G., Larsson, N.G., Neupert, W. and Reichert, A.S. (2006) 'Proteolytic processing of OPA1 links mitochondrial dysfunction to alterations in mitochondrial morphology', *J Biol Chem*, 281(49), pp. 37972-9.

Dyall, S.D. and Johnson, P.J. (2000) 'Origins of hydrogenosomes and mitochondria: evolution and organelle biogenesis', *Curr Opin Microbiol*, 3(4), pp. 404-11.

Efremov, R.G., Baradaran, R. and Sazanov, L.A. (2010) 'The architecture of respiratory complex I', *Nature*, 465(7297), pp. 441-445.

Elson, J.L., Samuels, D.C., Turnbull, D.M. and Chinnery, P.F. (2001) 'Random Intracellular Drift Explains the Clonal Expansion of Mitochondrial DNA Mutations with Age', *The American Journal of Human Genetics*, 68(3), pp. 802-806.

Elston, T., Wang, H. and Oster, G. (1998) 'Energy transduction in ATP synthase', *Nature*, 391(6666), pp. 510-3.

Engel, W.K. and Cunningham, G.G. (1963) 'Rapid examination of muscle tissue: An improved trichrome method for fresh-frozen biopsy sections', *Neurology*, 13(11), pp. 919-923.

Escobar-Henriques, M. and Anton, F. (2013) 'Mechanistic perspective of mitochondrial fusion: Tubulation vs. fragmentation', *Biochimica et Biophysica Acta (BBA) - Molecular Cell Research*, 1833(1), pp. 162-175.

Faxen, K., Gilderson, G., Adelroth, P. and Brzezinski, P. (2005) 'A mechanistic principle for proton pumping by cytochrome c oxidase', *Nature*, 437(7056), pp. 286-289.

Ferguson, S.J. (2010) 'ATP synthase: From sequence to ring size to the P/O ratio', *Proceedings of the National Academy of Sciences*, 107(39), pp. 16755-16756.

Fernández-Vizarra, E. and Zeviani, M. (2015) 'Nuclear gene mutations as the cause of mitochondrial complex III deficiency', *Frontiers in Genetics*, 6, p. 134.

Ferreira, R., Vitorino, R., Alves, R.M., Appell, H.J., Powers, S.K., Duarte, J.A. and Amado, F. (2010) 'Subsarcolemmal and intermyofibrillar mitochondria proteome differences disclose functional specializations in skeletal muscle', *Proteomics*, 10(17), pp. 3142-54.

Finkel, T. (1998) 'Oxygen radicals and signaling', *Curr Opin Cell Biol*, 10(2), pp. 248-53.
Fisher, R.P., Topper, J.N. and Clayton, D.A. (1987) 'Promoter selection in human mitochondria involves binding of a transcription factor to orientation-independent upstream regulatory elements', *Cell*, 50(2), pp. 247-58.

Frederiksen, A.L., Andersen, P.H., Kyvik, K.O., Jeppesen, T.D., Vissing, J. and Schwartz, M. (2006) 'Tissue specific distribution of the 3243A→G mtDNA mutation', *Journal of Medical Genetics*, 43(8), pp. 671-677.

Frey, T.G. and Mannella, C.A. (2000) 'The internal structure of mitochondria', *Trends Biochem Sci*, 25(7), pp. 319-24.

Fukui, H. and Moraes, C.T. (2009) 'Mechanisms of formation and accumulation of mitochondrial DNA deletions in aging neurons', *Human Molecular Genetics*, 18(6), pp. 1028-1036.

Garrido, N., Griparic, L., Jokitalo, E., Wartiovaara, J., van der Bliek, A.M. and Spelbrink, J.N. (2003) 'Composition and dynamics of human mitochondrial nucleoids', *Mol Biol Cell*, 14(4), pp. 1583-96.

Gaubatz, J., Prashad, N. and Cutler, R.G. (1976) 'Ribosomal RNA gene dosage as a function of tissue and age for mouse and human', *Biochim Biophys Acta*, 418(3), pp. 358-75.

Gehlert, S., Bloch, W. and Suhr, F. (2015) 'Ca2+-Dependent Regulations and Signaling in Skeletal Muscle: From Electro-Mechanical Coupling to Adaptation', *International Journal of Molecular Sciences*, 16(1), p. 1066.

Gellerich, F.N., Deschauer, M., Chen, Y., Muller, T., Neudecker, S. and Zierz, S. (2002) 'Mitochondrial respiratory rates and activities of respiratory chain complexes correlate linearly with heteroplasmy of deleted mtDNA without threshold and independently of deletion size', *Biochim Biophys Acta*, 1556(1), pp. 41-52.

Gerber, J., Neumann, K., Prohl, C., Mühlenhoff, U. and Lill, R. (2004) 'The Yeast Scaffold Proteins Isu1p and Isu2p Are Required inside Mitochondria for Maturation of Cytosolic Fe/S Proteins', *Molecular and Cellular Biology*, 24(11), pp. 4848-4857.

Gillies, A.R. and Lieber, R.L. (2011) 'Structure and function of the skeletal muscle extracellular matrix', *Muscle Nerve*, 44(3), pp. 318-31.

Giorgi, C., Agnoletto, C., Bononi, A., Bonora, M., De Marchi, E., Marchi, S., Missiroli, S., Patergnani, S., Poletti, F., Rimessi, A., Suski, J.M., Wieckowski, M.R. and Pinton, P. (2012) 'Mitochondrial calcium homeostasis as potential target for mitochondrial medicine', *Mitochondrion*, 12(1), pp. 77-85.

Gorman, G.S., Schaefer, A.M., Ng, Y., Gomez, N., Blakely, E.L., Alston, C.L., Feeney, C., Horvath, R., Yu-Wai-Man, P., Chinnery, P.F., Taylor, R.W., Turnbull, D.M. and McFarland, R. (2015) 'Prevalence of nuclear and mitochondrial DNA mutations related to adult mitochondrial disease', *Annals of Neurology*, 77(5), pp. 753-759.

Goto, Y., Koga, Y., Horai, S. and Nonaka, I. (1990) 'Chronic progressive external ophthalmoplegia: a correlative study of mitochondrial DNA deletions and their phenotypic expression in muscle biopsies', *J Neurol Sci*, 100(1-2), pp. 63-9.

Goto, Y., Nonaka, I. and Horai, S. (1990) 'A mutation in the tRNALeu(UUR) gene associated with the MELAS subgroup of mitochondrial encephalomyopathies', *Nature*, 348(6302), pp. 651-653.

Goto, Y., Nonaka, I. and Horai, S. (1991) 'A new mtDNA mutation associated with mitochondrial myopathy, encephalopathy, lactic acidosis and stroke-like episodes (MELAS)', *Biochimica et Biophysica Acta (BBA) - Molecular Basis of Disease*, 1097(3), pp. 238-240.

Goto, Y., Horai, S., Matsuoka, T., Koga, Y., Nihei, K., Kobayashi, M. and Nonaka, I. (1992) 'Mitochondrial myopathy, encephalopathy, lactic acidosis, and stroke-like episodes (MELAS): A correlative study of the clinical features and mitochondrial DNA mutation', *Neurology*, 42(3), p. 545.

Grady, J.P., Campbell, G., Ratnaike, T., Blakely, E.L., Falkous, G., Nesbitt, V., Schaefer, A.M., McNally, R.J., Gorman, G.S., Taylor, R.W., Turnbull, D.M. and McFarland, R. (2014) 'Disease progression in patients with single, large-scale mitochondrial DNA deletions', *Brain*, 137(2), pp. 323-334.

Grady, J.P., Murphy, J.L., Blakely, E.L., Haller, R.G., Taylor, R.W., Turnbull, D.M. and Tuppen, H.A.L. (2014) 'Accurate Measurement of Mitochondrial DNA Deletion Level and Copy Number Differences in Human Skeletal Muscle', *PLOS ONE*, 9(12), p. e114462.

Greaves, L.C., Yu-Wai-Man, P., Blakely, E.L., Krishnan, K.J., Beadle, N.E., Kerin, J., Barron, M.J., Griffiths, P.G., Dickinson, A.J., Turnbull, D.M. and Taylor, R.W. (2010) 'Mitochondrial DNA defects and selective extraocular muscle involvement in CPEO', *Invest Ophthalmol Vis Sci*, 51(7), pp. 3340-6.

Griffiths, E.J. and Rutter, G.A. (2009) 'Mitochondrial calcium as a key regulator of mitochondrial ATP production in mammalian cells', *Biochim Biophys Acta*, 1787(11), pp. 1324-33.

Grigorieff, N. (1999) 'Structure of the respiratory NADH:ubiquinone oxidoreductase (complex I)', *Curr Opin Struct Biol*, 9(4), pp. 476-83.

Guillausseau, P.J., Massin, P., Dubois-LaForgue, D., Timsit, J., Virally, M., Gin, H., Bertin, E., Blickle, J.F., Bouhanick, B., Cahen, J., Caillat-Zucman, S., Charpentier, G., Chedin, P., Derrien, C., Ducluzeau, P.H., Grimaldi, A., Guerci, B., Kaloustian, E., Murat, A., Olivier, F., Paques, M., Paquis-Flucklinger, V., Porokhov, B., Samuel-Lajeunesse, J. and Vialettes, B. (2001) 'Maternally inherited diabetes and deafness: a multicenter study', *Ann Intern Med*, 134(9 Pt 1), pp. 721-8.

Haber, J.E. (2000) 'Partners and pathways: repairing a double-strand break', *Trends in Genetics*, 16(6), pp. 259-264.

Hagerhall, C. (1997) 'Succinate: quinone oxidoreductases. Variations on a conserved theme', *Biochim Biophys Acta*, 1320(2), pp. 107-41.

Hammans, S.R., Sweeney, M.G., Hanna, M.G., Brockington, M., Morgan-Hughes, J.A. and Harding, A.E. (1995) 'The mitochondrial DNA transfer RNALeu(UUR) A-->G(3243) mutation. A clinical and genetic study', *Brain*, 118 (Pt 3), pp. 721-34.

Hammans, S.R., Sweeney, M.G., Holt, I.J., Cooper, J.M., Toscano, A., Clark, J.B., Morgan-Hughes, J.A. and Harding, A.E. (1992) 'Evidence for intramitochondrial complementation between deleted and normal mitochondrial DNA in some patients with mitochondrial myopathy', *J Neurol Sci*, 107(1), pp. 87-92.

Hammarsund, M., Wilson, W., Corcoran, M., Merup, M., Einhorn, S., Grander, D. and Sangfelt, O. (2001) 'Identification and characterization of two novel human mitochondrial elongation factor genes, hEFG2 and hEFG1, phylogenetically conserved through evolution', *Hum Genet*, 109(5), pp. 542-50.

Hanson, J. and Huxley, H.E. (1953) 'Structural basis of the cross-striations in muscle', *Nature*, 172(4377), pp. 530-2.

Hardie, D.G., Ross, F.A. and Hawley, S.A. (2012) 'AMPK: a nutrient and energy sensor that maintains energy homeostasis', *Nat Rev Mol Cell Biol*, 13(4), pp. 251-62.

Hardy, S.A., Blakely, E.L., Purvis, A.I., Rocha, M.C., Ahmed, S., Falkous, G., Poulton, J., Rose, M.R., O'Mahony, O., Bermingham, N., Dougan, C.F., Ng, Y.S., Horvath, R., Turnbull, D.M., Gorman, G.S. and Taylor, R.W. (2016) 'Pathogenic mtDNA mutations causing mitochondrial myopathy: The need for muscle biopsy', *Neurology: Genetics*, 2(4), p. e82.

Hatefi, Y. (1985) 'The mitochondrial electron transport and oxidative phosphorylation system', *Annu Rev Biochem*, 54, pp. 1015-69.

Hattori, K., Tanaka, M., Sugiyama, S., Obayashi, T., Ito, T., Satake, T., Hanaki, Y., Asai, J., Nagano, M. and Ozawa, T. (1991) 'Age-dependent increase in deleted mitochondrial DNA in the human heart: possible contributory factor to presbycardia', *Am Heart J*, 121(6 Pt 1), pp. 1735-42.

Hayashi, J., Ohta, S., Kikuchi, A., Takemitsu, M., Goto, Y. and Nonaka, I. (1991) 'Introduction of disease-related mitochondrial DNA deletions into HeLa cells lacking mitochondrial DNA results in mitochondrial dysfunction', *Proceedings of the National Academy of Sciences*, 88(23), pp. 10614-10618.

He, J., Mao, C.-C., Reyes, A., Sembongi, H., Di Re, M., Granycome, C., Clippingdale, A.B., Fearnley, I.M., Harbour, M., Robinson, A.J., Reichelt, S., Spelbrink, J.N., Walker, J.E. and Holt, I.J. (2007) 'The AAA(+) protein ATAD3 has displacement loop binding properties and is involved in mitochondrial nucleoid organization', *The Journal of Cell Biology*, 176(2), pp. 141-146.

He, L., Chinnery, P.F., Durham, S.E., Blakely, E.L., Wardell, T.M., Borthwick, G.M., Taylor, R.W. and Turnbull, D.M. (2002) 'Detection and quantification of mitochondrial DNA deletions in individual cells by real-time PCR', *Nucleic Acids Res*, 30(14), p. e68.

Head, B., Griparic, L., Amiri, M., Gandre-Babbe, S. and van der Bliek, A.M. (2009) 'Inducible proteolytic inactivation of OPA1 mediated by the OMA1 protease in mammalian cells', *The Journal of Cell Biology*, 187(7), pp. 959-966.

Hegde, M.L., Izumi, T. and Mitra, S. (2012) 'Oxidized Base Damage and Single-Strand Break Repair in Mammalian Genomes: Role of Disordered Regions and Posttranslational Modifications in Early Enzymes', *Progress in molecular biology and translational science*, 110, pp. 123-153.

Helm, M., Brulé, H., Degoul, F., Cepanec, C., Leroux, J.-P., Giegé, R. and Florentz, C. (1998) 'The presence of modified nucleotides is required for cloverleaf folding of a human mitochondrial tRNA', *Nucleic Acids Research*, 26(7), pp. 1636-1643.

Henderson, A.S., Warburton, D. and Atwood, K.C. (1972) 'Location of Ribosomal DNA in the Human Chromosome Complement', *Proceedings of the National Academy of Sciences of the United States of America*, 69(11), pp. 3394-3398.

Herlan, M., Vogel, F., Bornhovd, C., Neupert, W. and Reichert, A.S. (2003) 'Processing of Mgm1 by the rhomboid-type protease Pcp1 is required for maintenance of mitochondrial morphology and of mitochondrial DNA', *J Biol Chem*, 278(30), pp. 27781-8.

Hess, J.F., Parisi, M.A., Bennett, J.L. and Clayton, D.A. (1991) 'Impairment of mitochondrial transcription termination by a point mutation associated with the MELAS subgroup of mitochondrial encephalomyopathies', *Nature*, 351(6323), pp. 236-239.

Hirano, M., Ricci, E., Koenigsberger, M.R., Defendini, R., Pavlakis, S.G., DeVivo, D.C., DiMauro, S. and Rowland, L.P. (1992) 'Melas: an original case and clinical criteria for diagnosis', *Neuromuscul Disord*, 2(2), pp. 125-35.

Hirst, J., Carroll, J., Fearnley, I.M., Shannon, R.J. and Walker, J.E. (2003) 'The nuclear encoded subunits of complex I from bovine heart mitochondria', *Biochim Biophys Acta*, 1604(3), pp. 135-50.

Hockenbery, D., Nunez, G., Milliman, C., Schreiber, R.D. and Korsmeyer, S.J. (1990) 'Bcl-2 is an inner mitochondrial membrane protein that blocks programmed cell death', *Nature*, 348(6299), pp. 334-6.

Hoekstra, A.S. and Bayley, J.P. (2013) 'The role of complex II in disease', *Biochim Biophys Acta*, 1827(5), pp. 543-51.

Hofer, A.M., Curci, S., Doble, M.A., Brown, E.M. and Soybel, D.I. (2000) 'Intercellular communication mediated by the extracellular calcium-sensing receptor', *Nat Cell Biol*, 2(7), pp. 392-398.

Hofhaus, G., Weiss, H. and Leonard, K. (1991) 'Electron microscopic analysis of the peripheral and membrane parts of mitochondrial NADH dehydrogenase (complex I)', *J Mol Biol*, 221(3), pp. 1027-43.

Holt, I.J., Harding, A.E. and Morgan-Hughes, J.A. (1988) 'Deletions of muscle mitochondrial DNA in patients with mitochondrial myopathies', *Nature*, 331(6158), pp. 717-719.

Holt, I.J., Harding, A.E., Cooper, J.M., Schapira, A.H., Toscano, A., Clark, J.B. and Morgan-Hughes, J.A. (1989) 'Mitochondrial myopathies: clinical and biochemical features of 30 patients with major deletions of muscle mitochondrial DNA', *Ann Neurol*, 26(6), pp. 699-708.

Holt, I.J., Harding, A.E., Petty, R.K. and Morgan-Hughes, J.A. (1990) 'A new mitochondrial disease associated with mitochondrial DNA heteroplasmy', *Am J Hum Genet*, 46(3), pp. 428-33.

Holt, I.J., Lorimer, H.E. and Jacobs, H.T. (2000) 'Coupled Leading- and Lagging-Strand Synthesis of Mammalian Mitochondrial DNA', *Cell*, 100(5), pp. 515-524.

Hood, D.A. (2001) 'Invited Review: contractile activity-induced mitochondrial biogenesis in skeletal muscle', *J Appl Physiol (1985)*, 90(3), pp. 1137-57.

Hopkins, P.M. (2006) 'Skeletal muscle physiology', *Continuing Education in Anaesthesia, Critical Care & Pain*, 6(1), pp. 1-6.

Howell, N., Bindoff, L.A., McCullough, D.A., Kubacka, I., Poulton, J., Mackey, D., Taylor, L. and Turnbull, D.M. (1991) 'Leber hereditary optic neuropathy: identification of the same mitochondrial ND1 mutation in six pedigrees', *Am J Hum Genet*, 49(5), pp. 939-50.

Huang, J., Tan, L., Shen, R., Zhang, L., Zuo, H. and Wang, D.W. (2016) 'Decreased Peripheral Mitochondrial DNA Copy Number is Associated with the Risk of Heart Failure and Long-term Outcomes', *Medicine (Baltimore)*, 95(15), p. e3323.

Huang, X., Sun, L., Ji, S., Zhao, T., Zhang, W., Xu, J., Zhang, J., Wang, Y., Wang, X., Franzini-Armstrong, C., Zheng, M. and Cheng, H. (2013) 'Kissing and nanotunneling mediate intermitochondrial communication in the heart', *Proc Natl Acad Sci U S A*, 110(8), pp. 2846-51.

Hüttemann, M., Pecina, P., Rainbolt, M., Sanderson, T.H., Kagan, V.E., Samavati, L., Doan, J.W. and Lee, I. (2011) 'The multiple functions of cytochrome c and their regulation in life and death decisions of the mammalian cell: from respiration to apoptosis', *Mitochondrion*, 11(3), pp. 369-381.

Huttenlocher, P.R., Solitare, G.B. and Adams, G. (1976) 'Infantile diffuse cerebral degeneration with hepatic cirrhosis', *Arch Neurol*, 33(3), pp. 186-92.

Ishikawa, Y., Goto, Y., Ishikawa, Y. and Minami, R. (2000) 'Progression in a case of Kearns-Sayre syndrome', *J Child Neurol*, 15(11), pp. 750-5.

Iwasaki, T., Matsuura, K. and Oshima, T. (1995) 'Resolution of the Aerobic Respiratory System of the Thermoacidophilic Archaeon, Sulfolobus sp. Strain 7:: I.The archaeal terminal oxidase supercomplex is a functional fusion of respiratory complexes iii and iv with no C-type cytochromes', *Journal of Biological Chemistry*, 270(52), pp. 30881-30892.

James, D.I., Parone, P.A., Mattenberger, Y. and Martinou, J.C. (2003) 'hFis1, a novel component of the mammalian mitochondrial fission machinery', *J Biol Chem*, 278(38), pp. 36373-9.

Janssen, A.J., Smeitink, J.A. and van den Heuvel, L.P. (2003) 'Some practical aspects of providing a diagnostic service for respiratory chain defects', *Ann Clin Biochem*, 40(Pt 1), pp. 3-8.

Jensen, P.K. (1966) 'Antimycin-insensitive oxidation of succinate and reduced nicotinamide-adenine dinucleotide in electron-transport particles. I. pH dependency and hydrogen peroxide formation', *Biochim Biophys Acta*, 122(2), pp. 157-66.

Jenuth, J.P., Peterson, A.C., Fu, K. and Shoubridge, E.A. (1996) 'Random genetic drift in the female germline explains the rapid segregation of mammalian mitochondrial DNA', *Nat Genet*, 14(2), pp. 146-151.

Jeppesen, T.D., Schwartz, M., Frederiksen, A.L., Wibrand, F., Olsen, D.B. and Vissing, J. (2006) 'Muscle phenotype and mutation load in 51 persons with the 3243A>G mitochondrial DNA mutation', *Arch Neurol*, 63(12), pp. 1701-6.

Johns, D.R., Neufeld, M.J. and Park, R.D. (1992) 'An ND-6 mitochondrial DNA mutation associated with Leber hereditary optic neuropathy', *Biochem Biophys Res Commun*, 187(3), pp. 1551-7.

Johnson, M.A., Polgar, J., Weightman, D. and Appleton, D. (1973) 'Data on the distribution of fibre types in thirty-six human muscles: An autopsy study', *Journal of the Neurological Sciences*, 18(1), pp. 111-129.

Jornayvaz, F.R. and Shulman, G.I. (2010) 'Regulation of mitochondrial biogenesis', *Essays in biochemistry*, 47, p. 10.1042/bse0470069.

José Antonio, E. (2016) 'Supramolecular Organization of Respiratory Complexes', *Annual Review of Physiology*, 78(1), pp. 533-561.

Kamiya, H. (2003) 'Mutagenic potentials of damaged nucleic acids produced by reactive oxygen/nitrogen species: approaches using synthetic oligonucleotides and nucleotides: survey and summary', *Nucleic Acids Res*, 31(2), pp. 517-31.

Kaneda, H., Hayashi, J., Takahama, S., Taya, C., Lindahl, K.F. and Yonekawa, H. (1995) 'Elimination of paternal mitochondrial DNA in intraspecific crosses during early mouse embryogenesis', *Proceedings of the National Academy of Sciences of the United States of America*, 92(10), pp. 4542-4546.

Kanki, T. and Klionsky, D.J. (2008) 'Mitophagy in yeast occurs through a selective mechanism', *J Biol Chem*, 283(47), pp. 32386-93.

Kasamatsu, H., Robberson, D.L. and Vinograd, J. (1971) 'A novel closed-circular mitochondrial DNA with properties of a replicating intermediate', *Proc Natl Acad Sci U S A*, 68(9), pp. 2252-7.

Kawakami, Y., Sakuta, R., Hashimoto, K., Fujino, O., Fujita, T., Hida, M., Horai, S., Goto, Y. and Nonaka, I. (1994) 'Mitochondrial myopathy with progressive decrease in mitochondrial tRNA(Leu)(UUR) mutant genomes', *Ann Neurol*, 35(3), pp. 370-3.

Kearns, T.P. and Sayre, G.P. (1958) 'Retinitis pigmentosa, external ophthalmophegia, and complete heart block: unusual syndrome with histologic study in one of two cases', *AMA Arch Ophthalmol*, 60(2), pp. 280-9.

Kelly, D.P. and Scarpulla, R.C. (2004) 'Transcriptional regulatory circuits controlling mitochondrial biogenesis and function', *Genes Dev*, 18(4), pp. 357-68.

Kelly, R.D.W., Mahmud, A., McKenzie, M., Trounce, I.A. and St John, J.C. (2012) 'Mitochondrial DNA copy number is regulated in a tissue specific manner by DNA methylation of the nuclear-encoded DNA polymerase gamma A', *Nucleic Acids Research*, 40(20), pp. 10124-10138.

Kerr, J.F., Wyllie, A.H. and Currie, A.R. (1972) 'Apoptosis: a basic biological phenomenon with wide-ranging implications in tissue kinetics', *Br J Cancer*, 26(4), pp. 239-57.

King, M.P., Koga, Y., Davidson, M. and Schon, E.A. (1992) 'Defects in mitochondrial protein synthesis and respiratory chain activity segregate with the tRNA(Leu(UUR)) mutation associated with mitochondrial myopathy, encephalopathy, lactic acidosis, and strokelike episodes', *Molecular and Cellular Biology*, 12(2), pp. 480-490.

Kirichok, Y., Krapivinsky, G. and Clapham, D.E. (2004) 'The mitochondrial calcium uniporter is a highly selective ion channel', *Nature*, 427(6972), pp. 360-364.

Kirino, Y., Goto, Y., Campos, Y., Arenas, J. and Suzuki, T. (2005) 'Specific correlation between the wobble modification deficiency in mutant tRNAs and the clinical features of a human mitochondrial disease', *Proceedings of the National Academy of Sciences of the United States of America*, 102(20), pp. 7127-7132.

Kirino, Y., Yasukawa, T., Ohta, S., Akira, S., Ishihara, K., Watanabe, K. and Suzuki, T. (2004) 'Codon-specific translational defect caused by a wobble modification deficiency in mutant tRNA from a human mitochondrial disease', *Proc Natl Acad Sci U S A*, 101(42), pp. 15070-5.

Kispal, G., Csere, P., Prohl, C. and Lill, R. (1999) 'The mitochondrial proteins Atm1p and Nfs1p are essential for biogenesis of cytosolic Fe/S proteins', *The EMBO Journal*, 18(14), pp. 3981-3989.

Koc, E.C. and Spremulli, L.L. (2002) 'Identification of mammalian mitochondrial translational initiation factor 3 and examination of its role in initiation complex formation with natural mRNAs', *J Biol Chem*, 277(38), pp. 35541-9.

Koga, Y., Akita, Y., Takane, N., Sato, Y. and Kato, H. (2000) 'Heterogeneous presentation in A3243G mutation in the mitochondrial tRNALeu(UUR) gene', *Archives of Disease in Childhood*, 82(5), pp. 407-411.

Koga, Y., Davidson, M., Schon, E.A. and King, M.P. (1993) 'Fine mapping of mitochondrial RNAs derived from the mtDNA region containing a point mutation associated with MELAS', *Nucleic Acids Research*, 21(3), pp. 657-662.

Korhonen, J.A., Gaspari, M. and Falkenberg, M. (2003) 'TWINKLE Has 5′ → 3′ DNA Helicase Activity and Is Specifically Stimulated by Mitochondrial Single-stranded DNA-binding Protein', *Journal of Biological Chemistry*, 278(49), pp. 48627-48632.

Korhonen, J.A., Pham, X.H., Pellegrini, M. and Falkenberg, M. (2004) 'Reconstitution of a minimal mtDNA replisome in vitro', *The EMBO Journal*, 23(12), pp. 2423-2429.

Korr, H., Kurz, C., Seidler, T.O., Sommer, D. and Schmitz, C. (1998) 'Mitochondrial DNA synthesis studied autoradiographically in various cell types in vivo', *Brazilian Journal of Medical and Biological Research*, 31, pp. 289-298.

Koshiba, T., Detmer, S.A., Kaiser, J.T., Chen, H., McCaffery, J.M. and Chan, D.C. (2004) 'Structural basis of mitochondrial tethering by mitofusin complexes', *Science*, 305(5685), pp. 858-62.

Kraytsberg, Y., Kudryavtseva, E., McKee, A.C., Geula, C., Kowall, N.W. and Khrapko, K. (2006) 'Mitochondrial DNA deletions are abundant and cause functional impairment in aged human substantia nigra neurons', *Nat Genet*, 38(5), pp. 518-520.

Krebs, C., Agar, J.N., Smith, A.D., Frazzon, J., Dean, D.R., Huynh, B.H. and Johnson, M.K. (2001) 'IscA, an Alternate Scaffold for Fe−S Cluster Biosynthesis', *Biochemistry*, 40(46), pp. 14069-14080.

Krebs, H.A. and Johnson, W.A. (1937) 'The role of citric acid in intermediate metabolism in animal tissues', *Enzymologia*, 4, pp. 148-156.

Krishnan, K.J., Bender, A., Taylor, R.W. and Turnbull, D.M. (2007) 'A multiplex real-time PCR method to detect and quantify mitochondrial DNA deletions in individual cells', *Anal Biochem*, 370(1), pp. 127-9.

Krishnan, K.J., Reeve, A.K., Samuels, D.C., Chinnery, P.F., Blackwood, J.K., Taylor, R.W., Wanrooij, S., Spelbrink, J.N., Lightowlers, R.N. and Turnbull, D.M. (2008) 'What causes mitochondrial DNA deletions in human cells?', *Nat Genet*, 40(3), pp. 275-279.

Kroemer, G., Dallaporta, B. and Resche-Rigon, M. (1998) 'The mitochondrial death/life regulator in apoptosis and necrosis', *Annu Rev Physiol*, 60, pp. 619-42.

Kruse, B., Narasimhan, N. and Attardi, G. (1989) 'Termination of transcription in human mitochondria: Identification and purification of a DNA binding protein factor that promotes termination', *Cell*, 58(2), pp. 391-397.

Kukat, C., Wurm, C.A., Spahr, H., Falkenberg, M., Larsson, N.G. and Jakobs, S. (2011) 'Super-resolution microscopy reveals that mammalian mitochondrial nucleoids have a uniform size and frequently contain a single copy of mtDNA', *Proc Natl Acad Sci USA*, 108(33), pp.13534-9.

Kunkel, T.A. and Loeb, L.A. (1981) 'Fidelity of mammalian DNA polymerases', *Science*, 213(4509), pp. 765-7.

Larsen, N.B., Rasmussen, M. and Rasmussen, L.J. (2005) 'Nuclear and mitochondrial DNA repair: similar pathways?', *Mitochondrion*, 5(2), pp. 89-108.

Larsson, N.G., Holme, E., Kristiansson, B., Oldfors, A. and Tulinius, M. (1990) 'Progressive increase of the mutated mitochondrial DNA fraction in Kearns-Sayre syndrome', *Pediatr Res*, 28(2), pp. 131-6.

Lax, N.Z., Grady, J., Laude, A., Chan, F., Hepplewhite, P.D., Gorman, G., Whittaker, R.G., Ng, Y., Cunningham, M.O. and Turnbull, D.M. (2016) 'Extensive respiratory chain defects in inhibitory interneurones in patients with mitochondrial disease', *Neuropathology and Applied Neurobiology*, 42(2), pp. 180-193.

Lax, N.Z., Hepplewhite, P.D., Reeve, A.K., Nesbitt, V., McFarland, R., Jaros, E., Taylor, R.W. and Turnbull, D.M. (2012) 'Cerebellar Ataxia in Patients With Mitochondrial DNA Disease: A

Molecular Clinicopathological Study', *Journal of Neuropathology & Experimental Neurology*, 71(2), pp. 148-161.

Lee, Y.J., Jeong, S.Y., Karbowski, M., Smith, C.L. and Youle, R.J. (2004) 'Roles of the mammalian mitochondrial fission and fusion mediators Fis1, Drp1, and Opa1 in apoptosis', *Mol Biol Cell*, 15(11), pp. 5001-11.

Legesse-Miller, A., Massol, R.H. and Kirchhausen, T. (2003) 'Constriction and Dnm1p Recruitment Are Distinct Processes in Mitochondrial Fission', *Molecular Biology of the Cell*, 14(5), pp. 1953-1963.

Leigh, T.F. and Thompson, E.A. (1951) 'Pulmonary metastatic sarcoma with associated pneumothorax', *Am J Roentgenol Radium Ther*, 66(6), pp. 900-2.

Lenaz, G. and Genova, M.L. (2010) 'Structure and organization of mitochondrial respiratory complexes: a new understanding of an old subject', *Antioxid Redox Signal*, 12(8), pp. 961-1008.

Lestienne, P. (1987) 'Evidence for a direct role of the DNA polymerase gamma in the replication of the human mitochondrial DNA in vitro', *Biochem Biophys Res Commun*, 146(3), pp. 1146-53.

Lestienne, P. and Ponsot, G. (1988) 'Kearns-Sayre syndrome with muscle mitochondrial DNA deletion', *Lancet*, 1(8590), p. 885.

Lexell, J. (1995) 'Human aging, muscle mass, and fiber type composition', *J Gerontol A Biol Sci Med Sci*, 50 Spec No, pp. 11-6.

Lieber, R.L. (2010) *Skeletal muscle structure, function and plastictity.* Philadelphia, USA: Wolters Kluwer/Lippincott Williams & Wilkins Health.

Lightowlers, R.N., Chinnery, P.F., Turnbull, D.M. and Howell, N. (1997) 'Mammalian mitochondrial genetics: heredity, heteroplasmy and disease', *Trends Genet*, 13(11), pp.450-5.

Lill, R., Diekert, K., Kaut, A., Lange, H., Pelzer, W., Prohl, C. and Kispal, G. (1999) 'The essential role of mitochondria in the biogenesis of cellular iron-sulfur proteins', *Biol Chem*, 380(10), pp. 1157-66.

Ling, M., Merante, F., Chen, H.-S., Duff, C., Duncan, A.M.V. and Robinson, B.H. (1997) 'The human mitochondrial elongation factor tu (EF-Tu) gene: cDNA sequence, genomic localization, genomic structure, and identification of a pseudogene', *Gene*, 197(1–2), pp. 325-336.

Linnane, A.W., Baumer, A., Maxwell, R.J., Preston, H., Zhang, C. and Marzuki, S. (1990) 'Mitochondrial gene mutation: The ageing process and degenerative diseases', *Biochemistry International*, 22(6), pp. 1067-1076.

Liu, V.W., Zhang, C. and Nagley, P. (1998) 'Mutations in mitochondrial DNA accumulate differentially in three different human tissues during ageing', *Nucleic Acids Research*, 26(5), pp. 1268-1275.

Lodish H, Berk A, Zipursky SL, et al. (2000a) *Molecular Cell Biology 4th edition*. *Section 16.2, Electron Transport and Oxidative Phosphorylation*. New York: W. H. Freeman and Company.

Lodish H, Berk A, Zipursky SL, et al. (2000b) *Molecular Cell Biology 4th edition*. *Section 11.6, Processing of rRNA and tRNA*. New York: W. H. Freeman and Company.

Lopez-Gallardo, E., Lopez-Perez, M.J., Montoya, J. and Ruiz-Pesini, E. (2009) 'CPEO and KSS differ in the percentage and location of the mtDNA deletion', *Mitochondrion*, 9(5), pp. 314-7.

Loschen, G., Azzi, A., Richter, C. and Flohé, L. (1974) 'Superoxide radicals as precursors of mitochondrial hydrogen peroxide', *FEBS Letters*, 42(1), pp. 68-72.

Luo, S.-M., Ge, Z.-J., Wang, Z.-W., Jiang, Z.-Z., Wang, Z.-B., Ouyang, Y.-C., Hou, Y., Schatten, H. and Sun, Q.-Y. (2013) 'Unique insights into maternal mitochondrial inheritance in mice', *Proceedings of the National Academy of Sciences of the United States of America*, 110(32), pp. 13038-13043.

Ma, L. and Spremulli, L.L. (1995) 'Cloning and sequence analysis of the human mitochondrial translational initiation factor 2 cDNA', *J Biol Chem*, 270(4), pp. 1859-65.

MacIntosh, B.R., Gardiner, P.F. and McComas, A.J. (2006) *Skeletal muscle: form and function (second edition)*. Second edition edn. USA: Human Kinetics.

Mancuso, M., Orsucci, D., Angelini, C., Bertini, E., Carelli, V., Comi, G.P., Donati, A., Minetti, C., Moggio, M., Mongini, T., Servidei, S., Tonin, P., Toscano, A., Uziel, G., Bruno, C., Ienco, E.C., Filosto, M., Lamperti, C., Catteruccia, M., Moroni, I., Musumeci, O., Pegoraro, E., Ronchi, D., Santorelli, F.M., Sauchelli, D., Scarpelli, M., Sciacco, M., Valentino, M.L., Vercelli, L., Zeviani, M. and Siciliano, G. (2014) 'The m.3243A>G mitochondrial DNA mutation and related phenotypes. A matter of gender?', *Journal of Neurology*, 261(3), pp. 504-510.

Mancuso, M., Orsucci, D., Angelini, C., Bertini, E., Carelli, V., Comi, G.P., Donati, M.A., Federico, A., Minetti, C., Moggio, M., Mongini, T., Santorelli, F.M., Servidei, S., Tonin, P., Toscano, A., Bruno, C., Bello, L., Caldarazzo Ienco, E., Cardaioli, E., Catteruccia, M., Da Pozzo, P., Filosto, M., Lamperti, C., Moroni, I., Musumeci, O., Pegoraro, E., Ronchi, D., Sauchelli, D., Scarpelli, M., Sciacco, M., Valentino, M.L., Vercelli, L., Zeviani, M. and Siciliano, G. (2015) 'Redefining phenotypes associated with mitochondrial DNA single deletion', *J Neurol*, 262(5), pp. 1301-9.

Mannella, C.A., Marko, M. and Buttle, K. (1997) 'Reconsidering mitochondrial structure: new views of an old organelle', *Trends Biochem Sci*, 22(2), pp. 37-8.

Mapolelo, D.T., Zhang, B., Randeniya, S., Albetel, A.-N., Li, H., Couturier, J., Outten, C.E., Rouhier, N. and Johnson, M.K. (2013) 'Monothiol glutaredoxins and A-type proteins: partners in Fe-S cluster trafficking', *Dalton Transactions*, 42(9), pp. 3107-3115.

Marcuello, A., González-Alonso, J., Calbet, J.A.L., Damsgaard, R., López-Pérez, M.J. and Díez-Sánchez, C. (2005) 'Skeletal muscle mitochondrial DNA content in exercising humans', *Journal of Applied Physiology*, 99(4), pp. 1372-1377.

Margulis, L. (1971) 'The Origin of Plant and Animal Cells: The serial symbiosis view of the origin of higher cells suggests that the customary division of living things into two kingdoms should be reconsidered', *American Scientist*, 59(2), pp. 230-235.

Mariotti, C., Savarese, N., Suomalainen, A., Rimoldi, M., Comi, G., Prelle, A., Antozzi, C., Servidei, S., Jarre, L., DiDonato, S. and Zeviani, M. (1995) 'Genotype to phenotype correlations in mitochondrial encephalomyopathies associated with the A3243G mutation of mitochondrial DNA', *J Neurol*, 242(5), pp. 304-12.

Mariotti, C., Tiranti, V., Carrara, F., Dallapiccola, B., DiDonato, S. and Zeviani, M. (1994) 'Defective respiratory capacity and mitochondrial protein synthesis in transformant cybrids harboring the tRNA(Leu(UUR)) mutation associated with maternally inherited myopathy and cardiomyopathy', *J Clin Invest*, 93(3), pp. 1102-7.

Martin, W. and Muller, M. (1998) 'The hydrogen hypothesis for the first eukaryote', *Nature*, 392(6671), pp. 37-41.

Marzuki, S., Berkovic, S.F., Saifuddin Noer, A., Kapsa, R.M., Kalnins, R.M., Byrne, E., Sasmono, T. and Sudoyo, H. (1997) 'Developmental genetics of deleted mtDNA in mitochondrial oculomyopathy', *J Neurol Sci*, 145(2), pp. 155-62.

Matthews, P.M., Hopkin, J., Brown, R.M., Stephenson, J.B., Hilton-Jones, D. and Brown, G.K. (1994) 'Comparison of the relative levels of the 3243 (A-->G) mtDNA mutation in heteroplasmic adult and fetal tissues', *J Med Genet*, 31(1), pp. 41-4.

Mattson, M.P. and Chan, S.L. (2003) 'Calcium orchestrates apoptosis', *Nat Cell Biol*, 5(12), pp. 1041-3.

McCormack, J.G., Halestrap, A.P. and Denton, R.M. (1990) 'Role of calcium ions in regulation of mammalian intramitochondrial metabolism', *Physiol Rev*, 70(2), pp. 391-425.

McDonnell, M.T., Schaefer, A.M., Blakely, E.L., McFarland, R., Chinnery, P.F., Turnbull, D.M. and Taylor, R.W. (2004) 'Noninvasive diagnosis of the 3243A>G mitochondrial DNA mutation using urinary epithelial cells', *Eur J Hum Genet*, 12(9), pp. 778-781.

McFarland, R., Taylor, R.W. and Turnbull, D.M. (2010) 'A neurological perspective on mitochondrial disease', *The Lancet Neurology*, 9(8), pp. 829-840.

McKinney, E.A. and Oliveira, M.T. (2013) 'Replicating animal mitochondrial DNA', *Genetics and Molecular Biology*, 36(3), pp. 308-315.

Mears, J.A., Lackner, L.L., Fang, S., Ingerman, E., Nunnari, J. and Hinshaw, J.E. (2011) 'Conformational changes in Dnm1 support a contractile mechanism for mitochondrial fission', *Nat Struct Mol Biol*, 18(1), pp. 20-26.

Mehrazin, M., Shanske, S., Kaufmann, P., Wei, Y., Coku, J., Engelstad, K., Naini, A., De Vivo, D.C. and DiMauro, S. (2009) 'Longitudinal changes of mtDNA A3243G mutation load and level of functioning in MELAS', *Am J Med Genet A*, 149a(4), pp. 584-7.

Meissner, C., Lorenz, H., Weihofen, A., Selkoe, D.J. and Lemberg, M.K. (2011) 'The mitochondrial intramembrane protease PARL cleaves human Pink1 to regulate Pink1 trafficking', *Journal of Neurochemistry*, 117(5), pp. 856-867.

Melov, S., Shoffner, J.M., Kaufman, A. and Wallace, D.C. (1995) 'Marked increase in the number and variety of mitochondrial DNA rearrangements in aging human skeletal muscle', *Nucleic Acids Research*, 23(20), pp. 4122-4126.

Miller, F.J., Rosenfeldt, F.L., Zhang, C., Linnane, A.W. and Nagley, P. (2003) 'Precise determination of mitochondrial DNA copy number in human skeletal and cardiac muscle by a PCR-based assay: lack of change of copy number with age', *Nucleic Acids Research*, 31(11), pp. e61-e61.

Milner, D.J., Mavroidis, M., Weisleder, N. and Capetanaki, Y. (2000) 'Desmin Cytoskeleton Linked to Muscle Mitochondrial Distribution and Respiratory Function', *The Journal of Cell Biology*, 150(6), pp. 1283-1298.

Mimaki, M., Wang, X., McKenzie, M., Thorburn, D.R. and Ryan, M.T. (2012) 'Understanding mitochondrial complex I assembly in health and disease', *Biochimica et Biophysica Acta (BBA) - Bioenergetics*, 1817(6), pp. 851-862.

Mita, S., Schmidt, B., Schon, E.A., DiMauro, S. and Bonilla, E. (1989) 'Detection of "deleted" mitochondrial genomes in cytochrome-c oxidase-deficient muscle fibers of a patient with Kearns-Sayre syndrome', *Proc Natl Acad Sci U S A*, 86(23), pp. 9509-13.

Mitchell, P. (1961) 'Coupling of phosphorylation to electron and hydrogen transfer by a chemi-osmotic type of mechanism', *Nature*, 191, pp. 144-8.

Mitchell, P. (1975) 'The protonmotive Q cycle: A general formulation', *FEBS Letters*, 59(2), pp. 137-139.

Montoya, J., Christianson, T., Levens, D., Rabinowitz, M. and Attardi, G. (1982) 'Identification of initiation sites for heavy-strand and light-strand transcription in human mitochondrial DNA', *Proc Natl Acad Sci U S A*, 79(23), pp. 7195-9.

Moraes, C.T., Ciacci, F., Silvestri, G., Shanske, S., Sciacco, M., Hirano, M., Schon, E.A., Bonilla, E. and DiMauro, S. (1993) 'Atypical clinical presentations associated with the MELAS mutation at position 3243 of human mitochondrial DNA', *Neuromuscular Disorders*, 3(1), pp. 43-50.

Moraes, C.T., DiMauro, S., Zeviani, M., Lombes, A., Shanske, S., Miranda, A.F., Nakase, H., Bonilla, E., Werneck, L.C., Servidei, S. and et al. (1989) 'Mitochondrial DNA deletions in progressive external ophthalmoplegia and Kearns-Sayre syndrome', *N Engl J Med*, 320(20), pp. 1293-9.

Moraes, C.T., DiMauro, S., Zeviani, M., Lombes, A., Shanske, S., Miranda, A.F., Nakase, H., Bonilla, E., Werneck, L.C., Servidei, S., Nonaka, I., Koga, Y., Spiro, A.J., W. Brownell, A.K., Schmidt, B., Schotland, D.L., Zupanc, M., DeVivo, D.C., Schon, E.A. and Rowland, L.P. (1989) 'Mitochondrial DNA Deletions in Progressive External Ophthalmoplegia and Kearns-Sayre Syndrome', *New England Journal of Medicine*, 320(20), pp. 1293-1299.

Moraes, C.T., Ricci, E., Petruzzella, V., Shanske, S., DiMauro, S., Schon, E.A. and Bonilla, E. (1992) 'Molecular analysis of the muscle pathology associated with mitochondrial DNA deletions', *Nat Genet*, 1(5), pp. 359-367.

Moreno-Lastres, D., Fontanesi, F., García-Consuegra, I., Martín, M.A., Arenas, J., Barrientos, A. and Ugalde, C. (2012) 'Mitochondrial Complex I plays an Essential Role in Human Respirasome Assembly', *Cell Metabolism*, 15(3), pp. 324-335.

Morgan-Hughes, J.A., Sweeney, M.G., Cooper, J.M., Hammans, S.R., Brockington, M., Schapira, A.H.V., Harding, A.E. and Clark, J.B. (1995) 'Mitochondrial DNA (mtDNA) diseases: correlation of genotype to phenotype', *Biochimica et Biophysica Acta (BBA) - Molecular Basis of Disease*, 1271(1), pp. 135-140.

Mozdy, A.D., McCaffery, J.M. and Shaw, J.M. (2000) 'Dnm1p Gtpase-Mediated Mitochondrial Fission Is a Multi-Step Process Requiring the Novel Integral Membrane Component Fis1p', *The Journal of Cell Biology*, 151(2), pp. 367-380.

Mühlenhoff, U., Gerber, J., Richhardt, N. and Lill, R. (2003) 'Components involved in assembly and dislocation of iron–sulfur clusters on the scaffold protein Isu1p', *The EMBO Journal*, 22(18), pp. 4815-4825.

Munn, E.A. (1974) *The Structure of Mitochondria*. Academic Press London and New York.
Murphy, J.L., Ratnaike, T.E., Shang, E., Falkous, G., Blakely, E.L., Alston, C.L., Taivassalo, T., Haller, R.G., Taylor, R.W. and Turnbull, D.M. (2012) 'Cytochrome c oxidase-intermediate fibres: Importance in understanding the pathogenesis and treatment of mitochondrial myopathy', *Neuromuscular Disorders*, 22(8), pp. 690-698.

Murphy, MP. (2009) 'How mitochondria produce reactive oxygen species', *Biochemical Journal*, 417(1), pp. 1-13.

Nakase, H., Moraes, C.T., Rizzuto, R., Lombes, A., DiMauro, S. and Schon, E.A. (1990) 'Transcription and translation of deleted mitochondrial genomes in Kearns-Sayre syndrome: implications for pathogenesis', *Am J Hum Genet*, 46(3), pp. 418-27.

Narendra, D., Tanaka, A., Suen, D.-F. and Youle, R.J. (2008) 'Parkin is recruited selectively to impaired mitochondria and promotes their autophagy', *The Journal of Cell Biology*, 183(5), pp. 795-803.

Nass, S. and Nass, M.M.K. (1963) 'INTRAMITOCHONDRIAL FIBERS WITH DNA CHARACTERISTICS : II. Enzymatic and Other Hydrolytic Treatments', *The Journal of Cell Biology*, 19(3), pp. 613-629.

Naviaux, R.K. and Nguyen, K.V. (2004) 'POLG mutations associated with Alpers' syndrome and mitochondrial DNA depletion', *Annals of Neurology*, 55(5), pp. 706-712.

Nesbitt, V., Pitceathly, R.D.S., Turnbull, D.M., Taylor, R.W., Sweeney, M.G., Mudanohwo, E.E., Rahman, S., Hanna, M.G. and McFarland, R. (2013) 'The UK MRC Mitochondrial Disease Patient Cohort Study: clinical phenotypes associated with the m.3243A>G mutation—implications for diagnosis and management', *Journal of Neurology, Neurosurgery & Psychiatry*.

Ng, Y.S., Grady, J.P., Lax, N.Z., Bourke, J.P., Alston, C.L., Hardy, S.A., Falkous, G., Schaefer, A.G., Radunovic, A., Mohiddin, S.A., Ralph, M., Alhakim, A., Taylor, R.W., McFarland, R., Turnbull, D.M. and Gorman, G.S. (2016) 'Sudden adult death syndrome in m.3243A>G-related mitochondrial disease: an unrecognized clinical entity in young, asymptomatic adults', *Eur Heart J*, 37(32), pp. 2552-9.

Nguyen, T.N., Padman, B.S., Usher, J., Oorschot, V., Ramm, G. and Lazarou, M. (2016) 'Atg8 family LC3/GABARAP proteins are crucial for autophagosome–lysosome fusion but not autophagosome formation during PINK1/Parkin mitophagy and starvation', *The Journal of Cell Biology*, 215(6), pp. 857-874.

Noji, H., Yasuda, R., Yoshida, M. and Kinosita, K., Jr. (1997) 'Direct observation of the rotation of F1-ATPase', *Nature*, 386(6622), pp. 299-302.
O'Brien, T.W. (2003) 'Properties of Human Mitochondrial Ribosomes', *IUBMB Life*, 55(9), pp. 505-513.

Ojala, D., Montoya, J. and Attardi, G. (1981) 'tRNA punctuation model of RNA processing in human mitochondria', *Nature*, 290(5806), pp. 470-4.

Okatsu, K., Oka, T., Iguchi, M., Imamura, K., Kosako, H., Tani, N., Kimura, M., Go, E., Koyano, F., Funayama, M., Shiba-Fukushima, K., Sato, S., Shimizu, H., Fukunaga, Y., Taniguchi, H., Komatsu, M., Hattori, N., Mihara, K., Tanaka, K. and Matsuda, N. (2012) 'PINK1 autophosphorylation upon membrane potential dissipation is essential for Parkin recruitment to damaged mitochondria', *Nature Communications*, 3, p. 1016.

Old, S.L. and Johnson, M.A. (1989) 'Methods of microphotometric assay of succinate dehydrogenase and cytochrome c oxidase activities for use on human skeletal muscle', *Histochem J*, 21(9-10), pp. 545-55.

Oldfors, A., Larsson, N.G., Holme, E., Tulinius, M., Kadenbach, B. and Droste, M. (1992) 'Mitochondrial DNA deletions and cytochrome c oxidase deficiency in muscle fibres', *J Neurol Sci*, 110(1-2), pp. 169-77.

Oldfors, A., Larsson, N.-G., Holme, E., Tulinius, M., Kadenbach, B. and Droste, M. (1992) 'Mitochondrial DNA deletions and cytochrome c oxidase deficiency in muscle fibres', *Journal of the Neurological Sciences*, 110(1–2), pp. 169-177.

Orrenius, S., Zhivotovsky, B. and Nicotera, P. (2003) 'Regulation of cell death: the calcium-apoptosis link', *Nat Rev Mol Cell Biol*, 4(7), pp. 552-65.

Palade, G.E. (1952) 'The fine structure of mitochondria', *The Anatomical Record*, 114(3), pp. 427-451.

Palade, G.E. (1953) 'An electron microscope study of the mitochondrial structure', *J Histochem Cytochem*, 1(4), pp. 188-211.

Pallotti, F., Chen, X., Bonilla, E. and Schon, E.A. (1996) 'Evidence that specific mtDNA point mutations may not accumulate in skeletal muscle during normal human aging', *American Journal of Human Genetics*, 59(3), pp. 591-602.

Palty, R., Silverman, W.F., Hershfinkel, M., Caporale, T., Sensi, S.L., Parnis, J., Nolte, C., Fishman, D., Shoshan-Barmatz, V., Herrmann, S., Khananshvili, D. and Sekler, I. (2010) 'NCLX is an essential component of mitochondrial Na+/Ca2+ exchange', *Proc Natl Acad Sci U S A*, 107(1), pp. 436-41.

Paradkar, P.N., Zumbrennen, K.B., Paw, B.H., Ward, D.M. and Kaplan, J. (2009) 'Regulation of Mitochondrial Iron Import through Differential Turnover of Mitoferrin 1 and Mitoferrin 2', *Molecular and Cellular Biology*, 29(4), pp. 1007-1016.

Paumard, P., Vaillier, J., Coulary, B., Schaeffer, J., Soubannier, V., Mueller, D.M., Brethes, D., di Rago, J.P. and Velours, J. (2002) 'The ATP synthase is involved in generating mitochondrial cristae morphology', *Embo j*, 21(3), pp. 221-30.

Pavlakis, S.G., Phillips, P.C., DiMauro, S., De Vivo, D.C. and Rowland, L.P. (1984) 'Mitochondrial myopathy, encephalopathy, lactic acidosis, and strokelike episodes: a distinctive clinical syndrome', *Ann Neurol*, 16(4), pp. 481-8.

Pearson, H.A., Lobel, J.S., Kocoshis, S.A., Naiman, J.L., Windmiller, J., Lammi, A.T., Hoffman, R. and Marsh, J.C. (1979) 'A new syndrome of refractory sideroblastic anemia with vacuolization of marrow precursors and exocrine pancreatic dysfunction', *J Pediatr*, 95(6), pp. 976-84.

Pejznochova, M., Tesarova, M., Honzik, T., Hansikova, H., Magner, M. and Zeman, J. (2008) 'The developmental changes in mitochondrial DNA content per cell in human cord blood leukocytes during gestation', *Physiol Res*, 57(6), pp. 947-55.

Petruzzella, V., Moraes, C.T., Sano, M.C., Bonilla, S.E., DiMauro, S. and Schon, E.A. (1994) 'Extremely high levels of mutant mtDNAs co-localize with cytocohrome c oxidase-negative ragged-red fibers in patients harboring a point mutation at nt 3243', *Human Molecular Genetics*, 3(3), pp. 449-454.

Pette, D. and Vrbova, G. (1992) 'Adaptation of mammalian skeletal muscle fibers to chronic electrical stimulation', *Rev Physiol Biochem Pharmacol*, 120, pp. 115-202.

Pfaffl, M.W. ‘Quantification strategies in real time PCR’. IUL biotechnology series; 5. In: *A-Z of quantitative PCR*. Edited by: Bustin SA. La Jolla, CA, International University Line; 2004.

Phillips, N.R., Sprouse, M.L. and Roby, R.K. (2014) 'Simultaneous quantification of mitochondrial DNA copy number and deletion ratio: A multiplex real-time PCR assay', *Scientific Reports*, 4, p. 3887.

Pitceathly, R.D.S., Rahman, S. and Hanna, M.G. (2012) 'Single deletions in mitochondrial DNA – Molecular mechanisms and disease phenotypes in clinical practice', *Neuromuscular Disorders*, 22(7), pp. 577-586.

Pohjoismäki, J.L.O., Wanrooij, S., Hyvärinen, A.K., Goffart, S., Holt, I.J., Spelbrink, J.N. and Jacobs, H.T. (2006) 'Alterations to the expression level of mitochondrial transcription factor A, TFAM, modify the mode of mitochondrial DNA replication in cultured human cells', *Nucleic Acids Research*, 34(20), pp. 5815-5828.

Porteous, W.K., James, A.M., Sheard, P.W., Porteous, C.M., Packer, M.A., Hyslop, S.J., Melton, J.V., Pang, C.Y., Wei, Y.H. and Murphy, M.P. (1998) 'Bioenergetic consequences of accumulating the common 4977-bp mitochondrial DNA deletion', *Eur J Biochem*, 257(1), pp. 192-201.

Pyle, A., Taylor, R.W., Durham, S.E., Deschauer, M., Schaefer, A.M., Samuels, D.C. and Chinnery, P.F. (2007) 'Depletion of mitochondrial DNA in leucocytes harbouring the 3243A->G mtDNA mutation', *J Med Genet*, 44(1), pp. 69-74.

Rahman, S., Poulton, J., Marchington, D. and Suomalainen, A. (2001) 'Decrease of 3243 A→G mtDNA Mutation from Blood in MELAS Syndrome: A Longitudinal Study', *American Journal of Human Genetics*, 68(1), pp. 238-240.

Rebelo, A.P., Dillon, L.M. and Moraes, C.T. (2011) 'Mitochondrial DNA transcription regulation and nucleoid organization', *J Inherit Metab Dis*, 34(4), pp. 941-51.

Rhee, S.G., Bae, Y.S., Lee, S.R. and Kwon, J. (2000) 'Hydrogen peroxide: a key messenger that modulates protein phosphorylation through cysteine oxidation', *Sci STKE*, 2000(53), p. pe1.

Rocha, M.C., Grady, J.P., Grünewald, A., Vincent, A., Dobson, P.F., Taylor, R.W., Turnbull, D.M. and Rygiel, K.A. (2015) 'A novel immunofluorescent assay to investigate oxidative phosphorylation deficiency in mitochondrial myopathy: understanding mechanisms and improving diagnosis', *Scientific Reports*, 5, p. 15037.

Rorbach, J. and Minczuk, M. (2012) 'The post-transcriptional life of mammalian mitochondrial RNA', *Biochem J*, 444(3), pp. 357-73.

Rossignol, R., Malgat, M., Mazat, J.-P. and Letellier, T. (1999) 'Threshold Effect and Tissue Specificity: implication for mitochondrial cytopathies', *Journal of Biological Chemistry*, 274(47), pp. 33426-33432.

Rotig, A., Bourgeron, T., Chretien, D., Rustin, P. and Munnich, A. (1995) 'Spectrum of mitochondrial DNA rearrangements in the Pearson marrow-pancreas syndrome', *Hum Mol Genet*, 4(8), pp. 1327-30.

Rowland L.P. and Hayes A.P. ‘Diverse clinical disorders associated with morphological abnormalities in mitochondria’. In: *Mitochondrial Pathology in Muscle Diseases*. Edited by Scarlato G. and Cerri C.. Piccin; Padua: 1983. pp. 141–158

Rygiel, K.A., Grady, J.P., Taylor, R.W., Tuppen, H.A.L. and Turnbull, D.M. (2015) 'Triplex real-time PCR–an improved method to detect a wide spectrum of mitochondrial DNA deletions in single cells', *Scientific Reports*, 5, p. 9906.

Sabatino, L., Botto, N., Borghini, A., Turchi, S. and Andreassi, M.G. (2013) 'Development of a new multiplex quantitative real-time PCR assay for the detection of the mtDNA(4977) deletion in coronary artery disease patients: a link with telomere shortening', *Environ Mol Mutagen*, 54(5), pp. 299-307.

Sacconi, S., Salviati, L., Nishigaki, Y., Walker, W.F., Hernandez-Rosa, E., Trevisson, E., Delplace, S., Desnuelle, C., Shanske, S., Hirano, M., Schon, E.A., Bonilla, E., De Vivo, D.C., DiMauro, S. and Davidson, M.M. (2008) 'A functionally dominant mitochondrial DNA mutation', *Human Molecular Genetics*, 17(12), pp. 1814-1820.

Sadikovic, B., Wang, J., El-Hattab, A., Landsverk, M., Douglas, G., Brundage, E.K., Craigen, W.J., Schmitt, E.S. and Wong, L.-J.C. (2010) 'Sequence Homology at the Breakpoint and Clinical Phenotype of Mitochondrial DNA Deletion Syndromes', *PLoS ONE*, 5(12), p. e15687.
Samuels, D.C., Schon, E.A. and Chinnery, P.F. (2004) 'Two direct repeats cause most human mtDNA deletions', *Trends in Genetics*, 20(9), pp. 393-398.

Saraste, M. (1999) 'Oxidative phosphorylation at the fin de siecle', *Science*, 283(5407), pp. 1488-93.

Satoh, M. and Kuroiwa, T. (1991) 'Organization of multiple nucleoids and DNA molecules in mitochondria of a human cell', *Exp Cell Res*, 196(1), pp. 137-40.

Sazanov, L.A. (2007) 'Respiratory complex I: mechanistic and structural insights provided by the crystal structure of the hydrophilic domain', *Biochemistry*, 46(9), pp. 2275-88.

Sazanov, L.A. (2015) 'A giant molecular proton pump: structure and mechanism of respiratory complex I', *Nat Rev Mol Cell Biol*, 16(6), pp. 375-388.

Schaefer, A.M., McFarland, R., Blakely, E.L., He, L., Whittaker, R.G., Taylor, R.W., Chinnery, P.F. and Turnbull, D.M. (2008) 'Prevalence of mitochondrial DNA disease in adults', *Annals of Neurology*, 63(1), pp. 35-39.

Schaefer, A.M., Phoenix, C., Elson, J.L., McFarland, R., Chinnery, P.F. and Turnbull, D.M. (2006) 'Mitochondrial disease in adults: a scale to monitor progression and treatment', *Neurology*, 66(12), pp. 1932-4.

Schäfer, E., Dencher, N.A., Vonck, J. and Parcej, D.N. (2007) 'Three-Dimensional Structure of the Respiratory Chain Supercomplex I1III2IV1 from Bovine Heart Mitochondria', *Biochemistry*, 46(44), pp. 12579-12585.

Schäfer, E., Seelert, H., Reifschneider, N.H., Krause, F., Dencher, N.A. and Vonck, J. (2006) 'Architecture of Active Mammalian Respiratory Chain Supercomplexes', *Journal of Biological Chemistry*, 281(22), pp. 15370-15375.

Schägger, H. and Pfeiffer, K. (2000) 'Supercomplexes in the respiratory chains of yeast and mammalian mitochondria', *The EMBO Journal*, 19(8), pp. 1777-1783.

Schiaffino, S., Murgia, M., Serrano, A.L., Calabria, E. and Pallafacchina, G. (1999) 'How is muscle phenotype controlled by nerve activity?', *Ital J Neurol Sci*, 20(6), pp. 409-12.

Schiaffino, S. and Reggiani, C. (2011) 'Fiber Types in Mammalian Skeletal Muscles', *Physiological Reviews*, 91(4), pp. 1447-1531.

Schmickel, R.D. (1973) 'Quantitation of Human Ribosomal DNA: Hybridization of Human DNA with Ribosomal RNA for Quantitation and Fractionation', *Pediatr Res*, 7(1), pp. 5-12.

Schon, E.A., DiMauro, S. and Hirano, M. (2012) 'Human mitochondrial DNA: roles of inherited and somatic mutations', *Nature reviews. Genetics*, 13(12), pp. 878-890.

Schon, E.A., Santra, S., Pallotti, F. and Girvin, M.E. (2001) 'Pathogenesis of primary defects in mitochondrial ATP synthesis', *Semin Cell Dev Biol*, 12(6), pp. 441-8.

Schröder, R., Vielhaber, S., Wiedemann, F.R., Kornblum, C., Papassotiropoulos, A., Broich, P., Zierz, S., Elger, C.E., Reichmann, H., Seibel, P., Klockgether, T. and Kunz, W.S. (2000) 'New Insights into the Metabolic Consequences of Large-Scale mtDNA Deletions: A Quantitative Analysis of Biochemical, Morphological, and Genetic Findings in Human Skeletal Muscle', *Journal of Neuropathology & Experimental Neurology*, 59(5), pp. 353-360.

Schultz, B.E. and Chan, S.I. (2001) 'Structures and proton-pumping strategies of mitochondrial respiratory enzymes', *Annu Rev Biophys Biomol Struct*, 30, pp. 23-65.

Schwartz, M. and Vissing, J. (2002) 'Paternal inheritance of mitochondrial DNA', *N Engl J Med*, 347(8), pp. 576-80.

Sciacco, M., Bonilla, E., Schon, E.A., DiMauro, S. and Moraes, C.T. (1994) 'Distribution of wild-type and common deletion forms of mtDNA in normal and respiration-deficient muscle fibers from patients with mitochondrial myopathy', *Hum Mol Genet*, 3(1), pp. 13-9.

Sen, K. and Beattie, D.S. (1986) 'Cytochrome b is necessary for the effective processing of core protein I and the iron-sulfur protein of complex III in the mitochondria', *Arch Biochem Biophys*, 251(1), pp. 239-49.

Sena, Laura A. and Chandel, Navdeep S. (2012) 'Physiological Roles of Mitochondrial Reactive Oxygen Species', *Molecular Cell*, 48(2), pp. 158-167.

Shadel, G.S. and Clayton, D.A. (1997) 'Mitochondrial DNA maintenance in vertebrates', *Annu Rev Biochem*, 66, pp. 409-35.

Shanske, S., Pancrudo, J., Kaufmann, P., Engelstad, K., Jhung, S., Lu, J., Naini, A., DiMauro, S. and De Vivo, D.C. (2004) 'Varying loads of the mitochondrial DNA A3243G mutation in different tissues: implications for diagnosis', *Am J Med Genet A*, 130a(2), pp. 134-7.

Shaw, G.C., Cope, J.J., Li, L., Corson, K., Hersey, C., Ackermann, G.E., Gwynn, B., Lambert, A.J., Wingert, R.A., Traver, D., Trede, N.S., Barut, B.A., Zhou, Y., Minet, E., Donovan, A., Brownlie, A., Balzan, R., Weiss, M.J., Peters, L.L., Kaplan, J., Zon, L.I. and Paw, B.H. (2006) 'Mitoferrin is essential for erythroid iron assimilation', *Nature*, 440(7080), pp. 96-100.

Shen, J., Platek, M., Mahasneh, A., Ambrosone, C.B. and Zhao, H. (2010) 'Mitochondrial copy number and risk of breast cancer: a pilot study', *Mitochondrion*, 10(1), pp. 62-8.

Shiraiwa, N., Ishii, A., Iwamoto, H., Mizusawa, H., Kagawa, Y. and Ohta, S. (1993) 'Content of mutant mitochondrial DNA and organ dysfunction in a patient with a MELAS subgroup of mitochondrial encephalomyopathies', *Journal of the Neurological Sciences*, 120(2), pp. 174-179.

Shoffner, J.M., Lott, M.T., Lezza, A.M., Seibel, P., Ballinger, S.W. and Wallace, D.C. (1990) 'Myoclonic epilepsy and ragged-red fiber disease (MERRF) is associated with a mitochondrial DNA tRNA(Lys) mutation', *Cell*, 61(6), pp. 931-7.

Shoffner, J.M., Lott, M.T., Voljavec, A.S., Soueidan, S.A., Costigan, D.A. and Wallace, D.C. (1989) 'Spontaneous Kearns-Sayre/chronic external ophthalmoplegia plus syndrome associated with a mitochondrial DNA deletion: a slip-replication model and metabolic therapy', *Proc Natl Acad Sci U S A*, 86(20), pp. 7952-6.

Shoubridge, E.A., Karpati, G. and Hastings, K.E.M. (1990) 'Deletion mutants are functionally dominant over wild-type mitochondrial genomes in skeletal muscle fiber segments in mitochondrial disease', *Cell*, 62(1), pp. 43-49.

Shoubridge, E.A. and Wai, T. (2007) 'Mitochondrial DNA and the mammalian oocyte', *Curr Top Dev Biol*, 77, pp. 87-111.

Sicheritz-Ponten, T., Kurland, C.G. and Andersson, S.G. (1998) 'A phylogenetic analysis of the cytochrome b and cytochrome c oxidase I genes supports an origin of mitochondria from within the Rickettsiaceae', *Biochim Biophys Acta*, 1365(3), pp. 545-51.

Silvestri, G., Bertini, E., Servidei, S., Rana, M., Zachara, E., Ricci, E. and Tonali, P. (1997) 'Maternally inherited cardiomyopathy: a new phenotype associated with the A to G at nt.3243 of mitochondrial DNA (MELAS mutation)', *Muscle Nerve*, 20(2), pp. 221-5.

Silvestri, G., Rana, M., Odoardi, F., Modoni, A., Paris, E., Papacci, M., Tonali, P. and Servidei, S. (2000) 'Single-fiber PCR in MELAS(3243) patients: correlations between intratissue distribution and phenotypic expression of the mtDNA(A3243G) genotype', *Am J Med Genet*, 94(3), pp. 201-6.

Simamura, E., Shimada, H., Hatta, T. and Hirai, K.-I. (2008) 'Mitochondrial voltage-dependent anion channels (VDACs) as novel pharmacological targets for anti-cancer agents', *Journal of Bioenergetics and Biomembranes*, 40(3), pp. 213-217.

Simonsz, H.J., Barlocher, K. and Rotig, A. (1992) 'Kearns-Sayre's syndrome developing in a boy who survived pearson's syndrome caused by mitochondrial DNA deletion', *Doc Ophthalmol*, 82(1-2), pp. 73-9.

Smeitink, J., van den Heuvel, L. and DiMauro, S. (2001) 'The genetics and pathology of oxidative phosphorylation', *Nat Rev Genet*, 2(5), pp. 342-352.

Smirnova, E., Griparic, L., Shurland, D.L. and van der Bliek, A.M. (2001) 'Dynamin-related protein Drp1 is required for mitochondrial division in mammalian cells', *Mol Biol Cell*, 12(8), pp. 2245-56.

Smits, P., Smeitink, J. and van den Heuvel, L. (2010) 'Mitochondrial Translation and Beyond: Processes Implicated in Combined Oxidative Phosphorylation Deficiencies', *Journal of Biomedicine and Biotechnology*, 2010, p. 24.

Smits, P., Smeitink, J.A.M., van den Heuvel, L.P., Huynen, M.A. and Ettema, T.J.G. (2007) 'Reconstructing the evolution of the mitochondrial ribosomal proteome', *Nucleic Acids Research*, 35(14), pp. 4686-4703.

Sochivko, D.G., Fedorov, A.A., Varlamov, D.A., Kurochkin, V.E. and Petrov, R.V. (2013) 'Accuracy of quantitative real-time PCR analysis', *Dokl Biochem Biophys*, 449, pp. 105-8.
Sone, N., Sekimachi, M. and Kutoh, E. (1987) 'Identification and properties of a quinol oxidase super-complex composed of a bc1 complex and cytochrome oxidase in the thermophilic bacterium PS3', *J Biol Chem*, 262(32), pp. 15386-91.

Song, Z., Chen, H., Fiket, M., Alexander, C. and Chan, D.C. (2007) 'OPA1 processing controls mitochondrial fusion and is regulated by mRNA splicing, membrane potential, and Yme1L', *The Journal of Cell Biology*, 178(5), pp. 749-755.

Southern, E.M. (1975) 'Detection of specific sequences among DNA fragments separated by gel electrophoresis', *Journal of Molecular Biology*, 98(3), pp. 503-517.

Spelbrink, J.N., Li, F.-Y., Tiranti, V., Nikali, K., Yuan, Q.-P., Tariq, M., Wanrooij, S., Garrido, N., Comi, G., Morandi, L., Santoro, L., Toscano, A., Fabrizi, G.-M., Somer, H., Croxen, R., Beeson, D., Poulton, J., Suomalainen, A., Jacobs, H.T., Zeviani, M. and Larsson, C. (2001) 'Human mitochondrial DNA deletions associated with mutations in the gene encoding Twinkle, a phage T7 gene 4-like protein localized in mitochondria', *Nat Genet*, 28(3), pp. 223-231.

Spendiff, S., Reza, M., Murphy, J.L., Gorman, G., Blakely, E.L., Taylor, R.W., Horvath, R., Campbell, G., Newman, J., Lochmuller, H. and Turnbull, D.M. (2013) 'Mitochondrial DNA deletions in muscle satellite cells: implications for therapies', *Hum Mol Genet*, 22(23), pp. 4739-47.

Stierum, R.H., Dianov, G.L. and Bohr, V.A. (1999) 'Single-nucleotide patch base excision repair of uracil in DNA by mitochondrial protein extracts', *Nucleic Acids Res*, 27(18), pp. 3712-9.

Stiles, A.R., Simon, M.T., Stover, A., Eftekharian, S., Khanlou, N., Wang, H.L., Magaki, S., Lee, H., Partynski, K., Dorrani, N., Chang, R., Martinez-Agosto, J.A. and Abdenur, J.E. (2016) 'Mutations in TFAM, encoding mitochondrial transcription factor A, cause neonatal liver failure associated with mtDNA depletion', *Mol Genet Metab*, 119(1-2), pp. 91-9.

Strauss, M., Hofhaus, G., Schröder, R.R. and Kühlbrandt, W. (2008) 'Dimer ribbons of ATP synthase shape the inner mitochondrial membrane', *The EMBO Journal*, 27(7), pp. 1154-1160.

Sue, C.M., Quigley, A., Katsabanis, S., Kapsa, R., Crimmins, D.S., Byrne, E. and Morris, J.G. (1998) 'Detection of MELAS A3243G point mutation in muscle, blood and hair follicles', *J Neurol Sci*, 161(1), pp. 36-9.

Sun, Y., Li, Y., Luo, D. and Liao, D.J. (2012) 'Pseudogenes as Weaknesses of ACTB (Actb) and GAPDH (Gapdh) Used as Reference Genes in Reverse Transcription and Polymerase Chain Reactions', *PLOS ONE*, 7(8), p. e41659.

Sutovsky, P., Van Leyen, K., McCauley, T., Day, B.N. and Sutovsky, M. (2004) 'Degradation of paternal mitochondria after fertilization: implications for heteroplasmy, assisted reproductive technologies and mtDNA inheritance', *Reprod Biomed Online*, 8(1), pp. 24-33.

Suzuki, T., Suzuki, T., Wada, T., Saigo, K. and Watanabe, K. (2002) 'Taurine as a constituent of mitochondrial tRNAs: new insights into the functions of taurine and human mitochondrial diseases', *The EMBO Journal*, 21(23), pp. 6581-6589.

t Hart, L.M., Jansen, J.J., Lemkes, H.H., de Knijff, P. and Maassen, J.A. (1996) 'Heteroplasmy levels of a mitochondrial gene mutation associated with diabetes mellitus decrease in leucocyte DNA upon aging', *Hum Mutat*, 7(3), pp. 193-7.

Tang, Y., Schon, E.A., Wilichowski, E., Vazquez-Memije, M.E., Davidson, E. and King, M.P. (2000) 'Rearrangements of human mitochondrial DNA (mtDNA): new insights into the regulation of mtDNA copy number and gene expression', *Mol Biol Cell*, 11(4), pp. 1471-85.

Taylor, R.W., Barron, M.J., Borthwick, G.M., Gospel, A., Chinnery, P.F., Samuels, D.C., Taylor, G.A., Plusa, S.M., Needham, S.J., Greaves, L.C., Kirkwood, T.B. and Turnbull, D.M. (2003) 'Mitochondrial DNA mutations in human colonic crypt stem cells', *J Clin Invest*, 112(9), pp. 1351-60.

Taylor, R.W., Schaefer, A.M., Barron, M.J., McFarland, R. and Turnbull, D.M. (2004) 'The diagnosis of mitochondrial muscle disease', *Neuromuscular Disorders*, 14(4), pp. 237-245.
Taylor, R.W. and Turnbull, D.M. (2005) 'Mitochondrial DNA mutations in human disease', *Nat Rev Genet*, 6(5), pp. 389-402.

Thyagarajan, B., Wang, R., Barcelo, H., Koh, W.P. and Yuan, J.M. (2012) 'Mitochondrial copy number is associated with colorectal cancer risk', *Cancer Epidemiol Biomarkers Prev*, 21(9), pp. 1574-81.

Thyagarajan, B., Wang, R., Nelson, H., Barcelo, H., Koh, W.-P. and Yuan, J.-M. (2013) 'Mitochondrial DNA Copy Number Is Associated with Breast Cancer Risk', *PLoS ONE*, 8(6), p. e65968.

Thyagarajan, D., Shanske, S., Vazquez-Memije, M., De Vivo, D. and DiMauro, S. (1995) 'A novel mitochondrial ATPase 6 point mutation in familial bilateral striatal necrosis', *Ann Neurol*, 38(3), pp. 468-72.

Tokunaga, M., Mita, S., Murakami, T., Kumamoto, T., Uchino, M., Nonaka, I. and Ando, M. (1994) 'Single muscle fiber analysis of mitochondrial myopathy, encephalopathy, lactic acidosis, and stroke-like episodes (MELAS)', *Annals of Neurology*, 35(4), pp. 413-419.

Tong, W.H. and Rouault, T. (2000) 'Distinct iron-sulfur cluster assembly complexes exist in the cytosol and mitochondria of human cells', *Embo j*, 19(21), pp. 5692-700.

Tong, W.-H., Jameson, G.N.L., Huynh, B.H. and Rouault, T.A. (2003) 'Subcellular compartmentalization of human Nfu, an iron–sulfur cluster scaffold protein, and its ability to assemble a [4Fe–4S] cluster', *Proceedings of the National Academy of Sciences*, 100(17), pp. 9762-9767.

Tovar, J., Leon-Avila, G., Sanchez, L.B., Sutak, R., Tachezy, J., van der Giezen, M., Hernandez, M., Muller, M. and Lucocq, J.M. (2003) 'Mitochondrial remnant organelles of Giardia function in iron-sulphur protein maturation', *Nature*, 426(6963), pp. 172-176.

Trumpower, B.L. (1990) 'Cytochrome bc1 complexes of microorganisms', *Microbiol Rev*, 54(2), pp. 101-29.

Truscott, K.N., Brandner, K. and Pfanner, N. (2003) 'Mechanisms of protein import into mitochondria', *Curr Biol*, 13(8), pp. R326-37.

Tsukihara, T., Aoyama, H., Yamashita, E., Tomizaki, T., Yamaguchi, H., Shinzawa-Itoh, K., Nakashima, R., Yaono, R. and Yoshikawa, S. (1996) 'The whole structure of the 13-subunit oxidized cytochrome c oxidase at 2.8 A', *Science*, 272(5265), pp. 1136-44.

Tuppen, H.A.L., Blakely, E.L., Turnbull, D.M. and Taylor, R.W. (2010) 'Mitochondrial DNA mutations and human disease', *Biochimica et Biophysica Acta (BBA) - Bioenergetics*, 1797(2), pp. 113-128.

Turrens, J.F. (2003) 'Mitochondrial formation of reactive oxygen species', *The Journal of Physiology*, 552(2), pp. 335-344.

Turrens, J.F. and Boveris, A. (1980) 'Generation of superoxide anion by the NADH dehydrogenase of bovine heart mitochondria', *Biochem J*, 191(2), pp. 421-7.

Twig, G., Elorza, A., Molina, A.J.A., Mohamed, H., Wikstrom, J.D., Walzer, G., Stiles, L., Haigh, S.E., Katz, S., Las, G., Alroy, J., Wu, M., Py, B.F., Yuan, J., Deeney, J.T., Corkey, B.E. and Shirihai, O.S. (2008) 'Fission and selective fusion govern mitochondrial segregation and elimination by autophagy', *The EMBO Journal*, 27(2), pp. 433-446.

Urbina, H.D., Silberg, J.J., Hoff, K.G. and Vickery, L.E. (2001) 'Transfer of Sulfur from IscS to IscU during Fe/S Cluster Assembly', *Journal of Biological Chemistry*, 276(48), pp. 44521-44526.

van den Ouweland, J.M., Lemkes, H.H., Ruitenbeek, W., Sandkuijl, L.A., de Vijlder, M.F., Struyvenberg, P.A., van de Kamp, J.J. and Maassen, J.A. (1992) 'Mutation in mitochondrial tRNA(Leu)(UUR) gene in a large pedigree with maternally transmitted type II diabetes mellitus and deafness', *Nat Genet*, 1(5), pp. 368-71.

van den Ouweland, J.M.W., Lemkes, H.H.P.J., Trembath, R.C., Ross, R., Velho, G., Cohen, D., Froguel, P. and Maassen, J.A. (1994) 'Maternally inherited diabetes and deafness is a distinct subtype of diabetes and associates with a single point mutation in the mitochondrial tRNA ^{Leu(UUR)} gene', *Diabetes*, 43(6), pp. 746-751.

Van Goethem, G., Dermaut, B., Lofgren, A., Martin, J.-J. and Van Broeckhoven, C. (2001) 'Mutation of POLG is associated with progressive external ophthalmoplegia characterized by mtDNA deletions', *Nat Genet*, 28(3), pp. 211-212.

Venegas, V. and Halberg, M.C. (2012) 'Measurement of mitochondrial DNA copy number', *Methods Mol Biol*, 837, pp. 327-35.

Virbasius, J.V. and Scarpulla, R.C. (1994) 'Activation of the human mitochondrial transcription factor A gene by nuclear respiratory factors: a potential regulatory link between nuclear and mitochondrial gene expression in organelle biogenesis', *Proc Natl Acad Sci U S A*, 91(4), pp. 1309-13.

Vogel, F., Bornhovd, C., Neupert, W. and Reichert, A.S. (2006) 'Dynamic subcompartmentalization of the mitochondrial inner membrane', *J Cell Biol*, 175(2), pp. 237-47.

Wagner, K., Mick, D.U. and Rehling, P. (2009) 'Protein transport machineries for precursor translocation across the inner mitochondrial membrane', *Biochim Biophys Acta*, 1793(1), pp. 52-9.

Walker, J.E. (1992) 'The Nadh: Ubiquinone oxidoreductase (complex I) of respiratory chains', *Quarterly Reviews of Biophysics*, 25(3), pp. 253-324.

Wallace, D.C. (1992) 'Mitochondrial genetics: a paradigm for aging and degenerative diseases?', *Science*, 256(5057), pp. 628-32.

Wallace, D.C., Singh, G., Lott, M.T., Hodge, J.A., Schurr, T.G., Lezza, A.M., Elsas, L.J., 2nd and Nikoskelainen, E.K. (1988) 'Mitochondrial DNA mutation associated with Leber's hereditary optic neuropathy', *Science*, 242(4884), pp. 1427-30.

Wang, C. and Youle, R.J. (2009) 'The role of mitochondria in apoptosis*', *Annu Rev Genet*, 43, pp. 95-118.

Wang, G.J., Nutter, L.M. and Thayer, S.A. (1997) 'Insensitivity of cultured rat cortical neurons to mitochondrial DNA synthesis inhibitors: evidence for a slow turnover of mitochondrial DNA', *Biochem Pharmacol*, 54(1), pp. 181-7.

Wang, J. and Pantopoulos, K. (2011) 'Regulation of cellular iron metabolism', *Biochem J*, 434(3), pp. 365-81.

Wanrooij, S., Fusté, J.M., Farge, G., Shi, Y., Gustafsson, C.M. and Falkenberg, M. (2008) 'Human mitochondrial RNA polymerase primes lagging-strand DNA synthesis in vitro', *Proceedings of the National Academy of Sciences of the United States of America*, 105(32), pp. 11122-11127.

Watt, I.N., Montgomery, M.G., Runswick, M.J., Leslie, A.G.W. and Walker, J.E. (2010) 'Bioenergetic cost of making an adenosine triphosphate molecule in animal mitochondria', *Proceedings of the National Academy of Sciences of the United States of America*, 107(39), pp. 16823-16827.

Weber, K., Wilson, J.N., Taylor, L., Brierley, E., Johnson, M.A., Turnbull, D.M. and Bindoff, L.A. (1997) 'A new mtDNA mutation showing accumulation with time and restriction to skeletal muscle', *Am J Hum Genet*, 60(2), pp. 373-80.

Wei, M.C., Zong, W.-X., Cheng, E.H.Y., Lindsten, T., Panoutsakopoulou, V., Ross, A.J., Roth, K.A., MacGregor, G.R., Thompson, C.B. and Korsmeyer, S.J. (2001) 'Proapoptotic BAX and BAK: A Requisite Gateway to Mitochondrial Dysfunction and Death', *Science (New York, N.Y.)*, 292(5517), pp. 727-730.

Wellauer, P.K. and Dawid, I.B. (1979) 'Isolation and sequence organization of human ribosomal DNA', *Journal of Molecular Biology*, 128(3), pp. 289-303.

Westermann, B. (2010) 'Mitochondrial fusion and fission in cell life and death', *Nat Rev Mol Cell Biol*, 11(12), pp. 872-84.

White, H.E., Durston, V.J., Seller, A., Fratter, C., Harvey, J.F. and Cross, N.C. (2005) 'Accurate detection and quantitation of heteroplasmic mitochondrial point mutations by pyrosequencing', *Genet Test*, 9(3), pp. 190-9.

Wilkens, V., Kohl, W. and Busch, K. (2013) 'Restricted diffusion of OXPHOS complexes in dynamic mitochondria delays their exchange between cristae and engenders a transitory mosaic distribution', *Journal of Cell Science*, 126(1), pp. 103-116.

Wittenhagen, L.M. and Kelley, S.O. (2002) 'Dimerization of a pathogenic human mitochondrial tRNA', *Nat Struct Mol Biol*, 9(8), pp. 586-590.

Wong, L.J., Perng, C.L., Hsu, C.H., Bai, R.K., Schelley, S., Vladutiu, G.D., Vogel, H. and Enns, G.M. (2003) 'Compensatory amplification of mtDNA in a patient with a novel deletion/duplication and high mutant load', *J Med Genet*, 40(11), p. e125.

Wu, Z., Puigserver, P., Andersson, U., Zhang, C., Adelmant, G., Mootha, V., Troy, A., Cinti, S., Lowell, B., Scarpulla, R.C. and Spiegelman, B.M. (1999) 'Mechanisms controlling

mitochondrial biogenesis and respiration through the thermogenic coactivator PGC-1', *Cell*, 98(1), pp. 115-24.

Xin, H., Woriax, V., Burkhart, W. and Spremulli, L.L. (1995) 'Cloning and expression of mitochondrial translational elongation factor Ts from bovine and human liver', *J Biol Chem*, 270(29), pp. 17243-9.

Yamashita, S., Nishino, I., Nonaka, I. and Goto, Y. (2008) 'Genotype and phenotype analyses in 136 patients with single large-scale mitochondrial DNA deletions', *J Hum Genet*, 53(7), pp. 598-606.

Yasukawa, T., Reyes, A., Cluett, T.J., Yang, M.Y., Bowmaker, M., Jacobs, H.T. and Holt, I.J. (2006) 'Replication of vertebrate mitochondrial DNA entails transient ribonucleotide incorporation throughout the lagging strand', *Embo j*, 25(22), pp. 5358-71.

Yasukawa, T., Suzuki, T., Suzuki, T., Ueda, T., Ohta, S. and Watanabe, K. (2000) 'Modification Defect at Anticodon Wobble Nucleotide of Mitochondrial tRNAsLeu(UUR) with Pathogenic Mutations of Mitochondrial Myopathy, Encephalopathy, Lactic Acidosis, and Stroke-like Episodes', *Journal of Biological Chemistry*, 275(6), pp. 4251-4257.

Ylikallio, E. and Suomalainen, A. (2012) 'Mechanisms of mitochondrial diseases', *Ann Med*, 44(1), pp. 41-59.

Yoneda, M., Miyatake, T. and Attardi, G. (1994) 'Complementation of mutant and wild-type human mitochondrial DNAs coexisting since the mutation event and lack of complementation of DNAs introduced separately into a cell within distinct organelles', *Mol Cell Biol*, 14(4), pp. 2699-712.

Yoneda, M., Miyatake, T. and Attardi, G. (1995) 'Heteroplasmic mitochondrial tRNA(Lys) mutation and its complementation in MERRF patient-derived mitochondrial transformants', *Muscle Nerve Suppl*, 3, pp. S95-101.

Yoneda, M., Tanno, Y., Horai, S., Ozawa, T., Miyatake, T. and Tsuji, S. (1990) 'A common mitochondrial DNA mutation in the t-RNA(Lys) of patients with myoclonus epilepsy associated with ragged-red fibers', *Biochem Int*, 21(5), pp. 789-96.

Yoon, T. and Cowan, J.A. (2003) 'Iron−Sulfur Cluster Biosynthesis. Characterization of Frataxin as an Iron Donor for Assembly of [2Fe-2S] Clusters in ISU-Type Proteins', *Journal of the American Chemical Society*, 125(20), pp. 6078-6084.

Youle, R.J. and van der Bliek, A.M. (2012) 'Mitochondrial fission, fusion, and stress', *Science*, 337(6098), pp. 1062-5.

Young, B.D., Hell, A. and Birnie, G.D. (1976) 'A new estimate of human ribosomal gene number', *Biochimica et Biophysica Acta (BBA) - Nucleic Acids and Protein Synthesis*, 454(3), pp. 539-548.

Young, M.J. and Copeland, W.C. (2016) 'Human mitochondrial DNA replication machinery and disease', *Curr Opin Genet Dev*, 38, pp. 52-62.

Yusuf, F. and Brand-Saberi, B. (2012) 'Myogenesis and muscle regeneration', *Histochem Cell Biol*, 138(2), pp. 187-99.

Zeviani, M., Gallera, C., Pannacci, M., Uziel, G., Prelle, A., Servidei, S. and DiDonato, S. (1990) 'Tissue distribution and transmission of mitochondrial DNA deletions in mitochondrial myopathies', *Annals of Neurology*, 28(1), pp. 94-97.

Zeviani, M., Moraes, C.T., DiMauro, S., Nakase, H., Bonilla, E., Schon, E.A. and Rowland, L.P. (1988) 'Deletions of mitochondrial DNA in Kearns-Sayre syndrome', *Neurology*, 38(9), pp. 1339-46.

Zhang, G., Qu, Y., Dang, S., Yang, Q., Shi, B. and Hou, P. (2013) 'Variable copy number of mitochondrial DNA (mtDNA) predicts worse prognosis in advanced gastric cancer patients', *Diagn Pathol*, 8, p. 173.

Zhou, Y., Duncan, T.M. and Cross, R.L. (1997) 'Subunit rotation in Escherichia coli FoF1–ATP synthase during oxidative phosphorylation', *Proceedings of the National Academy of Sciences*, 94(20), pp. 10583-10587.

Zhu, J., Vinothkumar, K.R. and Hirst, J. (2016) 'Structure of mammalian respiratory complex I', *Nature*, 536(7616), pp. 354-358.

Zick, M., Rabl, R. and Reichert, A.S. (2009) 'Cristae formation—linking ultrastructure and function of mitochondria', *Biochimica et Biophysica Acta (BBA) - Molecular Cell Research*, 1793(1), pp. 5-19.

Zickermann, V., Kerscher, S., Zwicker, K., Tocilescu, M.A., Radermacher, M. and Brandt, U. (2009) 'Architecture of complex I and its implications for electron transfer and proton pumping', *Biochimica et biophysica acta*, 1787(6), pp. 574-583.

Zierz, C.M., Joshi, P.R. and Zierz, S. (2015) 'Frequencies of myohistological mitochondrial changes in patients with mitochondrial DNA deletions and the common m.3243A>G point mutation', *Neuropathology*, 35(2), pp. 130-6.

Zollo, O., Tiranti, V. and Sondheimer, N. (2012) 'Transcriptional requirements of the distal heavy-strand promoter of mtDNA', *Proceedings of the National Academy of Sciences*, 109(17), pp. 6508-6512.

Zong, H., Ren, J.M., Young, L.H., Pypaert, M., Mu, J., Birnbaum, M.J. and Shulman, G.I. (2002) 'AMP kinase is required for mitochondrial biogenesis in skeletal muscle in response to chronic energy deprivation', *Proc Natl Acad Sci U S A*, 99(25), pp. 15983-7.